Aus dem Institut für Prophylaxe und Epidemiologie der Kreislaufkrankheiten

der Ludwig-Maximilians-Universität München

Dissertation

zum Erwerb des Doctor of Philosophy (Ph.D.) an der

Medizinischen Fakultät der

Ludwig-Maximilians-Universität zu München

Targets of let-7b in endothelial cells

vorgelegt von:

Saffiyeh Saboor Maleki

aus

Mashhad, Iran

Jahr:

2023

Mit Genehmigung der Medizinischen Fakultät der

Ludwig-Maximilians-Universität zu München

First evaluator: Prof. Dr. Andreas Schober

Second evaluator: Prof. Dr. Alexander Bartelt

Dean: Prof. Dr. med. Thomas Gudermann

Datum der Verteidigung:
13th June 2023

To my dear Morteza and my loving parents

Table of content

Table of content 2
Abstract 5
List of figures 7
List of tables 9
List of abbreviations 11
1 Introduction 13
1.1. Atherosclerosis 13
1.2. Endothelial cells 14
1.3. Properties of ECs 16
1.3.1 Barrier and transport 16
1.3.2 Hemostasis and thrombus prevention 16
1.3.3 Vasoregulation 16
1.3.4 Leukocyte recruitment 17
1.4. Effects of blood flow dynamics on ECs 17
1.5. Endothelial maladaptation 18
1.6. MicroRNAs 20
1.6.1 miRNA biogenesis and function 21
1.6.2 Canonical targeting of miRNAs 22
1.6.3 Role of ncRNAs in endothelial maladaptation 24
1.7. The let-7 family of miRNAs 26
1.7.1 Let-7 biogenesis and regulation 28
1.7.2 Biological roles of let-7 family members 29
1.7.3 Roles of let-7b in ECs 29
1.8. Hypothesis and aims 30
2. Materials and methods 30
2.1. Equipment 30
2.2. Consumables and solutions 32
2.3. Cells 33
2.4. Kits 34
2.5. Oligonucleotides 35
2.6. Primers 36

2.7. Let-7b target identification in ECs....36
2.8. Calculation of let-7b target enrichment....37
2.9. In silico analysis of let-7b target binding sites....37
2.10. Cell culture....38
2.11. Transfection of oligonucleotides....38
2.12. Liquid chromatography-tandem mass spectrometry (LC-MS/MS)....39
2.13. Enzyme-linked immunosorbent assay (ELISA)....39
2.14. RNA extraction....39
2.15. miRCURY LNA miRNA probe PCR assays....40
2.16. cDNA synthesis....41
2.17. Quantitative real-time PCR....42
2.18. Reporter vector preparation....43
2.19. Site-directed mutagenesis....46
2.20. Dual transfection of plasmids and oligonucleotides....47
2.21. Luciferase reporter assay....47
2.22. Preparation of oxidized LDL....47
2.23. Preparation of 4% paraformaldehyde (PFA)....48
2.24. Wound healing assay....48
2.25. EdU labeling and proliferation assay....48
2.26. Apoptosis assessment....49
2.27. DNA damage assessment....49
2.28. Micronuclei (MN) Formation evaluation....49
2.29. Reactive oxygen species (ROS) production assay....49
2.30. Statistical analysis....50
3. Results....51
3.1. Expression of Let-7 family members in mouse and human ECs....51
3.2. Let-7b targets in MECs and HECs....53
3.2.1 Endothelial protein-coding targets of let-7b....54
3.2.2 Endothelial lncRNA targets of let-7b....57
3.3. Let-7b target enrichment....60
3.4. Predicted let-7b BSs in endothelial protein-coding targets....64
3.5. Predicted let-7b BSs in endothelial lncRNA targets....72
3.6. Let-7b-mediated regulation of protein expression in ECs....78

3.6.1 Let-7b-mediated downregulation of protein expression in ECs 83
3.6.2 Let-7b-mediated upregulation of protein expression in ECs 91
3.7. Let-7b-mediated regulation of UHRF2 expression in ECs 97
3.8. Target transcript expression regulation by let-7b 99
3.9. Validation of the let-7b BSs in targets 100
3.10. Inhibiting let-7b-mediated repression of targets with TSBs 102
3.11. Functional effects of let-7b-mediated target inhibition in ECs 105
3.11.1 Effects of let-7b on EC wound healing 105
3.11.2 Effects of let-7b on EC proliferation 110
3.11.3 Effects of Let-7b on EC apoptosis 112
3.11.4 Effects of let-7b on DNA damage formation in ECs 115
3.11.5 Role of let-7b in EC micronuclei formation 117
3.11.6 Effects of let-7b on reactive oxygen species production in ECs 118
4 Discussion 120
4.1. Let-7 family members in MECs and HECs 120
4.2. Assessment of protein-coding genes in the let-7b interactome 121
4.3. Conservation of canonical let-7b BSs in protein-coding genes 122
4.4. Differences between mouse and human ECs in post-transcriptional regulation of let-7b targets 123
4.5. Assessment of ncRNA and lncRNA gene expression in ECs 127
4.6. Assessment of lncRNA targets of let-7b in ECs 127
4.7. Canonical let-7b BSs in lncRNA genes 128
4.8. Effects of let-7b on endothelial gene expression 130
4.9. The let-7b targeting effect on ECs 131
4.10. The effect of let-7b/UHRF2 interaction on ECs 133
4.11. Differences between MECs and HECs 135
References 136
Acknowledgements 151
Affidavit 152
Confirmation of congruency 153

Abstract

Background: Atherosclerosis mainly affects the branched regions of the vasculature where blood flow is turbulent. Endothelial cells (ECs) residing in these regions are inflammatory activated and cannot adapt to unstable conditions. These ECs have high cell turnover rates providing an entry site for circulating lipoproteins into the intima, marking the initiation of atherosclerotic plaque formation. MicroRNAs (miRNAs) are short (~20-23 nucleotides long) non-coding RNAs that negatively regulate post-transcriptional gene expression by targeting mRNAs and long non-coding RNAs (lncRNAs) in the RNA-induced silencing complex (RISC). The canonical targeting occurs through the binding of the "seed" sequence, which consists of nucleotides 2 to 7 at the 5' end of the miRNA, with a complementary sequence in the 3'–UTR of the mRNA. Our previous results suggest that EC maladaptation is controlled partly by Dicer-generated miRNAs like let-7b. Let-7b, which is highly conserved among various species, plays an important role in the function of aortic endothelial cells. However, the RNA targets of let-7b in ECs and their conservation in humans are largely unknown. This study aimed to identify mRNA and lncRNA targets of let-7b in aortic ECs that are conserved in humans and mice because evolutionarily conserved targets are more likely to be biologically relevant. Moreover, this study aimed to investigate the functional effects of let-7b mediated inhibition of targets that were conserved in mouse and human ECs.

Methods: Expression levels of let-7 family members were assessed by quantitative Real-Time PCR in ECs with and without let-7b up-regulation. To identify the targeting network of let-7b in ECs, data generated from mouse and human aortic ECs using the RISC-trap approach combined with RNA sequencing were analyzed. Genes significantly enriched in the RISC of let-7b mimic-treated ECs were obtained by comparing the logarithmically transformed ratio of the read count in the immunoprecipitate to the read count in the whole cell lysate to that of GAPDH using Dunnett's multiple comparison test. Significantly enriched mouse and human RNA transcripts were analyzed for let-7b canonical binding site (BS)s (8-mer, 7-mer-A1, 7-mer-m8) using the RNAhybrid target prediction tool. The BS conservation of the mRNA targets was evaluated by obtaining the P_{CT} values from Targetscan database. UHRF2 and MLLT10 were selected from among the most significantly enriched let-7b targets in the RISC with the highest BS conservation and LINCPINT was selected as the only significantly enriched lncRNA with an identical BS in mice and humans. The BSs of the selected targets were validated by luciferase reporter assays. Differential expression of selected targets was studied by qRT-PCR in ECs treated with let-7b inhibitors or target site blockers (TSBs) and control oligonucleotides. Let-7b-mediated regulation of total protein expression was assessed by LC-MS/MS in ECs treated with let-7b mimics and control mimics. Let-7b mediated UHRF2 protein regulation was determined by ELISA in ECs treated with let-7b inhibitor, UHRF2-TSB, and control oligonucleotides. To study the effects of let-7b mediated inhibition of UHRF2 and m-Mllt10 on endothelial maladaptation, wound healing and cell proliferation were assessed in an *in vitro* injury model, using the CytoSmart Omni live cell imager and Click-iT® EdU kit, respectively, in ECs treated with let-7b inhibitor, TSBs, and control oligonucleotides. The effect of let-7b mediated DNA damage formation was assessed by flow cytometric measurement of γ-H2AX foci in let-7b inhibitor,

TSBs, and control oligonucleotide treated ECs. Effect of let-7b on apoptosis and reactive oxygen species (ROS) production, were assessed by CellEvent Caspase-3/7 kit and DCFDA/H2DCFDA Cellular ROS Assay, respectively in ECs treated with let-7b inhibitor or TSBs and oligonucleotide controls.

Findings: Let-7 family member expression profile differs among MECs and HECs. The results show that although let-7b is highly conserved, most let-7b targets differ in mice and humans. While most mRNA and lncRNA genes did not have a canonical binding site (BS) in their transcript sequence, they are enriched in the RISC by let-7b indicating that non-canonical BSs are functional. The mRNA and lncRNA let-7b targets in HECs were more abundant compared to in MECs and only 153 protein-coding targets were common in the two species of which 23, including *ubiquitin-like with PHD and ring finger domains 2 (UHRF2)* and *histone lysine methyltransferase DOT1L cofactor (MLLT10)* contained conserved canonical binding sites in their 3'–UTRs. LINCPINT was identified as a lncRNA with canonical conserved BS in its sequence. Upregulation of let-7b resulted in regulation of 3% of total proteins in MECs and HECs. The downregulated proteins were mainly involved in increase of cell proliferation. Treatment of MECs and HECs with let-7b inhibitors upregulated Uhrf2, Mllt10, and Lincpint mRNA expression compared with control treatments in MECs and upregulated UHRF2 protein expression in ECs from both species. Moreover, transfection with let-7b mimics decreased luciferase activity in HEK293 cells expressing the human UHRF2-3'–UTR, or mouse Mllt10-3'–UTR, demonstrating that let-7b targets UHRF2 and m-Mllt10 in ECs. Let-7b mediated UHRF2 downregulation decreased wound healing and cell proliferation in ECs from both species, and Let-7b mediated Mllt10 downregulation decreased wound healing and cell proliferation in MECs, promoting endothelial maladaptation. Let-7b mediated down-regulation of UHRF2 and Mllt10 did not affect ROS production, DNA damage, and apoptosis in MECs the same way as in HECs.

Conclusion: This study identifies RNA targets of let-7b in ECs, the proteins that are regulated by let-7b overexpression in ECs, and their differences among mice and humans. Moreover, this study shows that let-7b downregulates UHRF2 gene expression in ECs from both species. The downregulation of UHRF2 expression by let-7b reduces EC proliferation and promotes EC maladaptation. TSBs can distinctively prevent EC maladaptation by masking the UHRF2 canonical BS and resulting in increased UHRF2 expression. This targeting pathway is conserved in mice and humans and attractive for further investigations *in vivo*. The downregulation of Mllt10 expression by let-7b reduces MEC proliferation similar to UHRF2, however, the conservation of this activity in HECs has to be studied further. The effects of let-7b on other EC properties that cause maladaptation may be mediated through non-conserved species-specific targets that are also valuable for further investigations.

List of figures

Fig. 1: Steps in plaque formation and progression. 14
Fig. 2: Histological properties of vessels. 15
Fig. 3: Effect of blood flow dynamics on localization of plaque formation in the aorta. 18
Fig. 4: Properties of maladapted ECs. 20
Fig. 5: Biogenesis of miRNAs. 22
Fig. 6: Canonical binding of miRNA to target RNAs in the RISC. 23
Fig. 7: Role of miRNAs in EC maladaptation. 25
Fig. 8: Sequence conservation of let-7 miRNA. 26
Fig. 9: pEZX-MT05 vector map. 43
Fig. 10: psiCHECK2 vector map. 45
Fig. 11: Maps of the hybridized oligonucleotides for psiCHECK2 insertion. 45
Fig. 12: Expression of let-7 family members in MECs and HECs. 52
Fig. 13: Expression of let-7 family members after let-7b mimic treatment. 53
Fig. 14: Protein-coding targets of let-7b in mouse and human ECs. 55
Fig. 15: Comparison of protein-coding let-7b targets between mouse and human ECs. 56
Fig. 16: Identification of lncRNA targets of let-7b in mouse and human ECs. 59
Fig. 17: Comparison of lncRNA targets of let-7b between mouse and human ECs. 60
Fig. 18: Comparison of mRNA and lncRNA let-7b targets between MECs and HECs. 64
Fig. 19: Similarity of mouse and human target fractions according to their BSs. 65
Fig. 20: Percentages of predicted canonical BSs in mouse and human protein-coding let-7b targets. 66
Fig. 21: Predicted canonical let-7b BSs in the 3'–UTRs of MLLT10 and UHRF2. 71
Fig. 22: Fractions of murine and human lncRNA targets according to their BSs. 75
Fig. 23: Percentages of predicted canonical BSs in mouse and human lncRNA targets. 76
Fig. 24: Canonical let-7b BS in mouse and human LINCPINT. 78
Fig. 25: Volcano plot presenting differentially regulated proteins after let-7b mimic treatment in ECs. 79
Fig. 26: Effect of let-7b inhibitor treatment on the expression levels of let-7 family members. 98
Fig. 27: UHRF2 protein quantification after let-7b inhibition in ECs. 99
Fig. 28: Relative gene expression of targets after let-7b inhibition. 100
Fig. 29: Luciferase activities of predicted target constructs. 102
Fig. 30: Effects of blocking let-7b/UHRF2 interaction on target regulation in MECs and HECs. 103
Fig. 31: Effects of blocking let-7b/MLLT10 interaction on target regulation in MECs and HECs. 104
Fig. 32: Effect of blocking let-7b/Lincpint interaction on target regulation in MECs. 105
Fig. 33: Role of let-7b in MEC wound healing. 106
Fig. 34: Role of let-7b in HECs on wound healing. 107
Fig. 35: Role of ox-LDL in EC wound healing. 108
Fig. 36: Effects of TSB treatment on MEC wound healing. 109
Fig. 37: Effects of TSB treatment on HECs wound healing. 110
Fig. 38: Role of let-7b in EC proliferation. 111
Fig. 39: Role of TSBs in EC proliferation. 112
Fig. 40: Apoptosis induction in MECs and HECs. 113
Fig. 41: Effects of let-7b on EC apoptosis. 114
Fig. 42: Effects of TSBs on EC apoptosis. 114
Fig. 43: DNA damage formation in MECs and HECs. 115

Fig. 44: Effect of let-7b on DNA damage formation in ECs. 116
Fig. 45: Effect of TSBs on DNA damage formation in ECs. 117
Fig. 46: Effect of let-7b on MN formation in ECs. 118
Fig. 47: Effect of let-7b on ROS production in MECs and HECs. 119
Fig. 48: Effect of TSBs on ROS production in MECs and HECs. 119
Fig. 49: Functional differences between let-7b inhibitors and TSBs 126
Fig. 50: Effects of let-7b inhibition on murine and human ECs. 133
Fig. 51: The effect of let-7b-mediated UHRF2 downregulation on mouse and human ECs 135

List of tables

Table. 1: let-7 family members in mouse and human. 27
Table. 2: List of general equipment. 30
Table. 3: List of consumables and solutions. 32
Table. 4: List of cell types used in this study. 33
Table. 5: List of kits used in this study. 34
Table. 6: Oligonucleotides used in this study and their sequences. 35
Table 7: Forward and reverse primer sequences used for gene expression studies. 36
Table 8: miRCURY LNA reverse transcription reaction setup per sample 40
Table 9: miRCURY LNA reverse transcription cycling protocol 40
Table 10: miRCURY Probe PCR reaction components 41
Table 11: Cycling conditions used for miRCURY Probe PCR assay 41
Table. 12: High-Capacity cDNA Reverse Transcription Kit components. 41
Table. 13: cDNA synthesis cycling conditions. 42
Table. 14: qRT-PCR reaction components. 42
Table. 15: Cycling conditions used for the qRT-PCR reaction. 42
Table. 16: Designed primer pair for mouse Mllt10 3'–UTR amplification. 43
Table. 17: Components and the volumes used for Mllt10 3'–UTR PCR amplification. 44
Table. 18: Cycling conditions used to amplify Mllt10 3'–UTR. 44
Table. 19: Oligonucleotide sequences designed for hybridization and cloning into the psiCHECK2 vector. 46
Table. 20: Designed primer pairs for site-directed mutagenesis PCR. 47
Table 21: Click-iT® reaction cocktail components. 48
Table. 22: The top ten highly expressed genes in MECs and HECs. 54
Table. 23: The biological processes regulated by the 153 common let-7b targets in mouse and human ECs. 57
Table. 24: The ten most highly expressed ncRNA genes in MECs and HECs. 58
Table. 25: Gene expression of the top ten highly enriched protein-coding let-7b targets. 61
Table. 26: The common biological processes regulated by the top 100 enriched genes in MECs and HECs. 62
Table. 27: Gene expression of the top ten highly enriched lncRNA let-7b targets. 63
Table. 28: Let-7b targets with identical conserved canonical BS. 67
Table. 29: Sum of mean enrichment and P-values in MECs and HECs of the 23 let-7b targets with identical BSs. 70
Table. 30: Mouse lncRNA let-7b targets with predicted canonical BSs. 72
Table. 31: Human lncRNA Let-7b targets with predicted canonical BSs. 73
Table. 32: Mouse lncRNA let-7b targets with conserved genomic loci. 76
Table. 33: Biological processes regulated by the differentially regulated proteins in MECs. 80
Table 34: Proteins related to the biological pathways regulated by let-7b in MECs. 80
Table. 35: Biological processes related to the proteins differentially regulated by let-7b mimics in HECs. 81
Table 36: Described functions of proteins related to the biological pathways regulated by let-7b in HECs. 82
Table. 37: Downregulated proteins after let-7b mimic treatment in MECs. 84
Table. 38: Downregulated proteins after let-7b mimic treatment in HECs. 88

Table 39: Effect of let-7b mimic treatment on the protein expression of the 23 targets identical in MECs and HECs. 91
Table. 40: Upregulated proteins after let-7b mimic treatment in MECs. 92
Table. 41: Upregulated proteins after let-7b mimic treatment in HECs. 94
Table. 42: Regulation of endothelial differentiation markers and inflammatory genes by let-7b in ECs. 97

List of abbreviations

Ago2	Argonaut 2
Ago2-IP	Ago2-immunoprecipitate
BS	Binding site
CDC25a	Cell Division Cycle 25A
CDK6	Cyclin Dependent Kinase 6
cDNA	complementary DNA
cGMP	cyclic guanosine monophosphate
cGTP	cyclic guanosine triphosphate
CLIP	Cross-linking immunoprecipitation
CuSO4	Copper(II) sulfate
DAPI	4', 6-diamidino-2-phenylindole
DGCR8	DiGeorge syndrome critical region 8
DMEM	Dulbecco's Modified Eagle Medium
DMSO	Dimethyl sulfoxide
DSB	double-strand break
ECM	extracellular matrix
ECs	Primary aortic Endothelial Cells
EDTA	Ethylenediminetetraacetic acid Disodium salt Dihydrate
eNOS	endothelial nitric oxide synthase
ER	endoplasmic reticulum
FBS	Fetal Bovine Serum
FC	Fold change
GAPDH	Glyceraldehyde 3-phosphate dehydrogenase
h-	human
HECs	Human Primary aortic Endothelial Cells
hnRNP	Heterogeneous nuclear ribonucleoproteins
ICAM1	Intercellular adhesion molecule 1
IEJs	interendothelial junctions
KLF-2/4	Krüppel like factor-2 and 4
LDL	Low density lipoprotein
LC-MS/MS	Liquid chromatography-tandem mass spectrometry
LNA	Locked nucleic acid
lncRNA	Long non-coding RNA
m-	mouse
MCP-1	monocyte chemotactic protein-1
MECs	Mouse Primary aortic Endothelial Cells
miRNA	MicroRNA
MLLT10	Histone Lysine Methyltransferase DOT1L Cofactor

MN	micronuclei
ncRNA	Non-coding RNA
NO	Nitric Oxide
ox-LDL	Oxidized LDL
PBS	Phosphate buffered saline
P_{CT}	Probability of conserved targeting
PDGFs	platelet-derived growth factors
PECAM-1	platelet-endothelial-cell adhesion molecule 1
PFA	Paraformaldehyde
pH	Potential of hydrogen
PKG	protein kinase G
pre-miRNA	Precursor miRNA
pri-miRNA	Primary miRNA
RISC	RNA induced silencing complex
ROS	induces reactive oxygen species
RT	reverse transcription
SMCs	smooth muscle cells
TM	thrombomodulin
TUT	terminal uridylyl transferase
UHRF2	Ubiquitin Like With PHD And Ring Finger Domains 2
UPR	unfolded protein response
VCAM1	vascular cell adhesion molecule 1
VE cadherin	vascular endothelial cadherin
vWF	von Willibrand Factor
WPBs	weibel-Palade bodies

1 Introduction

Cardiovascular disease remains the highest mortality rate in Europe, comprising 45% of all deaths (1). Atherosclerosis is the leading cause of cardiovascular disease. It is characterized by the formation of atheromatous plaques in arteries, leading to narrowing of the vessel lumen and occasionally thrombosis due to unstable plaque rupture (2). The main risk factor for this chronic inflammatory disease is the high cholesterol-containing low-density lipoprotein (LDL) levels in the bloodstream. High blood pressure and high glucose levels have an accompanying role in this regard (3, 4).

1.1. Atherosclerosis

Vertebrates have evolved a network of vessels carrying oxygen and nutrient-rich blood to all body parts. This circulatory system is lined by a thin layer of endothelial cells (ECs) that maintain blood fluidity (5). Atherosclerotic lesion formation starts when the ECs lining the innermost layer of arteries at bifurcation sites cannot adapt to the blood flow properties (Fig. 1A) (6). ECs in these regions display a low level of chronic inflammation, which is present in healthy individuals, mice, and other mammals (7). The injured endothelium in these arterial regions allows the entry of blood LDL particles to the intimal region. These lipoproteins contain cholesterol and are chemically modified in the sub-endothelial region, imitating damage-associated molecular patterns (DAMPS) and pathogen-associated molecular patterns (PAMPS), thus further activating an inflammatory response. Inflammatory-activated ECs express adhesion molecules that attract monocytes in the blood flow. The monocytes attach and enter the intima, differentiating from tissue macrophages (Fig. 1B). These macrophages engulf the modified lipids and subsequently perform reverse cholesterol transport. Due to excess lipid uptake, these macrophages turn into foam cells that cannot handle the extra load of lipids. Therefore they undergo apoptosis (Fig. 1C). Phagocytes engulf the apoptotic lipid-containing macrophages, a process termed efferocytosis. Likewise, lipid-loaded macrophages known as efferocytes cannot handle the lipid load and thus undergo secondary necrosis. These events lead to the accumulation of lipids and apoptotic cell debris in the intimal plaques and produce a thrombogenic necrotic core in advanced plaques (3, 4, 8).

The plaques can remain asymptomatic and at the same time cause stenosis of the vessels. Lesions can be either stable, imposing less threat to the individual, or unstable, meaning they are more prone to rupture and erosion. The extent of collagen and smooth muscle cells (SMCs) covering the necrotic core defines the stability of the plaque. In unstable advanced plaques, the thrombogenic material is released after rupture and activates blood coagulation. This event leads to thrombosis and, depending on the location of an artery, causes myocardial infarction, stroke, and tissue damage (9) (Fig. 1D).

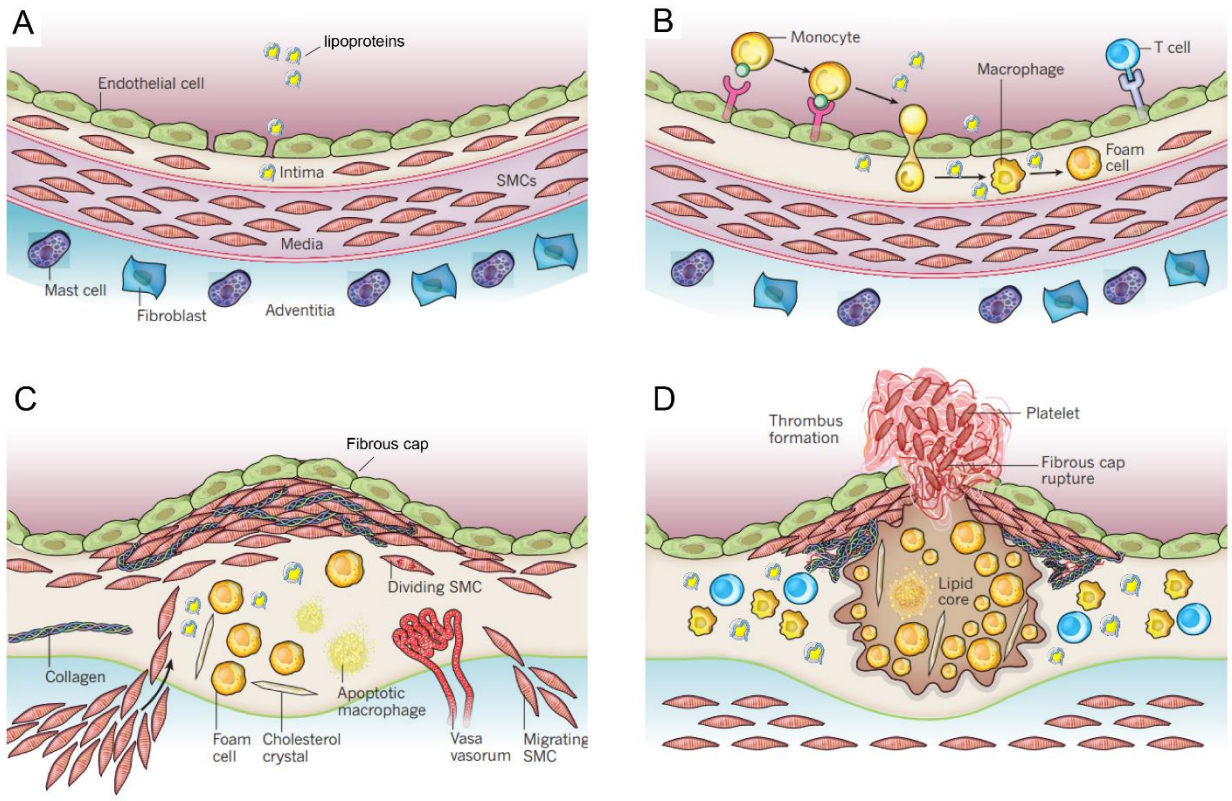

Fig. 1: Steps in plaque formation and progression.

The inflammatory-activated ECs located at branching points of arteries lose cell-to-cell contacts and allow the entry of lipoproteins to the intimal layer. (B) The activated ECs express adhesion molecules on the cell surface that mediates monocyte attraction and their access to the intima, where they develop into tissue macrophages. Macrophages initiate endocytosis of modified LDL particles and turn into lipid-loaded foam cells (C). Macrophages further phagocytose apoptotic foam cells, a process termed efferocytosis. Apoptosis of the efferocytes and the further accumulation of lipids result in the build-up of a thrombogenic necrotic core, which is covered by a fibrous cap. (D) In unstable advanced lesions, the fibrous cap is ruptured or eroded, exposing the thrombogenic material to the blood and initiating thrombus formation (modified from (3)).

1.2. Endothelial cells

ECs are flat and long with dimensions of 20-40 µm length, 10-15 µm width, and 0.1-0.5 µm height (10). The vasculature is branched throughout the body, providing an approximate endothelium surface of 3000-6000 m^2, allowing efficient nutrient and gas exchange. As a result of this extensive branching, the ECs located at different parts of the endothelium, i.e., arteries, arterioles, capillaries, venules, and veins, have distinct properties (11).

Vessels generally consist of three histologically distinct layers termed “tunic,” meaning “membrane.” The innermost layer is termed “tunica intima.” This layer consists of a single layer of ECs adherent to a basement membrane (Fig. 2). Below this layer is a network of the internal elastic membrane and connective tissue that support EC adhesion. Perivascular cells or pericytes are located in this layer and surround the ECs to provide a balanced cellular microenvironment. The pericytes are mesenchymal stem cells that can differentiate into

many cell types, including fibroblasts, connective tissue cells, and SMCs (12). The ECs secrete various proteins that make up the extracellular matrix (ECM). The ECM consists of collagen IV, fibronectin, entactin, laminin, chondroitin sulfate, heparin sulfate, and matricellular proteins (13). The ECM and the ECs comprise the tunica intima (10).

The tunica media consists of SMCs and elastin fibers. These layers are highly organized in large arteries due to their role in regulating the movement of large blood volumes. Below this layer is another network of elastic lamina that provides structural support. After this layering, the "tunica adventitia" or "tunica externa," which is the outermost layer of vessels, is present. Tunica externa mainly comprises fibro-elastic connective tissue and nerve endings (Fig. 2) (12).

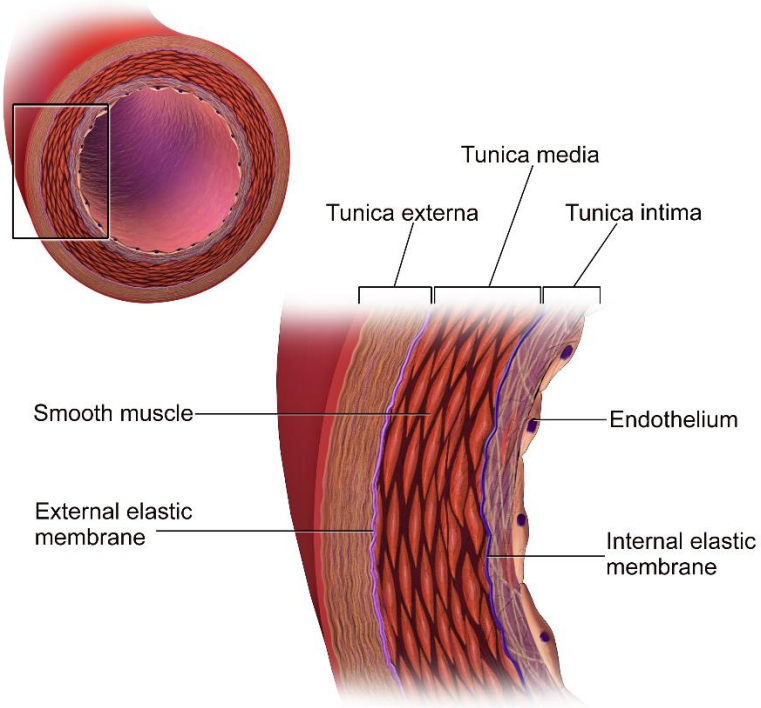

Fig. 2: Histological properties of vessels.

Vessels are composed of three distinct histological layers: the tunica intima, tunica media, and tunica externa (or tunica adventitia). The innermost layer or tunica intima comprises ECs and the ECM. The tunica media contains SMCs and elastic fibers. The outermost layer, the tunica externa, is composed of fibro-elastic tissue. Between these layers, an elastic lamina provides structural support (14).

1.3. Properties of ECs

The endothelium, previously thought to be only a barrier, is now regarded as an organ due to its various properties (10). ECs have multiple roles that are effected by their membrane receptors and the cell-cell or cell-ECM interactions (15).

1.3.1 Barrier and transport

The endothelium maintains a semi-permeable barrier to control the transport of fluid and macromolecules between the blood and the interstitial space (16). Endothelial transport can be via paracellular or transcellular pathways. The paracellular route is through the inter-endothelial junctions (IEJs) and is mainly regulated by the balance among cellular adhesive and counter adhesive forces. Urea, glucose, and water are among the molecules that are transported via this route (16). Macromolecules use the transcellular pathway that guides the active form of transport. Vesicular carriers called "caveolae" function through this route and transverse through the cytoplasm to reach the basolateral side of the cell, where they exocytose their contents (16). The organization of IEJ could be disrupted by activating inflammatory mediators like thrombin and histamine or mechanical factors such as disturbance in shear stress (reviewed in section 1.2.2).

1.3.2 Hemostasis and thrombus prevention

The endothelium can provide an antithrombotic vascular lumen for blood fluidity and prevent thrombosis via different mechanisms. Maintaining blood fluidity and preventing thrombus formation is done by controlling the expression of cell surface receptors of pro-coagulant and anti-coagulant factors. The expression of tissue factor pathway inhibitors is one of the essential anti-coagulant mechanisms in ECs that block the coagulation onset. The expression of heparin sulfate proteoglycans that inactivate thrombin and the expression of thrombomodulin from ECs are other mechanisms blocking coagulation initiation (17). The protein C/protein S pathway is active in quiescent ECs and inactivates several components of the coagulation cascade (15).

1.3.3 Vasoregulation

ECs cooperate with smooth muscle cells to control local vasoregulation of arteries and blood tension. ECs produce nitric oxide (NO) from the oxidation of arginine in response to chemical and physical stimuli. The NO can activate guanylate cyclase in SMCs and turn cGTP into cGMP. Thus, the cGMP-dependant protein kinase G (PKG) becomes active and causes SMC relaxation and vasodilation (13). Prostaglandin I_2 (also known as prostacyclin) is a lipid molecule released from ECs and causes SMC relaxation and vasodilation. Endothelin, thromboxane A2, angiotensin II, and superoxide are among the vasoconstrictors released by ECs (15).

1.3.4 Leukocyte recruitment

ECs control immune cell infiltration as one of their main tasks. Adhesion of platelets and rolling of leukocytes are the initial steps in recruiting immune cells to the site of infection or inflammation (15). Quiescent ECs do not interact with leukocytes since they do not express adhesion molecules such as E-selectin, vascular cell adhesion molecule 1 (VCAM1), and Intercellular adhesion molecule 1 (ICAM1). ECs at rest sequester leukocyte interacting proteins such as p-selectins and chemokines within the Weibel-Palade bodies (WPBs) (17). Leukocyte recruitment is initiated by factors released from the endothelium, like von Willibrand Factor (vWF) from the WPBs and p-selectins (15).

1.4. Effects of blood flow dynamics on ECs

Blood flow mechanics determine the functional fate of ECs, meaning that the hemodynamic forces induced on the endothelium modulate gene expression and cell signaling pathways that result in changes in the EC properties (18). The ECs that encounter high laminar shear stress in non-branched arterial regions have a different gene expression signature from the ECs located at branching sites of the vasculature that experience turbulent blood flow. This is partly due to the EC mechanic sensors like primary cilia, ion channels, tyrosine kinase receptors, platelet-endothelial-cell adhesion molecule 1 (PECAM 1), and vascular endothelial (VE)-cadherin that convey the physical stimulus into biochemical signals (7).

Flow mechanics regulates the expression of endothelial Krüppel-like factor-2 and 4 (KLF-2/4) transcription factors in ECs lining the arteries. KLF-2/4 expression regulates 15% of flow-regulated genes, resulting in a quiescent EC phenotype defined by low permeability, low inflammatory activation, and low thrombogenicity (19, 20). Increased expression of KLF-2/4 in the endothelium, induced by laminar blood flow, upregulates endothelial nitric oxide synthase (eNOS) and thrombomodulin (TM) expression in ECs and provides an anti-thrombotic endothelial phenotype at non-branching sites (21, 22). Moreover, NF-E2-related factor 2 (Nrf2) is activated by laminar flow through Extracellular signal-regulated kinase 5 (ERK5), contributing to anti-inflammatory and anti-apoptotic mechanisms in ECs (23). Laminar flow inhibits activation of ER stress and apoptosis of ECs through the PI3K/Akt signaling pathway (24). In areas with the disturbed flow, atherogenic genes like monocyte chemotactic protein-1 (MCP-1) and platelet-derived growth factors (PDGFs), as well as inflammatory genes in ECs, are activated, resulting in monocyte infiltration to the arterial wall, high proliferation rate of ECs, and increase of their turnover (3, 8, 18).

Due to the different responses of ECs to the flow dynamics, atherosclerotic lesion formation throughout the vasculature is non-randomly localized at bifurcation regions and regions with the disturbed flow, i.e., carotid bifurcations, aortic arch, and branch points of coronary, infra-renal, and femoral arteries (Fig. 3) (18).

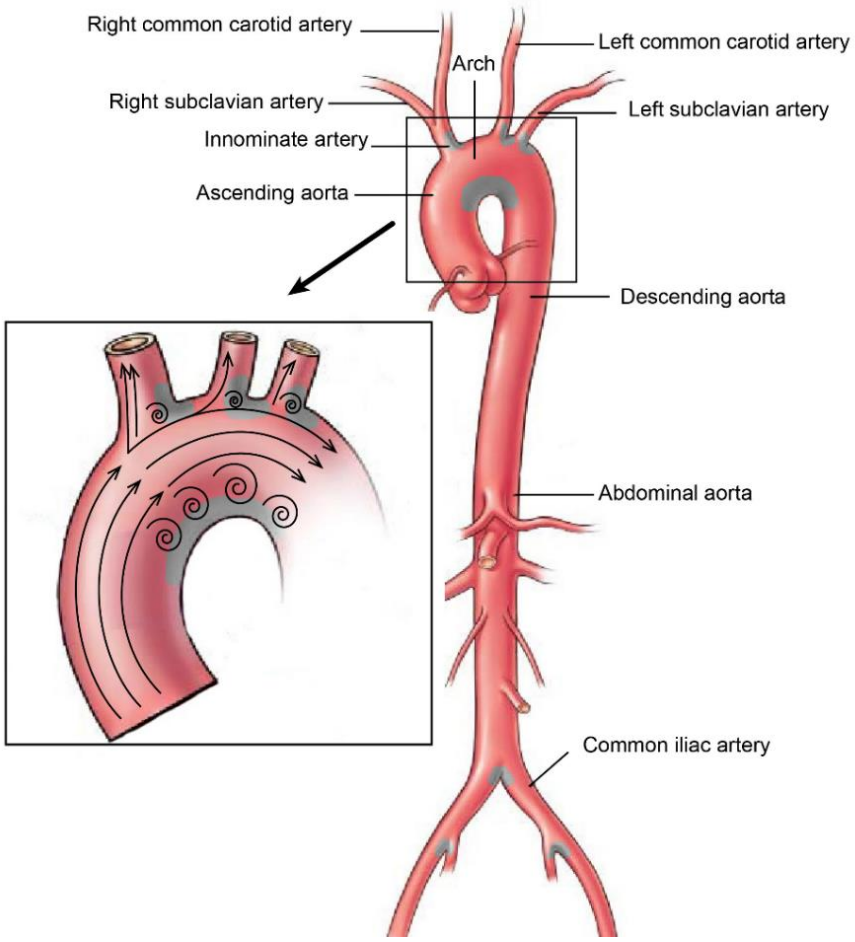

Fig. 3: Effect of blood flow dynamics on localization of plaque formation in the aorta.

The vasculature is branched throughout the body to ensure oxygenated, nutrient-rich blood reaches all tissues and organs. The branched nature of arteries induces changes in blood flow dynamics from regions encountering high laminar shear stress versus parts in arteries that experience turbulent blood flow. Blood flow turbulence defines the properties of ECs located at branching sites in the arteries, and atherosclerotic plaque formation initiation is mainly found in these sites (presented in gray). Black lines and arrows show blood flow dynamics. Image modified from (25).

1.5. Endothelial maladaptation

Endothelial dysfunction is the underlying cause of site-specific plaque localization in the circulation. Endothelial dysfunction is characterized as the modulation of EC phenotype so that they no longer are adapted to the extracellular environment (7). Blood-flow dynamics in different parts of the vasculature define the EC functional outcome. A healthy state of ECs is generally defined as tightly linked quiescent cells that are elongated in the flow direction and have a low cell turnover. The ECs that are naturally found in straight arterial regions and encounter a stable uni-directional blood flow are perfectly adaptable to the stable, extracellular environment. The adapted ECs rarely become apoptotic, and proliferation in these cells is rare (26).

The direction of the flow in branching points of arteries is random. The unpredictable multi-directional blood flow builds an unstable extracellular environment for ECs in these regions. Adaptation of ECs to this unstable environment is impossible. The flow initiates a heterogeneous stress response in these maladapted ECs (6) (Fig. 4). Disturbed flow initiates the endoplasmic reticulum (ER) stress response as well as the unfolded protein response in ECs, leading to their apoptosis (24). Apoptotic ECs are replaced by the proliferating and the migrating ECs located at the injury site to repair the generated damage (6). Cell death and the change in EC shapes, i.e., non-elongated and round, increase permeability of the endothelium to plasma macromolecules such as LDL (16). Dietary LDL can cross the endothelial barrier and reside in the tunica intima, where they are oxidized by the ECs (27). Oxidized LDL (ox-LDL) is toxic and induces further inflammation, apoptosis, and necrosis of the ECs and the subsequent increase in their turnover (28). Ox-LDL induces reactive oxygen species (ROS) production in ECs (29, 30) and increases DNA double-strand break (DSB)s (31). EC mitotic divisions without DSB repair are highly toxic for the cells. Unrepaired DSBs lead to incorrect chromosome segregation during mitosis and micronuclei (MN) formation, resulting in genomic instability. MN comprises a broken chromatin section from DSB enclosed by the nuclear membrane (32). The aberrant proliferation and MN formation in ECs exacerbates chronic endothelial wound healing in ECs. Collectively, these events cause endothelial maladaptation.

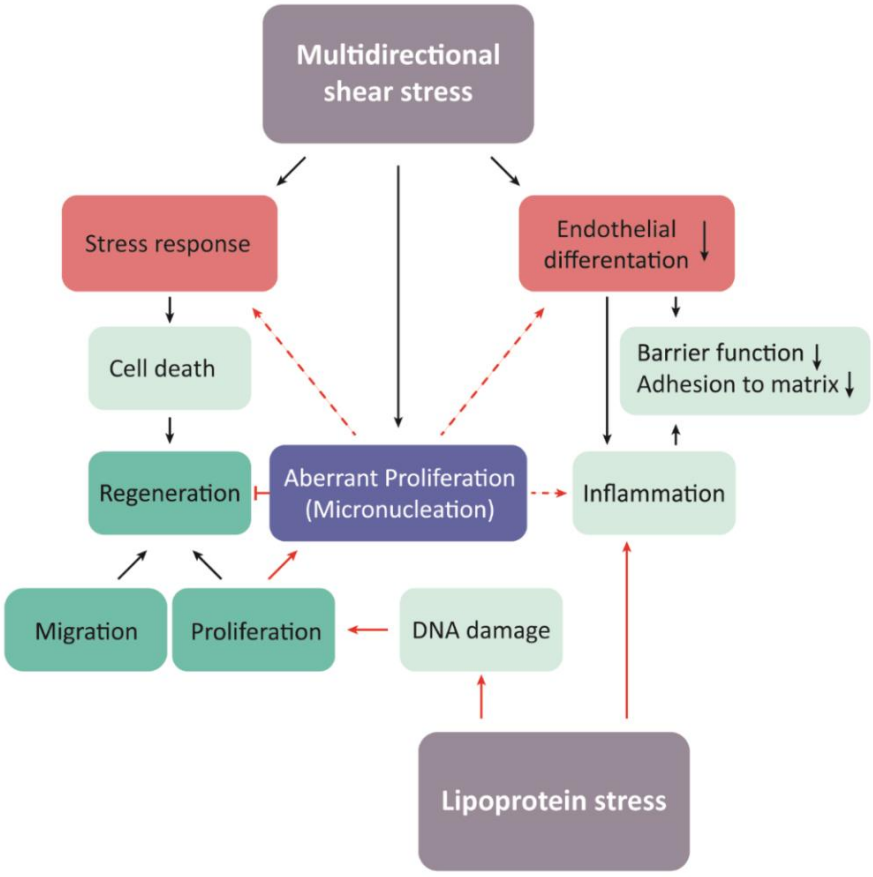

Fig. 4: Properties of maladapted ECs.

Adaptation of ECs to the blood flow at arterial branching points is impossible due to the multidirectional shear stress. Thus, these ECs are less differentiated, and a stress response leads to their activation. Proliferating and migrating cells partly compensate for cell death; however, the presence of external stimuli such as lipoprotein stress induces inflammation and DNA damage in ECs. DNA damage in proliferating ECs increases the risk of aberrant proliferation and further apoptosis (image acquired from (6)).

1.6. MicroRNAs

Only less than 2% of the genome codes for proteins and most of the remaining fraction, which was once identified as junk DNA is now known to be transcribed and functional. Non-coding (nc) RNAs are transcribed but not translated and mainly play a role in gene regulation. Regulatory non-coding RNAs are classified into microRNAs (miRNAs) and long non-coding RNAs (lncRNAs) (33).

miRNAs were discovered in the nematodes for the first time as short non-coding RNAs that regulate post-transcriptional gene expression (34). The development of evolutionary genetics, whole transcriptome sequencing techniques, and the available databases shed light on the presence of conserved miRNAs and their location in the genome (35). The short, ~21 nucleotide long miRNAs regulate protein-coding genes by binding to their 3´–UTRs in the

RNA-induced silencing complex (RISC). The degree of regulation by miRNAs is mainly mild, and the target repression by miRNAs is either through down-regulation of mRNA levels or translational repression of the target (36, 37). miRNAs regulate many genes related to EC inflammation and atherosclerosis development. These ncRNAs can even be considered diagnostic markers for determining the severity of atherosclerosis (38). Several miRNAs are flow-sensitive and regulate critical pathways in endothelial proliferation, apoptosis, and inflammation (39).

1.6.1 miRNA biogenesis and function

The biogenesis of miRNAs starts with the transcription of the hairpin structured primary (pri-) miRNA by mainly RNA polymerase II. The next step is processing pri-miRNA in the nucleus by microprocessor Drosha-DGCR8, an RNAse III endonuclease. DGCR8 (DiGeorge syndrome critical region 8) has two RNA binding domains that help identify the substrate and its correct positioning for cleavage. At the same time, Drosha cleaves the pri-miRNA from the 3' and 5' ends (40). This step leads to forming a 60-90 N hairpin RNA sequence called precursor (pre)-miRNA with a two-nucleotide overhang at the 3'-end. The pre-miRNA is transferred to the cytoplasm by Ran-GTP dependent exportin-5 (EXP5-Ran-GTP) and is further processed by the RNAse III endonuclease, Dicer-TRBP (Trans-activation response RNA-binding protein), resulting in the cleavage of the terminal hairpin loop and formation of a 21-22 nucleotide mature miRNA duplex (Fig. 5) (41, 42). The two strands enter the RISC with the help of Argonaut (Ago), and while one strand is degraded, the other strand, named the guide strand, forms a complex with Ago. The nucleotides 2 to 7 at the 5'- end of the guide strand comprise the seed sequence. MiRNA guide strand identifies the RNA target through complementary binding of the seed sequence to the target 3´–UTR or target transcript. Depending on the degree of complementarity, this process can result in translational inhibition of the target or degradation through GW182 proteins (42, 43).

miRNAs with identical seed sequences are usually grouped into miRNA families (44, 45). The miRNA genes from the same family can be located at different genomic locations (monocistronic genes) or be found as clusters in one single locus (polycistronic). miRNA genes are located in intergenic regions or exons and introns of other genes, and they can be transcribed either using their promoter or the promoter of the host gene (40).

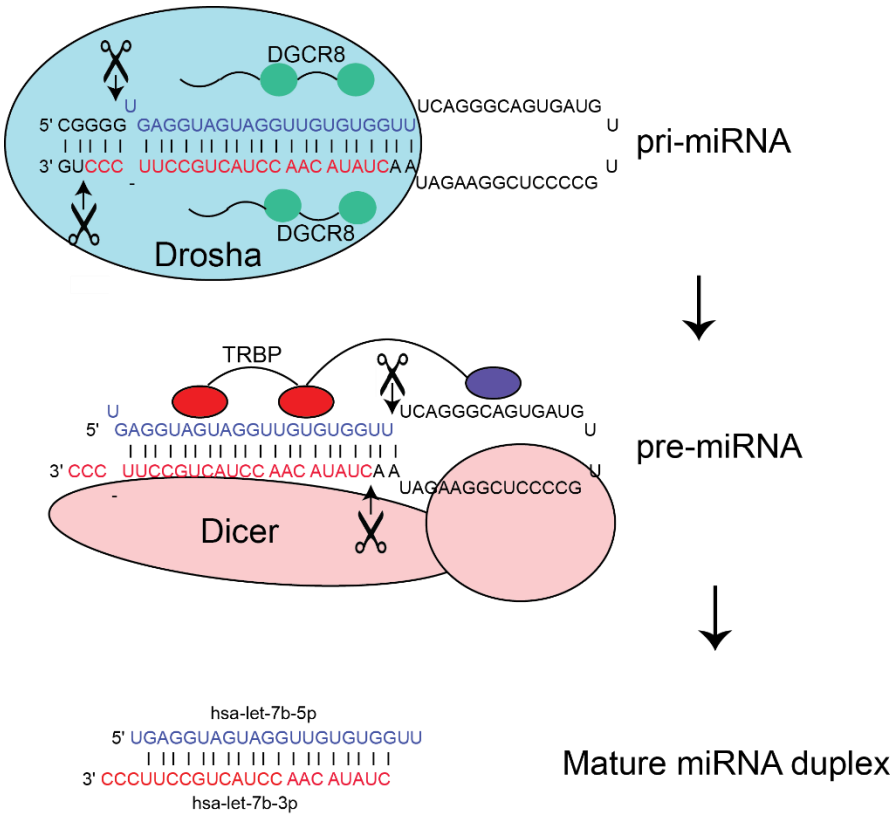

Fig. 5: Biogenesis of miRNAs.

The stem-loop structure of miRNAs contains the two 5p and 3p strands embedded in its stem sequence, presented in blue and red, respectively. Drosha and Dicer cleave the sites indicated by arrows to produce the pre-miRNA and mature miRNA duplex, respectively.

1.6.2 Canonical targeting of miRNAs

The 5‘-end sequence of miRNAs is usually more evolutionary conserved compared with the rest of the sequence. This is due to the miRNA seed sequence at nucleotide positions 2 to 7. The seed sequence is the essential component of every miRNA that is required for target recognition by the RISC. For mRNA targeting, Watson-crick base-pairing usually occurs between the 3’–UTR binding site and the miRNA seed sequence (46). The perfect base-pairing of miRNA with its target site is rare in animals but is usual in plants leading to the endo-nucleolytic degradation of the target by Ago. In animals, the base-pairing is partial, leading to RNA target translation repression or RNA destabilization (47, 48). miRNA recognition is not limited to mRNAs' 3’–UTR sequence. The open reading frame (ORF) and 5’–UTR of an mRNA can also contain functional miRNA recognition sites, although to a less extent (46).

The recognition of RNA targets by miRNA in the RISC is carried out step by step. First, the Ago2 exposes the nucleotides 2-5 of the miRNA for pairing with the target. Then, a conformational change occurs that exposes the nucleotides 2 to 8 and 13 to 16 of the miRNA,

allowing the additional recognition of the target. Interestingly, an adenosine nucleotide at the position opposite to the first miRNA nucleotide facilitates the target recognition (49).

miRNAs base-pairing to the target occurs through diverse binding sites (BSs). If nucleotides 2-7 of the miRNA pair with the target RNA, the BS is called a 6mer BS. There are three well-known canonical BSs that extend this six nucleotide base-pairing. The canonical BSs, in order of their binding efficiency, are the 8mer, the 7mer-m8, and the 7mer-A1 site. If in a 6mer site, adenosine is also present opposite to the 1st nucleotide of the miRNA, this BS is called a 7mer-A1 site. If there is an additional base pairing with the 8th nucleotide of the miRNA instead, this BS is a 7mer-m8 site. Finally, if both features exist (an adenosine opposite to the 1st nucleotide and a base-pairing with the 8th nucleotide of the miRNA), the BS is an 8mer site (Fig. 6) (46).

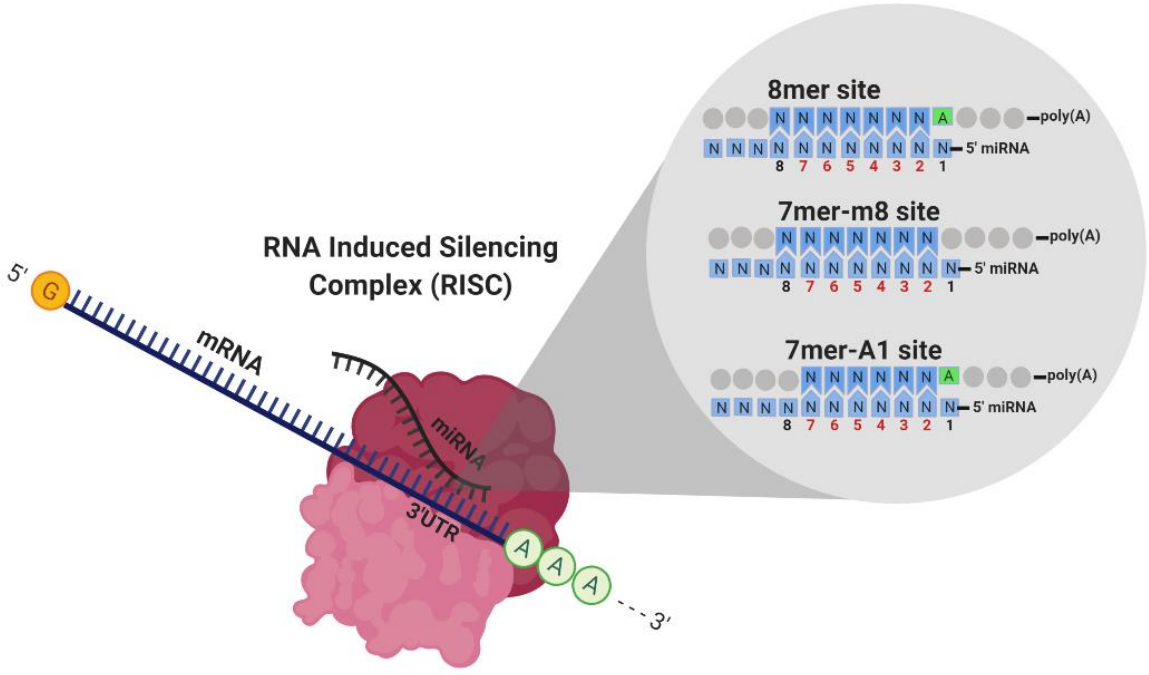

Fig. 6: Canonical binding of miRNA to target RNAs in the RISC.

The seed sequence of the miRNA (nucleotides 2-7) is the main feature of canonical binding to the target. The three canonical BSs in order of efficiency are the 8mer, the 7mer-m8, and the 7mer-A1 sites. A represents adenosine, and N represents any nucleotide.

Apart from the canonical BSs, other functional BSs exist but are not frequent. Non-canonical sites include marginal sites (6mer and the offset 6mer sites) and atypical sites (3' supplementary site and 3' compensatory sites) (46). Apart from these binding sites, G:U wobble base pairing and base pairing with bulges in the sequence are also non-canonical BSs that can be functional (48). miRNA family members with the same seed sequence differ in the nucleotides outside the seed. These members are often called sister miRNAs. The sister miRNAs can have specific base-pairing outside the seed on the 3'-end. Due to this, the

members of the same miRNA family can have different targets, which can explain the specificity of targeting for members of the same seed family (48). The presence of more than one BS for a miRNA in the target sequence leads to a cooperation of the two sites and can enhance the targeting outcome of the miRNA (46).

1.6.3 Role of ncRNAs in endothelial maladaptation

Endothelial microRNA (endo-miRNA) profiling has revealed different expression signatures in ECs according to the cell type, developmental stage, and environmental cues affecting the cells (50). The most abundant miRNA families expressed in ECs are the miR-126, miR-10, and the let-7 families (50).

MiR-126 partly regulates endothelial maladaptation to disturbed flow. The miR-126-3p reduces permeability and apoptosis of ECs, through direct inhibition of transforming growth factor beta (TGF-β) (51). Interestingly, in maladapted ECs that encounter disturbed laminar flow, the expression of the other miR-126 strand, miR-126-5p, is reduced. MiR-126-5p increases EC proliferative reserve at bifurcation sites by inhibiting delta-like 1 homolog (DLK1) and activation of Notch1, partly ameliorating EC adaptation (52).

Flow-sensitive miRNAs or mechano-miRs regulate several genes that play a role in endothelial maladaptation (39). Endothelial miR-92a regulates KLF2/4 expression, which results in EC heterogeneity in different flow regions (53). Moreover, ox-LDL mediated activation of ECs in low shear stress regions is regulated by miR-92a. Endothelial miR-92a targets the suppressor of cytokine signaling 5 (SOCS5) and KLF2/4, resulting in activation of the NFκB pathway (54). In atherosclerotic ECs, the hyperlipidemia-induced Hypoxia-inducible factor 1-alpha (HIF-1α) activation increases miR-19a expression, triggering NF-κB activation and CXCL1 expression, and CXCL1-dependent monocyte adhesion that are characteristics of EC maladaptation (55). Additionally, miR-19a post-transcriptionally targets cyclin D1, decreasing proliferation in human umbilical vein ECs (56) and further promoting EC maladaptation. miR-103-3p is generated by Dicer and is highly conserved in deuterostomes (57). This miRNA is highly expressed in ECs located at branching sites of arteries and is upregulated in ECs in the presence of ox-LDL and hyperlipidemia. MiR-103-3p contributes partly to the maladapted endothelial phenotype by targeting KLF-4 resulting in CXCL1-mediated monocyte adhesion promotion (58).

MiRNAs can also regulate endothelial dysfunction through complementary base pairing with long non-coding (lnc) RNAs (59, 60). lncRNAs are a group of regulatory non-coding (NC) RNAs with lengths of >200 nucleotides. lncRNAs serve as a scaffold for transcription factors and epigenetic regulators, are enhancers of gene regulation, and sequester miRNAs away, known as the sponging effect (61). Conversely, miRNAs can target lncRNAs in the RISC resulting in their downregulation. MiR-103-3p promotes EC maladaptation by suppressing the lncWDR59 lncRNA and promoting aberrant EC proliferation. LncWDR59 activates Notch1 and EC proliferation by competitively binding to Numb, which is the Notch1 inhibitor (60) (Fig. 7).

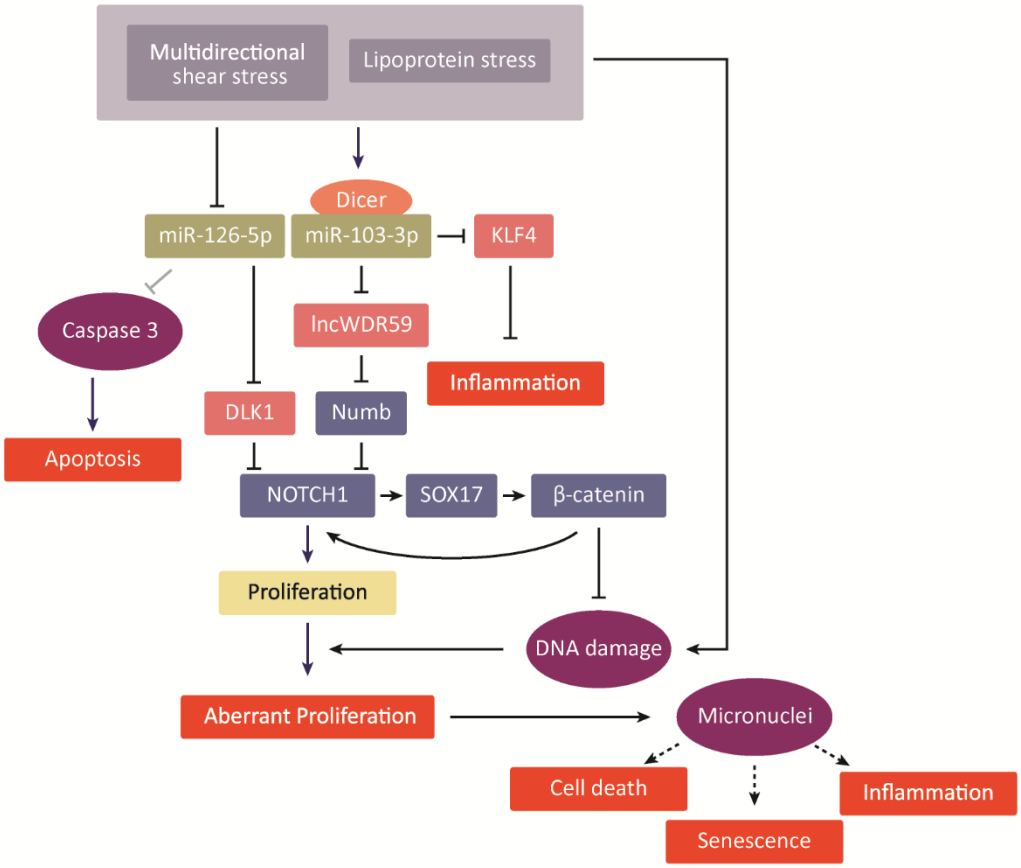

Fig. 7: Role of miRNAs in EC maladaptation.

MiR-126-5p decreases EC apoptosis and increases the proliferation of ECs through Notch1, ameliorating EC maladaptation. MiR-103-3p promotes EC maladaptation through KLF-4 mediated increase of inflammation. MiR-103-3p impairs wound healing by inhibiting proliferation and promoting DNA damage. Image from (6).

Apoe$^{-/-}$ mice with a deletion of *Dicer* in ECs develop less atherosclerosis than endothelial *Dicer*$^{+/+}$ mice after feeding an HFD (58). *Dicer*$^{-/-}$ in ECs results in down-regulation of a group of miRNAs, including miR-103 and the let-7 family members such as let-7b/i/d, suggesting that these miRNAs play a role in EC maladaptation (58). Target prediction analysis revealed that nearly half of downregulated miRNAs' targets are lncRNAs. Let-7b, highly expressed in ECs (62), was predicted to interact with a group of down-regulated mRNAs and many lncRNAs. This suggested that let-7b downregulates a group of mRNA and lncRNAs that play a crucial role in endothelial maladaptation (63). Thus, studying let-7b targets and their role can provide insights into the causes of EC maladaptation.

1.7. The let-7 family of miRNAs

Let-7 was one of the first miRNAs discovered and the first miRNA detected in humans. This miRNA was found in *Caenorhabditis elegans* (*C. elegans*) for the first time while searching for genes related to developmental timing. It was realized that the transition of larval stage 4 to the adult stage in this nematode is controlled by a short RNA that negatively regulates the *lin-41* gene expression. This regulatory RNA was complementary to the 3'–UTR of *lin-41,* and mutations of the RNA resulted in non-stop cell divisions that led to the burst of the vulva and were lethal at this stage. Based on the lethal phenotype observed, the gene was named *lethal-7* (*let-7*) (64). It was found later that the let-7 miRNA sequence is conserved in bilaterian animal species, including humans, but is not present in cnidarians, ctenophores, fungi, plants, or basal eukaryotes. Apart from the let-7 sequence conservation, its role in temporal development is also conserved (65). A conserved seed sequence for let-7 across vertebrates (Fig. 8A) suggests that let-7 targets are also most probably conserved. While the fruit fly, *Drosophila melanogaster* (*D. melanogaster*) has a single member of *let-7* (66), and four let-7 members are identified in *C. elegans* (*let-7*, *miR-84*, *miR-48*, and *miR-241*) (44), higher mammals have evolved into containing multiple family members. The let-7 miRNA family members are transcribed from different genomic loci on different chromosomes, and some of them are clustered in a region. In humans, ten let-7 family members are located in 12 distinct genomic loci and are distinguished by a letter. The let-7a, b, c, d, e, f, g, i, miR-98, and miR-202 are the members in humans. The mouse has 12 let-7 members, ten similar to humans, and two members (let-7j and let-7k) present only in the mouse (66). The let-7 members have the same seed sequence and differ only by a few point nucleotides in the 3'-end of the sequence (Fig. 8B) (45).

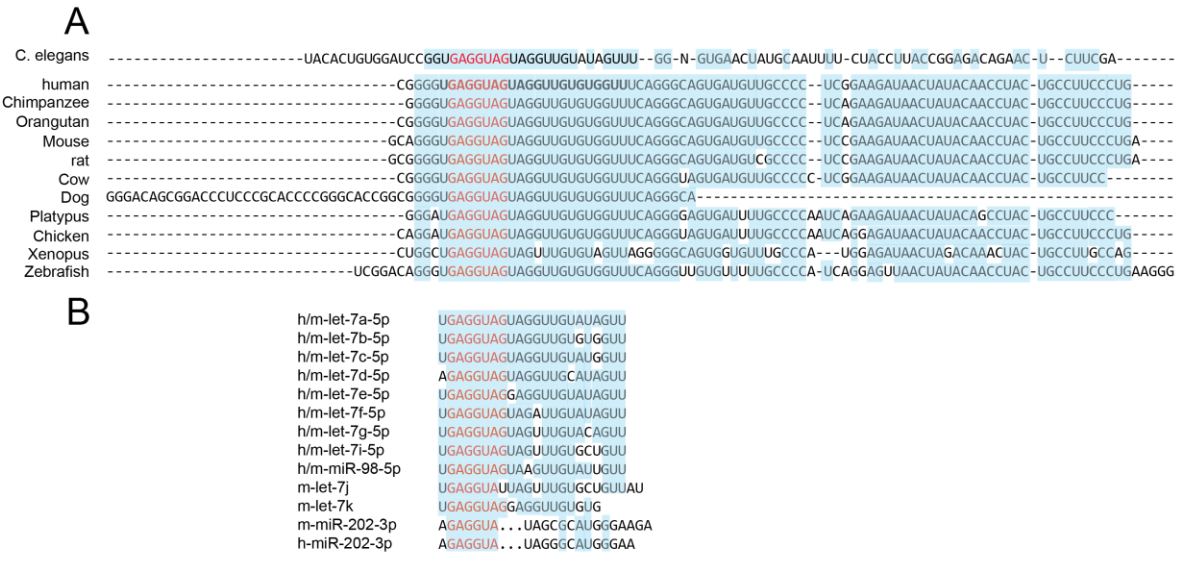

Fig. 8: Sequence conservation of let-7 miRNA.

(A) The C. elegans let-7 primary sequence compared to the let-7b primary sequence in various vertebrates. Blue shading indicates the conserved sequence, and red presents the seed sequence. (B) Conservation of mouse (m) and human (h) let-7 family members. The blue shaded region indicates the conserved region, and the seed sequence is red. Sequences were taken from miRBase.

On the one hand, having the same seed sequence in different family members suggests that let-7 members might target the same genes and thus have the same functions in the cell, making the let-7 resistant to genetic losses. On the other hand, the sequence difference in the 3'-end of these members suggests that each member might regulate specific genes leading to the control of different functions in the cell (6). Let-7b is transcribed from a mutual genomic region containing let-7c-2 in mice and a joint genomic region containing let-7a-3 in humans (Table. 1).

Table. 1: let-7 family members in mouse and human.

The miRBase ID for the guide sequence is presented. Mouse and human let-7 family member precursors are located as clusters with other miRNAs or as individual genes. The chromosomal location and the conserved genomic cluster are presented for comparison (n.a not applicable).

let-7 member	**Mouse/ Human miRBase ID**	**Mouse Gene**	**Human gene**
		(Chromosomal location: conserved genomic cluster)	
h/m-let-7a-5p	MIMAT0000521/ MIMAT0000062	*Mirlet7a1* (Chr13: let-7a-1, let-7f-1, let-7d)	*MIRLET7A-1* (Chr9: let-7a-1, let-7f-1, let-7d)
		Mirlet7a2 (Chr9: mir-100, let-7a-2)	*MIRLET7A-2* (Chr11: mir-100, mir-10526, let-7a-2)
		n.a	*MIRLET7A-3* (Chr22: let-7a-3, mir-4763, let-7b)
h/m-let-7b-5p	MIMAT0000522/ MIMAT0000063	*Mirlet7b* (Chr15: mmu-let-7c-2, mmu-let-7b)	*MIRLET7B* (Chr22: let-7a-3, mir-4763, let-7b)
h/m-let-7c-5p	MIMAT0000523/ MIMAT0000064	*Mirlet7c1* (Chr16 :mir-99a, let-7c-1)	*MIRLET7C* (Chr12: mir-99a, let-7c)
		Mirlet7c2 (Chr15: let-7c-2, let-7b)	n.a
h/m-let-7d-5p	MIMAT0000383/ MIMAT0000065	*Mirlet7d* (Chr13: let-7a-1, let-7f-1, let-7d)	*MIRLET7D* (Chr9: let-7a-1, let-7f-1, let-7d)
h/m-let-7e-5p	MIMAT0000524/ MIMAT0000066	*Mirlet7e* (Chr17: mir-99b, let-7e, mir-125a)	*MIRLET7E* (Chr19: mir-99b, let-7e, mir-125a)
h/m-let-7f-5p	MIMAT0000525/ MIMAT0000067	*Mirlet7f1* (Chr13: let-7a-1, let-7f-1, let-7d)	*MIRLET7F-1* (Chr9: let-7a-1, let-7f-1, let-7d)
		Mirlet7f2 (ChrX: let-7f-2, mir-98)	*MIRLET7F-2* (ChrX: let-7f-2, mir-98)
h/m-let-7g-5p	MIMAT0000121/	*Mirlet7g*	*MIRLET7G*

	MIMAT0000414	(Chr9)	(Chr3)
h/m-let-7i-5p	MIMAT0000122/ MIMAT0000415	*Mirlet7i* (Chr10)	*MIRLET7I* (Chr12)
h/m-miR-98-5p	MIMAT000054/ MIMAT0000096	*Mir98* (ChrX: let-7f-2, mir-98)	*MIR98* (ChrX: let-7f-2, mir-98)
m-let-7j	MIMAT0025123	*Mir7j* (Chr3)	n.a
m-let-7k	MIMAT0025580	*Mir7k* (Chr5)	n.a
m-miR-202-3p	MIMAT0000235	*Mir202* (Chr7: mir-202, mir-7686)	n.a
h-miR-202-3p	MIMAT0002811	n.a	*MIR202* (Chr10)

1.7.1 Let-7 biogenesis and regulation

The let-7 primary transcripts are transcribed by RNA polymerase II. They are 5'end-capped and 3'-end polyadenylated. The let-7 primary transcript in *C. elegans* undergoes an extra trans-splicing step by adding a "spliced leader sequence" to the 5'-end, common in nematodes (67). In human let-7 biogenesis, pre-let-7a-2, pre-let-7c, and pre-let-7e members follow the canonical miRNA biogenesis pathway and are called group I pre-miRNAs. The group I pre-miRNAs are canonically processed by Drosha and thus contain a two-nucleotide overhang at the 3'-end identified by Dicer. The other nine members, namely pre-let-7a-1, pre-let-7a-3, pre-let-7b, pre-let-7d, pre-let-7f-1, pre-let-7f-2, pre-let-7g, pre-let-7i, and pre-miR-98, are referred to as group II pre-miRNAs and contain a bulged adenine or uridine at the processing site that Drosha cannot identify, thus the processing of the group II pre-miRNAs results in a single nucleotide overhang at the 3'-end. To enable identification of the pre-miRNA by Dicer in these members, terminal uridylyl transferases (TUTs) mono-uridylate the 3'-end of these pre-miRNAs, thus producing a two-nucleotide overhang at the 3'-end that Dicer can identify for further processing. This process confers an extra regulatory step during the let-7 miRNAs' biogenesis (68). MYC, targeted by let-7a (69), regulates let-7 transcription in human cancer by binding to the promoter of the let-7a-1/let-7f-1/let-7d cluster and inhibiting its transcription (70), therefore, creating a regulatory feedback loop.

Post-transcriptional regulation of let-7 is performed through Lin28A and Lin28B RNA binding proteins. Lin28A/B, bind the pri-let-7 in the nucleus to prevent Drosha activity. Interestingly, Lin28A binds to pre-let-7 in the cytoplasm and blocks Dicer identification and processing (71). Overexpression of Lin28A in HEK293 cells results in the poly-uridylation of the pre-let-7 by TUTs. Lin28 recruits TUT4 to pre-let-7 sequences by recognizing a four nucleotide sequence (GGAG) (72). Addition of a 10 to 14 nucleotide long uridine chain by Lin28 limits the identification of the pre-miRNA by Dicer and its cleavage. Instead, the RNase II/R 3'-5'exonuclease named Dis3l2 (DIS3-like exonuclease 2) identifies and degrades the poly-uridylated pre-miRNA (71, 73). hnRNP A1 is a nucleo-cytoplasmic protein involved in splicing and protein shuttling. In the absence of Lin28, hnRNP A1 blocks

the processing of pre-let-7a by Drosha through binding to the conserved terminal loop sequence of pre-let-7a (74). These processes inhibit the maturation of the pre-let-7.

KH-type splicing regulatory protein (KSRP), an mRNA decay regulator, is required for miRNA maturation regulation. KSRP promotes the maturation of a group of miRNAs, including let-7-a, -b, -c, -d, -f, and -i, by high-affinity binding to G-rich sequences in their terminal loop (75). hnRNP A1 and KSRP are competitors for binding to the conserved terminal loop sequence of pre-let-7a. Therefore, hnRNP A1 antagonizes KSRP activity (74).

1.7.2 Biological roles of let-7 family members

The initial studies on let-7 clarified that this miRNA is required to properly develop the *C. elegans* from the larval stage 4 to the adult stage. In *D. melanogaster*, developmental entry to the adult stage and adequate neuromuscular maturation requires let-7 expression (65). Moreover, let-7 expression levels are high during embryogenesis and neural development in mammals (65). In a study by Johnson *et al.*, the 3'–UTR sequences of *C.elegans* were computationally screened to find let-7 complementary sites. Let-60, the Rat sarcoma (Ras) oncogene ortholog, was the top candidate containing let-7 sites. The regulation of let-60 by let-7 and miR-84 in *C. elegans* suggests that the same gene can be targeted by different let-7 family members (76).

Studies in humans have revealed that let-7 activity has anti-oncogenic properties, and nowadays, it is a well-known tumor suppressor (77). Studies in human lung cancer showed that let-7 directly regulates *RAS* oncogene (76) and inhibits the development of non-small cell lung cancer. Let-7g expression in murine lung cancer cells induces cell cycle arrest and cell death by down-regulation of *RAS* oncogene (78). These studies suggest that let-7 targets ortholog genes, i.e., common genes in different species, resulting in the same functional outcome.

Let-7 limits cell growth and proliferation by directly targeting the 3'–UTR of *CDC25a*, *CDK6*, and *CYCLIN D* cell cycle progression genes, limiting the G1 to S transition (79). Let-7 directly regulates the high-mobility group AT-hook 2 (*Hmga2*) gene, inhibiting cell growth and mammosphere formation in mouse breast cancer (80, 81). Studies have shown that the expression of the two genomic clusters (*let-7a-2-miR-100-miR-125b-1* and *let-7c-miR-99a-miR-125b-2*) is required for hematopoietic stem cell proliferation and differentiation (82). Let-7 members could be functionally redundant, and the exact role of let-7 in mammals has not yet been defined due to the technical difficulty of knocking out all let-7 members at the same time (66).

1.7.3 Roles of let-7b in ECs

Let-7 is a highly expressed miRNA in cardiovascular tissue, e.g., ECs, SMCs, and cardiomyocytes (83). Let-7 expression varies significantly among diverse EC types (84). Let-7b is highly expressed in human aortic ECs (HECs), human pulmonary and dermal microvascular ECs (HMVECs), and human pulmonary artery ECs (HPAECs). However, it

is low expressed in human umbilical vein ECs (HUVECs) and the brain microvasculature, suggesting that the differences among the various ECs are partly due to let-7b expression (84).

Studies have suggested that endothelial let-7b increases angiogenesis. Inhibition of angiogenesis in the corpus luteum of *Dicer1* knockout mice is partly rescued by let-7b and miR-17-5p expression (85). Moreover, Let-7 members appear to be essential mediators of Inflammation in ECs. Let-7b, let-7a, and let-7g target the lectin-like low-density lipoprotein receptor-1 (LOX-1), a receptor for oxidized LDL (ox-LDL) in ECs, and thus decrease ox-LDL mediated inflammatory response of ECs (62, 63).

Although studies show an athero-protective role of endothelial let-7 (62, 63, 86), the precise mechanism and functions of the let-7b during atherosclerosis progression in ECs have not yet been defined.

1.8. Hypothesis and aims

In this study, the hypothesis that let-7b regulates endothelial maladaptation by targeting a group of conserved mRNAs and lncRNAs in ECs was tested. To investigate this hypothesis, the following aims were addressed:

I. To identify the targeting network of let-7b in human and mouse ECs.

II. To identify the conserved mRNA and lncRNA targets of let-7b in ECs in humans and mice because evolutionarily conserved targets are more functionally relevant and translatable in the clinic.

III. To discover the functional outcome of let-7b-mediated target inhibition in mouse and human ECs that result in EC maladaptation.

2. Materials and methods

2.1. Equipment

Table. 2: List of general equipment.

Equipment	Company
Precisa 92SM-202A analytical balance	Sartorius Mechatronics, Göttingen, Germany
Heraeus Pico 17 centrifuge	ThermoFisher Scientific, Waltham, MA, USA
Heraeus Megafuge 1.0R centrifuge	ThermoFisher Scientific, Waltham, MA, USA
Heraeus Varifuge 3.0 R centrifuge	ThermoFisher Scientific, Waltham, MA, USA
Eppendorf 5430R centrifuge	Eppendorf AG, Hamburg, Germany
Eppendorf 5420 centrifuge	Eppendorf AG, Hamburg, Germany
Eppendorf 5425R centrifuge	Eppendorf AG, Hamburg, Germany
Panasonic MDF-C2156VAN-PE ultra-low temperature freezer (-150 °C)	Panasonic, Osaka, Japan
NewBrunswick Premium U570 comfort (-80 °C)	Eppendorf AG, Hamburg, Germany
DM6000B microscope	Leica Microsystem, Wetzlar, Germany
Olympus IX50	Olympus optical Co., Tokyo, Japan
Zeiss 47 30 11-9901	Carl Zeiss, Oberkochen, Germany
DMi8 invert thunder microscope	Leica Microsystem, Wetzlar, Germany
Leica Application Suite (LAS) X version 3.6.0.20104 imaging software	Leica Microsystem, Wetzlar, Germany
Master Cycler Nexus PCR thermal cycler	Eppendorf AG, Hamburg, Germany
Master cycler Gradient 22331	Eppendorf AG, Hamburg, Germany
2720 Thermal cycler	Applied Biosystems, Darmstadt, Germany
7900HT Fast Real-Time PCR System	Applied Biosystems, Darmstadt, Germany
QuantStudio 6 Pro Real-Time PCR System	Applied Biosystems, Darmstadt, Germany
Intas UV trans illumination AF100 312nm/16x20cm gel documentation	INTAS Science Imaging Instruments GmbH, Göttingen, Germany
HERA Cell VIOS 250i CO2 Incubator	ThermoFisher Scientific, Waltham, MA, USA
HERA Cell VIOS 160i CO2 Incubator	ThermoFisher Scientific, Waltham, MA, USA
Maxisafe 2020 biological Safety Cabinet	ThermoFisher Scientific, Waltham, MA, USA
HERA safe biological Safety Cabinet	ThermoFisher Scientific, Waltham, MA, USA
BD FACS Canto II flow cytometer	Becton, Dickinson and Company, NJ, USA
Infinite F200 PRO	Tecan Trading AG, Männedorf, Switzerland
WTW Labour-pH-Meters pH 526	Xylem Analytics Germany Sales GmbH & Co. KG, Weilheim, Germany
MR 2002 magnetic stirrer	Heidolph, Schwabach, Germany
Implen NP80-Touch Spectrophotometer	Implen, Munich, Germany
Thermostat Plus and Thermomixer comfort thermoblocks	Eppendorf AG, Hamburg, Germany
Vortex-Genie 2 vortex mixer	Scientific Industries, Inc., Bohemia, NY,USA
Systec VX-95 Autoclave	Systec GmbH, Wettenberg, Germany

Memmert U40 oven	Memmert GmbH + Co. KG, Schwabach, Germany
Memmert WB14 water bath	Memmert GmbH + Co. KG
CytoSMART Omni live cell imaging system	CytoSMART Technologies, The Netherlands
Power Pac Basic Power supply	Bio-Rad, California, USA
Consort EV243 Power Supply	Sigma Aldrich, Germany
Heraeus B15 Incubator	ThermoFisher Scientific, Waltham, MA, USA
AF 100 ice machine	Scotsman, USA
Milli-Q water purification system	Merck, Darmstadt, Germany
TRANSSONIC 310 sonicator	Elma, Singen, Germany

2.2. Consumables and solutions

Milli-Q water generated from the Milli-Q water purification system (Merck, Darmstadt, Germany) was used to prepare all solutions.

Table. 3: List of consumables and solutions.

Reagent	Company
DMSO	Carl Roth, Karlsruhe, Germany
Lipofectamin 2000	Thermo Fisher Scientific Inc., Waltham, MA, USA
Lipofectamin RNAiMax	Thermo Fisher Scientific Inc., Waltham, MA, USA
Antifade Mounting Medium with DAPI	Vector laboratories, INC., Burlingame, CA, USA
PFA	Carl Roth, Karlsruhe, Germany
PBS solution (for cell culture, pH: 7.4)	Thermo Fisher Scientific Inc., Waltham, MA, USA
RNaseZap® decontamination solution	Thermo Fisher Scientific Inc., Waltham, MA, USA
Triton X-100	Sigma-Aldrich, Germany
Tween® 20	Sigma-Aldrich, Germany
NotI HF	New England Biolabs (NEB), Ipswich, MA, USA
XhoI	New England Biolabs (NEB), Ipswich, MA, USA
CutSmart buffer	New England Biolabs (NEB), Ipswich, MA, USA
T4 DNA Ligase	New England Biolabs (NEB), Ipswich, MA, USA
Phusion High-Fidelity DNA Polymerase	Thermo Fisher scientific
Agarose	Biozym Scientific GmbH, Hessisch Oldendorf, Germany
Endothelial Cell Growth Medium (Ready-to-use)	PromoCell, Germany
Gentamicin (0.05 mg/ml)	Thermo Fisher Scientific Inc., Waltham, MA, USA
DMEM high glucose, pyruvate	Gibco, Germany
FBS	Sigma-Aldrich, Germany
0.2% Gelatin	ScienCell, USA
0.01% Collagen, Type I solution from rat tail	Sigma-Aldrich, Germany
Accutase solution	Sigma-Aldrich, Germany
LDL from human plasma	Sigma-Aldrich, Germany
CuSO4 (5 µM)	Sigma-Aldrich, Germany
EDTA (10 µM)	Sigma-Aldrich, Germany

2.3. Cells

Table. 4: List of cell types used in this study.

Cell type	**organism**	**company**
Primary Mouse Aortic Endothelial Cells (MECs)	mouse	PELOBiotech, Germany
Primary Human Aortic Endothelial Cells (HECs)	human	PromoCell, Germany
Human Embryonic Kidney Cells (HEK 293)	human	Sigma Aldrich, Germany

2.4. Kits

Table. 5: List of kits used in this study.

Kit	Company
NucleoSpin miRNA extraction	Machery Nagel, Germany
High-Capacity cDNA Reverse Transcription	Applied Biosystems, Germany
GoTaq qPCR Master Mix (SybrGreen)	Promega, USA
miRCURY LNA RT Kit	Qiagen, Germany
miRCURY Probe PCR Kit	Qiagen, Germany
hsa/mmu-U6 snRNA miRCURY LNA miRNA Probe PCR Assay	Qiagen, Germany
hsa/mmu -let-7a-5p miRCURY LNA miRNA Probe PCR Assay	Qiagen, Germany
hsa/mmu -let-7b-5p miRCURY LNA miRNA Probe PCR Assay	Qiagen, Germany
hsa/mmu -let-7c-5p miRCURY LNA miRNA Probe PCR Assay	Qiagen, Germany
hsa/mmu -let-7d-5p miRCURY LNA miRNA Probe PCR Assay	Qiagen, Germany
hsa/mmu -let-7e-5p miRCURY LNA miRNA Probe PCR Assay	Qiagen, Germany
hsa/mmu -let-7g-5p miRCURY LNA miRNA Probe PCR Assay	Qiagen, Germany
hsa/mmu -let-7i-5p miRCURY LNA miRNA Probe PCR Assay	Qiagen, Germany
hsa/mmu -let-7b-3p miRCURY LNA miRNA Probe PCR Assay	Qiagen, Germany
Qiaquick gel extraction kit	Qiagen, Germany
Secrete-Pair™ Dual Luminescence Assay	GeneCopoeia, USA
Dual-Glo Luciferase Assay System	Promega, USA
Human E3 ubiquitin-protein ligase (UHRF2) ELISA Kit	MyBioSource, USA
Mouse E3 ubiquitin-protein ligase (UHRF2) ELISA Kit	MyBioSource, USA
Click-iT® EdU Alexa Fluor® 488 Imaging Kit	Invitrogen, USA
DCFDA / H2DCFDA Cellular ROS Assay Kit	Abcam, Germany
CellEvent™ Caspase-3/7 Green Detection Reagent	Invitrogen, USA
iST Sample Preparation kit	PREOMICS, Germany

2.5. Oligonucleotides

Table. 6: Oligonucleotides used in this study and their sequences.

Oligonucleotide	Symbol	Sequence
hsa (mmu)-let-7b-5p miRCURY LNA miRNA Power Inhibitor	let-7b inhibitor	ACCACACAACCTACTACCCTC
miRCURY LNA miRNA Inhibitor Control	control inhibitor	TAACACGTCTATACGCCCA
hsa (mmu)-let-7b-5p miRCURY LNA miRNA Mimic	let7b mimic	UGAGGUAGUAGGUUGUGUGGUU
miRCURY LNA miRNA Mimic negative control	control mimic	UCACCGGGUGUAAAUCAGCUUG
hsa (mmu)-UHRF2/let-7b-miRCURY LNA miRNA Power TSB	UHRF2-TSB	CTGAGGTAGTTGCAAA
mmu-Mllt10/let-7b miRCURY LNA miRNA Power TSB	Mllt10-TSB	GTGAGGTAAGAGGTGT
hsa-MLLT10/let-7b miRCURY LNA miRNA Power TSB	MLLT10-TSB	TGAGGTAAGAACTGTG
mmu-Lincpint/let-7b miRCURY LNA miRNA Power TSB	Lincpint-TSB	GTGAGGTATGAAGCCA
miRCURY LNA miRNA Power TSB negative control	control-TSB	ACGTCTATACGCCCA

2.6. Primers

Table 7: Forward and reverse primer sequences used for gene expression studies.

Primer	Forward Sequence	Reverse sequence
m-Uhrf2	CCTTCCTGTAAAACTGACTCC	GACCAACACAAGCCATTCC
h-UHRF2	CTCTACTTGACCTTTTCTTCCC	ACCATTTCTTCCACCCTCC
m-Mllt10	AGCCAGAGTGTTGTTGCTTACT	ATGGGGACACAGCTCACATC
h-MLLT10	ATGTTCAGGGGAATTTTAAAGTCAA	TGTTACAGAATAACAACCAGTGGG
m-Lincpint	GCCCGGTTCTGGTTGTTATT	ATCCTTTCCTGCAGTCACCA
h-LINCPINT	GGCTTGGCTAGTTGGAGAGTTAC	AACTGAAACCAGACCTAAGGTTTTG
m-B2m	TCGGTGACCCTGGTCTTTCT	TTTGAGGGGTTTTCTGGATAGCA
h-GAPDH	AGGGCTGCTTTTAACTCTGGT	CCCCACTTGATTTTGGAGGGA

2.7. Let-7b target identification in ECs

To identify targets of let-7b in aortic endothelial cells (ECs), Lucia Natarelli co-transfected primary mouse and human ECs (n=7 and 6, respectively) with let-7b mimic and the Mir Trap vector (87) for 24 h, followed by RNA isolation from the whole cell lysates and Ago2-immunoprecipitates (method explained in detail in (60)). After sequencing the RNA from the whole cell lysates and Ago2-immunoprecipitates by Dr. Jan Haas' group (Universitätsklinik Heidelberg, Internal Medicine III, Cardiology, Heidelberg, Germany) using the Illumina HiSeq2000 platform, the reads were mapped and annotated by Prof. Ralf Zimmer's group (Institute for Informatics, Ludwig-Maximilians University Munich, Germany).

This study obtained raw read counts of the total annotated genes from EC lysates and Ago2-immunoprecipitates. Protein-coding genes were annotated according to Ensembl 98, and the detected lncRNA genes were annotated according to the NONCODE v5.0 database. The annotated genes were only included in the analysis if detected in all sample replicates. Among the detected genes in EC lysates, the genes that were also detected in Ago2-immunoprecipitates in all sample replicates were defined as putative miRNA targets.

To identify the significantly enriched genes in the RISC compared to GAPDH, initially, the ratio of "gene count in immunoprecipitate" to "gene count in EC lysate" was calculated for all putative miRNA targets. Next, the percentage for each gene was log10 transformed and compared to that of GAPDH, using paired multiple comparisons with Dunnett test (88, 89). GAPDH gene was highly expressed in ECs but had a very low mean ratio. Thus, it was selected as the control gene for enrichment comparison. The significantly enriched genes with let-7b mimic treatment in ECs compared to GAPDH enrichment were identified as let-

7b targets. To investigate the functional enrichment of the genes g:GOSt functional profiling tool in the g:Profiler database (https://biit.cs.ut.ee/gprofiler_archive3/e98_eg45_p14/gost) was used (90).

2.8. Calculation of let-7b target enrichment

To obtain the enrichment values of let-7b targets in mouse and human ECs, the calculated ratio of "gene count in immunoprecipitate" to "gene count in EC lysate" for each gene in each replicate was divided by the corresponding ratio of GAPDH in that replicate. Next, the mean of the calculated ratios was determined and reported as the mean enrichment of each gene.

2.9. In silico analysis of let-7b target binding sites

To find the binding site (BS)s of the identified let-7b targets, all of the 3'–UTR sequences of protein-coding genes were extracted from Ensembl 98 database (https://www.ensembl.org/index.html) using BioMart (91). The ncRNA genes were annotated according to NONCODE. Therefore, the complete transcript sequences of all lncRNA genes were extracted from NONCODE v5.0 (http://www.noncode.org) (92). The let-7b guide strand sequence (h/m-let-7b-5p, MIMAT0000063) was taken from miRBase 22.1 (http://www.mirbase.org/) (93). Next, all the 3'–UTR transcript sequences of protein-coding genes and the full transcript sequences of lncRNA genes were screened for let-7b canonical BSs (8-mer, 7-mer m8, 7-mer A1) using the RNAhybrid target prediction tool (https://bibiserv.cebitec.uni-bielefeld.de/rnahybrid), selecting no G:U in seed, and helix constraint from 2-7, as the parameters (94).

The mRNA targets were examined against the broadly conserved microRNA family, let-7-5p/98-5p in mouse TargetScan 7.2 (http://www.targetscan.org/mmu_72/) and human TargetScan 7.2 (http://www.targetscan.org/vert_72/) databases (95) and the P_{CT} value for the BS in each mouse and human transcript was obtained to assess the BS conservation. P_{CT} value for each BS estimates the probability of its conservation due to miRNA targeting and is equal to (S/B-1)/(S/B), where S/B is the signal-to-background ratio for the BS at the phylogenic branch length (96). Next, the targets that contained a conserved BS were explored for experimentally supported interactions with let-7b in DIANA tools, TarBase v.8 (97) database (http://carolina.imis.athena-innovation.gr/diana_tools/web/index.php?r=tarbasev8%2Findex).

To find common lncRNA targets in mice and humans, all the mouse lncRNA transcripts that had a canonical BS were blasted against the mouse genome to identify the loci and the flanking genes of the lncRNA gene of interest. Next, the flanking gene loci were found in the human genome, and the loci were screened for the presence of a lncRNA gene that was included in the human let-7b targets with a canonical BS. This was done using the Ensembl 98 BLAST tool (https://www.ensembl.org/Multi/Tools/Blast) (91).

2.10. Cell culture

Primary human aortic endothelial cells (HECs) (Cat#: C-12271, PromoCell, Germany) and primary mouse aortic Endothelial Cells (MECs) (Cat#: PB-C57-6052, PELOBiotech, Germany) were cultured in Endothelial Cell Growth Medium (Ready-to-use) (Cat#: C-22010, PromoCell, Germany) containing gentamicin (0.05 mg/ml, ThermoFisher, USA) according to manufacturer's instructions. MECs and HECs were cultured in plates (Corning (Costar), USA) coated with 0.2% Gelatin (ScienCell, USA) and used up to passage 6.

Human embryonic kidney 293 (HEK 293) cells (Sigma, Germany) were cultured in complete Dulbecco's Modified Eagle Medium (DMEM) (Gibco, Germany) with 10% fetal bovine serum (FBS, Sigma-Aldrich, Germany) and 0.05 mg/ml gentamicin. The culture plates (Corning (Costar), USA) were coated with 0.01% collagen, type I solution from rat tail (Sigma-Aldrich, Germany).

Cells were grown in a humidified atmosphere at 37°C and 5% CO_2 (HERA Cell VIOS CO2 Incubator) and detached when confluent using accutase solution (Cat#: A6964, Sigma-Aldrich, Germany). Sterile 1×PBS solution (Thermo Fisher Scientific, USA) was used to wash the cells before detachment. Cells were seeded at a density of 2×10^5 cells/ml for experiments.

2.11. Transfection of oligonucleotides

Cells were transfected with 50 nM h/m-let-7b-5p miRCURY LNA miRNA mimics (let-7b mimic) or miRCURY LNA miRNA mimic negative control (control mimics) to overexpress let-7b *in vitro*. To inhibit let-7b, cells were transfected with 50 nM h/m-let-7b-5p miRCURY LNA miRNA power inhibitor (let-7b inhibitor) or miRCURY LNA miRNA inhibitor control (control inhibitor) (Qiagen, Germany) for 24 h.

To block the interaction between let-7b and the targets (UHRF2, MLLT10, and Lincpint) in ECs, short antisense LNA oligonucleotide target site blockers (TSBs) were designed to mask let-7b binding sites on these targets. Cells were transfected with 50 nM h/m-UHRF2/let-7b miRCURY LNA miRNA Power TSB (m/h-UHRF2-TSB), m-Mllt10/let-7b miRCURY LNA miRNA Power TSB (m-Mllt10-TSB), h-MLLT10/let-7b miRCURY LNA miRNA Power TSB (h-MLLT10-TSB) and m-Lincpint/let-7b miRCURY LNA miRNA Power TSB (m-Lincpint-TSB) or miRCURY LNA miRNA Power TSB negative control (control-TSB) (Qiagen Germany) for 24 h.

Transfection of oligonucleotides was carried out using Lipofectamine RNAiMax or Lipofectamine 2000 (Invitrogen, USA). Briefly, the oligonucleotides and transfection reagents were diluted in serum-free media. The oligonucleotides and lipofectamine solutions were then mixed and let stand at room temperature for 20 min to form the lipofectamine complexes. The complexes were then added to the cell cultures and incubated at 37°C for 24 h.

2.12. Liquid chromatography-tandem mass spectrometry (LC-MS/MS)

MECs and HECs were cultured in T25 flasks and treated with let-7b or control mimics for 24 h. Cells were then washed, pelleted, and frozen until further processing. Next, the frozen cell pellets were transferred to the ZfP facility of the LMU Biomedical center, and cell pellets were processed using the iST sample preparation kit as recommended by the manufacturer (PreOmics, Germany). Dr. Ignasi Forne (Zentrallabor für Proteinanalytik, LMU Biomedical centre) performed LC-MS/MS assessment and data analysis. Detailed LC-MS/MS conditions are described in Kaseder *et al*. (98). The detected proteins from let-7b mimic and control mimic treated samples were compared using Limma in ImShot_1.0.1. Significant proteins ($P<0.05$) in the treatment group compared to the control group were identified with a cut-off of FC>1.3.

2.13. Enzyme-linked immunosorbent assay (ELISA)

Mouse and human ECs were cultured in 6-well plates and transfected with let-7b inhibitor, control inhibitor, UHRF2-TSB, and control-TSB for 24h. Cells were harvested in M-PER™ Mammalian Protein Extraction Reagent (Thermo Scientific, USA) containing 1X Halt™ Protease Inhibitor Cocktail (Thermo Scientific, USA). Lysates were sonicated at 20 kHz (TRANSSONIC 310, Germany). UHRF2 protein was quantified in the homogenized lysates using a human E3 ubiquitin-protein ligase UHRF2 ELISA Kit (MyBioSource, USA) and a plate reader. UHRF2 protein concentrations were normalized to the total protein concentrations obtained from DC Protein Assay Kit (BioRad, Germany). Data were compared between the treatment and relevant control groups using an unpaired Student's t-Test.

2.14. RNA extraction

Small and large RNAs were isolated using the NucleoSpin miRNA (Machery Nagel, Germany) kit. Briefly, the cells were lysed with 300 µl buffer ML after washing twice with ice-cold 1X PBS. Lysates were homogenized after passing through the column provided, and 150 µl %70 ethanol was added to the lysates. The precipitated nucleic acids were added to a silica membrane column, and on-column DNAse treatment was done for 15 min. Protein from the flow-through was precipitated and removed via protein removal columns provided in the kit. The small RNA from the flow-through was added to the columns after DNAse digestion. The silica membrane was washed three times with the wash buffers provided in the kit. RNA was eluted using RNAse-free H2O, after drying the column completely. RNA was quantified and qualified for impurities (A260/A280=1.8-2.1 and A260/A230≥2) using a spectrophotometer (Implen NP80-Touch, Germany).

2.15. miRCURY LNA miRNA probe PCR assays

The miRCURY LNA miRNA probe assays combine universal reverse transcription with LNA-enhanced, miRNA-specific primers and probe. Compared with other miRNA assays, it can specifically discriminate between highly similar targets down to one nucleotide difference. First, 10 ng RNA (total volume = 2 µl) was converted to cDNA (Table 8) using the miRCURY LNA Reverse Transcription Kit (Qiagen, Germany).

Table 8: miRCURY LNA reverse transcription reaction setup per sample

Component	**Volume (10 µl)**
5x miRCURY RT Probe Reaction buffer	2 µl
RNase-free water	4.5 µl
10x miRCURY RT Enzyme Mix	1 µl
UniSp6 RNA spike-in	0.5 µl
Template RNA (5 ng/µl)	2 µl

In this universal reverse transcription step, a poly(A) tail is added to the miRNAs, which are not polyadenylated in nature, and the cDNA is synthesized using a poly(T) primer with a 3' degenerate anchor and a 5' universal tag. The 3'degenerate anchor allows amplification of the mature miRNA in the real-time PCR step. Polyadenylation and reverse transcription occur at 40°C (60 min) and are inactivated at 95°C (Table 9).

Table 9: miRCURY LNA reverse transcription cycling protocol

Step	**Temperature**	**Time**
Reverse Transcription	40 °C	60 min
Inactivation	95 °C	5 min
Storage	4 °C	∞

miRNA expression levels were quantified using the miRCURY Probe PCR Kit (Qiagen, Germany). 2 µl of diluted (1:40) cDNA was added to each PCR reaction. The PCR mix was prepared as in Table 10, and the cycling conditions are presented in Table 11.

Table 10: miRCURY Probe PCR reaction components

Component	Volume (per 10 µl reaction)
2x QuantiNova Probe Master Mix	5 µl
10x miRCURY Probe Universal Primer	1 µl
LNA PCR assay	1 µl
RNase-free water	1 µl
cDNA template	2 µl

Table 11: Cycling conditions used for miRCURY Probe PCR assay

Stage	Temperature	Time
Hold	95 °C	2 min
Cycle (40 Cycles)	95 °C	5 sec
	56 °C	30 sec

miRNA Probe PCR Assays were run on QuantStudio 6 Pro Real-Time PCR System (Applied Biosystems). Relative miRNA gene expressions were normalized to U6 snRNA for human and mouse EC samples. Normalized data were Log10 transformed (Design and analysis software 2.4.1, Applied Biosystems) and were compared between the control and the treatment groups using unpaired Student's t-Test.

2.16. cDNA synthesis

500 ng to 1 µg RNA (total volume =14.2 µl) was converted to DNA using the High-Capacity cDNA Reverse Transcription Kit (Applied Biosystems, Germany). The master mix was prepared according to table 12. 14.2 µl of RNA was added to a 5.8 µl master mix, and the sample was run with thermal cycling conditions in table 13.

Table. 12: High-Capacity cDNA Reverse Transcription Kit components.

Component	Volume (for one sample = 5.8 µl)
10✕ RT Buffer	2 µl
25✕ dNTP Mix (100 mM)	0.8 µl
10✕ RT Random Primers	2 µl
MultiScribe™ Reverse Transcriptase	1 µl

Table. 13: cDNA synthesis cycling conditions.

Stage	Temperature	Time
Hold	25 °C	10 min
Reverse transcription	37 °C	120 min
Hold	85 °C	5 min
Hold	4 °C	∞

2.17. Quantitative real-time PCR

mRNA expression levels were quantified using GoTaq qPCR Master Mix (SybrGreen) (Promega, USA). PCR mix was prepared (Table 14), and 300 ng (2 µl) cDNA was added to each PCR reaction. Cycling conditions used were according to Table 15.

Table. 14: qRT-PCR reaction components.

Component	Volume (per 20-µl reaction)
2xGoTaq qPCR Master Mix (incl.CXR dye)	10 µl
Primer F (10uM)	0.6 µl
Primer R (10uM)	0.6 µl
Nuclease-free water	6.8 µl

Table. 15: Cycling conditions used for the qRT-PCR reaction.

Stage	Temperature	Time
Hold	95 °C	5 min
Cycle (40 Cycles)	95 °C	15 sec
	60 °C	60 sec

Real-time PCR experiments were run on a 7900HT thermocycler (Applied Biosystems) or QuantStudio 6 Pro Real-Time PCR System (Applied Biosystems). Relative mRNA gene expressions were normalized to GAPDH for human EC samples or B2M for mouse EC samples. Normalized data were Log10 transformed (qbase software, Biogazelle or Design and analysis software 2.4.1, Applied Biosystems) and were compared between the control and the treatment groups using an unpaired Student's t-Test.

2.18. Reporter vector preparation

pEZX-MT05 vectors containing the full length of human UHRF2 3'–UTR (>82% sequence similarity with the mouse) or human MLLT10 3'–UTR, were custom-made by GeneCopoeia (USA). Fig. 9 depicts the pEZX-MT05 vector map and the miR target location, which was replaced by the UHRF2 3'–UTR or MLLT10 3'–UTR.

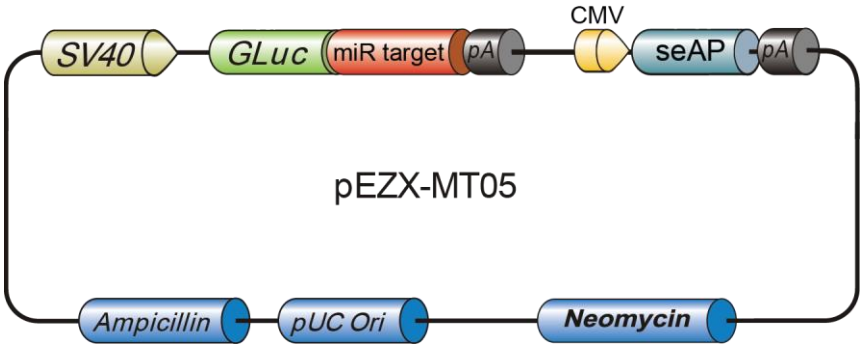

Fig. 9: pEZX-MT05 vector map.

The miR target is cloned in front of the Gaussia Luciferase (GLuc) gene. The Secreted Alkaline Phosphatase (seAP) gene is used as an internal control for transfection.

To prepare the mouse Mllt10 3'–UTR construct, initially, primers were designed in a way to introduce NotI and XhoI restriction sites, flanking the amplified fragment (Table 16). Next, the full length of mouse Mllt10 3'–UTR was amplified from 250 ng mouse endothelial cell cDNA, using Phusion High-Fidelity DNA Polymerase (ThermoFisher scientific) and the components mentioned in Table 17. Amplification was performed using the cycling conditions presented in Table 18.

Table. 16: Designed primer pair for mouse Mllt10 3'–UTR amplification.

Primer	Sequence
m-Mllt10-3UTR-F	CTCGAGAACCACCCACTGGAAC
m-Mllt10-3UTR-R	GCGGCCGCTAAACCACACTGATTC

Table. 17: Components and the volumes used for Mllt10 3'–UTR PCR amplification.

Component	Volume (per 50 µl reaction)
Phusion High-Fidelity DNA Polymerase (2,0 U/µl)	0.5 µl
5x Phusion GC buffer	10 µl
dNTP 100mM	1 µl
Primer F (10uM)	2.5 µl
Primer R (10uM)	2.5 µl
Nuclease-free water	27 µl
DMSO	1.5 µl

Table. 18: Cycling conditions used to amplify Mllt10 3'–UTR.

Stage	Temperature	Time
Hold	98 °C	10 min
Cycle (35 Cycles)	98 °C	30 sec
	57 °C	30 sec
	72 °C	150 sec

The amplified sequence was run on a 1% agarose gel to confirm the size. Subsequently, the fragment was extracted from the gel using the Qiaquick gel extraction kit (Qiagen, Germany). The purified fragment was treated with NotI and XhoI enzymes to produce sticky ends. Finally, the fragment was cloned into the psiCHECK2 vector (Promega, USA) at the NotI and XhoI sites (Fig. 10). The vector product was sequenced (Eurofins Genomics, Ebersberg, Germany) to ensure the sequence precision.

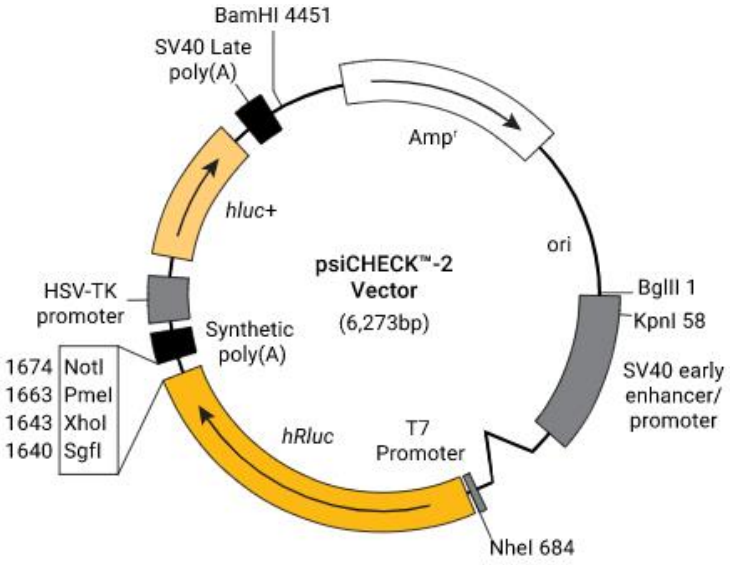

Fig. 10: psiCHECK2 vector map.

The miR target is cloned in front of the Renilla luciferase (hRluc) gene. The firefly luciferase (hluc+) gene is used as an internal control for transfection.

For m-Lincpint lncRNA, the predicted binding site with left and right flanking sequence (46 bp) was ordered as complementary oligonucleotides (Eurofins, Germany). The oligonucleotides were mixed at a 1:1 ratio and hybridized by heating the solution at 95°C for 5 min and slowly cooling to room temperature (99, 100). The hybridized oligonucleotides containing sticky ends were then cloned in the psiCHECK2 vector (Promega, USA) at the NotI and XhoI sites (Fig. 11A and Table 19). To ensure the validity of this experiment, a vector containing four BSs of let-7 (101) was made using the same procedure. The hybridized oligonucleotides, in this case, were treated with NotI and XhoI enzymes to generate sticky ends (Fig. 11B). For preparing the mutated m-Lincpint-psiCHECK2 vector, the mutation (TACC > CCTA) was introduced into the oligonucleotides (Eurofins) (Table 19 and Fig. 11A). The four nucleotides were shuffled in the BS sequence to form the mutation without changing the nucleotide composition.

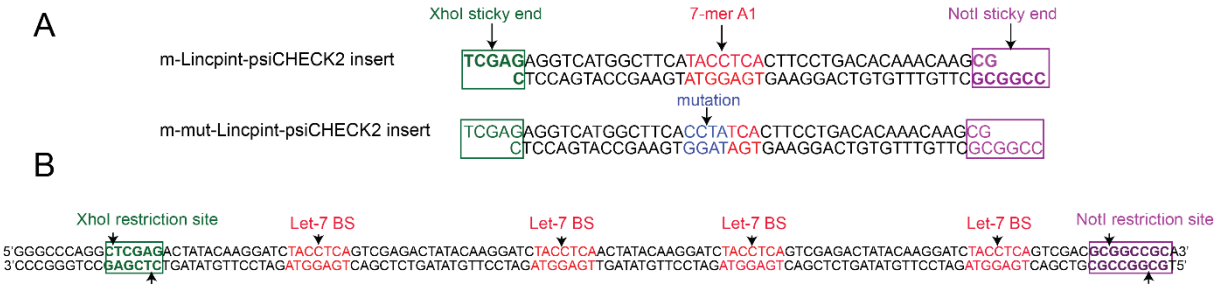

Fig. 11: Maps of the hybridized oligonucleotides for psiCHECK2 insertion.

(A) m-Lincpint sequence inserts with the predicted let-7b BS (red sequence) or the mutated let-7b BS (blue sequence), and the flanking XhoI and NotI sticky ends are represented with green and purple, respectively. (B) Hybridized oligonucleotides contain XhoI and NotI enzyme restriction sites represented with green and purple, respectively, flanking x4 let-7 BSs (red sequence).

Table. 19: Oligonucleotide sequences designed for hybridization and cloning into the psiCHECK2 vector.

Vector	Complementary oligonucleotides
m-Lincpint-psiCHECK2	5‘[PHO]TCGAGAGGTCATGGCTTCATACCTCACTTCCTGACACAAACAAGCG
	5‘[PHO]CCGGCGCTTGTTTGTGTCAGGAAGTGAGGTATGAAGCCATGACCTC
m-mut-Lincpint-psiCHECK2	5‘[PHO]TCGAGAGGTCATGGCTTCATACCTCACTTCCTGACACAAACAAGCG
	5‘[PHO]CCGGCGCTTGTTTGTGTCAGGAAGTGATAGGTGAAGCCATGACCTC
X4 Let-7 BS-psiCHECK2	5‘GGGCCCAGGCTCGAGACTATACAAGGATCTACCTCAGTCGAGACTATACAAG GATCTACCTCAACTATACAAGGATCTACCTCAGTCGAGACTATACAAGGATCT ACCTCAGTCGACGCGGCCGCA
	5‘TGCGGCCGCGTCGACTGAGGTAGATCCTTGTATAGTCTCGACTGAGGTAGATC CTTGTATAGTTGAGGTAGATCCTTGTATAGTCTCGACTGAGGTAGATCCTTGTA TAGTCTCGAGCCTGGGCCC

2.19. Site-directed mutagenesis

To introduce point mutations in the predicted BSs of UHRF2 and Mllt10 3’–UTRs, site-directed mutagenesis PCR was performed using h-UHRF2-3’–UTR-pEZX-MT05 and m-Mllt10-3’–UTR-psiCHECK2 vectors as templates and the designed primer pairs (Table 20). The PCR reaction components and conditions were the same as in Tables 17 and 18. To introduce point mutations in the predicted BSs of the MLLT10 3’–UTR, an h-MLLT10-pEZX-MT05 luciferase reporter vector with a custom point mutation (TAC > ACT) was purchased from GeneCopoeia. In all constructs, 3-4 nucleotides were shuffled in the BS sequence to generate the mutation without changing the nucleotide composition.

Table. 20: Designed primer pairs for site-directed mutagenesis PCR.

Template Vector	Primer pair	Mutation
h-UHRF2-3'–UTR-pEZX-MT05	F: TTTTGCAATCCACTCAGGACAGAAAAG	CTAC > TCCA
	R: CCTGAGTGGATTGCAAAATAAATCATAAC	
m-Mllt10-3'–UTR-psiCHECK2	F: CACCTCTACTCTCACTTCTGTAAATAAG	TAC > ACT
	R: AAGTGAGAGTAGAGGTGTGCAGTG	

2.20. Dual transfection of plasmids and oligonucleotides

Dual transfection of vectors with oligonucleotides was carried out using Lipofectamine 2000 (Invitrogen, USA). Briefly, 500 ng of the vectors and 50 nM of the oligonucleotides were diluted in the same serum-free media solution. Lipofectamine 2000 was diluted separately in serum-free media. The vector-oligonucleotide and lipofectamine solutions were mixed and incubated at room temperature for 20 min. The lipofectamine complexes were added to the cultured cell at 37°C for 48 h.

2.21. Luciferase reporter assay

HEK293 cells were cultured in 12-well-plates and co-transfected with 50 nM let-7b mimics or control mimics and 500 ng of pEZX-MT05 or psiCHECK2 luciferase reporter vectors containing the respective insert using Lipofectamine 2000. Bioluminescence activity was measured 48 h after co-transfection using Secrete-Pair™ Dual Luminescence Assay Kit (GeneCopoeia, USA) for the pEZX-MT05 vectors or Dual-Glo Luciferase Assay System (Promega, USA) for the psiCHECK2 vectors by a plate reader (Infinite F200 PRO, TECAN). Bioluminescence values from cells treated with let-7b mimics and control mimics were normalized to the mean values of control mimics-treated samples and expressed as percentages. Data were compared between the treatment and control groups using an unpaired Student's t-test.

2.22. Preparation of oxidized LDL

Low-density lipoproteins (LDL) from human plasma (10 mg, Merck, Germany) were dialyzed using D-Tube™ Dialyzer Midi tubes (MWCO 6-8 kDa, Merck, Germany) and treated with 5 µM $CuSO_4$ for up to 8 h at 37°C. Conjugated diene formation was monitored by measuring the UV absorbance at 234 nm every 30 min (Nanophotometer, Implen). The reaction was stopped when the absorbance reached a plateau by adding 10 µM EDTA. The oxLDL was purified with PD-10 desalting columns (Cytiva, Germany) and sterilized using a 0.22 µM filter. Sterile oxLDL was adjusted to a stock concentration of 1 mg/ml with 1×PBS and kept at 4°C in the dark until further use.

2.23. Preparation of 4% paraformaldehyde (PFA)

To prepare 4% PFA in 400 ml volume, 16 g of PFA was dissolved in 184 ml of 1×PBS by adding 5 ml of 10 M NaOH and heating to 60°C. After adjusting the pH to 7.4-8, 200 ml 1×PBS was added, and the solution was filtered through a filter paper.

2.24. Wound healing assay

MECs and HECs were plated in 96-well plates at 2×10^5 cells/ml density and transfected with let-7b inhibitor, TSBs, and controls the next day. After 24 h, a wound was mechanically made with a pipette tip in the middle of the confluent wells, the media was changed, and oxLDL (150 µg/ml) was added. The plate was subsequently placed on the CytoSMART Omni (CytoSMART Technologies, Netherlands) inside an incubator (37°C and 5% CO2). The entire plate was scanned every 2 h for 48 h, and images from each well were uploaded to the CytoSMART cloud. The wound area was automatically analyzed at each time point by the CytoSmart algorithm and reported as a percentage of the wound area at time point 0 h. Data were compared between the treatment groups and the relevant controls using multiple t-tests.

2.25. EdU labeling and proliferation assay

MECs and HECs were plated in 96-well plates at a density of 2×10^5 cells/ml and transfected the next day with let-7b inhibitor, TSBs, and controls for 24 h. Next, a wound was made mechanically in the middle of the confluent cells, and 20 µM EdU (5-ethynyl-2´-deoxyuridine) was added to each well. After 40 h, cells were fixed with 4% PFA for 15 min. Fixed cells were washed with 3% BSA in PBS and permeabilized with 0.5% Triton for 20 min. Click-iT® reaction cocktail was prepared according to Table 21 (Click-iT® EdU Alexa Fluor® 488 Imaging Kit, Invitrogen) and added to each well for 30 min. The injured area of each well was imaged using the DMi8 invert thunder microscope (Leica, Germany). The number of proliferating cells (EdU-positive cells) was counted in the injured area (same area for all samples) using Fiji (Image J). Proliferation was reported as the percent of EdU-positive cells. Data were compared between the treatment groups and the relevant controls using an unpaired t-test (2 groups) or one-way ANOVA (>2 groups).

Table 21: Click-iT® reaction cocktail components.

Reaction components	**Volume**
1×Click-iT® reaction buffer	430 µl
CuSO4	20 µl
Alexa Fluor® azide	1.2 µl
Reaction buffer additive	50 µl

2.26. Apoptosis assessment

MECs and HECs were cultured in black 96-well plates with a transparent bottom (Perkin Elmer, USA) at 2×10^5 cells/ml density. They were transfected the next day with let-7b inhibitor, control inhibitor, TSBs, and control TSBs for 21 h. Cells were then treated with 2 µM CellEvent™ Caspase-3/7 Green Detection Reagent (Invitrogen, USA), and the required wells were treated with 100 µg/ml oxLDL at the same time. Plates were kept at 37°C for 3 h, and the fluorescent intensity (Ex/Em = 502/530 nm) was measured using a plate reader (Infinite F200 PRO, TECAN). Human cells were treated with 10 µM staurosporine (a protein kinase inhibitor) as an apoptosis inducer and control positive treatment for this assay. Data were compared using multiple t-tests.

2.27. DNA damage assessment

MECs and HECs were cultured in 6-well plates and treated at 60% confluency with let-7b inhibitor, control inhibitor, TSBs, and control TSB for 24 h. Next, the wells were treated with 100 µg/ml oxLDL for 24 h. Cells were then detached using Accutase solution (Sigma Aldrich, Germany), fixed with 70% ethanol on ice, washed once with 1% BSA in PBS, and stained with 0.5 µg/ml APC-conjugated anti-H2A.X-Phosphorylated (Ser139) antibody (BioLegend, USA). Control positive cells were treated for 10 min with UV before staining. The negative control cells were stained similarly with 0.5 µg/ml APC Mouse IgG1, κ Isotype Ctrl (ICFC) antibody (BioLegend, USA). The stained cells' median fluorescent intensity (MFI) was obtained by a flow cytometer (BD FACS Canto II flow cytometer, Becton, Dickinson and Company, USA). Data were analyzed using Flowing Software 2.5.1 (Turku Bioscience Centre) and compared using multiple t-tests.

2.28. Micronuclei (MN) Formation evaluation

MECs and HECs were seeded in 4-well removable chamber slides (Nunc™ Lab-Tek™ Chamber Slide System, Thermo Scientific, Germany) and treated with let-7b inhibitor and control inhibitor for 24 h. Next, the cells were fixed with 2% PFA, and the chambers were removed. Cells were stained with 4′,6-diamidino-2-phenylindole (DAPI, VECTOR Labs, USA) and imaged using a DM6000B fluorescent microscope (Leica microsystem, Germany). The number of MN was counted manually and normalized to the number of cells (reported as MN%). Additionally, the percentage of cells containing an MN was reported. Data were compared between the let-7b inhibitor-treated and control groups using an unpaired Student’s t-test.

2.29. Reactive oxygen species (ROS) production assay

MECs and HECs were seeded in black 96-well plates with the transparent bottom (Perkin Elmer, USA) at a density of 2×10^5 cells/ml and transfected with let-7b inhibitor, control inhibitor, TSBs, and control TSBs for 21 h. The media of the wells was replaced with phenol

red-free media containing 25 µM DCFDA dye (DCFDA / H2DCFDA Cellular ROS Assay Kit, Abcam, Germany). The required wells were treated with 100 µg/ml oxLDL simultaneously, and the cells were incubated at 37°C for 3 h. Next, the fluorescent intensity (FI, Ex/Em = 485/535 nm) was measured by a plate reader (Infinite F200 PRO, TECAN). Tert-butyl hydrogen peroxide (TBHP, 500µM) was used as a positive control according to the kit instructions. Data were compared using one-way ANOVA.

2.30. Statistical analysis

Prism versions 7 and 8 (GraphPad) were used to analyze the data statistically. Shapiro-Wilk test ($n<5$) and Kolmogorov-Smirnov test ($n>5$) were used to test whether the data are normally distributed.

A paired analysis was performed to compare the enrichment of putative miRNA targets by let-7b treatment in ECs with that of GAPDH using the Dunnett test with adjustment for multiple comparisons (88, 89).

To compare let-7b target percentages and BS percentages in MECs and HECs, Fisher's exact test (2 groups) and Chi-square test (>2 groups) were used.

Data were compared between the treatment and the control groups using multiple t-tests, a two-tailed Student’s t-test (2 groups), and a one-way analysis of variances (ANOVA) (>2 groups). All data are presented as mean ± SEM.

Proteomics data were compared between samples treated with let-7b mimic and control mimic using Limma (ImShot_1.0.1). Significant proteins in the treatment group compared to the control group ($P<0.05$) were identified using a fold change cut-off of >1.3.

3. Results

3.1. Expression of Let-7 family members in mouse and human ECs

The expression levels of seven let-7 members and let-7b-3p (let-7b*) were determined in MECs and HECs by qRT-PCR using miRCURY LNA-modified primers. In MECs, let-7c expression levels were significantly higher than all other family members, followed by let-7b and let-7d, the next highly expressed members (Fig. 12A). Let-7a was not detectable in MECs or HECs. In HECs, let-7g was significantly higher than let-7e and let-7b* expression (Fig. 12B). Moreover, let-7b* expression levels were similar to let-7b (*P*=ns, Fig. 12B), and let-7b* was expressed in HECs but was not detectable in MECs. Let-7b, let-7c, and let-7d expression levels were significantly higher in MECs than HECs (Fig. 12C). This result indicates that the seven let-7 members were variably expressed in MECs, whereas in HECs, their expression levels were more comparable.

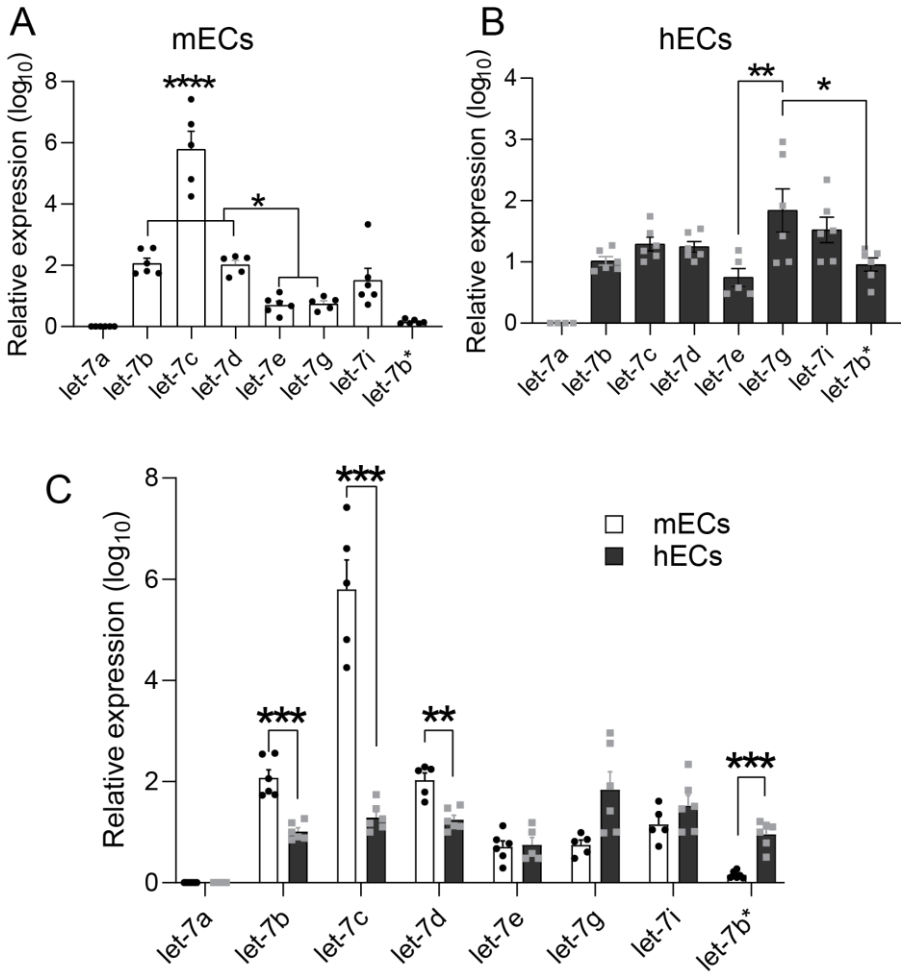

Fig. 12: Expression of let-7 family members in MECs and HECs.

Gene expression of let-7a, b, c, d, e, g, i, and let-7b* were studied relative to U6 snRNA by qRT-PCR in mouse and human ECs (n=5-6) and compared with each other in (A) MECs and (B) HECs using one-way ANOVA. (C) Relative gene expression of let-7 family members to U6 snRNA was compared between MECs and HECs using multiple t-tests with multiple comparison corrections using the Holm-Sidak method (*P<0.05 **P<0.01, ***P<0.001, and ****P<0.0001). Data are presented as mean ± SEM.

Next, the effect of let7b mimic treatment on the expression level of the seven let-7 family members was determined in MECs and HECs by qPCR using miRCURY LNA assays.

Let-7b mimic treatment (n=5-6) upregulated let-7b expression 13-fold in MECs and 19-fold in HECs (Fig. 13A), indicating high efficiency of let-7b mimic transfection. The let-7b mimics treatment downregulated let-7c, let-7d, and let-7e in MECs (Fig. 13B). In HECs, let-7b mimics increased let-7c and let-7g expression and reduced let-7b* expression (Fig. 13C) compared with control mimic treatment. This result indicates that let-7b mimic treatment affects other let-7-member expression levels differently in mouse and human ECs.

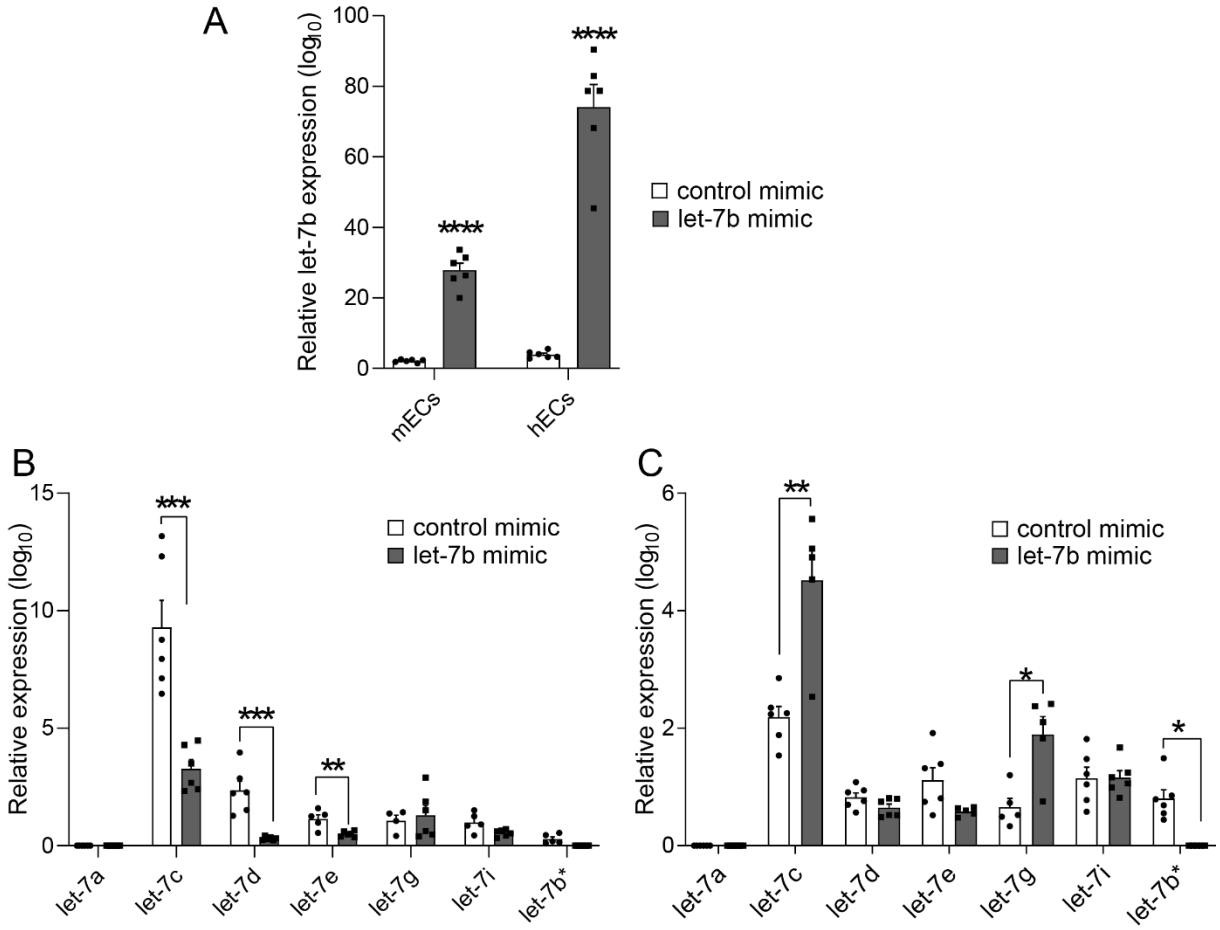

Fig. 13: Expression of let-7 family members after let-7b mimic treatment.

(A, B) MECs and (A, C) HECs (n=5-6) were treated with 50 nM of let-7b mimics and control mimics for 24 h. Expression of (A) let-7b, (B, C) let-7a, let-7c, let-7d, let-7e, let-7g, let-7i, and let-7b* were studied relative to U6 snRNA by qRT-PCR. Let-7b mimic-treated sample and the control sample were compared using multiple t-tests with multiple comparison corrections using the Holm-Sidak method (*P<0.05, **P<0.01, ***P<0.001, and ****P<0.0001). Data are presented as mean ± SEM.

3.2. Let-7b targets in MECs and HECs

To study mRNA and lncRNA targets of let-7b in ECs, MECs and HECs were co-transfected with let-7b mimics and the miRTrap vector (performed by Dr. Lucia Natarelli). The read counts from the expressed genes in whole EC cell lysates and the transcript read counts in Ago2 immunoprecipitates (Ago2-IP) were obtained by RNA sequencing (n=6-7). The accepted read counts for protein-coding and lncRNA genes were annotated according to Ensembl 98 and NONCODE v5.0 databases, respectively. Next, the transcripts significantly enriched by let7b mimic treatment in the RISC compared to GAPDH were defined as let-7b targets. The transcripts detected in the RISC but not enriched by let-7b were probably targets of other endothelial miRNAs.

3.2.1 Endothelial protein-coding targets of let-7b

Reads in all replicates were mapped to 3572 genes in MECs and 7092 in HECs. Mitochondrial-encoded genes, including cytochrome c oxidase I (*MT-CO1*), NADH dehydrogenase 4 (*MT-ND4*), and NADH dehydrogenase 2 (*MT-ND2*), were among the ten most highly expressed genes in MECs and HECs (Table 22).

Table. 22: The top ten highly expressed genes in MECs and HECs.

MECs			**HECs**		
Gene ID	**Gene name**	**Expression level (read count)**	**Gene ID**	**Gene name**	**Expression level (read count)**
ENSMUSG00000064351	mt-Co1	138896	ENSG00000198804	MT-CO1	244364
ENSMUSG00000064370	mt-Cytb	45686	ENSG00000198886	MT-ND4	134800
ENSMUSG00000005397	Nid1	44723	ENSG00000198786	MT-ND5	89890
ENSMUSG00000024661	Fth1	39543	ENSG00000198712	MT-CO2	85954
ENSMUSG00000038587	Akap12	36844	ENSG00000106366	SERPINE1	62401
ENSMUSG00000064363	mt-Nd4	25104	ENSG00000198938	MT-CO3	61128
ENSMUSG00000057113	Npm1	19143	ENSG00000198727	MT-CYB	60020
ENSMUSG00000064345	mt-Nd2	19027	ENSG00000115414	FN1	57349
ENSMUSG00000030787	Lyve1	18974	ENSG00000026025	VIM	53244
ENSMUSG00000022283	Pabpc1	18482	ENSG00000198763	MT-ND2	50555

Among the 3572 expressed genes in MECs, 1846 (51%) were found in the Ago2-immunoprecipitates. Let-7b mimics treatment significantly enriched the transcript abundance of 402 protein-coding genes in the RISC (adj. $P<0.05$). In HECs, 5215 transcripts out of 7092 expressed genes (74%) were detectable in the RISC of all replicates (Fig. 14). Let-7b mimic treatment enriched 1354 protein-coding transcripts in the Ago2-IP compared with GAPDH (adj. $P<0.05$) (Fig. 14). The number of expressed genes and putative miRNA targets were nearly twofold higher in HECs than in MECs. In addition, the protein-coding let-7b targets were threefold higher in HECs compared to MECs. Together, these findings indicate that let-7b has a more influential role in regulating protein-coding genes in HECs than in MECs.

Notably, let-7b enriched transcripts of 153 genes in MECs and HECs (i.e., conserved let-7b targets). Moreover, 249 and 1201 expressed genes were selectively enriched in MECs and HECs, respectively (Fig. 14). This data indicates that let-7b targets a substantial proportion of the genes expressed in ECs; however, only a limited number of the let-7b targets are conserved between mice and humans.

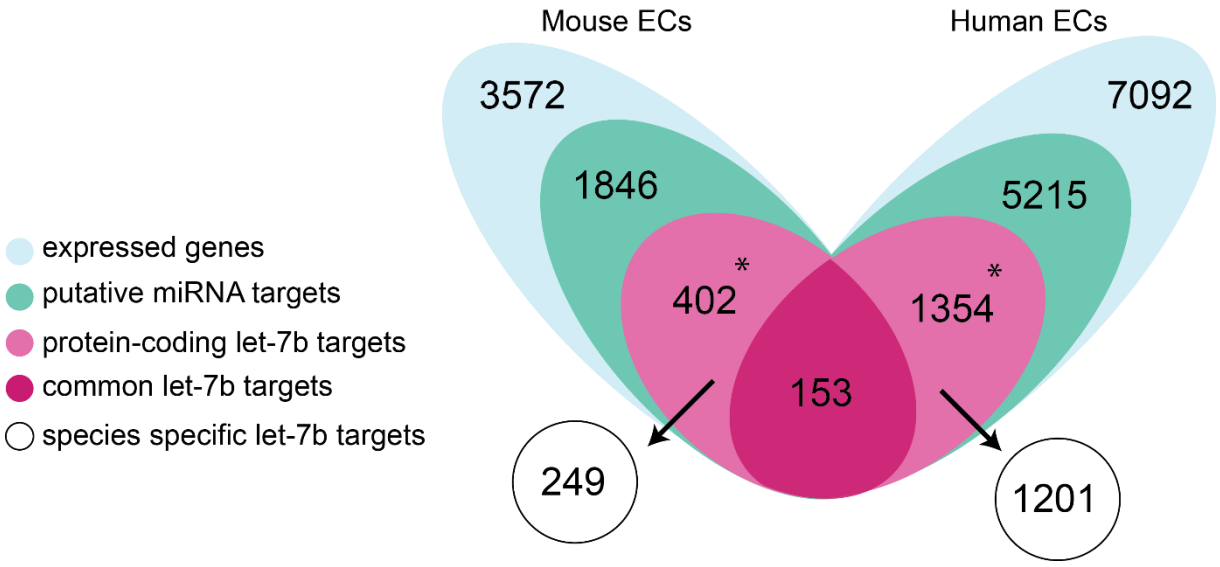

Fig. 14: Protein-coding targets of let-7b in mouse and human ECs.

The number of genes (annotated in Ensembl 98) detected in all replicates (n = 6-7) is shown in blue. Putative miRNA targets were found in all replicates of the Ago2-IPs (green). For each putative miRNA target, the ratio of "read count in Ago2-IP" to "read count in EC lysate" was calculated and compared to that of GAPDH using paired multiple comparison Dunnett test. The putative miRNA targets significantly enriched in the RISC by let-7b mimic compared to GAPDH were defined as let-7b targets (* adj. $P<0.05$; pink). The number of common let-7b targets in mice and humans are shown in the merged oval (red). The white circles indicate the number of let-7b targets detected only in mouse or human ECs.

The percentage of let-7b targets among the expressed genes was significantly lower in MECs than in HECs (11% versus 19%; $P<0.0001$; Fig. 15A). Similarly, the percentage of let-7b targets among the putative miRNA targets in MECs was significantly lower than that in HECs (22% versus 26% of putative miRNA targets) ($P<0.001$, Fig. 15B). However, the 153 let-7b targets commonly found in mouse and human ECs comprised a significantly higher fraction of the let7b targets in MECs than in HECs (38% versus 11%; $P<0.0001$; Fig. 15C). This data suggests that HECs contain more let-7b targets that cannot be found in MECs.

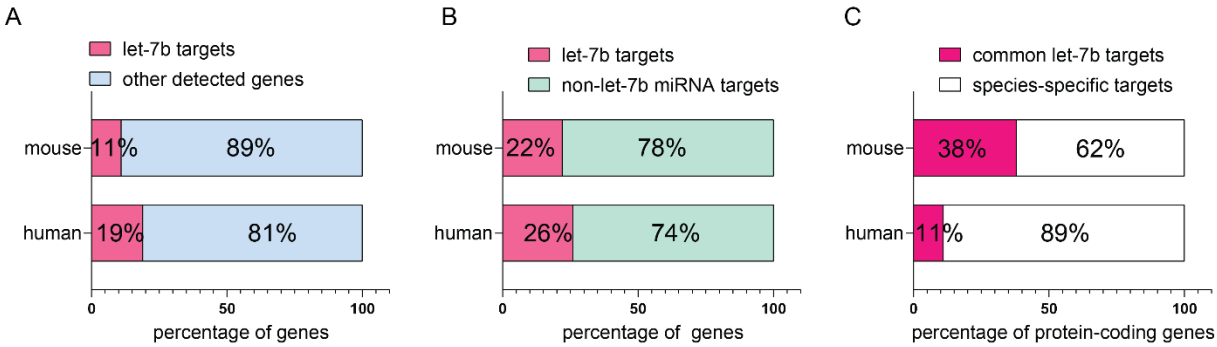

Fig. 15: Comparison of protein-coding let-7b targets between mouse and human ECs.

(A) Comparison of the percentage of protein-coding let-7b targets out of all genes expressed in all replicates between mouse and human ECs (Fisher's exact test, $P<0.0001$). (B) Comparison of the percentage of protein-coding let-7b targets out of all miRNA targets between mouse and human ECs (Fisher's exact test, $P<0.001$). (C) Comparison of the percentage of let-7b targets that are the same in mouse and human ECs (153) out of all protein-coding let-7b targets (Fisher's exact test, $P<0.0001$).

Functional enrichment analysis by g:Profiler revealed that the 153 common let-7b targets in MECs and HECs were related to chromatin organization and RNA splicing. Cell cycle and DNA binding were other enriched GO terms related to these genes (Table 23).

Table. 23: The biological processes regulated by the 153 common let-7b targets in mouse and human ECs.

The identical mouse and human genes related to a similar biological process are presented in bold (GO, gene ontology).

GO.ID	description	mouse adj. *P* Value	mouse genes	human adj. *P* value	human genes
GO:0006325	chromatin organization	1.57546E-05	**Kdm5a**, **Ubr2**, **Shprh**, **Resf1**, **Atrx**, **Pml**, **Tlk2**, **Setd2**, **Baz1a**, **Bptf**, **Emsy**, **Ogt**, **Rere**, **Smchd1**, **Tpr**, **Trip12**, Oga, **Msl2**, **Chd9**, **Kmt2e**, **Slk**, **Tet2**, **Chd4**	6.11229E-05	CAMK2D, **SMCHD1**, **TRIP12**, **SHPRH**, GATAD2B, **KDM5A**, **BPTF**, **SETD2**, **ATRX**, **BAZ1A**, CBX3, **EMSY**, **OGT**, **PML**, **RERE**, **RESF1**, **TLK2**, **TPR**, **UBR2**, USP7, **MSL2**, **CHD9**, **KMT2E**, **TET2**, **CHD4**
GO:0008380	RNA splicing	0.00040	**Rbm39**, **Son**, **Sfswap**, **Rbm6**, **Pnn**, **Fus**, **Hnrnpa2b1**, **Hnrnpk**, **Mbnl1**, **Mbnl2**, **Rbm25**, **Hnrnph1**, **Srrm2**, **Dyrk1a**, **Syncrip**	3.32623E-06	**SFSWAP**, **HNRNPA2B1**, **PNN**, **RBM39**, **FUS**, AHNAK2, HNRNPD, **HNRNPK**, **MBNL1**, **MBNL2**, PAPOLA, **RBM25**, **RBM6**, **SON**, U2SURP, PCF11, **SRRM2**, **HNRNPH1**, **DYRK1A**, **SYNCRIP**
GO:0007049	cell cycle	0.00104	**Son**, **Ubr2**, **Cyld**, **Cdh13**, Camk2d, **Cep192**, **Sptbn1**, **Rock2**, **Atrx**, **Pml**, **Tlk2**, **Setd2**, **Apc**, **Ccnt1**, **Cep295**, **Cltc**, **Ddx3x**, **Myh9**, **Pafah1b1**, **Pcm1**, **Ppp1r12a**, **Tpr**, **Xpo1**, **Nes**, **Itgb1**, **Csnk2a1**, **Kmt2e**, **Senp5**, **Tet2**, **Uhrf2**, **Pkn2**	0.01959	**CEP192**, **DDX3X**, **PCM1**, IPO7, **CYLD**, **XPO1**, **CCNT1**, PHIP, **ROCK2**, **APC**, **SETD2**, **SPTBN1**, **ATRX**, CBX3, **CDH13**, **CEP295**, **CLTC**, **MYH9**, **PAFAH1B1**, **PML**, **PPP1R12A**, **SON**, TENT4B, **TLK2**, **TPR**, **UBR2**, **NES**, **ITGB1**, **CSNK2A1**, **KMT2E**, **SENP5**, **TET2**, **UHRF2**, **PKN2**
GO:0003677	DNA binding	0.00437	**Kdm5a**, **Son**, **Nfat5**, **Pnn**, **Shprh**, **Lrrfip1**, **Trim33**, **Klf6**, **Atrx**, **Fus**, **Pml**, **Hnrnpd**, **Elf2**, **Bptf**, **Ccnt1**, **Ddx3x**, **Egr1**, **Hnrnpa2b1**, **Hnrnpk**, **Mbnl2**, **Rere**, **Samhd1**, **Smchd1**, **Smg7**, **Sos1**, **Swap70**, **Tiparp**, **Zeb2**, **Xrn2**, **Zbtb38**, **Gatad2b**, **Chd9**, **Rbms1**, **Tet2**, **Uhrf2**, **Chd4**	0.00137	**SMCHD1**, **HNRNPA2B1**, **LRRFIP1**, **DDX3X**, **PNN**, **TRIM33**, **NFAT5**, **SHPRH**, **FUS**, **CCNT1**, **GATAD2B**, **KDM5A**, **BPTF**, **ATRX**, **EGR1**, **ELF2**, HIPK1, **HNRNPD**, **HNRNPK**, **KLF6**, **MBNL2**, **PML**, RBM6, **RERE**, **SAMHD1**, **SMG7**, **SON**, **SOS1**, **SWAP70**, TENT4B, **TIPARP**, **ZEB2**, **XRN2**, **ZBTB38**, **CHD9**, MLLT10, **RBMS1**, **TET2**, **UHRF2**, XRN1, **CHD4**, SBNO1

3.2.2 Endothelial lncRNA targets of let-7b

LncRNAs play a widespread role in gene regulation. One of the lncRNA functions is to regulate miRNA activity by binding to miRNAs and titrating them away from their mRNA targets, known as the “sponging effect.” Conversely, miRNAs also can regulate LncRNAs through base-pairing interactions in the RISC (59, 60). Therefore, the next aim was to identify lncRNA targets of let-7b in mouse and human ECs. The non-coding (nc) RNA genes expressed in the aortic ECs were annotated according to the NONCODE database (v5.0). In murine ECs, 647 ncRNA genes were expressed in all replicates, whereas 5551 expressed ncRNAs were detected in human ECs. The evolutionarily conserved miRNA sponge metastasis-associated lung adenocarcinoma transcript 1 (MALAT1), which regulates endothelial dysfunction contributing to atherosclerosis development, was among the top ten highly expressed lncRNA genes in HECs (Table 24) (6, 102).

Table. 24: The ten most highly expressed ncRNA genes in MECs and HECs.

MECs				HECs			
lncRNA ID	**Gene name**	**Chromosomal localization**	**Expression level (read count)**	**lncRNA ID**	**Gene name**	**Chromosomal localization**	**Expression level (read count)**
NONMMUG015781.2	NA	Chr16:11143905-11144315(+)	150032	**NONHSAG103252.1**	NA	ChrM:3246-15886(-)	1047104
NONMMUG016749.2	NA	Chr16:57391106-57391681(+)	45480	**NONHSAG053892.2**	NA	ChrM:3317-15887(+)	525189
NONMMUG026007.2	NA	Chr3:5860337-6049710(+)	15816	**NONHSAG005322.2**	NA	Chr10:17229544-17237584(+)	57650
NONMMUG007938.3	NA	Chr11:109011560-109012415(-)	11087	**NONHSAG005323.3**	lnc-TRDMT1-5	Chr10:17231002-17237311(-)	49422
NONMMUG044356.2	NA	ChrM:11719-14070(-)	9203	**NONHSAG013412.2**	NA	Chr13:45337219-45341155(-)	44707
NONMMUG091736.1	NA	Chr18:68691947-68692411(-)	5806	**NONHSAG063480.2**	lnc-LTBP3-2	Chr11:65408383-65511027(-)	32253
NONMMUG044358.2	NA	ChrM:15355-16294(+)	3281	**NONHSAG025023.2**	lnc-RAB8A-1-2	Chr19:16081012-16103000(+)	30852
NONMMUG044354.2	NA	ChrM:1148-3703(+)	1893	**NONHSAG008675.3 (ENSG00000251562)**	MALAT1	Chr11:65496266-65509085(+)	27423
NONMMUG007013.2	NA	Chr11:83215124-83218272(+)	1666	**NONHSAG053180.2**	lnc-C9orf152-5-1_dup1	Chr9:110170268-110176436(-)	26585
NONMMUG020586.2	NA	Chr19:4062438-4065879(-)	1104	**NONHSAG008515.2**	lnc-ROM1-7	Chr11:62515915-62532883(+)	20754

Among the 647 identified ncRNA genes in MEC lysates, the transcripts of 99 ncRNA genes were detectable in Ago2-IPs, indicating that they are putative miRNA targets. Furthermore, let-7b mimic treatment of MECs significantly enriched transcripts of 50 lncRNA genes in the RISC compared to GAPDH (adj. $P<0.05$). In HECs, 1342 out of 5551 ncRNA gene transcripts were detected in Ago2-IPs. Among those, 330 lncRNA transcripts were significantly enriched by the let-7b mimic treatment compared to GAPDH (adj. $P<0.05$, Fig. 16). This data indicates that let-7b interacts with lncRNAs in ECs in addition to mRNAs.

The sequences of lncRNAs are frequently not conserved between species (103). Therefore, the number of lncRNA targets that are common between mouse and human ECs could not be evaluated using the same procedure as for mRNA targets (Fig. 16, empty yellow merged oval).

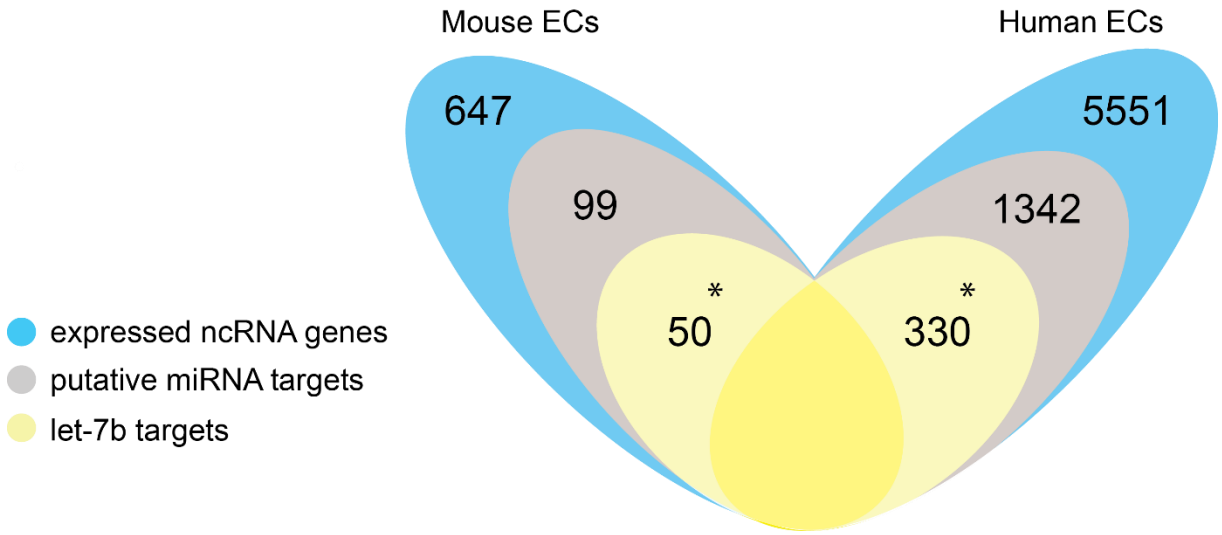

Fig. 16: Identification of lncRNA targets of let-7b in mouse and human ECs.

The total number of ncRNA genes detected in all EC lysates (n=6-7) is shown in blue, and the number of ncRNAs that were also detectable in all Ago2-IP samples is shown in grey. ncRNAs detected in EC lysates and Ago2-IP samples were considered putative targets of any miRNA. LncRNA targets of let-7b that were significantly enriched in the Ago2-IP samples by let-7b mimic treatment compared to GAPDH (* adj. $P<0.05$ by paired multiple comparison Dunnett test) are shown in yellow.

Compared with MECs, the number of expressed ncRNA genes in all replicates and the number of let-7b ncRNA targets were eight-fold and six-fold higher, respectively, in HECs (Fig. 16). However, the number of ncRNAs considered putative miRNA targets was 13-fold higher in HECs than in MECs (Fig. 16). The percentage of let-7b targets among the expressed ncRNA genes in all replicates in MECs was not significantly different from that in HECs (7% versus 6% of lncRNA genes) (P= ns, Fig. 17A). Although the number of lncRNA targets of let-7b was six-fold higher in human than in MECs, the percent of let-7b targets among the total miRNA targets was significantly higher in MECs than in HECs (50% versus 25% of the putative miRNA targets) ($P<0.0001$, Fig. 17B). Taken together, this result indicates that let-7b plays a crucial role in lncRNA regulation in MECs. In contrast, in HECs, other miRNAs than let-7b appear to contribute more to the targeting of ncRNAs.

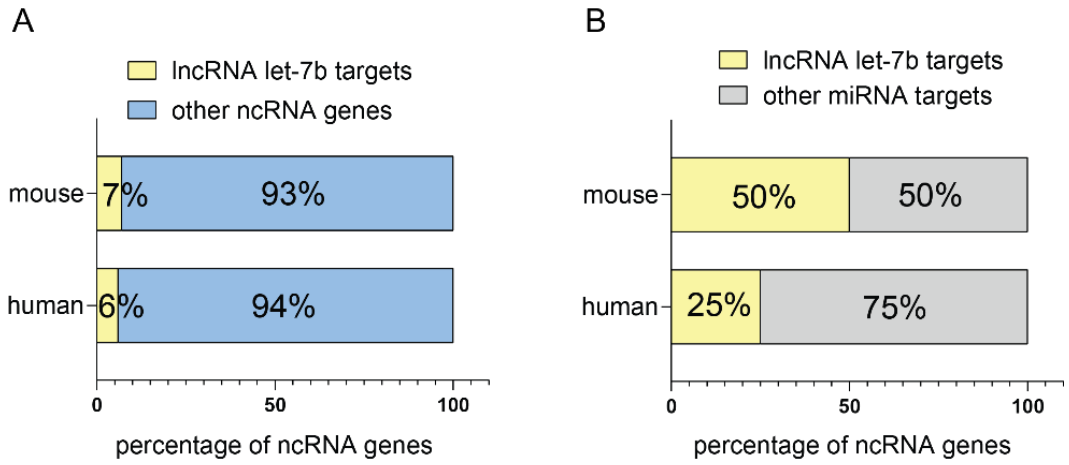

Fig. 17: Comparison of lncRNA targets of let-7b between mouse and human ECs.

(A) Comparison of the percentage of let-7b targets out of all expressed ncRNA genes in all replicates between mouse and human ECs (Fisher's exact test, *P*=ns). (B) Comparison of the percentage of let-7b targets out of all miRNA targets between mouse and human ECs (Fisher's exact test, *P*<0.0001).

3.3. Let-7b target enrichment

The mean enrichment of all protein-coding let-7b targets (i.e., genes significantly enriched in the RISC by let-7b mimic compared to GAPDH) was determined in mouse and human ECs. *O-linked N-acetylglucosamine (GlcNAc) transferase* (*OGT*) was the highest enriched gene in MECs and HECs (Table. 25). Notably, the mean enrichment was more than 100-fold in HECs. In contrast, the maximum mean enrichment in MECs was 79-fold.

Table. 25: Gene expression of the top ten highly enriched protein-coding let-7b targets.

The enrichment of 402 murine and 1354 human let-7b targets was calculated by dividing the "gene count in AgoIP" by "gene count in EC lysate" ratios from each gene in each replicate by the corresponding ratio for GAPDH in that replicate. Next, the mean enrichment of each gene was calculated. The genes were ranked according to the highest mean enrichment in MECs and HECs. Gene expression level is provided as gene counts.

MECs				HECs			
gene ID	gene name	mean enrichment	expression (gene count)	gene ID	gene name	mean enrichment	expression (gene count)
ENSMUSG00000034160	Ogt	79	299	ENSG00000147162	OGT	290	431
ENSMUSG00000026131	Dst	71	3952	ENSG00000163138	PACRGL	192	102
ENSMUSG00000029823	Luc7l2	70	300	ENSG00000089280	FUS	118	573
ENSMUSG00000026349	Ccnt2	65	220	ENSG00000129197	RPAIN	110	186
ENSMUSG00000031196	F8	52	344	ENSG00000146414	SHPRH	104	215
ENSMUSG00000041297	Cdk13	46	478	ENSG00000166135	HIF1AN	104	186
ENSMUSG00000038535	Zfp280d	45	231	ENSG00000173559	NABP1	102	964
ENSMUSG00000020255	D10Wsu102e	45	469	ENSG00000205268	PDE7A	101	164
ENSMUSG00000054387	Mdm4	43	399	ENSG00000213096	ZNF254	100	152
ENSMUSG00000025019	Lcor	42	225	ENSG00000128534	LSM8	96	113

Functional profiling of the top 100 significantly enriched genes in mouse and human ECs by g:Profiler revealed that in both cell types, they are related to the cell nucleus, mRNA metabolic process, and cellular nitrogen compound metabolism (Table 26).

Table. 26: The common biological processes regulated by the top 100 enriched genes in MECs and HECs.

The identical mouse and human genes related to a common process are presented in bold (GO, gene ontology).

GO.ID	Description	mouse adj. *P* value	mouse genes	human adj. *P* value	Human genes
GO:0005634	nucleus	6.97E-10	**Ogt**, Dst, Luc7l2, Ccnt2, Cdk13, Zfp280d, Mdm4, Lcor, Tet2, Ralgapa1, Lcorl, Jmjd1c, Syne1, Phf20l1, Iqgap1, Sptbn1, Ikbkb, **Sfswap**, Camk2d, Asxl2, Emsy, Setd5, Cers4, Rbm25, Klf3, Nktr, Mob1b, Phf10, Tbp, Haus3, Son, Qrich1, Kdm5a, Zfp142, Srrm2, Chd9, Rbm5, Golga4, Pbx1, **Rbm6**, Bclaf1, Strn3, Pcf11, **Fus**, Cilk1, Zc3hav1, Aftph, **Mllt10**, Nbea, Btbd7, **Pnn**, Zfp407, Nfat5, Thoc2, Bod1l, **Elf2**, Baz1a, Zfp644, Nars2, Tgif1, Egr1, Tet3, Dmtf1, Mcl1, Apc, Tcf4	0.00032	**OGT**, **FUS**, RPAIN, SHPRH, HIF1AN, NABP1, ZNF254, LSM8, MED28, **PNN**, MAPK10, FNBP4, UBN2, KHNYN, TRA2B, HERC4, HMGA2, PNISR, **MLLT10**, DARS2, OGA, SRSF5, MECP2, CRMP1, DCAF13, KAT6B, PCGF3, **SFSWAP**, ZFPM2, HCLS1, RBM39, TSPYL2, KANSL1, SAP30BP, LUC7L3, HDX, ZNF773, BRWD3, PLAGL2, RUBCN, WDR55, PIAS2, STAT2, MARS1, RBM28, FBXW7, PPM1B, ATR, RNF213, **RBM6**, NAA30, NLRC5, UBR4, RORA, **ELF2**, UBP1, RAB3IP, CTNNB1, MPHOSPH8, ELP2
GO:0016070	RNA metabolic process	5.74E-08	Ogt, Luc7l2, Ccnt2, Cdk13, Zfp280d, Mdm4, Lcor, Tet2, Ralgapa1, Riok3, Lcorl, Jmjd1c, Phf20l1, Ikbkb, **Sfswap**, Asxl2, Emsy, Setd5, Rbm25, Klf3, Tbp, Son, Qrich1, Kdm5a, Tsc22d2, Zfp142, Rnf141, Srrm2, Rbm5, Pbx1, **Rbm6**, Bclaf1, Strn3, Pcf11, Phip, **Fus**, Zc3hav1, **Mllt10**, **Pnn**, Zfp407, Nfat5, Fnip1, Thoc2, **Elf2**, Zfp644, Nars2, Tgif1, Egr1, Tet3, Dmtf1, Tcf4	0.00522	OGT, **FUS**, HIF1AN, NABP1, ZNF254, LSM8, **PNN**, MAPK10, KHNYN, TRA2B, HMGA2, **MLLT10**, DARS2, ACVR2A, SRSF5, MECP2, DCAF13, KAT6B, PCGF3, **SFSWAP**, ZFPM2, LARS2, HCLS1, RBM39, SAP30BP, LUC7L3, HDX, ZNF773, BRWD3, METTL2B, PLAGL2, WDR55, PIAS2, STAT2, MARS1, RBM28, **RBM6**, NLRC5, RORA, **ELF2**, UBP1, CTNNB1, MPHOSPH8, ELP2
GO:0034641	cellular nitrogen compound metabolic process	0.00010	Ogt, Luc7l2, Ccnt2, Cdk13, Zfp280d, Mdm4, Lcor, Tet2, Ralgapa1, Riok3, Lcorl, Jmjd1c, Phf20l1, Ikbkb, **Sfswap**, Camk2d, Asxl2, Emsy, Setd5, Cers4, Rbm25, Klf3, Tbp, Son, Qrich1, Kdm5a, Tsc22d2, Zfp142, Rnf141, Srrm2, Shprh, Rbm5, Pbx1, **Rbm6**, Bclaf1, Strn3, Pcf11, Phip, Fus, Zc3hav1, **Mllt10**, **Pnn**, Zfp407, Nfat5, Fnip1, Thoc2, Bod1l, **Elf2**, Zfp644, Nars2, Tgif1, Egr1, Tet3, Dmtf1, Tcf4	0.00280	OGT, FUS, RPAIN, SHPRH, HIF1AN, NABP1, PDE7A, ZNF254, LSM8, **PNN**, MAPK10, KHNYN, TRA2B, HMGA2, **MLLT10**, SUCLA2, DARS2, ACVR2A, SRSF5, MECP2, CRMP1, DCAF13, KAT6B, PCGF3, **SFSWAP**, DIP2A, ZFPM2, LARS2, HCLS1, NADSYN1, RBM39, ENTPD4, SAP30BP, LUC7L3, HDX, ZNF773, BRWD3, METTL2B, ACAT1, PLAGL2, WDR55, PIAS2, ACO1, STAT2, MARS1, RBM28, ATR, **RBM6**, NLRC5, RORA, **ELF2**, UBP1, CTNNB1, MPHOSPH8, ELP2

Similar to protein-coding targets, the mean enrichment of the lncRNA targets was determined in mouse and human ECs (Table 27). Although protein-coding let-7b targets have higher expression values (> 200 in MECs and > 100 in HECs) compared to lncRNA target expressions (mostly <100), the mean enrichment values of lncRNA targets were up to ten-fold higher than of the protein-coding targets. This data suggests that in mouse and human ECs, let-7b targets lncRNA transcripts more effectively than mRNAs.

Table. 27: Gene expression of the top ten highly enriched lncRNA let-7b targets.

The enrichment of 50 and 330 mouse and human let-7b targets was calculated by dividing the "read count in AgoIP" to "read count in EC lysate" ratio in each replicate (n=6-7) by the ratio of GAPDH in that replicate. Next, the mean enrichment of each gene was calculated. The genes are ordered according to the highest mean enrichment in mouse and human ECs. Finally, the absolute expression level of each gene was calculated from the mean of the read counts.

MECs				HECs			
lncRNA ID	**lncRNA name**	**Mean enrichment**	**Expression level (read count)**	**lncRNA ID**	**lncRNA name**	**Mean enrichment**	**Expression level (read count)**
NONMMUG042674.2	NA	17819	30	**NONHSAG038995.3**	(Lnc-INPP4B-4)	4111	73
NONMMUG023935.2	NA	17063	237	**NONHSAG069030.2**	NA	3503	123
NONMMUG055601.1	NA	2968	12	**NONHSAG097191.2**	NA	2475	78
NONMMUG055605.1	NA	2491	4	**NONHSAG099774.2**	(lnc-ZFAT-1-2)	2228	58
NONMMUG040020.2	NA	2441	19	**NONHSAG079293.2**	(LINC01473)	1646	158
NONMMUG018876.2	NA	1554	42	**NONHSAG057260.2**	NA	1149	113
NONMMUG002995.2	NA	888	6	**NONHSAG027351.3**	(FLJ31356)	986	65
NONMMUG055596.1	NA	723	79	**NONHSAG032560.3**	(MIR155HG)	888	82
NONMMUG038263.2	NA	668	25	**NONHSAG094315.2**	(lnc-SNX14-1-3)	809	10
NONMMUG014085.2	NA	589	5	**NONHSAG004226.2**	(LINC02535)	774	15

lncRNA targets comprised 11% of the total 452 let-7b targets (protein-coding and lncRNA) in MECs and 21% of the 1684 let-7b targets (protein-coding and lncRNA) in HECs. LncRNAs comprise a significantly higher proportion of let-7b targets in HECs than in MECs (P<0.0001, Fig. 18).

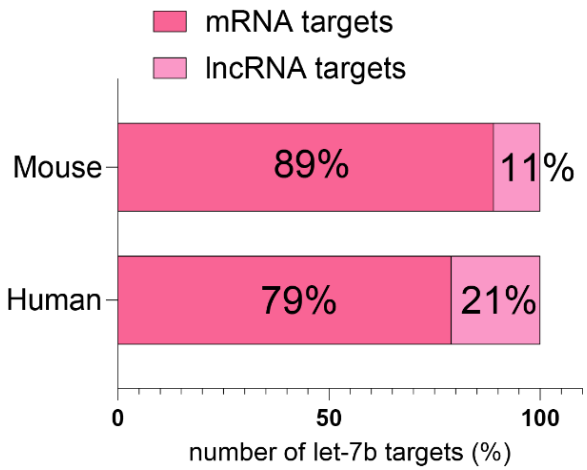

Fig. 18: Comparison of mRNA and lncRNA let-7b targets between MECs and HECs.

The percentage of protein-coding and lncRNA let-7b targets was compared between MECs and HECs by Fisher's exact test (P<0.0001).

3.4. Predicted let-7b BSs in endothelial protein-coding targets

Canonical let-7b binding sites (BSs), including 8mer, 7mer-m8, and 7mer-A1 BSs, were predicted in the 3'–UTR sequences of the protein-coding targets using RNAhybrid. Among the 153 common let-7b targets (Fig. 14 and 15 C), 50 (33%) and 58 (38%) of the mouse and human targets, respectively, contained a putative canonical BS (Fig. 19A). Moreover, the predicted canonical BS was identical between mouse and human in 23 of the common let-7b targets (15%). Accordingly, 103 (67%) and 95 (62%) of the common let-7b targets in MECs and HECs, respectively, did not contain a predicted canonical BS (Fig. 19A). The fractions of common targets with or without a predicted canonical BS did not statistically differ between MECs and HECs (P=ns) (Fig. 19A).

Among the 249 let-7b targets that were only found in MECs, a conserved (P_{CT}>0.3) and a non-conserved (P_{CT}<0.3) canonical BS was predicted in 37 (15%) and 53 (21%) targets, respectively (Fig. 19B). Moreover, among the 1202 human-specific let-7b targets, 152 (13%) and 268 (22%) contained a conserved and not conserved predicted canonical BSs, respectively (Fig. 19B). The percentage of species-specific targets with (36% versus 35%, P=ns) and without a predicted canonical BS (64% versus 65%, P=ns) was similar between mouse and human ECs (Fig. 19B).

This data reveals that only one-third of the let-7b targets in MECs or HECs contain a canonical BS, suggesting that two-thirds of the targets have functional non-canonical BSs.

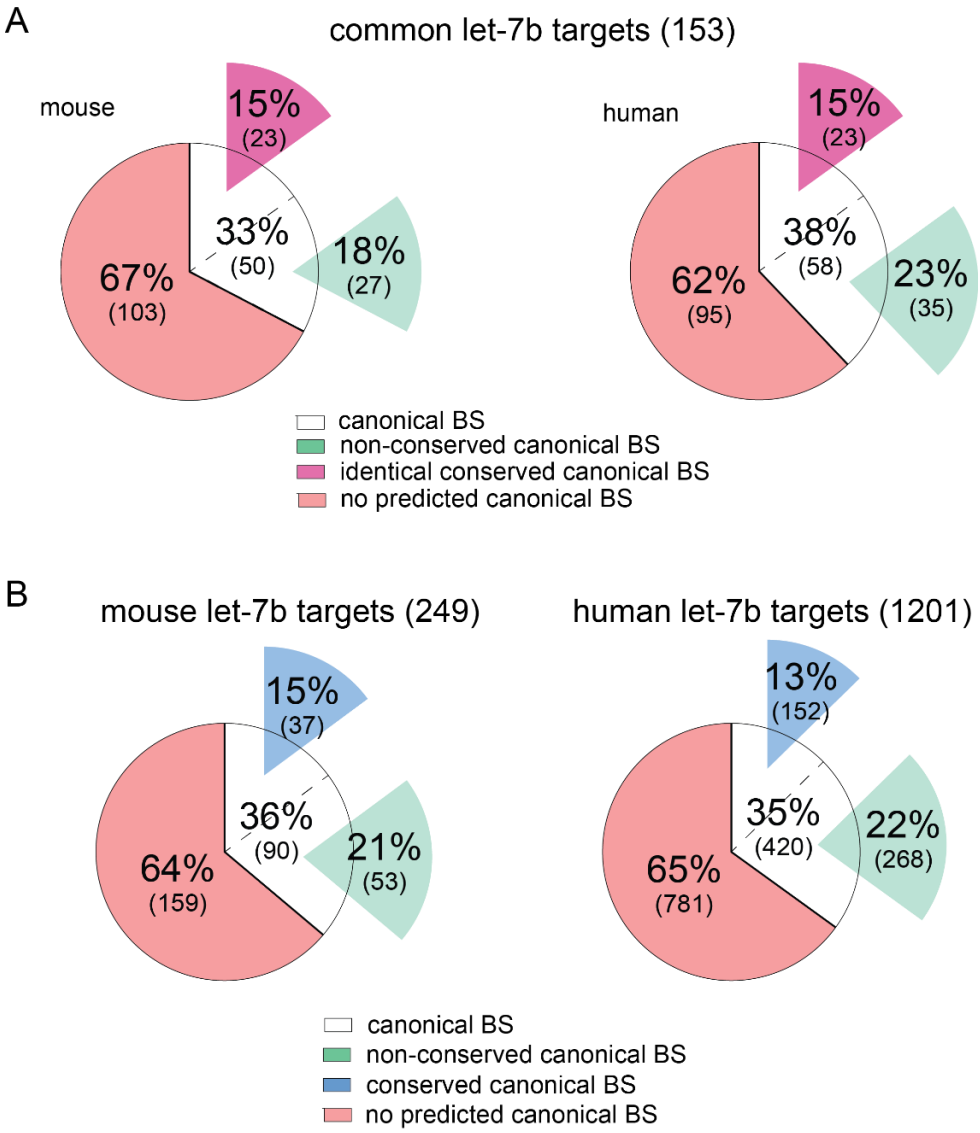

Fig. 19: Similarity of mouse and human target fractions according to their BSs.

Canonical BSs in endothelial let-7b targets were predicted by RNAhybrid, and their conservation was assessed by TargetScan (P_{CT}>0.3). (A) The fraction of targets containing a canonical BS (identical conserved and non-conserved) or no canonical BS in their 3'–UTR was compared between MECs and HECs using Fisher's exact test (*P*= ns). (B) The fraction of mouse or human let-7b targets containing a conserved canonical BS, a non-conserved canonical BS, or no canonical BS in their 3'–UTR was compared between MECs and HECs by Chi-square test (*P*= ns). Characters in brackets show the number of targets.

Among the 229 predicted BSs in all let-7b target transcripts in MECs, the percentage of predicted 8mer, 7mer-m8, and 7mer-A1 BSs were 18%, 48%, and 34%, respectively (Fig. 20A). Omitting 63 replicate BSs (which were found more than once in different transcripts of the same protein-coding gene) revealed that among the remaining 166 BSs 20% were 8mer, 39% were 7mer-m8, and 41% were 7mer-A1 BSs (Fig. 20C). Out of 1065, BSs predicted in human let-7b target transcripts, the percentage of predicted 8mer, 7mer-m8, and 7mer-A1 BSs were 14%, 41% and 45%, respectively (Fig. 20B). Omitting the replicate BSs resulted in 635 predicted BSs in human protein-coding targets including 18% 8mer, 33%

7mer-m8 and 49% 7mer-A1 BSs (Fig. 20D). The percentages of the three types of canonical BSs predicted in mRNA transcripts were different between murine and human ECs (P<0.05), e.g., more 7mer-A1 BSs were found in HECs than in MECs. However, this difference in the proportions of BSs was not observed when the replicate BSs were omitted (P=ns).

The observed distribution of different BS types predicted in targets deviated from equally distributed values in mouse and human ECs (P<0.01).

This data suggests that 8mer BS are the least common BSs for targeting protein-coding genes by let-7b.

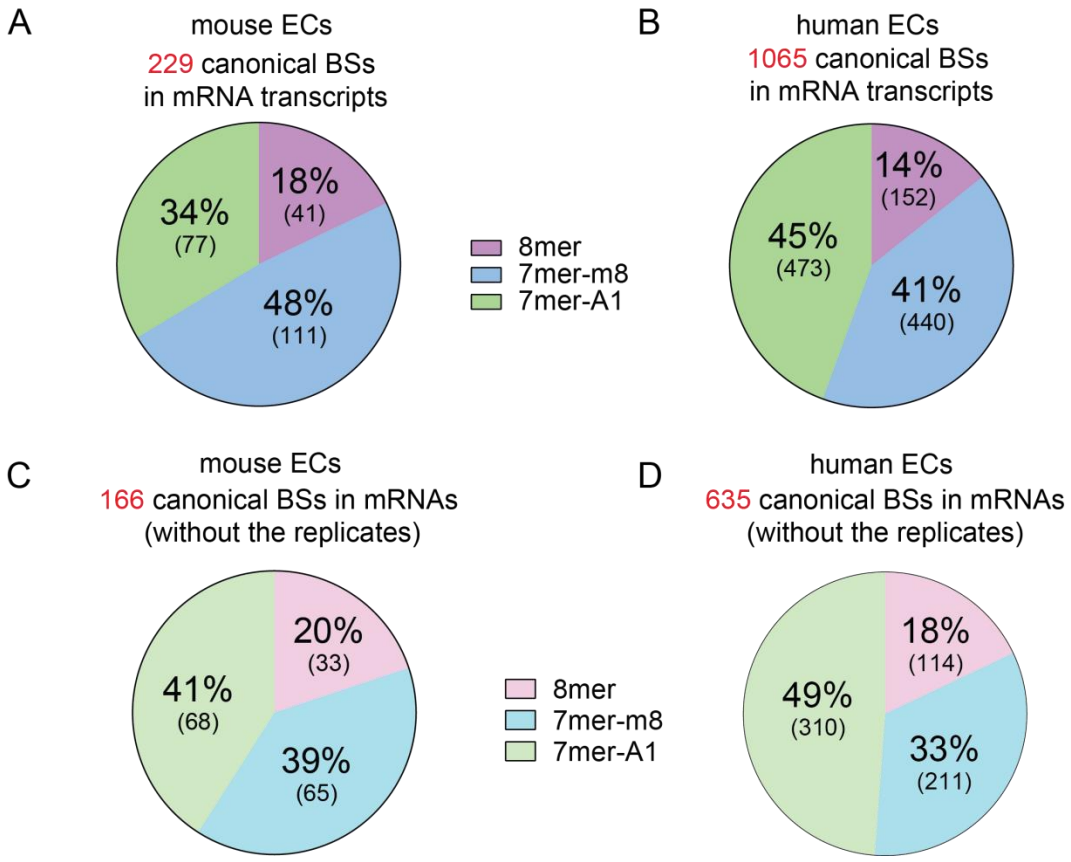

Fig. 20: Percentages of predicted canonical BSs in mouse and human protein-coding let-7b targets.

Canonical BSs were predicted in common and species-specific transcripts of the endothelial let-7b targets by RNAhybrid. The percentage of 8mer, 7mer-m8, and 7mer-A1 sites out of all predicted BSs at the transcript level in (A) MECs and (B) HECs (P<0.05) and at the gene level in (C) MECs and (D) HECs (P= ns) were compared between the two species using Chi-square test. Characters in brackets show the number of BSs.

The 23 identical common targets contained four 8mer sites (17%), eight 7mer-m8 sites (35%), and eleven 7mer-A1 sites (48%), which were conserved in mouse and human transcripts (P_{CT} > 0.3) (Table 28). This result suggests that 8mer sites are less frequent than 7mer-m8 and 7mer-A1 sites in conserved let-7b targets of mouse and human ECs. The P_{CT} value was higher than 0.9 for 13 targets in MECs (52%) and 11 targets in HECs (48%) (Table

28).

Table. 28: Let-7b targets with identical conserved canonical BS.

The P_{CT} values of the predicted canonical BSs and the respective murine and human transcripts were obtained from TargetScan.

Gene	Gene name	Identical conserved let-7b BS	Mouse		Human	
			transcript ID (gene ID)	**P_{CT} value**	**transcript ID (gene ID)**	**P_{CT} value**
MLLT10	Histone lysine methyltransferase DOT1L cofactor	7mer-A1	ENSMUST00000114671.2 (ENSMUSG00000026743)	0.88	ENST00000377072.3 (ENSG00000078403)	0.86
TET2	tet methylcytosine dioxygenase 2	7mer-A1	ENSMUST00000098603.3 (ENSMUSG00000040943)	0.91	ENST00000545826.1 (ENSG00000168769)	0.96
RBMS1	RNA binding motif, single stranded interacting protein 1	8mer	ENSMUST00000028347.7 (ENSMUSG00000026970)	0.97	ENST00000348849.3 (ENSG00000153250)	0.95
UHRF2	ubiquitin-like with PHD and ring finger domains 2, E3 ubiquitin-protein ligase	8mer	ENSMUST00000025739.8 (ENSMUSG00000024817)	0.96	ENST00000276893.5 (ENSG00000147854)	0.95
KMT2E	lysine (K)-specific methyltransferase 2E	8mer	ENSMUST00000094962.3 (ENSMUSG00000029004)	0.85	ENST00000334877.4 (ENSG00000005483)	0.82
CHD9	chromodomain helicase DNA binding protein 9	7mer-A1	ENSMUST00000109614.3 (ENSMUSG00000056608)	0.86	ENST00000566029.1 (ENSG00000177200)	0.85
TSC22D2	TSC22 domain family, member 2	7mer-A1	NSMUST00000099090.2 (ENSMUSG00000027806)	0.95	ENST00000361875.3 (ENSG00000196428)	0.96
CSNK2A1	casein kinase 2, alpha 1 polypeptide	7mer-A1	ENSMUST00000099224.4 (ENSMUSG00000074698)	0.95	ENST00000349736.5 (ENSG00000101266)	0.89
XRN1	5'-3' exoribonuclease 1	7mer-A1	ENSMUST00000185633.1 (ENSMUSG00000032410)	0.83	ENST00000264951.4 (ENSG00000114127)	0.86
DYRK1A	dual-specificity tyrosine-(Y)-phosphorylation regulated kinase 1A	7mer-m8	NSMUST00000023614.4 (ENSMUSG00000022897)	0.89	ENST00000339659.4 (ENSG00000157540)	0.77
CHD4	chromodomain helicase DNA binding protein 4	7mer-m8	ENSMUST00000056889.9 (ENSMUSG00000063870)	0.9	ENST00000544484.1 (ENSG00000111642)	0.79
SBNO1	strawberry notch homolog 1 (Drosophila)	7mer-m8	ENSMUST00000065263.6 (ENSMUSG00000038095)	0.94	ENST00000420886.2 (ENSG00000139697)	> 0.99
EIF5B	eukaryotic translation initiation factor 5B	7mer-A1	ENSMUST00000027252.7 (ENSMUSG00000026083)	0.95	ENST00000289371.6 (ENSG00000158417)	0.95
GOLGA4	golgin A4	7mer-A1	ENSMUST00000084820.4 (ENSMUSG00000038708)	0.95	ENST00000361924.2 (ENSG00000144674)	0.73
SENP5	SUMO1/sentrin specific peptidase 5	7mer-A1	ENSMUST00000023457.6 (ENSMUSG00000022772)	0.95	ENST00000323460.5 (ENSG00000119231)	0.96
PKN2	protein kinase N2	7mer-A1	ENSMUST00000043812.9 (ENSMUSG00000004591)	0.75	ENST00000370521.3 (ENSG00000065243)	0.85
SLK	STE20-like kinase	7mer-m8	ENSMUST00000026043.6 (ENSMUSG00000025060)	0.88	ENST00000335753.4 (ENSG00000065613)	0.76

MSN	moesin	7mer-m8	ENSMUST00000117399.1 (ENSMUSG00000031207)	0.88	ENST00000360270.5 (ENSG00000147065)	0.56
MGAT4A	mannosyl (alpha-1,3-)-glycoprotein beta-1,4-N-acetylglucosaminyltransferase, isozyme A	7mer-m8	ENSMUST00000151952.2 (ENSMUSG00000026110)	0.96	ENST00000264968.3 (ENSG00000071073)	> 0.99
SYNCRIP	synaptotagmin binding, cytoplasmic RNA interacting protein	8mer	ENSMUST00000174391.2 (ENSMUSG00000032423)	0.97	ENST00000355238.6 (ENSG00000135316)	0.95
CGNL1	cingulin-like 1	7mer-m8	ENSMUST00000121322.2 (ENSMUSG00000032232)	0.54	ENST00000281282.5 (ENSG00000128849)	0.98
KPNA1	karyopherin alpha 1 (importin alpha 5)	7mer-A1	ENSMUST00000004054.7 (ENSMUSG00000022905)	0.91	ENST00000344337.6 (ENSG00000114030)	0.93
EXOC5	exocyst complex component 5	7mer-m8	ENSMUST00000162175.2 (ENSMUSG00000061244)	0.63	ENST00000413566.2 (ENSG00000070367)	0.37

To identify interactions between let-7 and its targets with similar functional roles in MECs and HECs, targets with highly conserved canonical BSs ($P_{CT} > 0.85$) in both cell types were selected, and the sum of the mean enrichment in MECs and HECs was calculated. The histone lysine methyltransferase DOT1L cofactor (*MLLT10*) showed the highest combined mean enrichment (80-fold) among the 23 common let-7b targets. Moreover, the sum of P-values of the comparisons between the target enrichment and that of GAPDH in MECs and HECs was determined. The lowest sum of P-values was calculated for ubiquitin-like with PHD and ring finger domains 2 (*UHRF2*) (sum of *P-value* 0.0104) (Table 29).

In addition to 13 common targets, the interaction between *MLLT10* and let-7b was experimentally validated by cross-linking immunoprecipitation (CLIP) according to the TarBase database version 8 (http://carolina.imis.athena-innovation.gr/diana_tools/web/index.php?r=tarbasev8%2Findex). In contrast, the interaction between *UHRF2* and let-7b has not been determined previously (Table 29).

Table. 29: Sum of mean enrichment and P-values in MECs and HECs of the 23 let-7b targets with identical BSs.

The sum of the mean enrichment of each gene in MECs and HECs was calculated. The sum of P-values derived from comparisons between the target enrichment and the enrichment of GAPDH was obtained by paired multiple Dunnett test and multiple comparison correction (n=6-7). In addition, TarBase v.8 was explored to find experimentally confirmed interactions of the targets with let-7b (references).

Gene	Mean enrichment		The sum of mean enrichment	*Adj. P-value*		Sum of *P-value*	TarBase Reference
	Mouse	**Human**		**Mouse**	**Human**		
MLLT10	19	61	80	0.0430	0.0118	0.0548	(104, 105)
TET2	40	36	76	0.0323	0.0493	0.0816	(104)
RBMS1	11	32	43	0.0403	0.0064	0.0467	(106-108)
UHRF2	14	30	44	0.0009	0.0095	0.0104	-
KMT2E	13	29	42	0.0150	0.0051	0.0201	(109)
CHD9	21	26	47	0.0127	0.0139	0.0266	-
TSC22D2	23	24	47	0.0331	0.0029	0.036	(106, 107, 109-112)
CSNK2A1	15	23	38	0.0081	0.0155	0.0236	(107)
XRN1	13	22	35	0.0271	0.0386	0.0657	(105)
DYRK1A	8	20	28	0.0223	0.0054	0.0277	-
EIF5B	5	19	24	0.0029	0.0214	0.0243	-
CHD4	10	18	28	0.0285	0.0350	0.0635	-
SBNO1	11	16	27	0.0239	0.0080	0.0319	(112)
GOLGA4	20	14	34	0.0164	0.0246	0.041	(104, 111)
SENP5	12	13	25	0.0484	0.0089	0.0573	(110, 112, 113)
SLK	8	11	19	0.0152	0.0163	0.0315	-
MGAT4A	13	11	24	0.0320	0.0164	0.0484	(109, 111)
MSN	6	11	17	0.0112	0.0147	0.0259	(106)
SYNCRIP	7	10	17	0.0116	0.0413	0.0529	(110)
KPNA1	6	10	16	0.0015	0.0128	0.0143	-
PKN2	8	10	18	0.0476	0.0280	0.0756	(109)
CGNL1	8	9	17	0.0203	0.0053	0.0256	-
EXOC5	10	6	16	0.0277	0.0493	0.077	-

A comparison of the transcript sequences revealed an identity between the murine and human MLLT10 3'–UTRs of more than 89% and between the 22 nucleotides of the BS region of 86%, including a 7mer-A1 BS conserved in vertebrates (Fig. 21A). Moreover, the nucleotide sequence identity between murine and human UHRF2 3'–UTRs is 82%. In contrast, the sequence identity of let-7b BS regions is 100% between the two species. The murine and human let-7b BS regions contain the same 8mer BS, which was conserved in vertebrates (Fig. 21B).

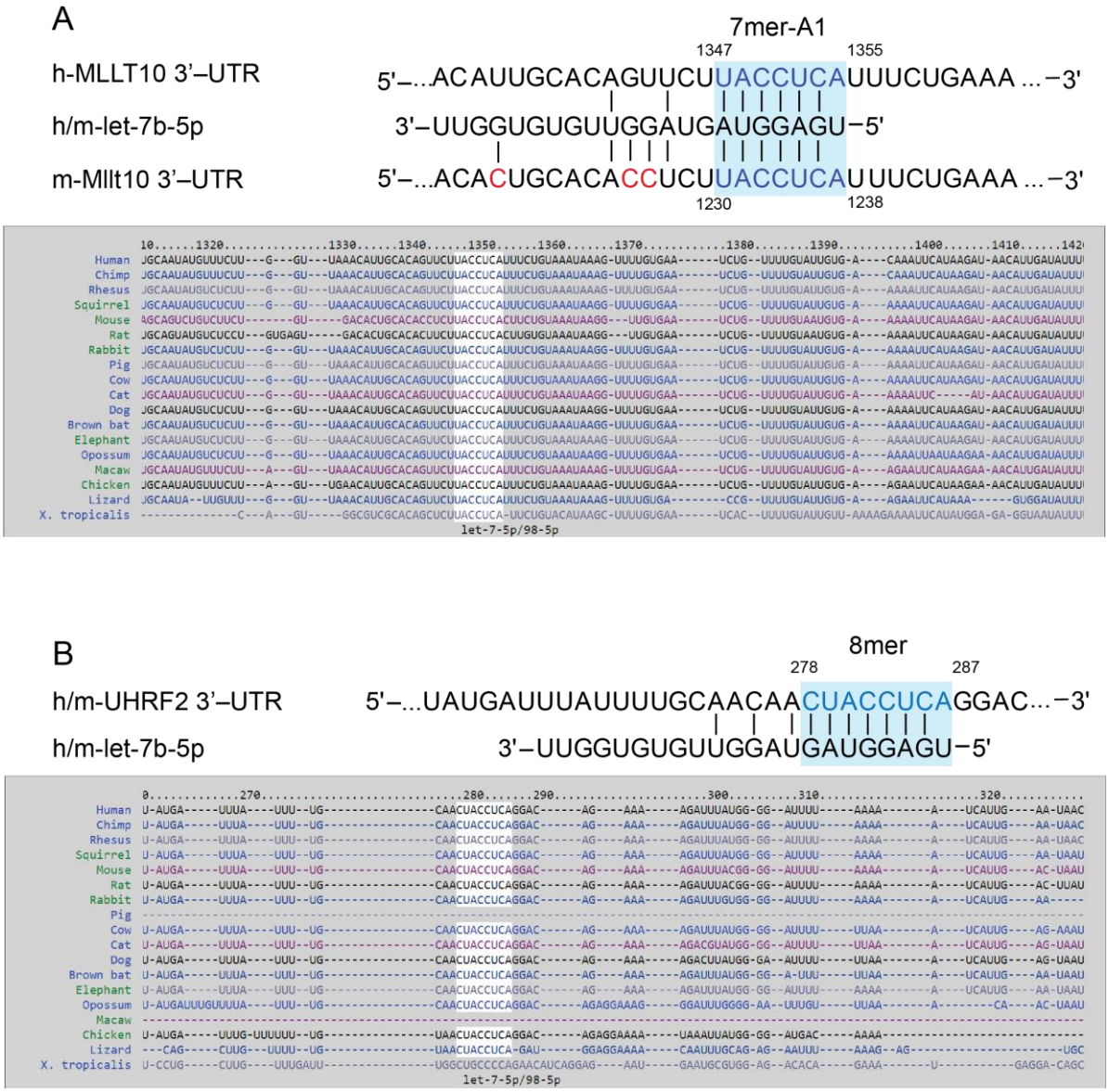

Fig. 21: Predicted canonical let-7b BSs in the 3'–UTRs of MLLT10 and UHRF2.

The predicted base pairing between the let-7b seed sequence (nucleotides 2 to 7) and the conserved region in the 3'–UTR of the targets is presented. (A) MLLT10 has a 7mer-A1 BS (blue shaded area) located between nucleotides 1347 and 1355 in humans and nucleotides 1230 and 1238 in mouse 3'–UTRs. The 22 nucleotides at the BS region were 86% identical in mice and humans (nucleotide variation shown in red). The BS is conserved in vertebrates (white highlighted sequence). (B) The 3'–UTR of UHRF2 contains an 8mer BS (blue shaded area) located between nucleotides 278 and 287 in both mouse and human sequences due to 100% sequence identity of the 22 nucleotides in the BS region. The BS is conserved among vertebrates (white highlighted sequence). Images showing BS conservation were obtained from human TargetScan.

3.5. Predicted let-7b BSs in endothelial lncRNA targets

LncRNAs are not translated and lack a 3'–UTR; thus, miRNA BSs can be located throughout the lncRNA transcript (59). The complete sequences of all the lncRNA target transcripts in mouse and human ECs were obtained from NONCODE v.5.0, and canonical let-7b BSs were predicted by RNAhybrid. Among the 50 mouse lncRNA targets (207 transcripts), 16 lncRNA genes (26 transcripts) contained at least one canonical BS in their sequence (Table 3.9), including long non-protein-coding RNA, Trp53 induced transcript (*Lincpint*) and Pvt1 oncogene (*Pvt1*).

Table. 30: Mouse lncRNA let-7b targets with predicted canonical BSs.

The 16 lncRNA targets in MECs predicted to contain canonical BSs (8mer, 7mer-m8, and 7mer-A1) by RNAhybrid in any of their transcript variants are shown. The genes are ranked based on the lowest adjusted P-value (significantly enriched in the RISC by let-7b mimic treatment using paired multiple comparisons Dunnett test, n=7) and the highest mean enrichment. NA, not applicable.

Gene ID	Gene name	Mean enrichment	*P-value*	Predicted BSs in transcripts
NONMMUG039682.2 (ENSMUSG00000059277)	expressed sequence R74862	44	0.0003	7mer-A1
NONMMUG055598.1 (ENSMUSG00000099115)	Gm17190-201	396	0.0004	8mer, 7mer-m8
NONMMUG010287.2	NA	138	0.0008	7mer-m8
NONMMUG055597.1	NA	249	0.0009	8mer
NONMMUG014644.3 (ENSMUSG00000097039)	Pvt1 oncogene	334	0.0011	8mer
NONMMUG034886.3 (ENSMUSG00000044471)	Lincpint	509	0.0018	7mer-m8, 7mer-A1
NONMMUG006955.2	NA	210	0.0019	7mer-m8
NONMMUG031918.3 (ENSMUSG00000073147)	5031425E22Rik	98	0.0027	8mer, 7mer-m8
NONMMUG083020.2	NA	45	0.0035	8mer, 7mer-m8
NONMMUG012930.2	NA	560	0.0036	7mer-m8, 7mer-A1
NONMMUG028848.2	NA	14	0.0048	7mer-m8, 7mer-A1
NONMMUG040020.2	NA	2441	0.0079	7mer-m8
NONMMUG034303.2	NA	147	0.0124	8mer
NONMMUG042674.2	NA	17819	0.026	7mer-A1
NONMMUG034874.2	NA	48	0.0346	8mer
NONMMUG016683.3	NA	9	0.0454	7mer-A1

Moreover, among the 330 human targets (2915 transcripts), 151 lncRNA genes (650 transcripts) contained at least one canonical BS in their sequence. Lnc-SERPINB9-3, lnc-DALRD3-1, Lnc-NLRP12-1, lnc-ZNF705D-1-1, DIRC3 Antisense RNA 1 (DIRC3-AS1), Lnc-KLF10-2, and MMADHC Divergent Transcript (MMADHC-DT) were among the ten targets with the lowest *P-value* (Table 31).

Table. 31: Human lncRNA Let-7b targets with predicted canonical BSs.

The top 20 out of 151 lncRNA targets in HECs that contain predicted canonical BSs (8mer, 7mer-m8, and 7mer-A1) in any of their transcript variants (predicted by RNAhybrid) are shown. The genes are ranked based on the lowest adjusted *P-value* (significantly enriched in mouse RISC by let-7b mimic treatment using paired multiple comparisons Dunnett test, n=6) and the highest mean enrichment. NA, not applicable.

Gene ID	Gene name	Mean enrichment	*P*P-value	Predicted BSs in transcripts
NONHSAG042704.2	Lnc-SERPINB9-3	15	0.0001	7mer-m8

NONHSAG035049.3 (ENSG00000223343)	lnc-DALRD3-1	24	0.0005	8mer, 7mer-A1, 7mer-m8
NONHSAG053956.3	NA	14	0.0006	7mer-A1
NONHSAG026480.3 (ENSG00000232220)	Lnc-NLRP12-1	8	0.0006	7mer-A1
NONHSAG056997.1	NA	14	0.0008	7mer-m8
NONHSAG049580.3	lnc-ZNF705D-1-1	641	0.0009	7mer-A1, 7mer-m8
NONHSAG030500.3 (ENSG00000233143)	DIRC3-AS1	363	0.0009	7mer-A1, 7mer-m8
NONHSAG113557.1	NA	11	0.0013	7mer-m8
NONHSAG050957.2	Lnc-KLF10-2	9	0.0013	7mer-m8
NONHSAG029518.3 (ENSG00000231969)	MMADHC-DT	465	0.0014	8mer, 7mer-A1, 7mer-m8
NONHSAG004868.3	NA	14	0.0022	7mer-m8
NONHSAG015483.2	NA	229	0.0023	7mer-A1
NONHSAG017690.2	Lnc-BTBD1-2	15	0.0027	7mer-A1
NONHSAG062967.2	NA	59	0.0029	7mer-A1
NONHSAG072221.2	lnc-AGRP-5-2	18	0.0035	8mer, 7mer-A1, 7mer-m8
NONHSAG079454.2	NA	13	0.0036	8mer, 7mer-A1, 7mer-m8
NONHSAG030106.2	NA	23	0.0038	8mer
NONHSAG109858.1	NA	501	0.0040	7mer-A1
NONHSAG093996.1	NA	35	0.0040	8mer, 7mer-m8
NONHSAG037225.3 (ENSG00000249592)	lnc-CPLX1-2-3	55	0.0043	7mer-A1

Next, the lncRNA genes were compared between mice and humans based on the presence of a predicted canonical BS in at least one of their transcript sequences. The percent of lncRNAs containing a canonical BS was not significantly different between murine and human ECs (32% versus 45%). This data suggests that let-7b targets lncRNAs via canonical BSs to a similar extent in mice and humans (Fig. 22).

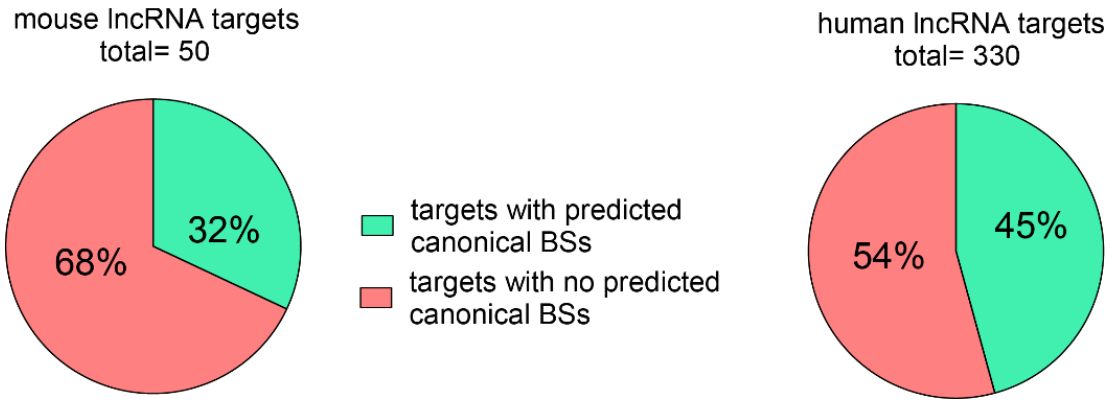

Fig. 22: Fractions of murine and human lncRNA targets according to their BSs.

Comparison of the percentage of lncRNA targets with or without a predicted canonical BS between MECs and HECs (Fisher's exact test, *P*= ns).

Among the total 34 BSs predicted in all let-7b lncRNA target transcripts in MECs, the percentage of 8mer, 7mer-m8, and 7mer-A1 BSs was 35%, 44%, and 21%, respectively (Fig. 23A). Additionally, omitting 11 replicate BSs (which were found more than once in different transcripts of the same lncRNA gene) revealed that among the remaining 23 BSs, 31% were 8mer, 44% were 7mer-m8, and 26% were 7mer-A1 BSs (Fig. 23C). Out of 1126 BSs predicted in human lncRNA transcripts, the percentage of 8mer, 7mer-m8, and 7mer-A1 BSs was 16.5%, 34%, and 50%, respectively (Fig. 23B). Omitting the replicate BSs resulted in 366 predicted BSs in human lncRNA targets that included 18% 8mer, 45% 7mer-m8, and 37% 7mer-A1 BSs (Fig. 23D).

The percentages of the three types of canonical BSs predicted in lncRNA transcripts were different between murine and human ECs ($P<0.01$) due to more 7mer-A1 BSs and fewer 8mer BSs in HECs than in MECs. However, this difference in the proportions of BSs was not observed when the replicate BSs were omitted (*P*=ns), indicating that the higher number of replicate lncRNA BSs in HECs were primarily 7mer-A1 BSs.

There was an equal distribution of different BS types in mouse lncRNAs on the transcript level (Fig. 23A) and gene level (Fig. 23C, *P*=ns). In contrast, in human lncRNAs, the observed distribution of different BSs deviated from an equal distribution (Fig. 23B and D, $P<0.0001$). These results indicate that 8mer let-7b BSs play a more critical role in murine than human lncRNAs.

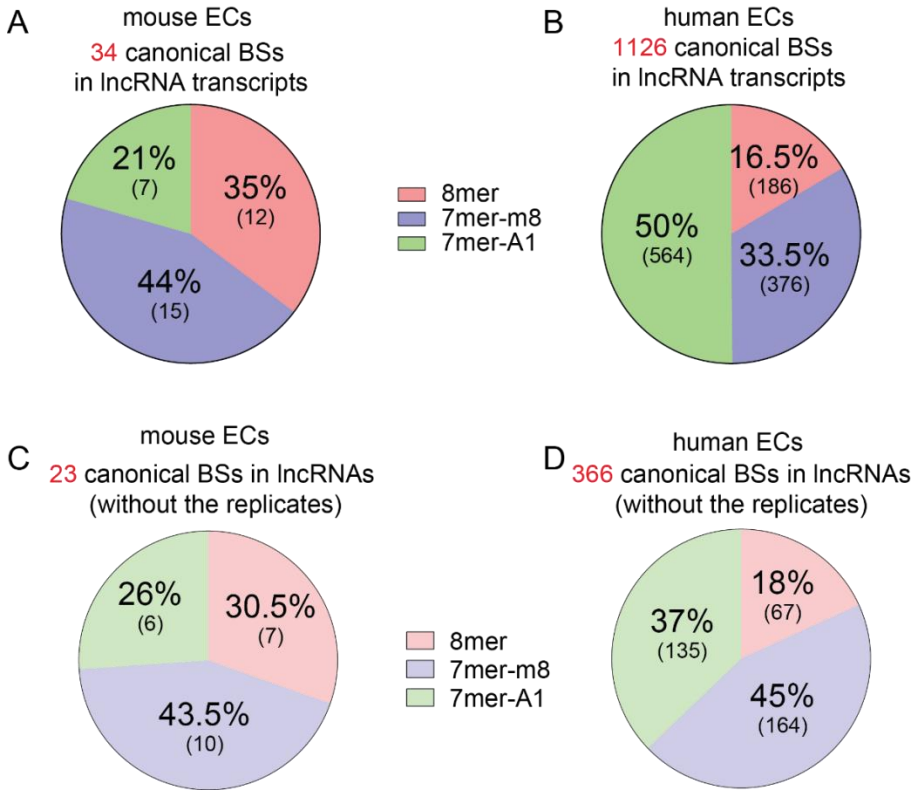

Fig. 23: Percentages of predicted canonical BSs in mouse and human lncRNA targets.

The canonical BSs in all transcripts of lncRNA let-7b targets were predicted by RNAhybrid. The percentage of the predicted 8mer, 7mer-m8, and 7mer-A1 BSs in lncRNA targets on the transcript level in mouse (A) and human (B) ECs were compared between the two species using the Chi-square test ($P<0.01$). The percentage of the predicted 8mer, 7mer-m8, and 7mer-A1 BSs in lncRNA targets on the gene level in mouse (C) and human (D) ECs were compared between the two species using the Chi-square test (P=ns). Characters in brackets show the number of BSs.

The presence of linked conserved genes in the loci of the 16 lncRNAs that contained a canonical BS in MECs was determined. Among those, six were located in a conserved stretch of linked genes also found in the human genome, including *LINCPINT*. Apart from LINCPINT, no other human lncRNA let-7b target was found in the remaining five conserved regions. Thus, LINCPINT is a conserved let-7b target in mouse and human ECs (Table 32 and Fig. 24 A-B).

Table. 32: Mouse lncRNA let-7b targets with conserved genomic loci.

The six lncRNA target genes in MECs (out of 16) located in the common stretch of linked genes in the murine and human genome are shown. Only LINCPINT was found in the conserved human region. NA, no conserved homologous lncRNA in this locus.

lncRNA mouse gene ID	lncRNA human gene ID	Mouse locus	Human locus	Linked genes in the locus
NONMMUG039682.2 (Expressed sequence R74862, ENSMUSG00000059277)	NA	Chr7 (q)	Chr11 (p15.5)	CD81, ASCL2, TSPAN32
NONMMUG034886.3 (Lincpint, ENSMUSG00000044471)	NONHSAG097344.2 (LINCPINT, ENSG00000231721)	Chr6 (q)	Chr7 (q32.3)	MKLN1, RNU6, MIR-29A, MIR29B1, KLF14, TSGA13
NONMMUG006955.2	NA	Chr11 (q)	Chr17 (q11.2)	PSMD11, CDK5R1, MYO1D, RHBLD
NONMMUG031918.3 (5031425E22Rik, ENSMUSG00000073147)	NA	Chr5 (q)	Chr7 (q22.3)	SRPK2, KMT2E, EIF4BP6
NONMMUG028848.2	NA	Chr4 (q)	Chr6 (q15)	RARS2 , AKININ2, SLC35A1, CFAP206
NONMMUG034874.2	NA	Chr6 (q)	Chr7 (q32.2)	MEST, TSGA13, COPG2, CEP41

Next, the sequence identity of the let-7b BSs between murine and human LINCPINT transcripts was studied. The LINCPINT transcript sequences were obtained from Ensembl 98, and canonical BSs were predicted by RNAhybrid. An identical 7mer-A1 BS was predicted in the ENSMUST00000230209.2 and ENST00000451786.5 LINCPINT transcripts (Fig. 24), which had a sequence homology of 84.5%. The identity of the 22 nucleotide-long sequences in let-7b BSs regions between mice and humans was 77% (Fig. 24C).

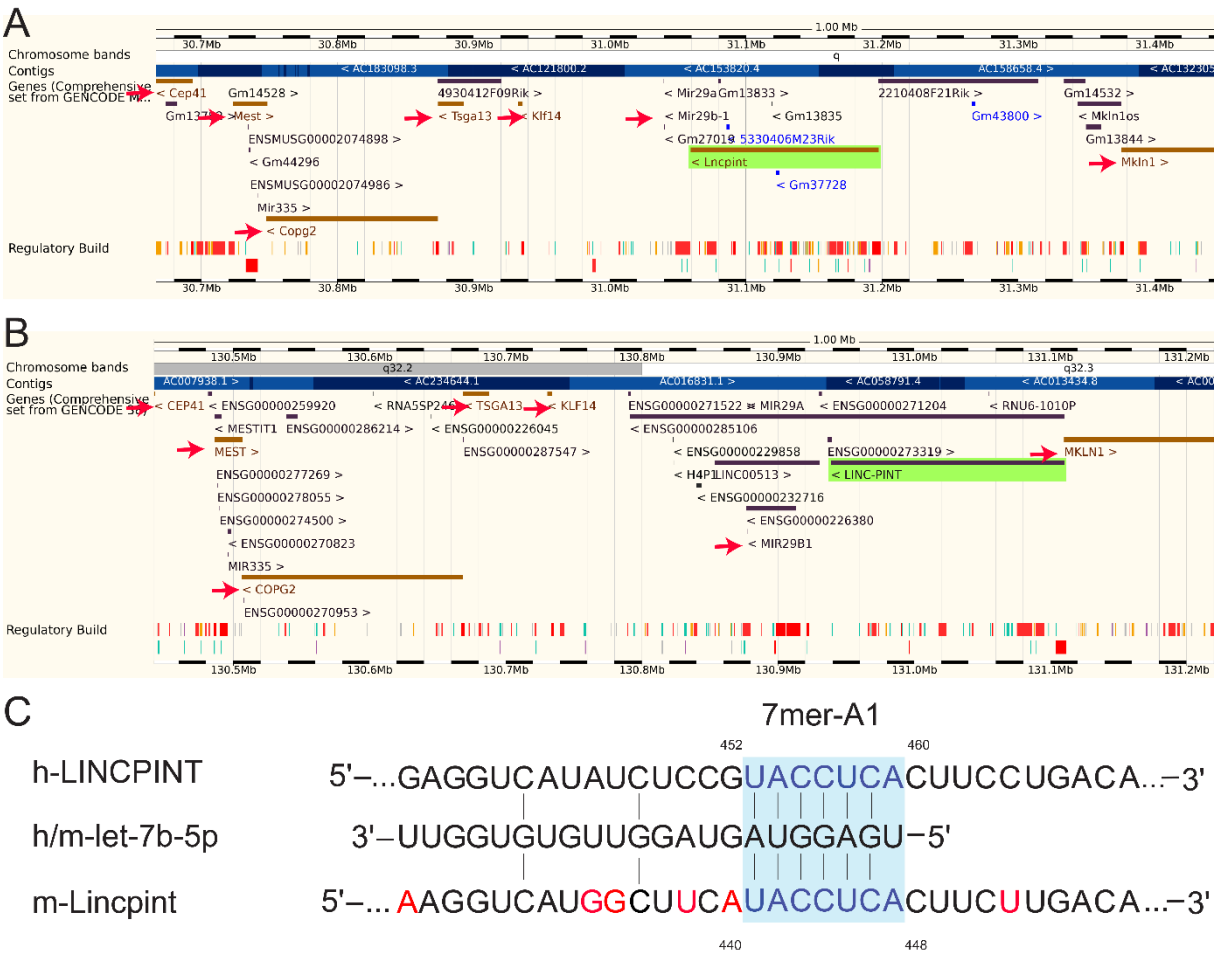

Fig. 24: Canonical let-7b BS in mouse and human LINCPINT.

The genomic locations of the LINCPINT gene (green) in (A) mice and (B) humans are shown (from Ensembl (91)). The gene is flanked by the same genes in both species (red arrows), indicating its conservation at the genomic level. (C) The 7mer-A1 BS (blue shaded area) in the LINCPINT transcript sequence is located between nucleotides 452 to 460 in humans (ENST00000451786.5) and nucleotides 440 to 448 in mice (ENSMUST00000230209.2). Red, mismatches between murine and human sequences in the BS region.

3.6. Let-7b-mediated regulation of protein expression in ECs

To investigate how overexpression of let-7b affects protein expression in MECs and HECs, liquid chromatography-tandem mass spectrometry (in collaboration with Prof. Imhof) was performed after treatment with let-7b mimics or control mimics for 24 h.

Among 3181 proteins detected in MECs (n = 4), 93 were differentially regulated [adj. P < 0.05, absolute fold change (FC) > 1.3] by let-7b mimic compared to control mimic treatment. Let-7b mimic treatment downregulated 60 proteins and upregulated 33 proteins in MECs (adj. P < 0.05, absolute FC > 1.3) (Fig. 25A). In HECs, 84 out of 3069 detected proteins (n = 4) were differentially regulated by let-7b mimic treatment (adj. P < 0.05, absolute FC > 1.3), including 40 downregulated and 44 upregulated proteins (Fig. 25B). Taken together, this data suggests that let-7b regulates protein expression in MECs and HECs to a similar extent (~ 3% of the proteome).

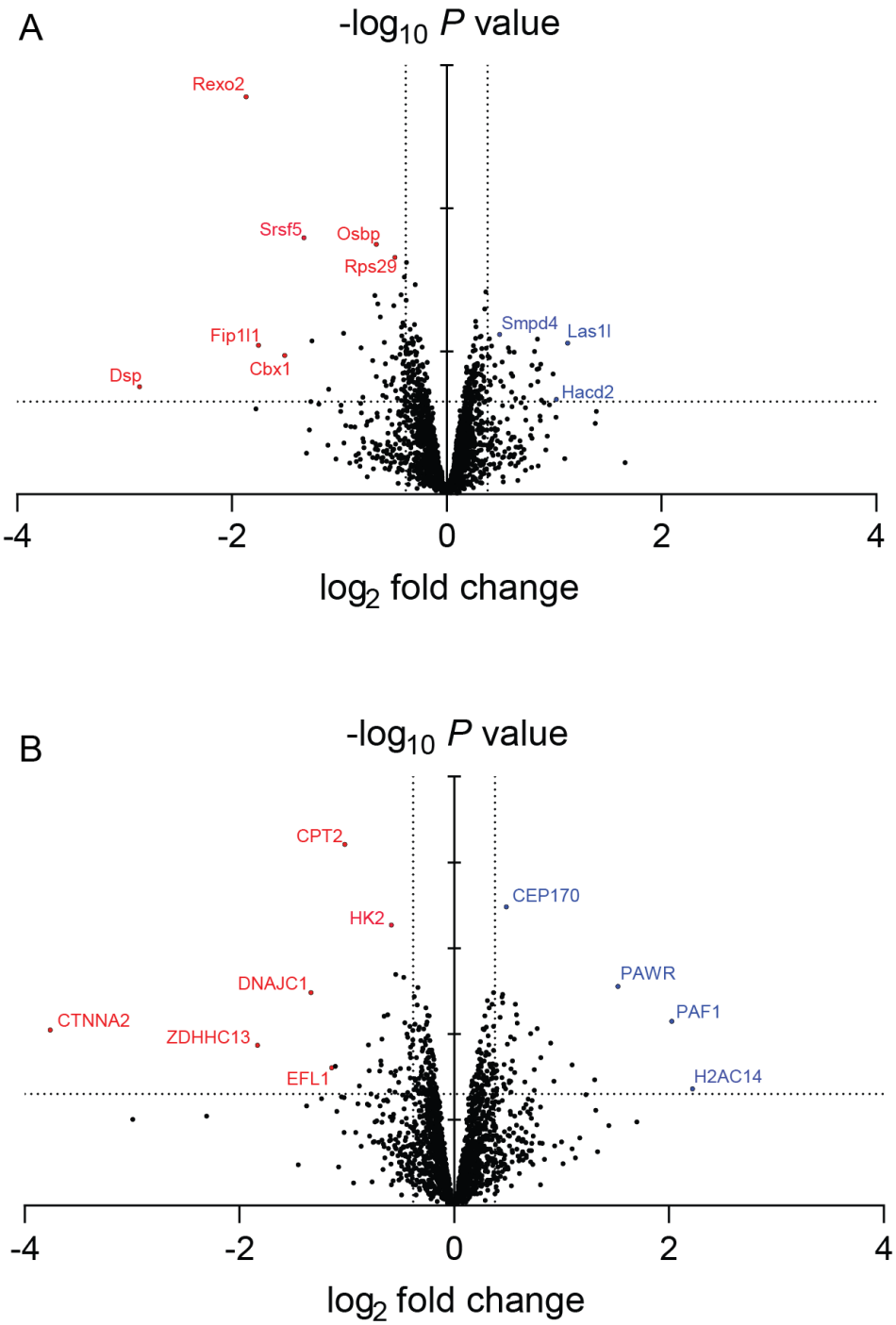

Fig. 25: Volcano plot presenting differentially regulated proteins after let-7b mimic treatment in ECs.

LC-MS/MS was performed on (A) MECs and (B) HECs treated with let-7b mimics and control mimics for 24 h (n=4). Proteins were quantified by MaxQuant, and data were compared between the let-7b mimic-treated cells and the control mimic-treated cells using the Limma test. An absolute 1.3-fold change (FC) cut-off was set for differentially regulated proteins (adj. P<0.05). Differential protein expression is shown in a Volcano plot. The top down- and upregulated proteins are shown in red and blue, respectively.

Functional enrichment analysis using g:GOSt in g:Profiler (https://biit.cs.ut.ee/gprofiler_archive3/e98_eg45_p14/gost) revealed that the proteins differentially regulated by let-7b in MECs were related to RNA binding, RNA processing, and splicing (Table 33).

Table. 33: Biological processes regulated by the differentially regulated proteins in MECs.

Significantly enriched biological process were determined by the g:profile web tool. Red and blue show down- and upregulated proteins by let-7b mimic treatment in MECs, respectively (GO; Gene Ontology, KEGG; Kyoto Encyclopedia of Genes and Genomes, REAC; Reactome, WP; WikiPathways).

Pathway ID	Description	*P* value	Genes
GO:0003723	RNA binding	0.0105	Srsf5, Ddx3y, Ddx39a, Eif3j1, Fus, Snrpe, Fip1l1, Tra2b, Ddx39b, Ascc3, Eif2ak2, Taco1, Mrpl13, Ddx51, Carhsp1, Mrps5, Zfp638
GO:0006396	RNA processing	0.0153	Fip1l1, Srsf5, Cdk11b, Ddx39b, Ddx39a, Snrpe, Fus, Ppp3ca, Tra2b, Zfp638, Ints6, Isy1, Ddx51, Prorp, Las1l
KEGG:03040	Spliceosome	0.0019	Srsf5, Ddx39b, Snrpe, Fus, Tra2b, Isy1
REAC:R-MMU-72203	Processing of capped intron-containing pre-mRNA	0.0143	Fip1l1, Srsf5, Ddx39b, Ddx39a, Snrpe, Fus, Tra2b, Isy1
REAC:R-MMU-8953854	Metabolism of RNA	0.0174	Srsf5, Rps29, Psmb6, Ddx39a, Fus, Snrpe, Fip1l1, Tra2b, Rplp1, Ddx39b, Las1l, Isy1
WP:WP310	mRNA processing	0.0033	Srsf5, Ddx39b, Ddx39a, Rps29, Eif2ak2, Snrpe, Fus, Tra2b, Zfp638, Fdx2

In MECs, downregulated proteins related to RNA metabolism and splicing (Table 33), such as Srsf5, Ddx39a/b, and Fus (Table 34), have been reported to promote proliferation. However, their effect on apoptosis has been reported to be variable (Table 34).

Table 34: Proteins related to the biological pathways regulated by let-7b in MECs.

The effects of these proteins on proliferation and apoptosis described in the literature are shown. NA; not applicable.

Gene ID	Gene description	Proliferation	Apoptosis	Reference
Ascc3	activating signal cointegrator 1 complex subunit 3	↑	NA	(114)
Ddx39a	DEAD box helicase 39a	↑	NA	(115)
Ddx39b	DEAD box helicase 39b	↑	NA	(116)
Ddx3y	DEAD-box helicase 3 Y-linked	↓	↓/↑	(117)/(118)
Eif2ak2	eukaryotic translation initiation factor 2-alpha kinase 2	NA	↑	(119)
Eif3j1	eukaryotic translation initiation factor 3, subunit J1	↑	↓	(120)
Fip1l1	FIP1 like 1 (S. cerevisiae)	↑	NA	(121)
Fus	fused in sarcoma	↑	↑	(122)/(123)
Ppp3ca	protein phosphatase 3 catalytic subunit alpha	↑	↓	(124)
Psmb6	proteasome 20S Subunit Beta 6	↑	NA	(125)
Rplp1	ribosomal protein lateral stalk subunit P1	↑	NA	(126)
Rps29	ribosomal protein S29	NA	↓	(127)
Snrpe	small nuclear ribonucleoprotein E	↑	NA	(128)
Srsf5	serine and arginine-rich splicing factor 5	↑	↓	(129)
Tra2b	transformer 2 beta	↑	↓	(130)/(131)

The proteins differentially regulated by let-7b in HECs were related to RNA-binding and metabolism, peptide biosynthesis, peptide metabolism, and translation (Table 35).

Table. 35: Biological processes related to the proteins differentially regulated by let-7b mimics in HECs.

Downregulated proteins are shown in red and upregulated proteins in blue. GO, Gene Ontology.

Pathway ID	Description	*P* value	Genes
GO:0003723	RNA binding	0.0016	RTF1, TIA1, PDIA4, MRPS31, EMG1, EFL1, NOL10, DIDO1, SF3B4, PUM1, TYMS, DDX19A, RPL29, TRIM21, CFAP20, GSPT1, MOV10, RPS29, PIN4, CELF1, ZNF638, ACO1, RNF20, PYM1
GO:0006518	peptide metabolic process	0.0011	DNAJC1, APP, TIA1, PDE12, MRPS31, PRNP, EFL1, PUM1, TYMS, RPL29, GSPT1, MTPN, MOV10, RPS29, CELF1, XPNPEP1, ACO1, PYM1
GO:0006412	translation	0.0014	DNAJC1, APP, TIA1, PDE12, MRPS31, EFL1, PUM1, TYMS, RPL29, GSPT1, MTPN, MOV10, RPS29, CELF1, ACO1, PYM1
GO:0043043	peptide biosynthetic process	0.0023	DNAJC1, APP, TIA1, PDE12, MRPS31, EFL1, PUM1, TYMS, RPL29, GSPT1, MTPN, MOV10, RPS29, CELF1, ACO1, PYM1
GO:0006417	regulation of translation	0.0072	DNAJC1, APP, TIA1, PDE12, PUM1, TYMS, GSPT1, MTPN, MOV10, CELF1, ACO1, PYM1
GO:0016071	mRNA metabolic process	0.0229	APP, SF3B4, TIA1, PSMA3, PDE12, PUM1, RPL29, PAF1, PRKACA, GSPT1, MOV10, RPS29 , CELF1, RNF20, PYM1

The downregulated proteins related to RNA metabolism in HECs were reported to promote cell proliferation, similar to MECs. In addition, these proteins' pro- and anti-apoptotic roles have been described (Table 36). These results indicate that let-7b overexpression regulates RNA metabolism in MECs and HECs via a separate set of proteins, which may increase proliferation. In contrast, their role in apoptosis appears variable (Table 36).

Table 36: Described functions of proteins related to the biological pathways regulated by let-7b in HECs.

The reported effects of these proteins on proliferation and apoptosis are shown. NA, not applicable.

Gene ID	Gene Description	Proliferation	Apoptosis	Reference
APP	amyloid beta precursor protein	↑	NA	(132)
DIDO1	death inducer obliterator	↑	↓/↑	(133)/(134)
EFL1	euphorbia factor L1	NA	↑	(135)
EMG1	EMG1 N1-specific pseudouridine methyltransferase	↑	NA	(136, 137)
PDIA4	protein disulfide isomerase 4	↑	↓	(138)/(139)
PUM1	pumilio RNA binding family member 1	↑	↓	(140)/(141)
SF3B4	splicing factor 3b subunit 4	↑	NA	(142)
TIA1	T-cell intracellular antigen-1	↑	↑	(143)/(144)
TYMS	thymidylate synthetase	↑	↓	(145)

3.6.1 Let-7b-mediated downregulation of protein expression in ECs

Among the proteins downregulated by let-7b mimic treatment in MECs, Ppp3ca was significantly enriched in the RISC by let-7b mimic treatment in MECs. It contained a predicted conserved 7mer-A1 BS (P_{CT}=0.84). In contrast, the down-regulated proteins high mobility group box 2 (Hmgb2), a let-7b target in MECs, and Fus, a common let-7b target in MECs and HECs, did not contain canonical BSs. Among the downregulated proteins in MECs, GA repeat binding protein alpha (Gabpa) and VPS26 retromer complex component B (Vps26b) had highly conserved canonical BSs (P_{CT}>0.8); however, they were not included in the analysis of gene enrichment by let-7b mimic in ECs (NA) (Table 37). Ankyrin repeat and FYVE domain containing 1 (Ankfy1) included a highly conserved 8mer BSs according to TargetScan; however, let-7b mimic treatment did not significantly enrich Ankfy1 in the RISC of MECs (see section 3.1.1).

Table. 37: Downregulated proteins after let-7b mimic treatment in MECs.

Downregulated proteins (adj. $P<0.05$, absolute FC>1.3, Limma test, n=4 replicates per group) are ranked according to the lowest *P* value and greatest fold change. The canonical BS and P_{CT} value was obtained from mouse TargetScan. The significantly enriched gene transcript in the RISC by let-7b mimic treatment in ECs was an identified let-7b target (NA, not applicable). Genes involved in RNA binding, processing, and metabolism are shown in red.

Protein	Gene description	Uniprot ID	Fold change	Adj. *P* value	Canonical BS (TargetScan P_{CT})	let-7b target (*P* value of enrichment compared to GAPDH)
Rexo2	RNA exonuclease 2	Q9D8S4	-3,65	0.0000027		NA
Srsf5	serine and arginine-rich splicing factor 5	Q9D8S5	-2,51	0.00026		no (0.101)
Osbp	oxysterol binding protein	Q3B7Z2	-1,58	0.00032		NA
Rps29	ribosomal protein S29	P62274	-1,40	0.00049		no (0.9999)
Gabpa	GA repeat binding protein. alpha	Q00422	-1,31	0.00091	7mer-A1 (0.82)	NA
Fgd5	FYVE, RhoGEF and PH domain containing 5	E9QKY4	-1,31	0.00094		no (0.6848)
Snx3	sorting nexin 3	Q78ZM0	-1,34	0.00162		no (0.8542)
Try10	trypsin 10	Q792Z1	-1,59	0.00166		NA
Psmb6	proteasome (prosome, macropain) subunit, beta type 6	Q60692	-1,30	0.00192		NA
Ddx3y	DEAD box helicase 3, Y-linked	Q62095	-1,56	0.00217		NA
Ddx39a	DEAD box helicase 39a	Q8VDW0	-1,41	0.00229	7merA1	NA
Kctd12	potassium channel tetramerisation domain containing 12	Q6WVG3	-1,54	0.00328		NA
Pdlim1	PDZ and LIM domain 1 (elfin)	O70400	-1,33	0.00397	7merA1	NA
Eif3j1	eukaryotic translation initiation factor 3, subunit J1	Q3UGC7	-1,32	0.00411		NA
Fus	fused in sarcoma	Q8CFQ9	-1,31	0.00434	no canonical	yes (0.0346)
Gopc	golgi associated PDZ and coiled-coil motif containing	A0A1W2P7V0	-1,34	0.00456		NA
Snrpe	small nuclear ribonucleoprotein E	P62305	-1,34	0.00463		NA
Ms4a6d	membrane-spanning 4-domains, subfamily A, member 6D	Q99N07	-1,95	0.00560		NA
Clint1	clathrin interactor 1	Q5SUH7	-1,34	0.00602		no (0.8542)
Clic4	chloride intracellular channel 4 (mitochondrial)	Q9QYB1	-1,32	0.00701		NA
Actr10	ARP10 actin-related protein 10	Q9QZB7	-2,39	0.00718		no (0.4995)
Csrp2	cysteine and glycine-rich protein 2	A0A1W2P845	-1,49	0.00749		NA
Fip1l1	FIP1 like 1 (S. cerevisiae)	Q9D824	-3,37	0.00820		no (0.1119)
Tra2b	transformer 2 beta	F8WJG3	-1,30	0.00862		NA
Hdgf	heparin binding growth factor	P51859	-1,34	0.00887		NA
Ppp4r2	protein phosphatase 4, regulatory subunit 2	A0A0N4SV05	-1,74	0.00893		no (0.5888)

Ppp3ca	protein phosphatase 3, catalytic subunit. alpha isoform	P63328	-1,30	0.01006	7mer-A1 (0.84)	yes (0.0255)
Adgrg1	adhesion G protein-coupled receptor G1	Q8K209	-1,30	0.01091		NA
Rplp1	ribosomal protein, large. P1	P47955	-1,35	0.01106		NA
Cbx1	chromobox 1	P83917	-2,84	0.01133		NA
Ddx39b	DEAD box helicase 39b	Q9Z1N5	-1,42	0.01199		NA
Sar1a	secretion associated Ras related GTPase 1A	Q99JZ4	-1,39	0.01231		no (0.9991)
Ascc3	activating signal cointegrator 1 complex subunit 3	E9PZJ8	-1,61	0.01340		no (0.9913)
Abcf1	ATP-binding cassette. sub-family F (GCN20). member 1	Q6P542	-1,32	0.01375		NA
Ptma	prothymosin alpha	P26350	-1,33	0.01492		no (0.9997)
Mlec	malectin	Q6ZQI3	-1,49	0.01498		NA
Pdlim7	PDZ and LIM domain 7	Q3TJD7	-1,30	0.01614	7merA1	no (0.8632)
Pip4k2c	phosphatidylinositol-5-phosphate 4-kinase, type II, gamma	Q91XU3	-1,31	0.01969		NA
Lgals1	lectin. galactose binding, soluble 1	P16045	-1,33	0.02026		NA
Nmt2	N-myristoyltransferase 2	O70311	-1,57	0.02239	7merA1	no (0,0913)
Washc5	WASH complex subunit 5	Q8C2E7	-1,41	0.02350		no (0.3233)
Ssrp1	structure specific recognition protein 1	A2AW05	-1,32	0.02504		NA
Smim7	small integral membrane protein 7	F8WIU9	-1,42	0.02559		NA
Igfbp4	insulin-like growth factor binding protein 4	P47879	-1,49	0.02636		no (0.4739)
Hao2	hydroxyacid oxidase 2	Q9NYQ2	-1,43	0.02907		NA
Rpl21	ribosomal protein L21	Q9CQM8	-1,48	0.02998		no (0.9994)
Lig3	ligase III, DNA, ATP-dependent	Q3UC82	-1,31	0.03070		NA
Dsp	desmoplakin	E9Q557	-7,27	0.03134		NA
Pip4k2b	phosphatidylinositol-5-phosphate 4-kinase, type II, beta	Q80XI4	-1,34	0.03384		NA
Metap1	methionyl aminopeptidase 1	Q8BP48	-2,14	0.03402		NA
Ankfy1	ankyrin repeat and FYVE domain containing 1	Q810B6	-1,32	0.03451	8mer (0.91)	no (0.186)
Mindy1	MINDY lysine 48 deubiquitinase 1	Q76LS9	-1,39	0.03555		NA
Hmgb2	high mobility group box 2	P30681	-1,31	0.03634	no canonical	yes (0.0046)
Vps13c	vacuolar protein sorting 13C	Q8BX70	-1,51	0.04131	7merA1	NA
Vps26b	VPS26 retromer complex component B	Q8C0E2	-1,31	0.04353	7mer-m8 (0.9)	NA

Cdk11b	cyclin-dependent kinase 11B	A2A9P6	-1,48	0.04354		NA
Osbpl9	oxysterol binding protein-like 9	Q5FWX7	-1,72	0.04369		no (0.2201)
Eif2ak2	eukaryotic translation initiation factor 2-alpha kinase 2	Q03963	-1,38	0.04523		no (0.9997)
Sec61b	Sec61 beta subunit	Q9CQS8	-1,34	0.04869		NA
Mcm7	minichromosome maintenance complex component 7	Q61881	-1,31	0.04895		NA

Among the proteins downregulated by let-7b mimic treatment in HECs, golgin A4 (GOLGA4) was among the common 23 let-7b targets with an identical BS in mice and humans (Table 38). Additionally, the downregulated protein heparan sulfate proteoglycan 2 (HSPG2), one of the 153 common let-7b targets, did not have a predicted canonical BS. Moreover, the downregulated proteins hexokinase 2 (HK2), DNA damage-inducible 1 homolog 2 (DDI2), amyloid beta precursor protein (APP) and nucleolar protein 10 (NOL10) were significantly enriched in the RISC by let-7b mimic treatment in HECs. However, in contrast to APP and NOL10, which did not contain a predicted canonical BS, conserved canonical BSs were predicted in the HK2 and DDI2 3'–UTR sequences. In addition, 7b mimic treatment downregulated phosphodiesterase 12 (PDE12), TIA1, and DnaJ heat shock protein family member C1 (DNAJC1) in HECs at the protein level but did not significantly enrich them in the RISC. However, PDE12, TIA1, and DNAJC1 had predicted conserved canonical BSs (Table 38).

Table. 38: Downregulated proteins after let-7b mimic treatment in HECs.

Downregulated proteins (adj. $P < 0.05$ by Limma test, absolute FC > 1.3, n = 4 per group) are ordered according to the lowest *P*-value and greatest fold change. The canonical BSs and P_{CT} values were derived from TargetScan. The significantly enriched gene transcripts in the RISC by let-7b mimic treatment in ECs were considered as let-7b targets. Genes involved in RNA-binding, RNA-translation, and RNA-metabolism are shown in red. NA, not applicable.

Protein	Gene description	Uniprot ID	Fold change	Adj. *P*-value	BS (P_{CT})	let-7b target (*P* value of enrichment compared to GAPDH)
CPT2	carnitine palmitoyltransferase 2	A0A1B0GTB8	-2.02	0,000062	7mer-A1	NA
HK2	hexokinase 2	E9PB90	-1.50	0.0005	7mer-A1 (0.81)	yes (0.0046)
RTF1	RTF1 homolog, Paf1/RNA polymerase II complex component	Q92541	-1.46	0.0020		no (0.0723)
GOLGA4	golgin A4	Q13439	-1.38	0.0022	7mer-A1 (0.73)	yes (0.0246)
DNAJC1	DnaJ heat shock protein family (Hsp40) member C1	Q96KC8	-2.52	0.0033	7mer-A1 (0.86)	no (0.9269)
APP	amyloid beta precursor protein	P05067	-1.54	0.0060	no canonical BS	yes (0.0299)
PNKP	polynucleotide kinase 3'-phosphatase	A0A0D9SFL2	-1.57	0.0062		NA
TIA1	TIA1 cytotoxic granule associated RNA binding protein	F8W8I6	-1.37	0.0074	7mer-m8 (0.6)	no (0.0546)
PSMA3	proteasome 20S subunit alpha 3	P25788	-1.37	0.0077		no (0.988)
RANBP3	RAN binding protein 3	Q9H6Z4	-1.33	0.0081		NA
CTNNA2	catenin alpha 2	P26232	-13.57	0.0090		NA
DDB2	damage specific DNA binding protein 2	Q92466	-1.30	0.0091		NA
PDIA4	protein disulfide isomerase family A member 4	A0A499FI48	-1.35	0.0099		no (0.9968)
PDE12	phosphodiesterase 12	F6T1Q0	-1.35	0.0109	8mer, 7mer-m8 (0.98)	no (0.121)
RFT1	RFT1 homolog	Q96AA3	-1.59	0.0115	8mer	NA
LAMA4	laminin subunit alpha 4	A0A0A0MTC7	-1.30	0.0116	7mer-A1	no (0.0743)
MRPS31	mitochondrial ribosomal protein S31	Q92665	-1.31	0.0133		NA
SORD	sorbitol dehydrogenase	Q00796	-1.74	0.0134		NA
ZDHHC13	zinc finger DHHC-type palmitoyltransferase 13	Q8IUH4	-3.56	0.0135		NA
GIPC2	GIPC PDZ domain containing family member 2	Q8TF65	-1.32	0.0142	7mer-A1	NA
NDUFAF4	NADH:ubiquinone oxidoreductase complex assembly factor 4	Q9P032	-1.33	0.0148		no (0.9966)
M6PR	mannose-6-phosphate receptor, cation dependent	P20645	-1.33	0.0169	7mer-m8	no (0.9587)
IGFBP7	insulin-like growth factor binding protein 7	Q16270	-1.33	0.0188		no (0.6267)
PRNP	prion protein	P04156	-1.61	0.0205		no (0.9961)
CLCC1	chloride channel CLIC like 1	Q96S66	-1.60	0.0228		no (0.9966)
EMG1	EMG1 N1-specific pseudouridine methyltransferase	Q92979	-2.15	0.0238		NA
EFL1	elongation factor like GTPase 1	Q7Z2Z2	-2.20	0.0248		NA

TNFRSF10B	TNF receptor superfamily member 10b	O14763	-1.34	0.0253		no (0.2249)
NOL10	nucleolar protein 10	Q9BSC4	-1.41	0.0253	no canonical BS	yes (0.0145)
DIDO1	death inducer-obliterator 1	Q9BTC0	-1.73	0.0267		no (0.1665)
BNIP1	BCL2 interacting protein 1	Q12981	-1.46	0.0270		NA
DDI2	DNA damage-inducible 1 homolog 2	Q5TDH0	-1.62	0.0270	8mer (0.96)	yes (0.0253)
ETV6	ETS variant transcription factor 6	P41212	-1.50	0.0282		NA
SF3B4	splicing factor 3b subunit 4	Q15427	-1.47	0.0305		NA
PUM1	pumilio RNA binding family member 1	H0YDK8	-1.33	0.0326		no (0.9993)
TYMS	thymidylate synthetase	P04818	-1.43	0.0364		NA
PTPRF	protein tyrosine phosphatase receptor type F	P10586	-1.84	0.0403		no (0.9968)
SEPTIN10	septin 10	E7EW69	-1.52	0.0459		no (0.9968)
HSPG2	heparan sulfate proteoglycan 2	P98160	-1.47	0.0475	no canonical BS	yes (0.0284)
PRKAA1	protein kinase AMP-activated catalytic subunit alpha 1	Q13131	-1.35	0.0479		no (0.4055)

This data indicates that let-7b can downregulate targets at the protein level via non-canonical BSs.

Among the 23 let-7b targets identical in mice and humans, only GOLGA4 was downregulated (adj. P = 0.0021, FC = –1.38) in HECs. Protein expression of the remaining targets was either not determined or was not significantly regulated by let-7b mimic treatment (Table 39).

Table 39: Effect of let-7b mimic treatment on the protein expression of the 23 targets identical in MECs and HECs.

The fold change of the protein expression after let-7b mimic compared with control treatment is shown. The adjusted *P*-values were obtained by the Limma test (n = 4 per group). NA, not applicable.

Protein	MECs		HECs	
	Fold change	Adj. *P*-value	Fold change	Adj. *P*-value
MLLT10	NA	NA	NA	NA
TET2	NA	NA	NA	NA
RBMS1	1.14	0.6677	1.07	0.5127
UHRF2	NA	NA	-1.0008	0.9893
KMT2E	NA	NA	NA	NA
CHD9	NA	NA	NA	NA
TSC22D2	NA	NA	NA	NA
CSNK2A1	-1.03	0.7186	1.01	0.8649
XRN1	NA	NA	NA	NA
DYRK1A	NA	NA	NA	NA
CHD4	-1.03	0.5763	-1.04	0.4839
SBNO1	NA	NA	NA	NA
EIF5B	-1.08	0.2789	1.06	0.2651
GOLGA4	NA	NA	-1.38	0.0021
SENP5	NA	NA	NA	NA
PKN2	NA	NA	NA	NA
SLK	-1.05	0.4600	1.15	0.1339
MSN	-1.19	0.0158	1.04	0.4994
MGAT4A	-1.12	0.7442	NA	NA
SYNCRIP	1.005	0.9241	-1.06	0.2906
CGNL1	1.103	0.1598	1.08	0.2770
KPNA1	-1.015	0.7895	1.21	0.0324
EXOC5	-1.16	0.0415	1.24	0.0105

3.6.2 Let-7b-mediated upregulation of protein expression in ECs

In MECs, let-7b mimic treatment upregulated lysophosphatidylglycerol acyltransferase 1 (Lpgat1), sacsin molecular chaperone (Sacs), and pleckstrin homology and RhoGEF domain containing G1 (Plekhg1) and significantly enriched them also in the RISC. Lpgat1 included a 7mer-A1 and a 7mer-m8 BS with a $P_{CT} > 0.99$ (predicted by TargetScan), and Sacs contained a predicted 7mer-A1 BS predicted by RNAhybrid. Additionally, among the proteins upregulated by let-7b mimic treatment, Plekhged had no predicted BS. Among the upregulated proteins with a conserved BS, let-7b mimic treatment enriched PRKC apoptosis

WT1 regulator (PAWR), phosphoglucomutase 2-like 1 (PGM2L1), and CUGBP Elav-like family member 1 (CELF1) in the RISC of HECs but not MECs (Table 40).

Table. 40: Upregulated proteins after let-7b mimic treatment in MECs.

Upregulated proteins ($P < 0.05$ by Limma test, FC > 1.3, n = 4) are ordered according to the lowest *P*-value and greatest fold change. The canonical BSs and P_{CT} values were determined by TargetScan. The significantly enriched gene transcript in the RISC by let-7b mimic treatment in ECs was considered a let-7b target. Genes involved in RNA-binding, RNA-processing, and RNA-metabolism are shown in blue. NA, not applicable.

Protein	Gene description	Uniprot ID	Fold change	Adj. *P* value	BS (TargetScan P_{CT})	let-7b target (*P* value of enrichment compared to GAPDH)
Smpd4	sphingomyelin phosphodiesterase 4	A0A338P735	1.41	0.0058		NA
Taco1	translational activator of mitochondrially encoded cytochrome c oxidase I	Q8K0Z7	1.32	0.0067		NA
P3h1	prolyl 3-hydroxylase 1	A2A7Q5	1.80	0.0067		NA
Las1l	LAS1-like (S. cerevisiae)	A2BE28	2.18	0.0076		NA
Scrib	scribbled planar cell polarity	Q80U72	1.34	0.0084		NA
Rer1	retention in endoplasmic reticulum sorting receptor 1	Q9CQU3	1.49	0.0090		NA
Clip2	CAP-GLY domain-containing linker protein 2	Q9Z0H8	1.76	0.0100		NA
Isy1	ISY1 splicing factor homolog	Q69ZQ2	1.50	0.0101		NA
Sacs	sacsin	E9QNY8	1.55	0.0102	7mer-A1	yes (0.0028)
Lpgat1	lysophosphatidylglycerol acyltransferase 1	Q91YX5	1.31	0.0117	7mer-A1/7mer-m8 (> 0.99)	NA
Nrbp1	nuclear receptor binding protein 1	Q99J45	1.32	0.0122		NA
Man1a2	mannosidase, alpha, class 1A, member 2	P39098	1.43	0.0140		NA
Erlin1	ER lipid raft associated 1	Q91X78	1.83	0.0151		NA
Rfc1	replication factor C (activator 1) 1	A0A0N5E9G7	1.73	0.0156		NA
Mrpl13	mitochondrial ribosomal protein L13	Q9D1P0	1.36	0.0157		NA
Cisd2	CDGSH iron sulfur domain 2	Q9CQB5	1.81	0.0173		NA
Swi5	SWI5 recombination repair homolog (yeast)	V9GXX7	1.79	0.0179		NA
Mlkl	mixed lineage kinase domain-like	Q9D2Y4	1.52	0.0205		NA
Atp8a1	ATPase, aminophospholipid transporter (APLT), class I, type 8A, member 1	A0A0M3HEP7	1.99	0.0206		NA
Ddx51	DEAD box helicase 51	Q6P9R1	1.53	0.0221		NA

Pdia5	protein disulfide isomerase associated 5	Q921X9	1.36	0.0232		NA
Carhsp1	calcium regulated heat stable protein 1	Q9CR86	1.42	0.0262		NA
Dnajc5	DnaJ heat shock protein family (Hsp40) member C5	P60904	1.32	0.0262		NA
Plekhg1	pleckstrin homology domain containing, family G (with RhoGef domain) member 1	F6S200	1.80	0.0265		yes (0.0118)
Emc4	ER membrane protein complex subunit 4	Q9CZX9	1.33	0.0295		NA
Mrps5	mitochondrial ribosomal protein S5	Q99N87	1.72	0.0299		NA
Ints6	integrator complex subunit 6	Q6PCM2	1.44	0.0308		NA
Ube3c	ubiquitin protein ligase E3C	Q80U95	1.52	0.0373		NA
Prorp	protein only RNase P catalytic subunit	V9GXP4	1.64	0.0443		NA
Fdx2	ferredoxin 2	Q9CPW2	1.56	0.0457		NA
Zfp638	zinc finger protein 638	A0A0N4SV80	1.32	0.0469		NA
Hacd2	3-hydroxyacyl-CoA dehydratase 2	Q9D3B1	2.03	0.0471		NA
Itgb4	integrin beta 4	A2A863	1.84	0.0480		NA

Screening of the human TargetScan database revealed that among the upregulated proteins in HECs, DEAD box polypeptide 19A (DDX19A) and ribonucleotide reductase M2 (RRM2) had a predicted canonical conserved 8mer BS (P_{CT}=0.96). In addition, ring finger protein 20 E3 ubiquitin-protein ligase (RNF20) contained a conserved 7mer-m8 site. Moreover, osteoclast stimulating factor 1 (OSTF1) had a conserved canonical 7mer-A1 BS. In addition to the enrichment in the RISC, let-7b mimic treatment upregulated myotrophin (MTPN), aconitase 1 (ACO1), centrosomal protein 170 (CEP170), NUMB endocytic adaptor protein (NUMB), glutamine--fructose-6-phosphate transaminase 1 (GFPT1), and spartin (SPART) at the protein level in HECs. Notably, RNAhybrid predicted a 7mer-A1 BS in the 3'-UTR of MTPN. This data indicates that the interaction between let-7b and the 3'–UTRs may upregulate the target at the protein level (Table 41).

Table. 41: Upregulated proteins after let-7b mimic treatment in HECs.

Upregulated proteins ($P < 0.05$ by Limma test, FC > 1.3) are ordered according to the lowest P-value and greatest fold change. The canonical BSs and PCT values were identified by TargetScan. Genes significantly enriched in the RISC by let-7b mimic treatment were considered let-7b targets. Genes involved in RNA-binding, RNA-translation, and RNA-metabolism are shown in blue. NA, not applicable.

Protein	Gene description	Uniprot ID	Fold change	Adj. *P* value	BS (TargetScan P_{CT})	let-7b target (*P* value of enrichment compared to GAPDH)
CEP170	centrosomal protein 170	H0Y2V6	1.40	0.0003		yes (0.032)
PAWR	pro-apoptotic WT1 regulator	Q96IZ0	2.88	0.0028	7mer-m8 (0.7)	yes (0.0291)
SPART	spartin	Q8N0X7	1.37	0.0034		yes (0.0044)
DDX19A	DEAD-box helicase 19A	I3L0H8	1.36	0.0037	8mer (0.96)	NA
RPL29	ribosomal protein L29	P47914	1.37	0.0043		NA
GAPVD1	GTPase activating protein and VPS9 domains 1	F8W9S7	1.49	0.0045		NA
GFPT1	glutamine--fructose-6-phosphate transaminase 1	Q06210	1.50	0.0060		yes (0.0448)
ERGIC3	ERGIC and golgi 3	H0Y621	1.35	0.0064		NA
PAF1	PAF1 homolog, Paf1/RNA polymerase II complex component	Q8N7H5	4.08	0.0071		NA
TBCB	tubulin folding cofactor B	K7EK42	1.50	0.0075		NA
RAP1GDS1	Rap1 GTPase-GDP dissociation stimulator 1	P52306	1.71	0.0087		NA
CHMP1A	charged multivesicular body protein 1A	F8VUA2	1.64	0.0099		NA
TRIM21	tripartite motif containing 21	P19474	1.44	0.0108		no (0.1313)
ACACA	acetyl-CoA carboxylase alpha	Q13085	1.47	0.0114		no (0.2105)
MIF	macrophage migration inhibitory factor	P14174	1.87	0.0127		NA
PRKACA	protein kinase cAMP-activated catalytic subunit alpha	P17612	1.41	0.0131		no (0.0931)
CFAP20	cilia and flagella associated protein 20	Q9Y6A4	1.75	0.0189		NA
OSTF1	osteoclast stimulating factor 1	Q92882	1.46	0.0205	7mer-A1 (0.93)	NA
GSPT1	G1 to S phase transition 1	P15170	1.38	0.0227		no (0.1265)
PRKD2	protein kinase D2	Q9BZL6	2.14	0.0228		NA
PKN1	protein kinase N1	Q16512	1.31	0.0229		no (0.7788)
KIF4A	kinesin family member 4A	O95239	1.44	0.0254		NA
HACL1	2-hydroxyacyl-CoA lyase 1	Q9UJ83	1.68	0.0261		NA
MTPN	myotrophin; leucine zipper protein 6	P58546	1.32	0.0268	7mer-A1	yes (0.0043)
MOV10	Mov10 RISC complex RNA helicase	Q9HCE1	1.48	0.0281		NA
PIGT	phosphatidylinositol glycan anchor biosynthesis class T	A0A1W2PNP0	1.36	0.0323		NA
UFC1	ubiquitin-fold modifier conjugating enzyme 1	Q9Y3C8	1.35	0.0324		no (0.9919)
PGLS	6-phosphogluconolactonase	O95336	1.31	0.0325		NA
RPS29	ribosomal protein S29	P62273	2.48	0.0343		no (0.8503)
VPS25	vacuolar protein sorting 25 homolog	K7EKV4	1.43	0.0350		NA
PGM2L1	phosphoglucomutase 2 like 1	Q6PCE3	1.44	0.0353	7mer-A1/7mer-m8 (> 0.99)	yes (0.0099)

PIN4	peptidylprolyl cis/trans isomerase, NIMA-interacting 4	Q9Y237	1.91	0.0356		NA
NUMB	NUMB endocytic adaptor protein	P49757	1.58	0.0360		yes (0.0051)
EML4	EMAP like 4	Q9HC35	1.43	0.0371		NA
CELF1	CUGBP Elav-like family member 1	Q92879	1.42	0.0374	7mer-A1 (> 0.99)	yes (0.0125)
XPNPEP1	X-prolyl aminopeptidase 1	Q9NQW7	1.38	0.0382		NA
ZNF638	zinc finger protein 638	Q14966	1.38	0.0410		no (0.0761)
ACO1	aconitase 1	P21399	1.32	0.0430		yes (0.0137)
H2AC14	H2A clustered histone 14	Q99878	4.66	0.0435		NA
RRM2	ribonucleotide reductase regulatory subunit M2	P31350	1.39	0.0437	8mer (0.96)	no (0.9994)
PLCB3	phospholipase C beta 3	Q01970	1.40	0.0441		no (0.2895)
RNF20	ring finger protein 20	Q5VTR2	1.68	0.0451	7mer-m8 (0.97)	NA
PYM1	PYM homolog 1, exon junction complex associated factor	Q9BRP8	1.31	0.0459		NA
IPO4	importin 4	Q8TEX9	1.44	0.0473		NA

Let-7b mimic treatment in MECs and HECs did not regulate endothelial differentiation markers or inflammatory factors compared to control-treated cells (Table 42). This data suggests that let-7b overexpression does not affect EC activation.

Table. 42: Regulation of endothelial differentiation markers and inflammatory genes by let-7b in ECs.

LC-MS/MS was performed on MECs and HECs treated with let-7b and control mimics for 24 h (n = 4). EC identification/activation markers have a fold change (FC) of less than 1.3 and a P-value of more than 0.05.

EC differentiation or activation marker	MECs		HECs	
	Fold change	**Adj. *P* value**	**Fold change**	**Adj. P value**
CDH2 (cadherin 2; neural cadherin)	1.612	0.215	NA	NA
CDH5 (cadherin 5; vascular endothelial cadherin)	1.038	0.544	-1.083	0.330
CCL2 (chemokine (C-C motif) ligand 2; monocyte chemotactic and activating factor)	1.161	0.153	NA	NA
CD34 (CD34 antigen)	-1.06	0.445	-1.153	0.065
EGFR (Epidermal growth factor receptor)	NA	NA	1.038	0.796
NOS3 (nitric oxide synthase 3, endothelial cell)	-1.002	0.973	1.006	0.967
VWF (Von Willebrand factor)	1.024	0.856	1.297	0.133
ICAM1 (intercellular adhesion molecule 1)	NA	NA	1.132	0.084
ICAM2 (intercellular adhesion molecule 2)	-1.052	0.337	-1.141	0.060
NCAM1 (neural cell adhesion molecule 1)	1.039	0.597	NA	NA
PECAM1 (platelet/endothelial cell adhesion molecule 1; CD31)	-1.014	0.820	1.007	0.917
VCAM1 (vascular cell adhesion molecule 1)	1.246	0.592	NA	NA
PTGS1 (prostaglandin-endoperoxide synthase 1; cyclooxygenase-1)	-1.001	0.988	1.067	0.370
SELP (selectin P; platelet activation dependent granule-external membrane protein)	1.022	0.802	NA	NA
TGFB1 (transforming growth factor, beta 1)	1.077	0.266	NA	NA
THBD (thrombomodulin)	1.138	0.230	1.032	0.783

3.7. Let-7b-mediated regulation of UHRF2 expression in ECs

UHRF2 was not detectable in let-7b mimic-treated MECs by mass spectrometry, probably due to its suppression by the endogenous let-7 expression. To test this hypothesis, MECs and HECs were treated with an inhibitor of let-7b, and the effect of this treatment on the UHRF2 protein level was determined by enzyme-linked immunosorbent assay (ELISA).

Let-7b inhibitor treatment (n= 4–6) decreased the let-7b expression level in MECs ($P < 0.0001$, (Fig. 26A) and HECs ($P < 0.0001$, Fig. 26B), indicating high efficiency of the let-7b inhibitor transfection. Furthermore, let-7b inhibitor transfection downregulated let-7c

(*P*<0.0001), let-7d (*P* < 0.001), let-7e (*P* < 0.001), and let-7i (*P* < 0.05) expression in MECs (Fig. 26A), and downregulated let-7c (*P* < 0.0001), let-7d (*P* < 0.0001), let-7i (*P* < 0.001) and let-7b* (*P* < 0.05) in HECs (Fig. 26B). However, let-7b inhibitor treatment upregulated let-7g expression in MECs (*P* < 0.05, Fig. 26A) after but not in HECs (*P*=ns, Fig. 26B). This result reveals that let-7b inhibitor treatment in ECs un-specifically downregulates most of the let-7 members.

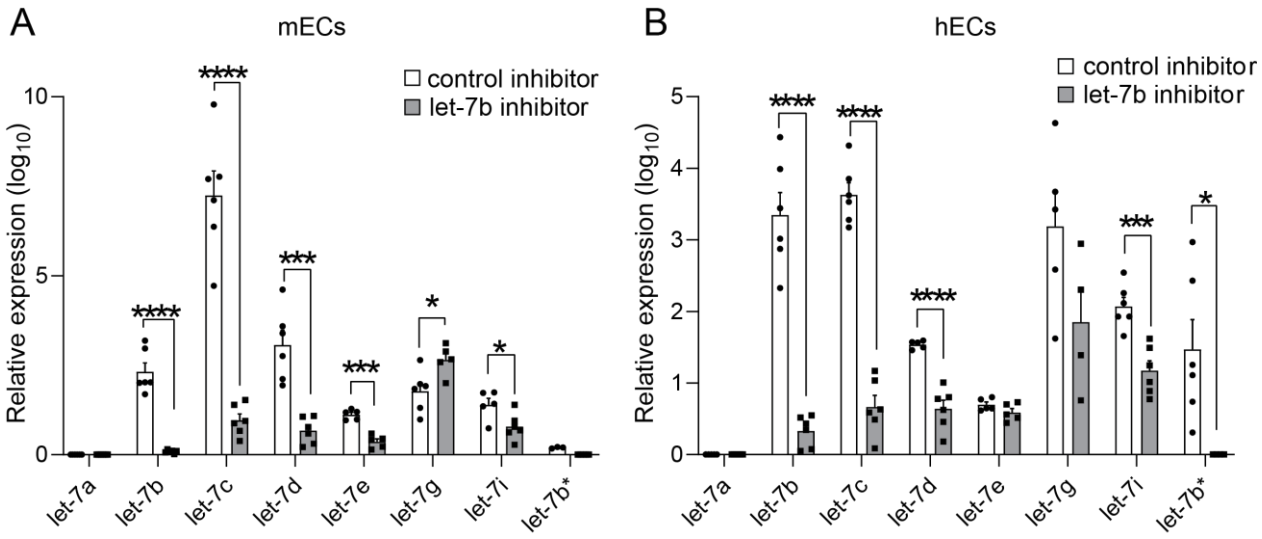

Fig. 26: Effect of let-7b inhibitor treatment on the expression levels of let-7 family members.

MECs (A; n = 5-6) and HECs (B; n = 5-6) were treated with 50 nM of let-7b inhibitors and control oligonucleotides for 24 h. Expression levels of let-7a, b, c, d, e, g, i, and let-7b-3p were determined relative to that of U6 snRNA by qRT-PCR. Let-7b inhibitor-treated sample and the control sample were compared using multiple t-tests with multiple comparison corrections using the Holm-Sidak method (**P* < 0.05, ****P* < 0.001, and *****P* < 0.0001). Data are presented as mean ± SEM.

The UHRF2 protein expression was increased after let-7b inhibitor treatment (n=3-4) in MECs (Fig. 27A) and HECs (Fig. 27B) compared to control treatment (*P*<0.05), indicating that let-7b post-transcriptionally downregulates UHRF2 expression in ECs from both species.

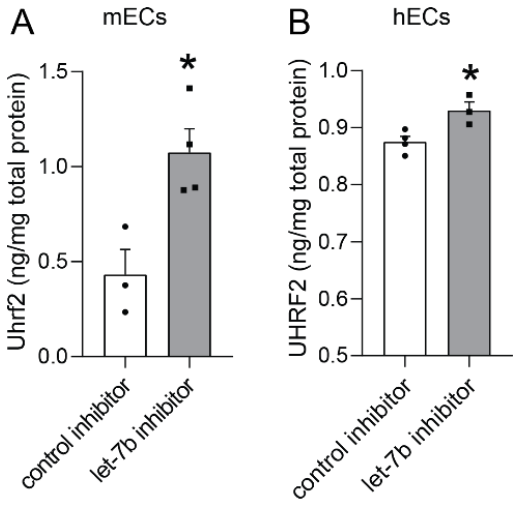

Fig. 27: UHRF2 protein quantification after let-7b inhibition in ECs.

(A) MECs and (B) HECs (n=3-4) were treated with 50 nM of let-7b inhibitor and control inhibitor for 24 h. UHRF2 protein levels and total protein levels were detected by ELISA and DC protein assay, respectively, in cell lysates. The UHRF2 protein levels were normalized to the total protein levels and were compared between the treatment group and the control group using a two-tailed Student's t-test (**P*<0.05). Data are presented as mean ± SEM.

3.8. Target transcript expression regulation by let-7b

To investigate whether let-7b inhibition changes *UHRF2*, *MLLT10,* and *LINCPINT* gene expression levels, RT-qPCR was performed in MECs and HECs transfected with let-7b inhibitor or control inhibitor.

Let-7b inhibition resulted in upregulation of Uhrf2 (*P*<0.0001), Mllt10 (*P*<0.05), and Lincpint (*P*<0.001) transcripts in MECs (Fig. 28A), indicating that let-7b mediates Uhrf2, Mllt10 and Lincpint transcript degradation in MECs. Downregulation of let-7b in HECs did not alter UHRF2 and MLLT10 mRNA levels (*P*=ns, Fig. 28B), suggesting that in HECs, let-7b targeting results in translational inhibition of mRNA targets. Let-7b downregulation did not alter LINCPINT transcript expression levels in HECs (*P*=ns, Fig. 28B), suggesting that LINCPINT is not regulated by RNA degradation in HECs. These results indicate that let-7b regulates its targets differently at the transcript level in MECs and HECs.

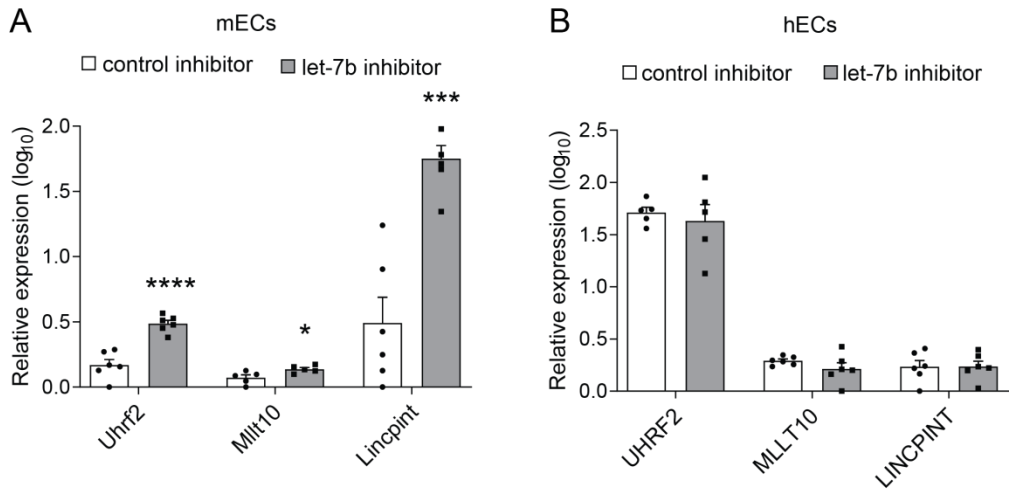

Fig. 28: Relative gene expression of targets after let-7b inhibition.

MECs and HECs were treated with 50 nM let-7b inhibitor or control inhibitor (n = 4-6) for 24h. (A) Expression of Uhrf2, Mllt10, and Lincpint relative to B2m was assessed by q-RT PCR in MECs. (B) The expression of UHRF2, MLLT10, and LINCPINT relative to GAPDH was evaluated by q-RT PCR in HECs. Gene expression of target genes was compared between the let-7b inhibited sample and the control sample using multiple t-tests with no comparison correction (*P<0.05, ***P<0.001, and ****P<0.0001). Data are presented as mean ± SEM.

3.9. Validation of the let-7b BSs in targets

A luciferase reporter assay was performed to study whether let-7b directly targets the UHRF2 and MLLT10 3'–UTRs. HEK293 cells were co-transfected with let-7b mimics or control mimics and a vector encoding the 3'–UTR of either UHRF2 or MLLT10 downstream of a luciferase reporter gene.

Let-7b mimic treatment significantly reduced luciferase activity in cells treated with h/m-UHRF2 3'–UTR (P<0.001), m-Mllt10 3'–UTR (P<0.001), and h-MLLT10 3'–UTR (P<0.01) reporter constructs compared to the control treatment (n=3-4). Furthermore, mutation of 3-4 nucleotides in the predicted BSs opposite to the seed sequence in the 3'–UTR encoding constructs prevented the suppression of luciferase activity by let-7b mimic, indicating that let-7b directly targets h/m-UHRF2 and h-MLLT10 (m-Mllt10) through the predicted BS (Fig. 29 A-C).

To assess whether let-7b directly targets Lincpint lncRNA, a luciferase reporter assay was performed in HEK293 cells co-transfected with let-7b mimics or control mimics, and a vector encoding the mouse Lincpint transcript sequence downstream of a luciferase reporter gene (m-Lincpint). To ensure the validity of our cloning method, a constructed vector containing four let-7 binding sites downstream of the luciferase reporter (x4 let-7 BS) was transfected in the positive control group. Luciferase activity of the m-Lincpint sequence construct as well as the positive control construct were significantly reduced by let-7b mimic treatment (n=4) compared to the control treatment (P< 0.05 and P<0.0001, respectively). Moreover, mutation of the predicted BSs opposite to the seed sequence in the m-Lincpint construct

prevented the suppression of luciferase activity by let-7b mimics (Fig. 29D), indicating that let-7b directly targets Lincpint through this predicted BS.

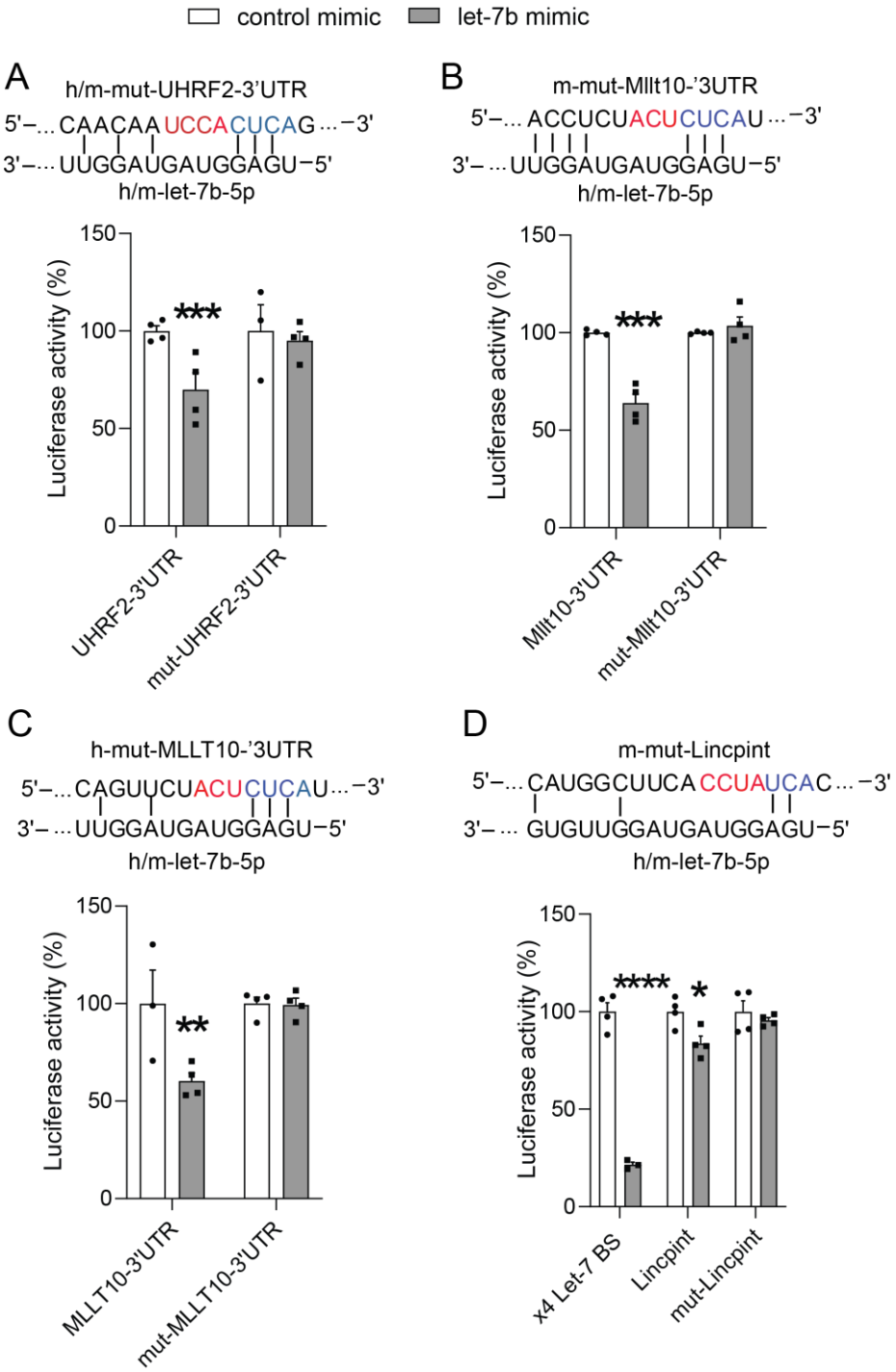

Fig. 29: Luciferase activities of predicted target constructs.

HEK293 cells (n=3-4) were co-transfected with 500 ng of luciferase reporter vector and 50 nM of let-7b mimic or control mimic for 48 h. Luciferase activity of the wild-type or mutated (A) m/h-UHRF2 3'–UTR, (B) m-Mllt10 3'–UTR, and (C) h-MLLT10 3'–UTR luciferase reporter vectors was determined and normalized to the control oligonucleotide treated group and presented as percentages for each replicate. (D) Wild-type or mutated m-Lincpint sequence construct and a control positive construct containing four let-7 BSs downstream of the reporter gene were co-transfected with let-7b mimics or control mimics in HEK 329 cells. Next, the luciferase activity of the constructs was determined and normalized to the control group and presented as percentages. Luciferase activities were compared between the treatment group and the control group using a two-tailed Student's t-test (**P* < 0.05, ***P*<0.01, ****P*<0.001, and *****P*<0.0001). Data are presented as mean ± SEM. The vector constructs contained let-7b BS sequences (red and blue). The mutated nucleotides are in red.

3.10. Inhibiting let-7b-mediated repression of targets with TSBs

To investigate whether blocking the let-7b BS changes *UHRF2*, *MLLT10*, and *LINCPINT* gene expression levels, locked nucleic acid (LNA) based oligonucleotide target site blockers (TSBs) were designed to pair with the target transcripts in the BS region, and prevent BS accessibility for let-7b. Next, the expression of targets on the transcript and protein level was assessed in MECs and HECs transfected with TSBs (Fig. 30 and 31).

h/m-UHRF2-TSB treatment upregulated UHRF2 expression at the transcript level (*P*<0.01, Fig. 30B) and at the protein level (*P*<0.05, Fig. 30C) in MECs but did not affect MLLT10 and LINCPINT gene expressions (Fig. 30B). Moreover, in HECs h/m-UHRF2-TSB treatment increased UHRF2 transcript (*P*<0.05, Fig. 30D) and protein (*P*<0.05, Fig. 30E) expression significantly compared to the control treatment. This data reveals that h/m-UHRF2-TSB binds to the 3'–UTR of UHRF2 and blocks let-7b targeting in MECs and HECs.

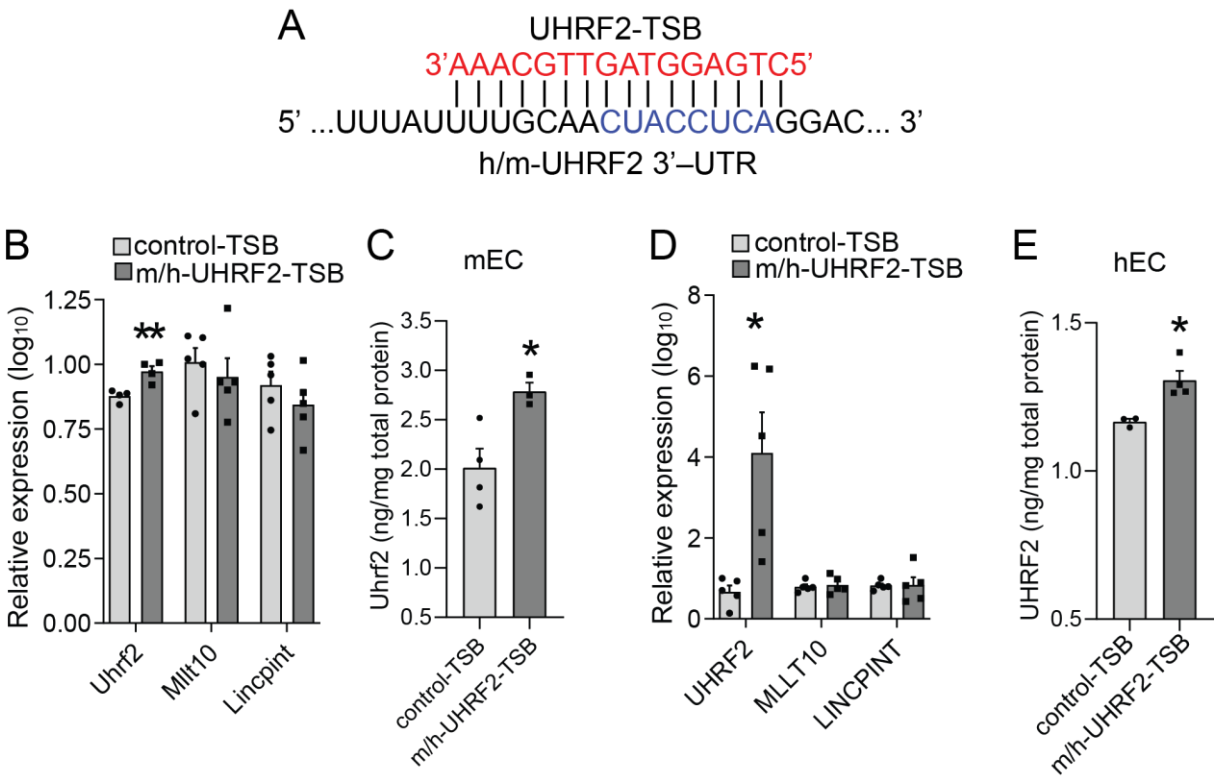

Fig. 30: Effects of blocking let-7b/UHRF2 interaction on target regulation in MECs and HECs.

(A) Short oligonucleotide TSBs were designed (red sequence) to mask the predicted BS (blue) on UHRF2 3'–UTR. (B-C) MECs and (D-E) HECs were transfected with 50 nM h/m-UHRF2-TSB or control-TSBs (n=4-5) for 24h. (B, D) Gene expression of UHRF2, MLLT10, and LINCPINT in MECs and HECs relative to B2m and GAPDH, respectively, were assessed by qRT-PCR. Relative gene expression was compared between the TSB treatment group and the control group using paired multiple t-tests with no comparison correction (**P*<0.05 and ***P*<0.01). (C, E) UHRF2 protein levels were detected by ELISA and were normalized to the total protein levels quantified by DC protein assay. UHRF2 protein levels were compared between the treatment and control groups using a two-tailed Student's t-test (**P*<0.05). Data are presented as mean ± SEM.

Treatment of the MECs with m-Mllt10-TSB (Fig. 31A) increased Mllt10 expression significantly (*P*<0.05) compared to the control treatment and did not affect Uhrf2 or Lincpint expression (Fig. 31C). Nevertheless, treating the HECs with h-MLLT10-TSB (Fig. 31B) significantly increased the MLLT10 (*P*<0.01) and UHRF2 (*P*<0.05) expressions compared to the control treatment and had no effect on Lincpint gene expression (Fig. 31D). This result indicates that only the mouse Mllt10-TSB specifically blocks the BS on mouse Mllt10 3'–UTR, and the human MLLT10-TSB is not specific to MLLT10 3'–UTR.

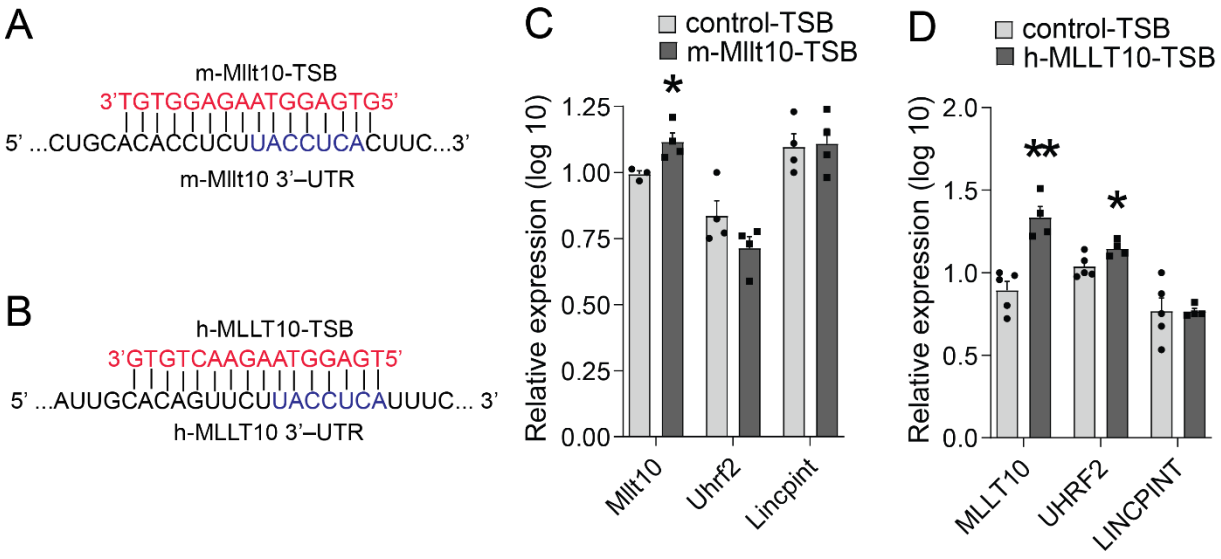

Fig. 31: Effects of blocking let-7b/MLLT10 interaction on target regulation in MECs and HECs.

(A-B) Short oligonucleotide TSBs were designed (red sequences) to mask the predicted BSs (blue) on Mllt10/MLLT10 3'–UTRs. MECs and HECs (n=4-5) were transfected with 50 nM MLLT10-TSB (A-B) or control-TSB for 24h. Expression of MLLT10, UHRF2, and LINCPINT was assessed relative to B2m in (C) MECs and relative to GAPDH (D) in HECs by qRT-PCR and compared between the treatment group and the control group using unpaired multiple t-tests with no comparison correction (**P*<0.05 and ***P*<0.01). Data are presented as mean ± SEM.

In MECs treated with m-Lincpint-TSB, Lincpint and Mllt10 expressions were not changed (Fig. 32). This data reveals that Lincpint is not regulated by TSB treatment.

These results prove that h/m-UHRF2-TSB specifically prevents let-7b interaction with UHRF2 3'–UTR in MECs and HECs. Moreover, m-Mllt10-TSBs prevent let-7b interaction with the m-Mllt10 3'–UTR in MECs.

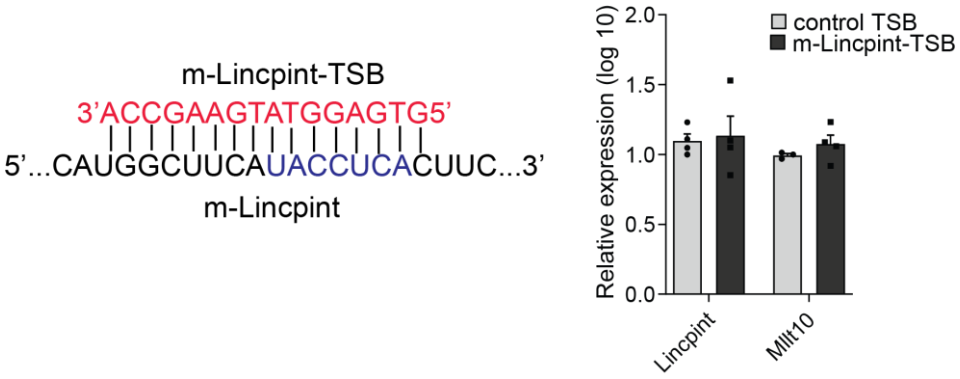

Fig. 32: Effect of blocking let-7b/Lincpint interaction on target regulation in MECs.

Short oligonucleotide TSB (red sequences) was designed to mask the predicted BSs (blue) on the m-Lincpint transcript. MECs (n=4-5) were transfected with 50 nM m-Lincpint-TSB or control-TSBs for 24h. Gene expression of mouse Lincpint and Mllt10 relative to B2m was assessed by qRT-PCR and compared between the groups using paired multiple t-tests with no comparison correction (*P*=ns). Data are presented as mean ± SEM.

3.11. Functional effects of let-7b-mediated target inhibition in ECs

To discover whether let-7b mediated inhibition of UHRF2 and m-Mllt10 affects endothelial maladaptation in MECs and HECs, the role of let-7b on EC properties (section 1.2.3), like wound healing, proliferation, apoptosis, DNA damage, and reactive oxygen species (ROS) production was studied.

3.11.1 Effects of let-7b on EC wound healing

To investigate the effect of let-7b on endothelial wound healing, MECs and HECs were treated with let-7b inhibitor, TSBs, and control oligonucleotides for 24 h (n=4-6). Next, the closure of the generated wound was continuously monitored in the presence and absence of ox-LDL for 48h.

In MECs, the generated wound area was reduced during 48 h, and there was no difference between let-7b inhibitor-treated cells and control-treated cells at all time points (Fig. 33).

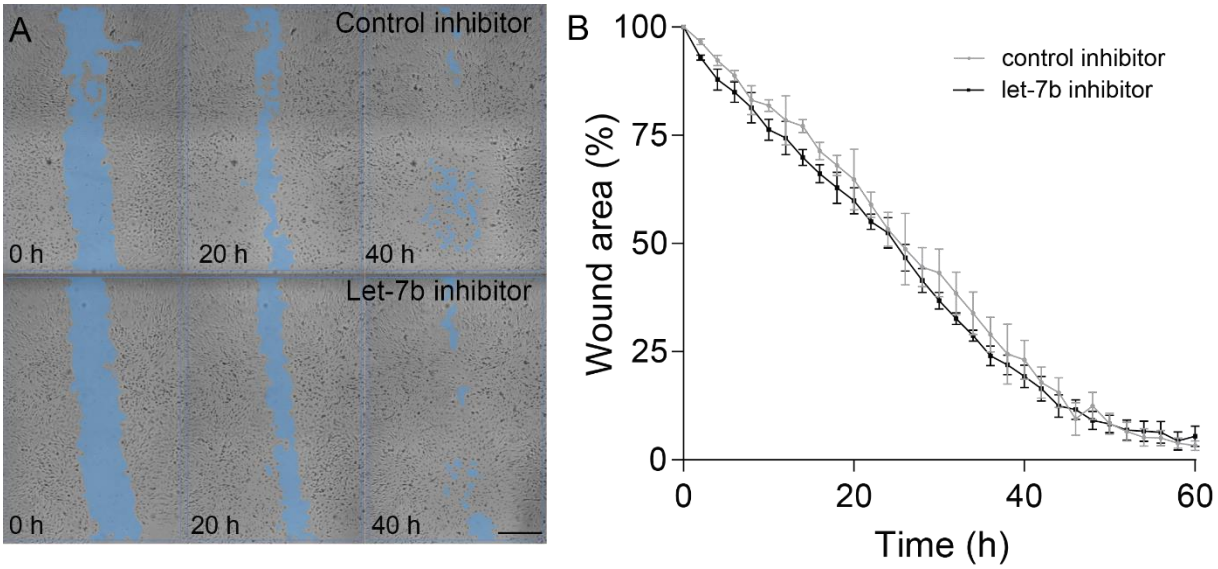

Fig. 33: Role of let-7b in MEC wound healing.

MECs were treated with 50 nM let-7b inhibitor and control inhibitor for 24 h, and a wound was generated in the middle of each confluent well. The damaged area was monitored with the CytoSMART Omni for 48 h. (A) The blue overlay indicates the wound area on brightfield images at 0, 20, and 40 h time points (scale bar, 2 mm). (B) The wound area (µm^2) of the acquired scans was normalized to that at 0 h and reported as a percent. Data were compared between the groups using multiple t-tests (*P*=ns) and shown as mean ± SEM.

In HECs, let-7b inhibitor treatment significantly reduced wound closure compared to control treatment between 8 to 38 h ($P<0.05$, Fig. 34). This result indicates that let-7b is required for wound healing in HECs.

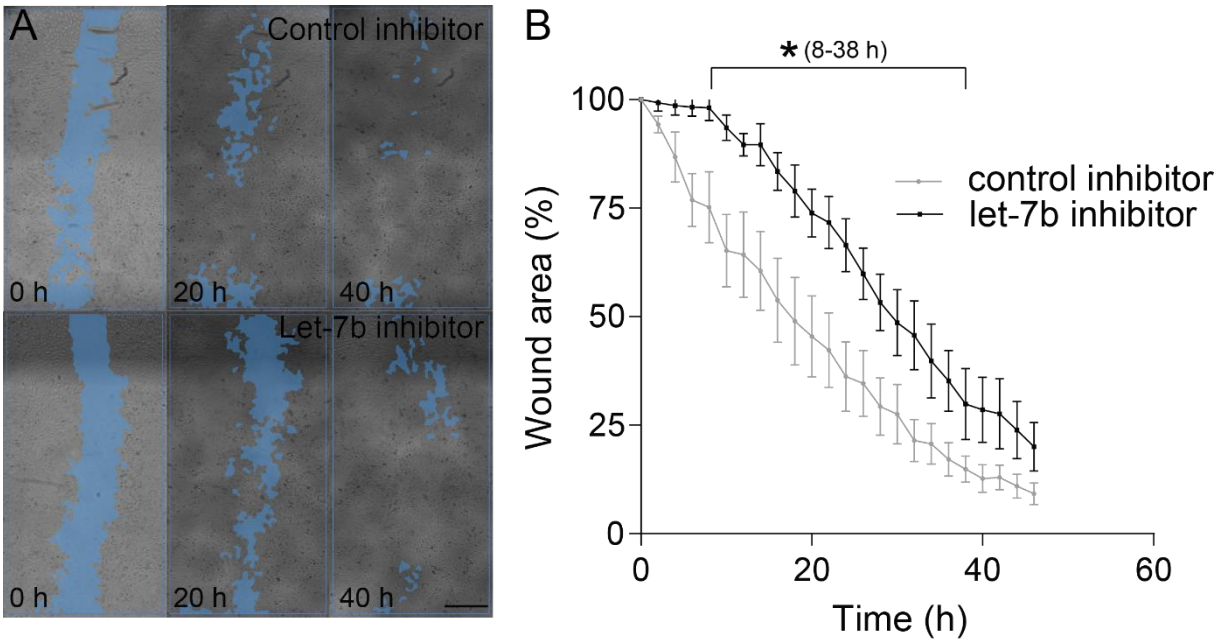

Fig. 34: Role of let-7b in HECs on wound healing.

HECs were treated with 50 nM let-7b inhibitor and control inhibitor for 24 h, and a wound was generated in the middle of each confluent well. The wound area was monitored with the CytoSMART Omni for 48 h. (A) The blue overlay indicates the wound area on bright-field images at 0, 20, and 40 h time points (scale bar, 2 mm). (B) The wound area (μm^2) of the acquired scans was normalized to that at 0 h and reported as a percent. Data were compared between the treatment and control groups using multiple t-tests ($P<0.05$) and are shown as mean ± SEM.

Ox-LDL treatment did not affect wound healing in MECs alone (Fig. 35A) or in the presence of let-7b inhibitor (Fig. 35B). However, ox-LDL treatment in HECs delayed the wound closure after 8 h compared to the control group ($P<0.05$, Fig. 35C). The increased wound closure in control inhibitor treated HECs compared to let-7b inhibitor-treated cells was attenuated in the presence of ox-LDL (Fig. 35D). These results suggest that ox-LDL limits wound healing in HECs.

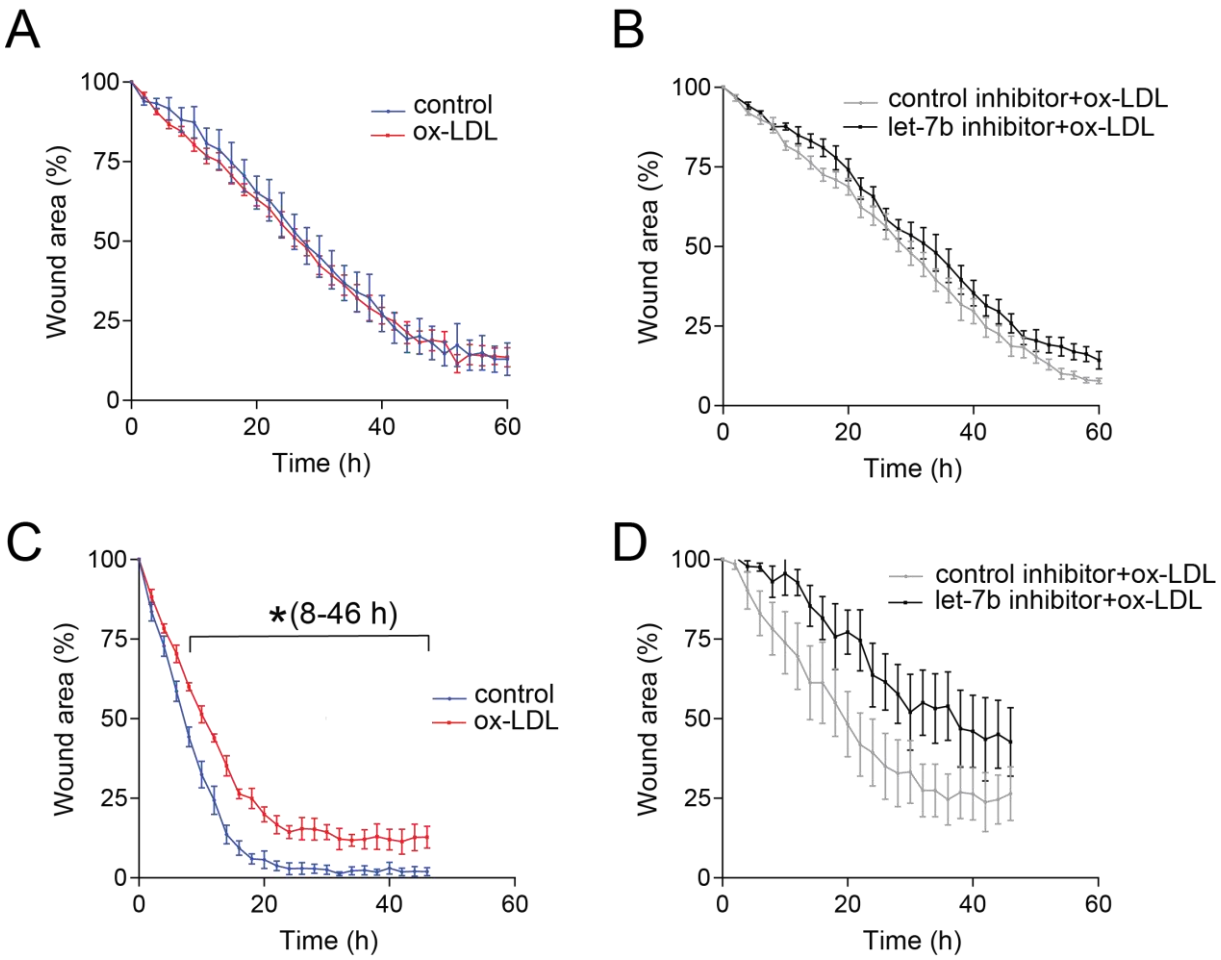

Fig. 35: Role of ox-LDL in EC wound healing.

(A) MECs and (C) HECs were treated with 150 µg/ml ox-LDL after generating a wound in the middle of each confluent well. (B) MECs and (D) HECs were treated with 50 nM let-7b inhibitor and control inhibitor for 24 h and treated with 150 µg/ml ox-LDL after wound generation. The wound area in all wells was monitored up to 48 h with the CytoSMART Omni. The computed wound areas (μm^2) were normalized to 0 h and reported as a percent. Data were compared between the treatment and control groups using multiple t-tests ($P<0.05$) and are reported as mean ± SEM.

To investigate the effect of let-7b-mediated downregulation of UHRF2 and Mllt10 on EC wound healing, a scratch injury experiment was performed in MECs and HECs treated with TSBs (n=4-6).

In MECs, h/m-UHRF2-TSB or m-Mllt10-TSB treatment significantly reduced wound area between 18 to 56 h compared to the control-TSB-treated cells. ($P<0.05$, Fig. 36A and B). However, treatment of the MECs with ox-LDL prevented the beneficial effects of the m/h-h/m-UHRF2-TSB and m-Mllt10-TSBs on wound healing (Fig. 36C).

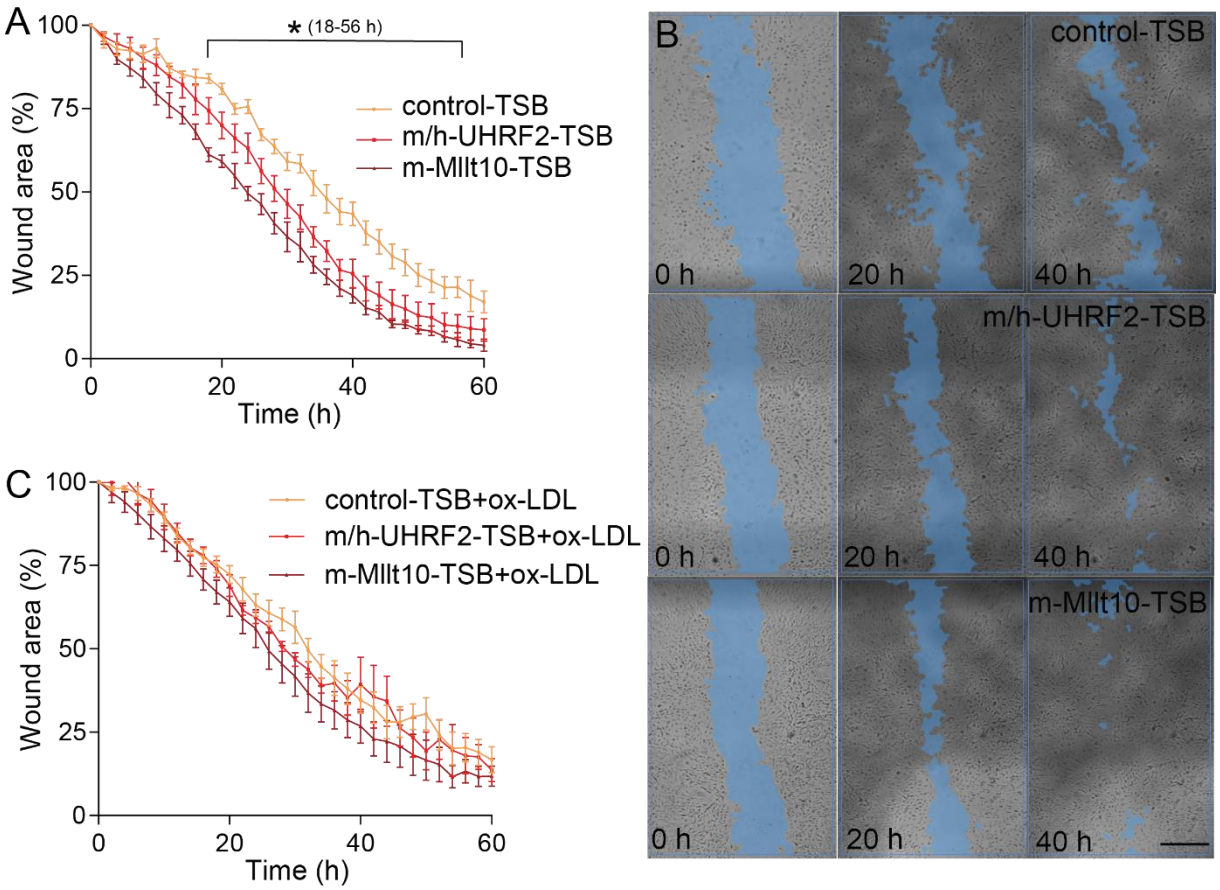

Fig. 36: Effects of TSB treatment on MEC wound healing.

(A) MECs were treated with 50 nM h/m-UHRF2-TSB, m-Mllt10-TSB, or control-TSB for 24h; a wound was made in the middle of each confluent well, and the generated wound was monitored for 48 h with the CytoSMART Omni. (B) The blue overlay indicates the wound area in MECs on brightfield images at 0, 20, and 40 h time points (scale bar, 2 mm). (C) MECs were treated with 50 nM h/m-UHRF2-TSB, m-Mllt10-TSB, or control-TSB for 24h. Next, the cells were treated with 150 µg/ml ox-LDL after wound generation. The generated wound area was then monitored for 48 h with the CytoSMART Omni. All samples' wound areas (μm^2) were normalized to 0 h and reported as a percent. Data were compared between the treatments and the control using multiple t-tests ($P<0.05$) and are reported as mean ± SEM.

In HECs, h/m-UHRF2-TSB treatment significantly reduced wound area compared to the control-treated cells at all time points after 6 h ($P<0.05$, Fig. 37A and B) and at all time points after 2 h in the presence of ox-LDL ($P<0.05$, Fig. 37C).

These results reveal that UHRF2 is required for wound healing in mouse and human ECs, and let-7b-mediated downregulation of UHRF2 limits wound healing. Moreover, let-7b-mediated downregulation of Mllt10 also limits wound healing in MECs.

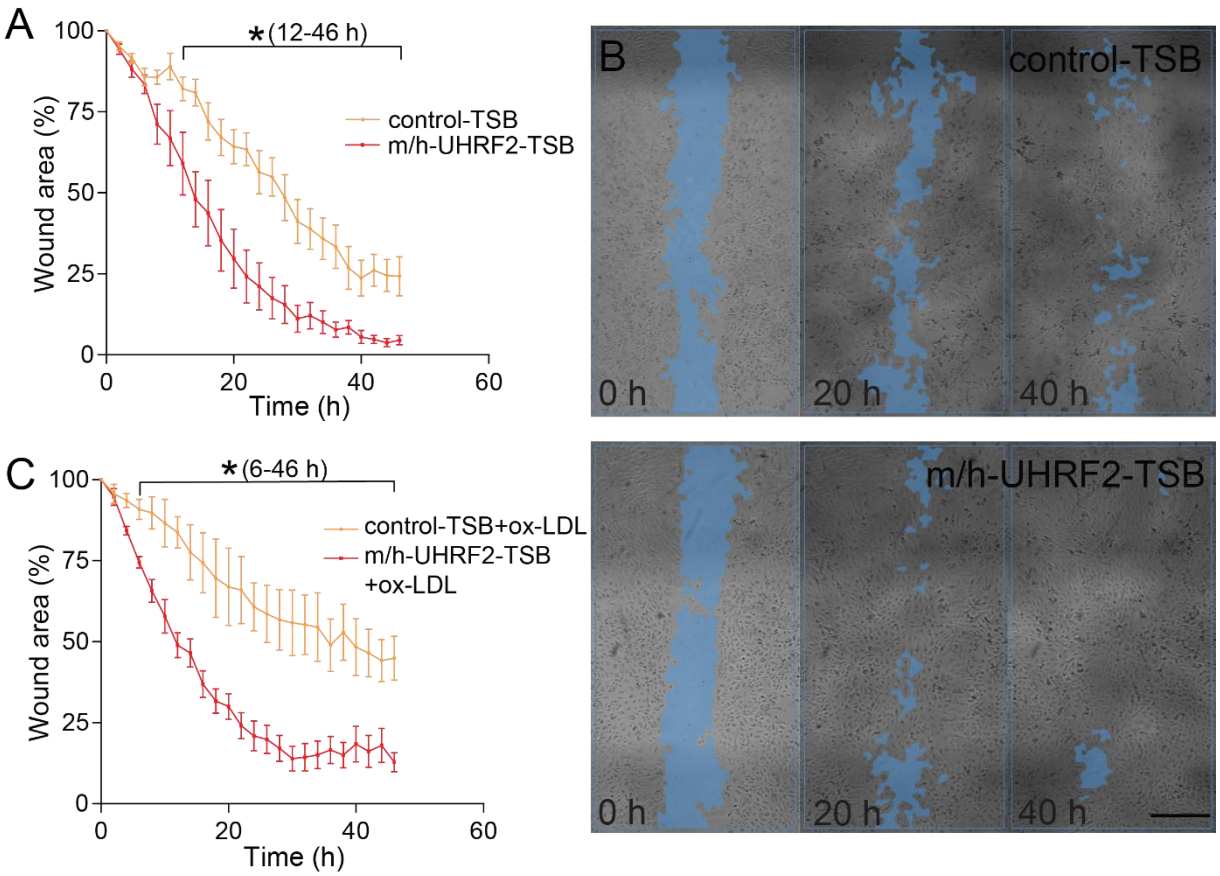

Fig. 37: Effects of TSB treatment on HECs wound healing.

(A) HECs were treated with 50 nM h/m-UHRF2-TSB or control-TSB for 24h; next, a wound was made in the middle of each confluent well, and the generated wound was monitored for 48 h with the CytoSMART Omni. (B) The blue overlay indicates the wound area on brightfield images at 0, 20, and 40 h time points (scale bar, 2 mm). (C) HECs were treated with 50 nM h/m-UHRF2-TSB or control-TSB for 24h. Next, the cells were treated with 150 µg/ml ox-LDL after wound generation. The generated wound area was then monitored for 48 h with the CytoSMART Omni. All wells' wound areas (μm^2) were normalized to T0 and reported as a percent. Data were compared between the TSB treatments and the controls using multiple t-tests with no multiple comparison correction ($P<0.05$) and is reported as mean ± SEM.

3.11.2 Effects of let-7b on EC proliferation

To understand whether let-7b affects cell proliferation during wound healing, MECs and HECs were treated with let-7b inhibitor, TSBs, and control oligonucleotides for 24 h (n=4-5). EC proliferation was assessed using Click-iT® EdU proliferation assay after wound generation with or without ox-LDL treatment.

Let-7b inhibitor treatment reduced the proliferation of MECs ($P<0.01$) and HECs ($P<0.05$) in the wound area compared to the control treatment (Fig. 38), suggesting that let-7b is required for EC proliferation during wound healing in MECs and HECs.

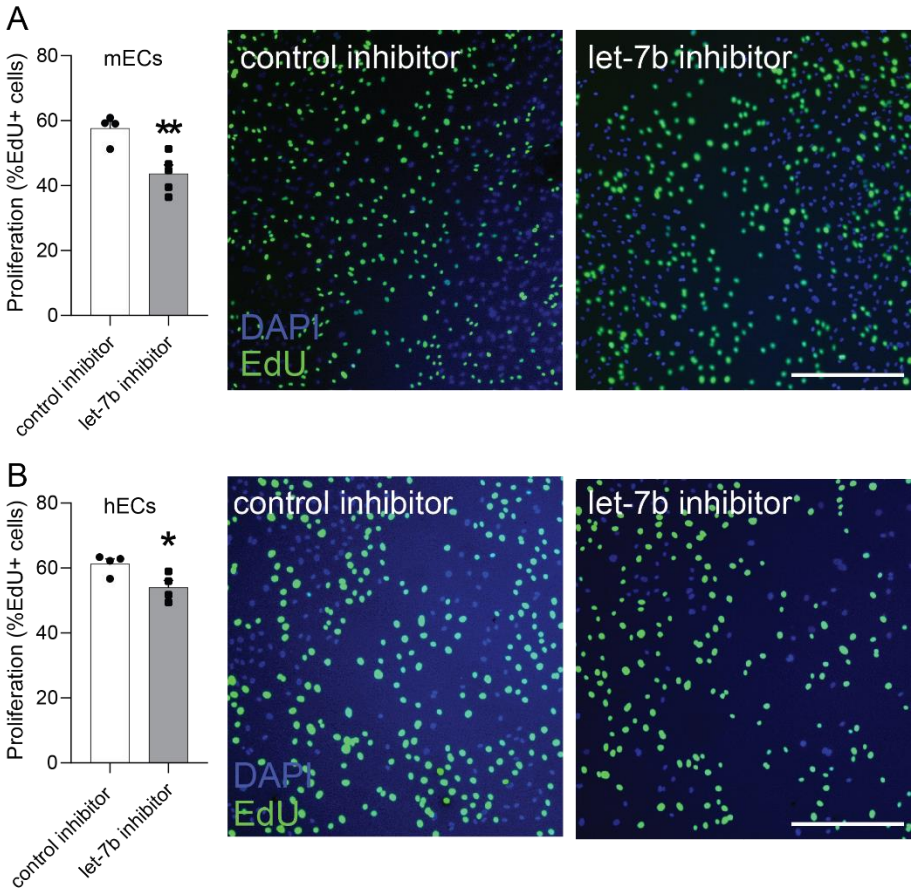

Fig. 38: Role of let-7b in EC proliferation.

(A) MECs and (B) HECs were transfected with let-7b inhibitor or control inhibitor for 24 h (n = 4-5). Next, a wound was made in the middle of each well, and cells were kept in media containing 20 µM EdU for 40 h. The cells were then stained with a Click-iT® EdU kit and imaged. The EdU-positive cells in the wound area were counted using ImageJ. The percentage of EdU positive cells in the wound area was compared among the treatment group and the control using a two-tailed Student's t-test (*P<0.05). Data are presented as mean ± SEM. Representative images show wound areas after EdU staining in (A) MECs and (B) HECs (EdU, green; DAPI, blue; scale bars represent 500 µm).

h/m-UHRF2-TSB treatment increased the proliferation of MECs and HECs in the wound area (P<0.01 and P<0.05, respectively) compared to the control treatment (Fig. 39A-B). Moreover, m-Mllt10-TSB treatment increased the proliferation of MECs significantly (P<0.001, Fig. 39A). These results reveal that UHRF2 and Mllt10 are required for EC proliferation during wound healing. This function is conserved for UHRF2 in MECs and HECs.

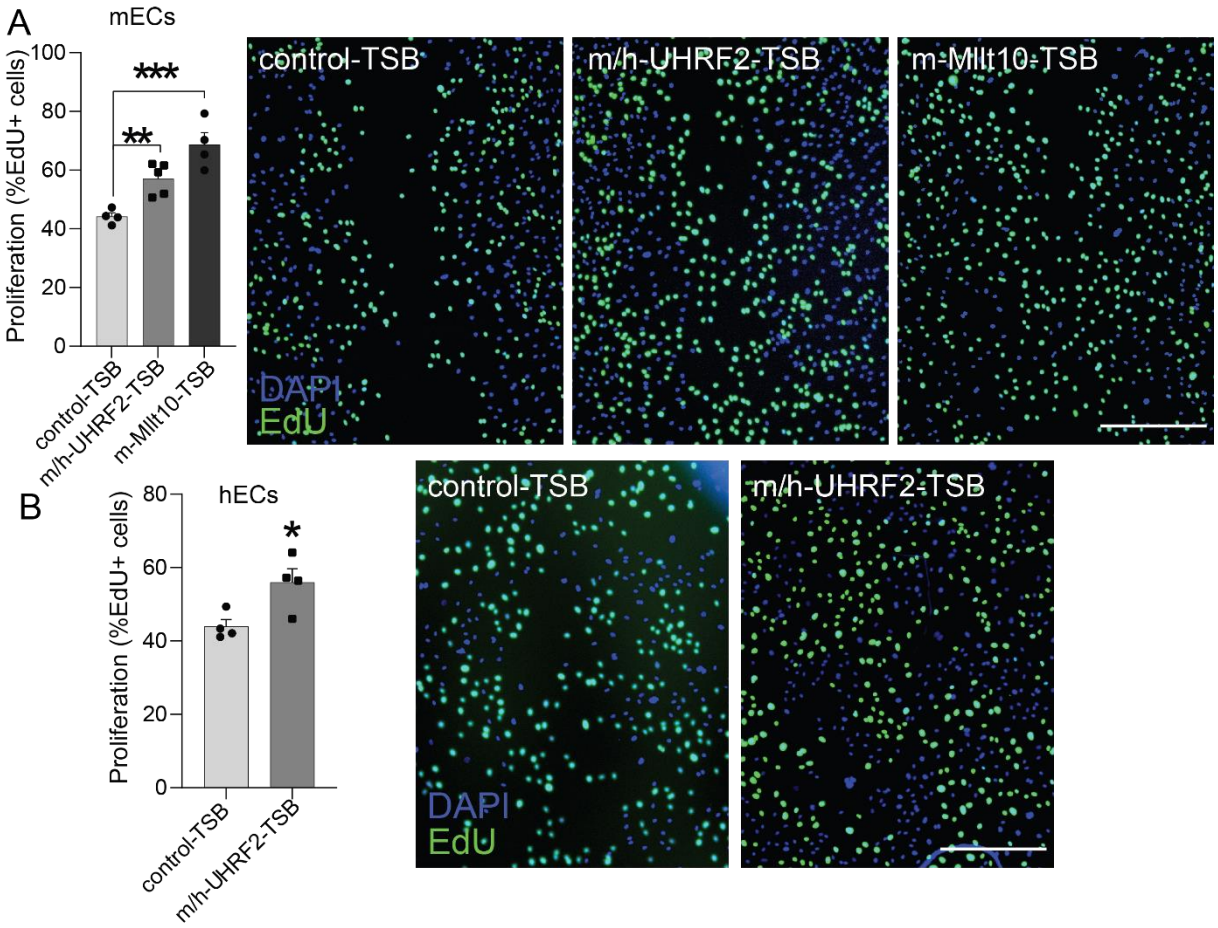

Fig. 39: Role of TSBs in EC proliferation.

(A) MECs were transfected with h/m-UHRF2-TSB, m-Mllt10-TSB, or control-TSB, and (B) HECs were transfected with h/m-UHRF2-TSB or control-TSB for 24 h (n = 4-5). Next, a wound was made in the middle of each well, and cells were kept in media containing 20 µM EdU for 40 h. The cells were then stained with a Click-iT® EdU kit and imaged after counterstaining of nuclei with DAPI. The EdU-positive cells in the wound area were counted using ImageJ. The percent of EdU positive cells in the wound area was compared among the treatment group and the control using (A) one-way ANOVA (***P*<0.01, and ****P*<0.001) or (B) two-tailed Student's t-test (**P*<0.05). Data are presented as mean ± SEM. Representative images show wound areas after EdU staining in (A) MECs and (B) HECs (EdU, green; DAPI, blue; scale bars represent 500 µm).

3.11.3 Effects of Let-7b on EC apoptosis

To study apoptosis induction in MECs and HECs, cells were treated with staurosporine (a protein kinase inhibitor) or ox-LDL (n=5-6), and apoptosis was assessed by measuring caspase 3/7 activation by CellEvent™ Caspase-3/7 kit. In HECs treated with staurosporine, apoptosis was increased more than 2-fold compared with MECs (P<0.001, n=2-4), indicating that HECs are more susceptible to staurosporine (Fig. 40A). Ox-LDL treatment in MECs or HECs did not alter apoptosis (Fig. 40B), suggesting that ox-LDL does not induce EC death at the time point studied.

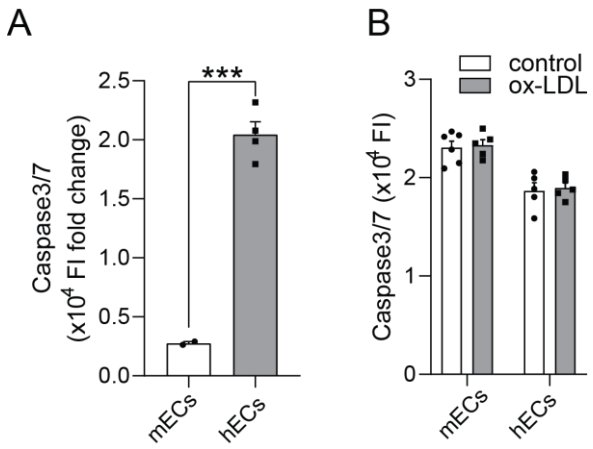

Fig. 40: Apoptosis induction in MECs and HECs.

(A) MECs and HECs were treated with 10 µM staurosporine for 3 h (n=2-4). Cells were then stained with CellEvent™ Caspase-3/7 Green Detection Reagent, and the apoptotic nuclei's fluorescent intensity (FI) was quantified. Fold change of FI after staurosporine treatment was compared between MECs and HECs using a two-tailed Student's t-test (***P<0.001). (B) MECs and HECs were treated with or without 100 µg/ml ox-LDL for 21 h (n=5-6). Cells were then stained with 2 µM CellEvent™ Caspase-3/7 Green Detection Reagent for 3h, and the FI of the apoptotic nuclei was measured. Data were compared among the ox-LDL treatment group and the control using multiple t-tests with no comparison correction (P=ns). Data are presented as mean ± SEM.

To investigate the role of let-7b in apoptosis, MECs and HECs were treated with let-7b inhibitors, TSBs, and oligonucleotide controls. Next, apoptosis was assessed by CellEvent™ Caspase-3/7 kit. Let-7b inhibition in MECs treated with or without ox-LDL did not alter apoptosis, whereas in HECs without ox-LDL treatment, apoptosis was increased after let-7b inhibition (P<0.05, n=5-6). This data reveals that let-7b limits spontaneous HEC apoptosis (Fig. 41).

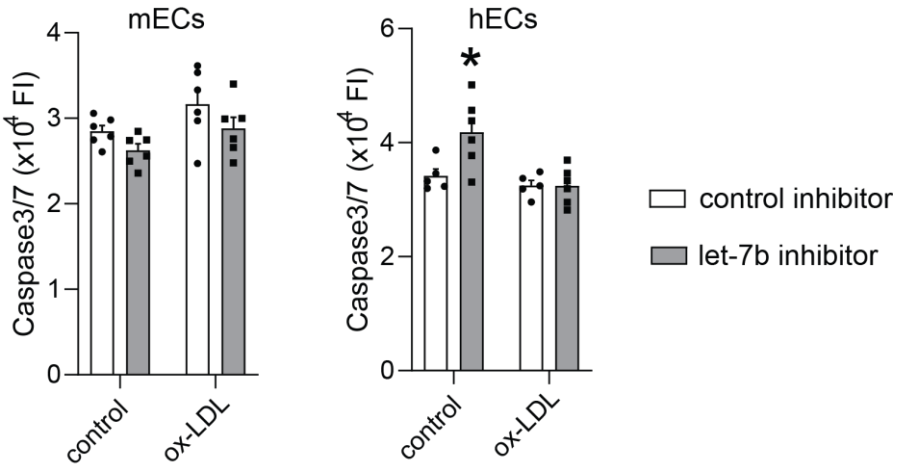

Fig. 41: Effects of let-7b on EC apoptosis.

MECs and HECs (n=5-6) were treated with let-7b inhibitor and control for 21 h and then with or without (control) 100 µg/ml ox-LDL for 3 h. Cells were then stained with CellEvent™ Caspase-3/7 Green Detection Reagent, and the apoptotic nuclei's FI was measured. Data were compared between the let-7b inhibitor group and the control group using multiple t-tests without multiple comparison corrections (*P<0.05). Data are presented as mean ± SEM.

h/m-UHRF2-TSB increased apoptosis in MECs treated with or without ox-LDL (P<0.05), whereas Mllt10-TSB did not affect MEC apoptosis (P=ns, Fig. 42A). h/m-UHRF2-TSB decreased apoptosis only in ox-LDL-treated HECs (Fig. 42B). These results reveal that the targeting of UHRF2 by let-7b results in different apoptotic cell fates in MECs and HECs.

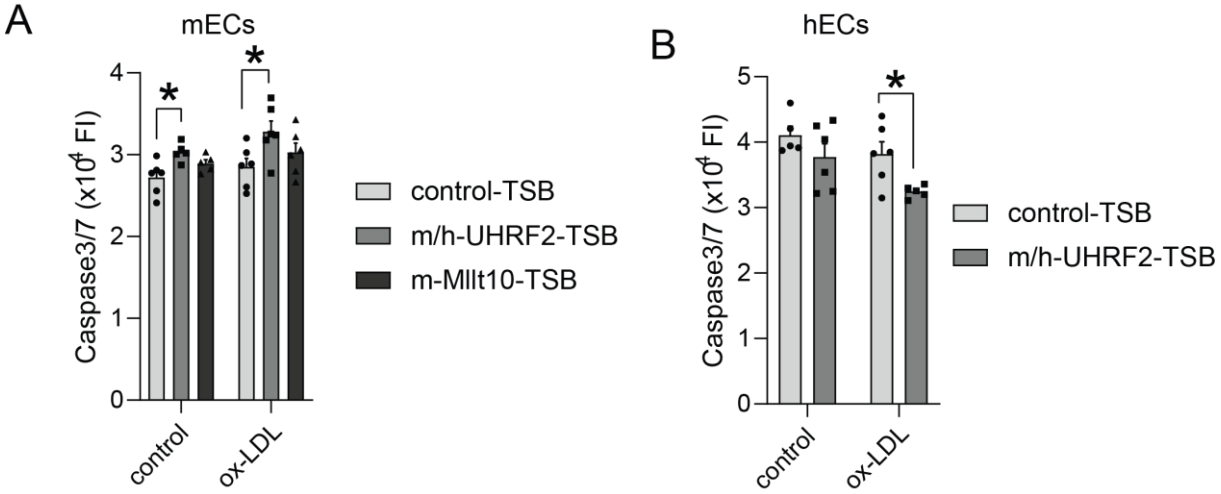

Fig. 42: Effects of TSBs on EC apoptosis.

MECs were treated with h/m-UHRF2-TSB, m-Mllt10-TSB, or control-TSB for 21 h and then with or without (control) 100 µg/ml ox-LDL for 3 h (n=5-6). (B) HECs were treated with h/m-UHRF2-TSB or control-TSB for 21 h and then with or without (control) 100 µg/ml ox-LDL for 3 h (n=5-6). Cells were then stained with CellEvent™ Caspase-3/7 Green Detection Reagent, and the apoptotic nuclei's FI was measured. Data were compared among the treatment and control groups using multiple t-tests without multiple comparison corrections (*P<0.05). Data are presented as mean ± SEM.

3.11.4 Effects of let-7b on DNA damage formation in ECs

To investigate DNA damage formation in ECs, γ-H2AX median fluorescent intensity (MFI) was measured by flow cytometry in ECs treated with ox-LDL or UV.

Treatment with UV light (10 min) increased γ-H2AX MFI in MECs (P<0.001) and HECs (P<0.01) (n=3-4, data not shown). The increase of DNA damage in UV treated cells was significantly higher in HECs compared to MECs (P<0.01), indicating that HECs are more susceptible to DNA damage induction (Fig. 43A). Ox-LDL (100 µg/ml) treatment (n=3-4) did not have an effect on DNA damage levels in MECs, whereas it increased DNA damage levels in HECs compared to the control (P<0.01, Fig. 43B) suggesting that the HECs are more sensitive to ox-LDL induced DNA damage compared to MECs.

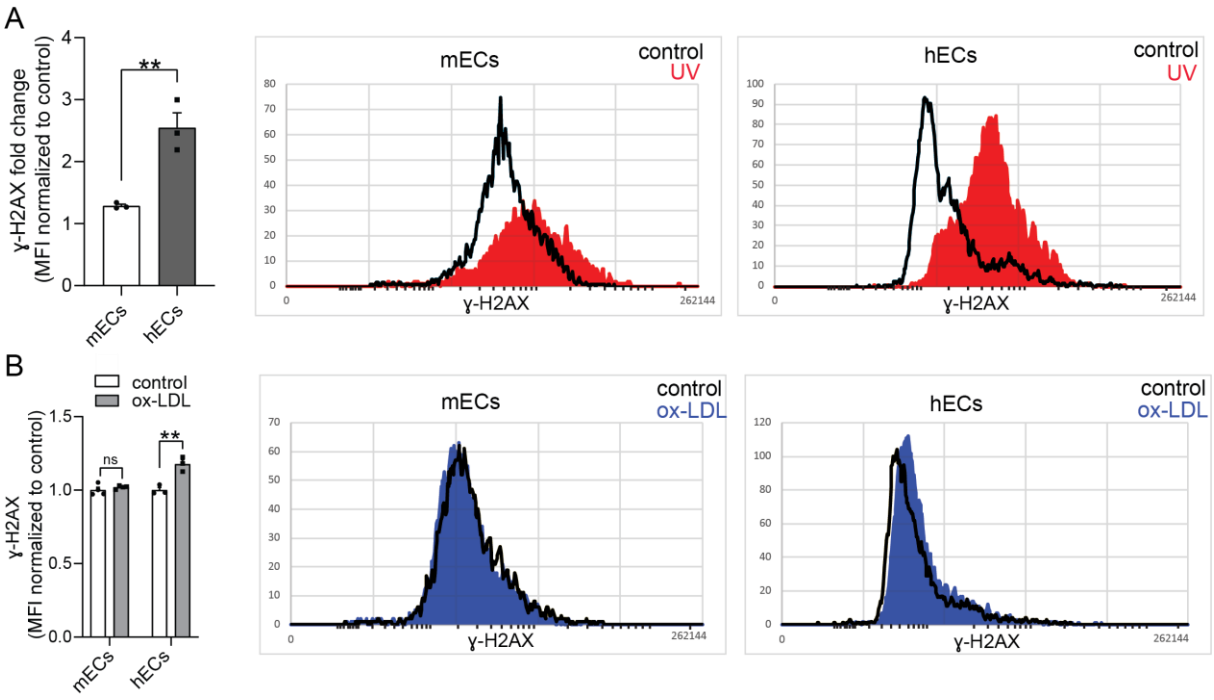

Fig. 43: DNA damage formation in MECs and HECs.

(A) MECs and HECs were treated with 10 min UV (n = 3). Next, they were labelled with APC-conjugated anti-γ-H2AX antibody. Median fluorescent intensity (MFI) of the labelled γ-H2AX foci in MECs and HECs was measured by flow cytometry and normalized to the control sample. The fold change of DNA damage increase in UV treated samples was compared between MECs and HECs using two-tailed Student's t-test (**P<0.01). Representative overlay histograms show γ-H2AX MFI difference between UV treatment (red) and control (black) in MECs and HECs. (B) MECs and HECs were treated with 100 µg/ml ox-LDL for 24 h (n = 3-4). Next, they were labelled with APC-conjugated anti-γ-H2AX antibody. The MFI of labelled γ-H2AX foci in MECs and HECs was measured by flow cytometry and normalized to the control sample. The control and ox-LDL treated groups were compared using multiple t-test with no multiple comparison correction (**P<0.01). Representative overlay histograms show γ-H2AX MFI difference between ox-LDL treatment (blue) and control (black) in MECs and HECs. Data is presented as mean ± SEM.

To assess the role of let-7b on DNA damage formation in ECs, cells were treated with let-7b inhibitor, TSBs and controls in the presence or absence of ox-LDL and the γ-H2AX MFI was measured by flow cytometry (n=3-6).

Let-7b inhibitor treatment did not change DNA damage levels compared to the control inhibitor treatment in the presence or absence of ox-LDL treatment in MECs or HECs (Fig. 3.30).

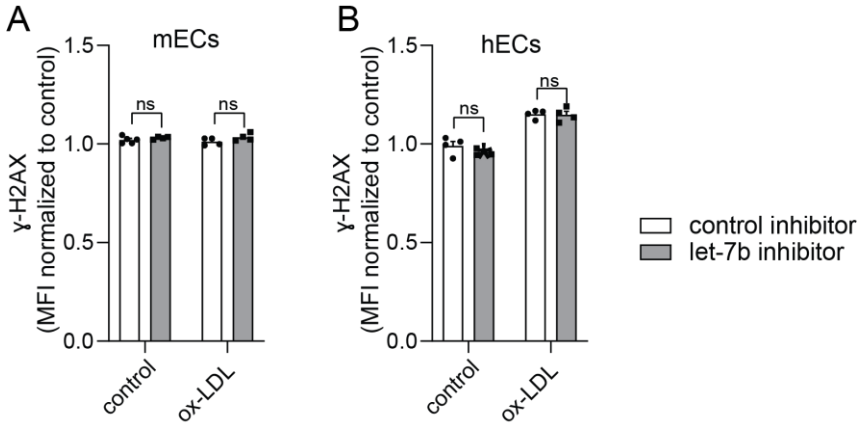

Fig. 44: Effect of let-7b on DNA damage formation in ECs.

(A) MECs and (B) HECs were treated with let-7b inhibitor and control for 24 h following 24 h of no treatment (control) or 100 µg/ml ox-LDL treatment (n = 3-5). γ-H2AX foci were then labelled by APC conjugated anti-H2AX antibody and the MFI of γ-H2AX was measured by flow cytometry. MFI was normalized to the control sample. The let-7b inhibitor and control inhibitor treated groups were compared using multiple t-test with no multiple comparison correction (P=ns). Data is presented as mean ± SEM.

Treating MECs with h/m-UHRF2-TSBs did not change DNA damage levels compared to the control in the presence or absence of ox-LDL treatment (Fig. 45A). In contrast, Mllt10-TSBs reduced significantly the γ-H2AX MFI in the absence but not in the presence of ox-LDL (P<0.05) (Fig. 45A). This data suggests that Mllt10 protects from DNA damage in MECs.

In HECs, h/m-UHRF2-TSB treatment increased DNA damage levels with (P<0.01) and without (P< 0.05) ox-LDL treatment. This result indicates that let-7b-mediated downregulation of UHRF2 reduces DNA damage formation in HECs (Fig. 45B).

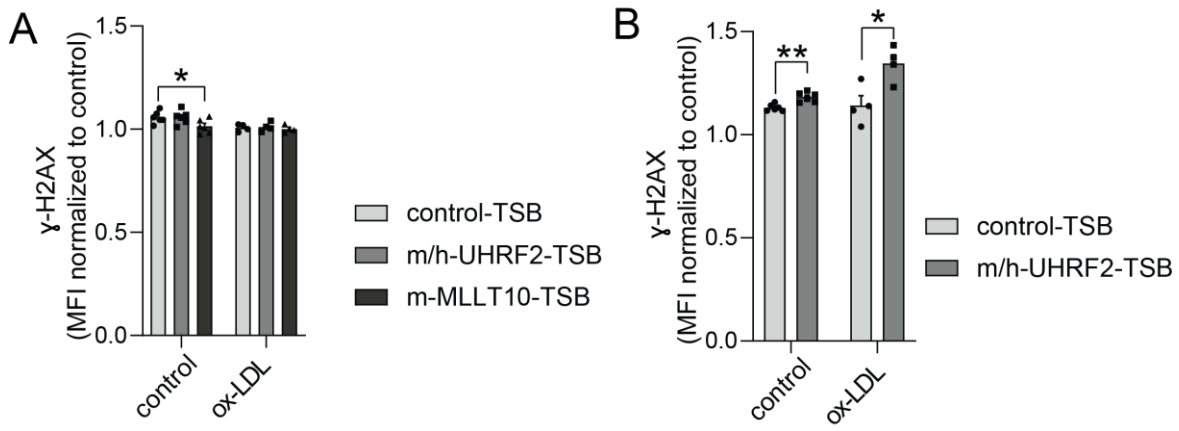

Fig. 45: Effect of TSBs on DNA damage formation in ECs.

(A) MECs were treated with h/m-UHRF2-TSB, Mllt10-TSB, or control-TSB for 24 h and treatment with or without ox-LDL (100 µg/ml for 24 h n = 3-6). (B) HECs were treated with h/m-UHRF2-TSB or control-TSB for 24 h following 24 h of no treatment (control) or 100 µg/ml ox-LDL (n = 3-6). Next, cells were labelled with APC conjugated anti-γ-H2AX antibody. γ-H2AX MFI was measured by flow cytometry and normalized to the control sample. Data was compared between the treatments and the controls using multiple t-test with no multiple comparison correction (**P*<0.05, ***P*<0.001). Data is presented as mean ± SEM.

3.11.5 Role of let-7b in EC micronuclei formation

To investigate whether let-7b affects micronuclei (MN) formation, MECs and HECs were stained with DAPI after let-7b inhibitor or control inhibitor treatment, and the number of MN in cells were assessed. Let-7b inhibition did not change the percent of cells containing a MN or the percentage of MN per cell in MECs (Fig. 46A) and HECs (Fig. 46B), suggesting that MN formation is not affected by let-7b expression levels.

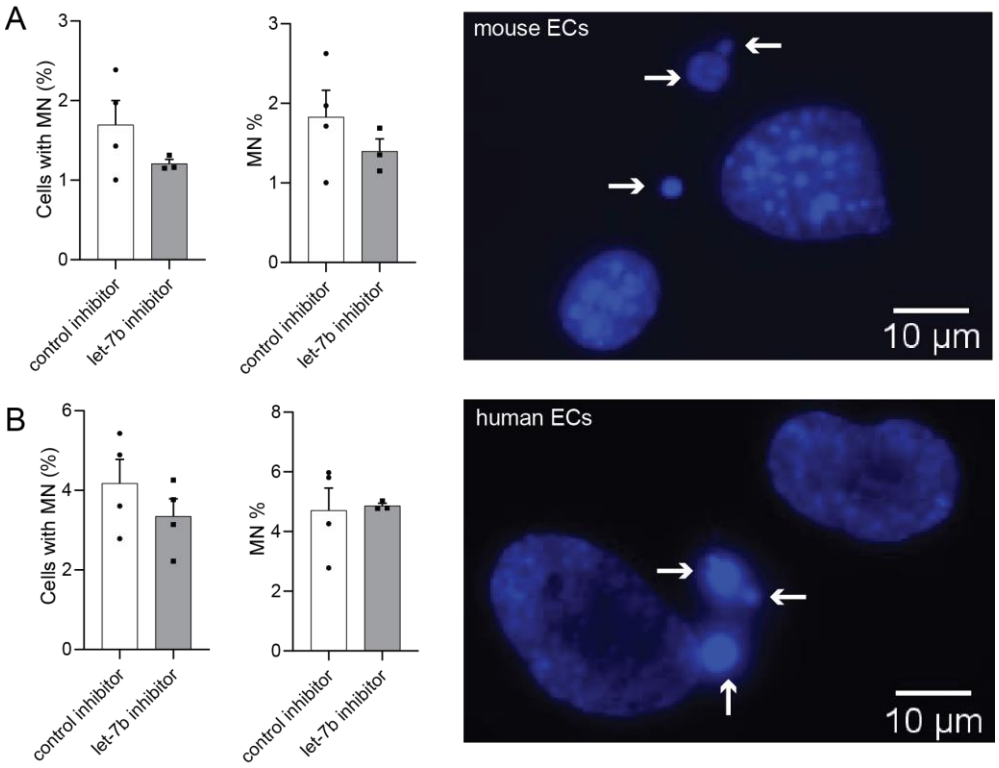

Fig. 46: Effect of let-7b on MN formation in ECs.

(A) MECs and (B) HECs were treated with 50 nM of let-7b inhibitor or control inhibitor for 24 h (n = 3-4). The number of MN were counted and reported as the percent of cells with a MN or the number of MN normalized to total cell numbers (MN %). Data was compared between the let-7b inhibitor treated sample and control using two-tailed Student's t-test and presented as mean ± SEM (*P*=ns). White arrows point to the MN detected in ECs.

3.11.6 Effects of let-7b on reactive oxygen species production in ECs

If reactive oxygen species (ROS) production is not balanced in the cell, it leads to oxidative stress and consecutively cell damage (146). To investigate ROS production in ECs, DCFDA/H2DCFDA Cellular ROS Assay was performed in MECs and HECs treated with oligonucleotides with and without ox-LDL treatment.

ROS was significantly increased in MECs and HECs treated with ox-LDL and *tert*-Butyl hydroperoxide (TBHP), represented by the increased Fluorescent intensity (FI) of DCFDA ($P<0.0001$, Fig. 47A). Let-7b inhibition significantly increased ROS production in MECs with ($P<0.01$) or without ($P<0.05$) ox-LDL treatment, but had no effect on HECs, suggesting that let-7b is protective against oxidative stress only in MECs (Fig. 47B).

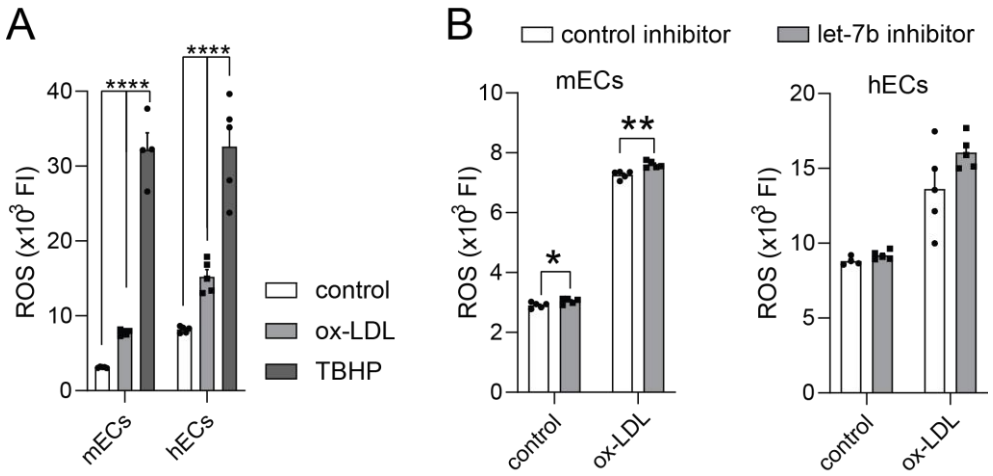

Fig. 47: Effect of let-7b on ROS production in MECs and HECs.

(A) MECs and HECs were treated with 100 µg/ml ox-LDL or 500 µM TBHP and ROS was measured after 3 h. (B) MECs and HECs were treated with let-7b inhibitor or control inhibitor for 24 h (n = 4-5). ROS was measured after 3 h of no treatment or 100 µg/ml ox-LDL treatment. Treatment groups were compared to the controls using multiple t-test (*P<0.05, **P<0.01, ****P<0.0001). Data is presented as mean ± SEM.

ROS production was increased in MECs treated with h/m-UHRF2-TSB with (P<0.05) and without ox-LDL treatment (P<0.01). Moreover, Mllt10-TSB treatment increased ROS in MECs in the presence of ox-LDL (P<0.0001, Fig. 48A) indicating that the protective effect of let-7b on oxidative stress is partly mediated through UHRF2 and Mllt10 in MECs. H/m-UHRF2-TSB did not have an effect on ROS production in HECs (Fig. 48B). These results reveal that let-7b mediated UHRF2 downregulation results in decreased ROS production only in MECs.

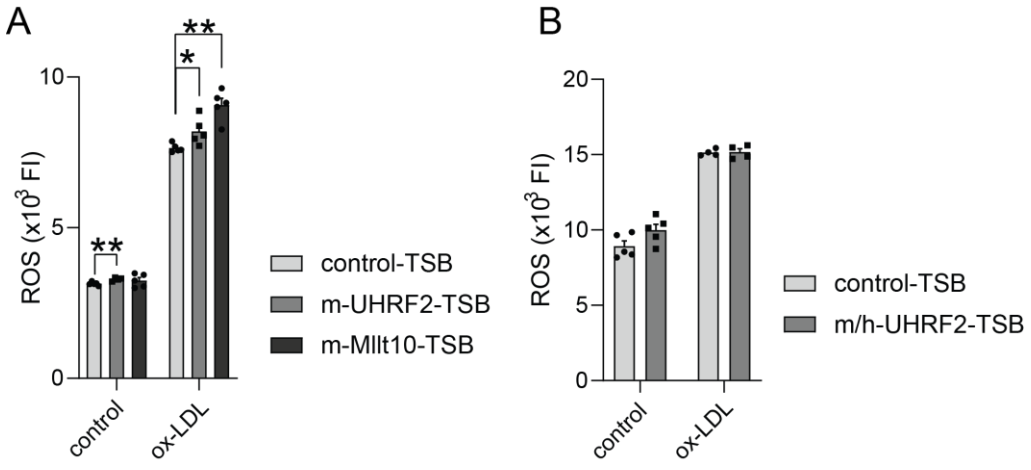

Fig. 48: Effect of TSBs on ROS production in MECs and HECs.

(A) MECs were treated with h/m-UHRF2-TSB, m-Mllt10-TSB and control-TSB for 24 h (n = 4-5). (B) HECs were treated with h/m-UHRF2-TSB and control-TSB for 24 h (n = 4-5). ROS was measured in mouse and human ECs in the presence or absence of ox-LDL treatment (100 µg/ml, 3h). Treatment groups were compared to the control using one-way ANOVA in MECs (*P<0.05, **P<0.01) and multiple t-test in HECs (P=ns). Data is presented as mean ± SEM.

4 Discussion

4.1. Let-7 family members in MECs and HECs

Let-7b shares its seed sequence with 11 other miRNAs in mice and with nine miRNAs in humans. Moreover, their whole sequences differ only in one or two nucleotides. This similarity makes it likely that let-7 family members have similar functions. However, it is unclear whether this assumption is correct because it is technically challenging to discriminate the individual family members, e.g., by standard qRT-PCR. To overcome this technical limitation, an LNA-based probe PCR was used in the current study, which can discriminate single nucleotide differences in DNAs and RNAs (147).

In contrast to previous results, which found high expression of let-7a in human umbilical cord vein endothelial cells (HUVECS) (63, 148) by Taqman RT-PCR and in HECs by microarray (84), let-7a was not detectable in MECs or HECs in the current study. This discrepancy is most likely due to cross-detection of other let-7 family members by microarray or Taqman RT-PCR. In addition, the potential cross-detection by Taqman RT-PCR may also be considered in interpreting data from other studies comparing the expression level of let-7 family members (63, 79, 149-154). Thus, the expression levels of the let-7 family members in ECs were quantified for the first time in the current study.

The expression levels differed substantially between the individual let-7 family members in aortic ECs. Let-7c was much higher expressed than all the other let-7 members in MECs, whereas the expression levels of all let-7 members except for let-7a were comparable in HECs. Thus, the let-7 family members were differentially expressed between MECs and HECs. However, this is only relevant if the individual let-7 members have specific functions independent of the same seed sequence. Interestingly, knockout of the let-7adf cluster increases antigen-dependent IgM production in mice. In contrast, the knockout of the let-7bc cluster did not affect IgM production, indicating that individual let-7 family members have specific effects despite their minor sequence difference (155). Moreover, the role of different let-7 family members on mitochondrial function in macrophages has been studied by treatment with let-7 mimics. The results show that only let-7b but not let-7i, let-7a, and miR-98 affect mitochondrial respiration in anti-inflammatory macrophages (156). Thus, these data indicate that at least two to three nucleotide difference between the let-7 family members can change their function. EC-specific Dicer deletion reduces let-7b expression in the atherosclerotic aorta. In contrast, the expression of a group of lncRNAs with predicted non-canonical BSs for let-7b is increased (60), suggesting that let-7b plays a more critical role in ECs than the other let-7 members.

Furthermore, it is unclear how overexpressing one family member affects the expression of the other members. Therefore, the best way to study whether individual let-7 family members have specific effects would be to use cells or mice with a genetic knockout of one individual let-7 member. In the current study, the role of let-7b was studied primarily by treatment with

let-7b mimics to overexpress this miRNA. Although this approach allows altering let7b levels specifically, let7b mimic treatment may affect the expression of the other let-7 family members. Indeed, let-7b mimic treatment downregulated let-7c, d, and e expression levels in MECs, which could be due to negative feedback regulation of the other let-7 members. In contrast, in HECs, let-7b overexpression upregulated let-7c and g levels, indicating that the regulation of the let-7 family members among each other differs considerably between mouse and human ECs. LIN28 post-transcriptionally downregulates let-7 expression, and for some family members like let-7g, this downregulation is stronger (155). Interestingly, in HEK293 cells, let-7b targets LIN28 (157). Thus, upregulation of let-7c and let-7g may be due to the downregulation of LIN28 by let-7b in HECs. However, in mouse ECs, the mechanism by which let-7b downregulates other family members needs further investigations. Nevertheless, let-7b mimic transfection in mouse and human ECs resulted in a 13- and 19-fold overexpression of let-7b, respectively. Therefore, the comparably minor changes in the expression level of the other let-7 members may not alter the effect of let-7b mimic treatment.

4.2. Assessment of protein-coding genes in the let-7b interactome

MicroRNAs target dozens to hundreds of mRNAs in a cell due to the short seed sequence interaction (49). However, some miRNAs, such as miR-200b, can interact only with one mRNA target (158). The interactome of all miRNAs in a cell can be investigated by techniques such as high-throughput sequencing of RNAs isolated by crosslinking immunoprecipitation (HITS-CLIP) (159) and photoactivatable-ribonucleoside-enhanced crosslinking and immunoprecipitation (PAR-CLIP) (160). Moreover, crosslinking, ligation, and sequencing of hybrids (CLASH) can even determine individual miRNA-RNA interactions directly using an extra ligating step to produce miRNA-mRNA hybrids (158). In the current study, overexpression of a mutated subunit of the RISC and let-7b by co-transfection of the miRTrap vector and let-7b mimic, respectively, allowed the pulldown of let-7b-bound targets that were trapped in the RISC and could not be further processed (87). Let-7b targeted a substantial fraction of the protein-coding transcriptome in MECs (11%) and HECs (19%). Moreover, a considerable fraction of the expressed protein-coding genes was detectable in the Ago2 immunoprecipitates but not enriched by let-7b, indicating that they are targets of other miRNAs. Among those miRNA targets, let-7b enriched 22% and 26% protein-coding transcripts in mouse and human ECs' RISC, respectively. In contrast, let-7b is involved in only 3% of all miRNA-mRNA interactions in HEK293 cells (158). This difference indicates that let-7b may play a more prominent role in ECs than HEK293 cells. The percent of let-7b interactions with mRNAs were 89% and 79% of the total interactions in mouse and human ECs, respectively. Interestingly, the percent of canonical let-7b interactions with mRNAs are 95% and 57% of all canonical let-7b interactions in mouse and human tissues, respectively (161), which further supports that let-7b interaction with mRNAs plays a central role in ECs.

Another reason for this discrepancy could be that a mutated Ago2 was expressed in the current study, which traps the mRNA target in the RISC. In contrast, an Ago2 protein without this trapping function was expressed in the study by Hellwag *et al.* (158). Furthermore, overexpression of let-7b in the current study may lead to the detection of a more significant number of transient interactions compared with the study by Hellwag *et al.*, where endogenous miRNA interactions were investigated (158). Moreover, the combination of overexpressing let-7b during 24 hours and the trapping function of the Ago2 protein may result in a cumulative number of interactions during this period rather than in the interactions at one-time point as in the study by Hellwag *et al.* (158). Thus, it is likely that a more comprehensive number of let-7b targets, including those with transient interactions, has been determined in the current study. To decrease the possibility of false positive let-7b targets, only mRNAs detected in all replicates were included in the present study.

Notably, one current study finding was that miRNAs more frequently targeted mRNAs in HECs (74%) than in MECs (51%). Interestingly, these data align with reports that validated targets of miRNAs are more frequent in humans than in mice (162). This difference could be related to the general increase in the number of miRNAs during the evolution of biological complexity. The human species has gained 179 out of its 585 miRNA genes after diverging from mouse (163). In addition, let-7b targeted more mRNAs in HECs (26% of the miRNA targets and 19% of all expressed mRNAs) than in MECs (22% of the miRNA targets and 11% of all expressed mRNAs), and human-specific let-7b targets were more frequent than mouse-specific targets. This difference between the two species could be due to an increase in targeting by let-7 family members in humans compared to other species like mice, rats, and zebrafish (162), indicating that the let-7 function expanded explicitly in humans, corresponding to their complexity (47).

A limitation of the miRtrap approach in the current study may be that more transient interactions between let-7b and its targets are detected, which do not affect protein expression and thus have no functional role. Moreover, mimic transfection reduces the possibility of detecting low-expressed targets because it may suppress the target to undetectable levels. To overcome these limitations, future studies may use let-7b inhibitor transfection in ECs or EC-specific knockout of let-7b combined with immunoprecipitation of endogenous Ago2. Thus, comparing the data between the two approaches will allow us to explore the probability of detecting irrelevant let-7b interactions in this study.

4.3. Conservation of canonical let-7b BSs in protein-coding genes

miRNA-mediated post-transcriptional gene regulation occurs through canonical interactions between miRNAs and the 3’–UTRs of protein-coding genes in the RISC (Fig. 1.6) (41). Although canonical BSs in the coding sequences and 5’–UTRs may also be functional (160, 164, 165), those predicted in the 3’–UTRs are more effectively repressing protein expression (166). Hence, the 3’–UTR sequences of protein-coding targets were screened for 8mer, 7mer-m8, and 7mer-A1 sites in the current study (46). In human and mouse ECs, nearly one-third

of the protein-coding let-7b targets were predicted to contain canonical BSs in their 3'–UTRs, indicating that most let-7b-target interactions are via non-canonical BSs, such as G:U base pairing in the seed match and 3' complementary binding. In line with this finding, 13% of the let-7b interactions with the 3'–UTRs contain canonical seed matches in HEK293 cells (158). Therefore, non-canonical interactions between let-7b and its targets may be more common than canonical interactions. However, it needs to be determined whether these non-canonical interactions are biologically relevant (95). For instance, the let-7 BS in the 3'–UTR of *C. elegans lin-41* gene contains two non-canonical 3'-compensatory sites that are conserved in the nematode species and are very efficient for *lin-41* regulation (34-36).

Canonical BSs are reported more effective in miRNA-mediated target repression than non-canonical BSs (37, 95). The 8mer BS is the most efficient canonical BSs, followed by 7mer-m8 and 7mer-A1 BSs (46, 95). Notably, the 8mer BSs were less common than the 7mer-m8 and 7mer-A1 BSs in ECs from both species. This finding contrasts with other reports showing that miRNAs, such as miR-1, mainly bind to 8mer BSs in cancer cells (166). The finding that let-7b targets less efficient canonical BSs in ECs may be due to their stable phenotypic nature, requiring a less efficient let-7b targeting. In contrast, the permanent phenotypic changes during proliferation in cancer cells may require more efficient target regulation by miRNAs.

Considering the high conservation of the let-7 seed (65), the let-7b BSs in the target mRNAs might also be conserved between species (46). In the current study, 23 out of 153 common protein-coding let-7b targets in mouse and human ECs (15%) contained an identical canonical BS in their 3'–UTR. Bioinformatics analysis of available 3'–UTR sequences of 14 non-fish vertebrate species showed that 7% of genes contained conserved BSs for conserved miRNA families (96). Indeed, 18-23% of common mouse and human let-7b targets had canonical non-identical BSs, which suggests that the functional conservation of let-7b targeting plays a critical role in ECs.

Targeting conserved BSs, mainly canonical, more strongly represses protein expression than non-conserved BSs (36), suggesting that targeting conserved, canonical BSs is critical for the functional role of miRNAs, including let-7b (167). The canonical and highly conserved let-7 BSs in the UHRF2 and MLLT10 3'–UTRs were verified by luciferase reporter assays, indicating that the strategy to identify let-7 targets in ECs was successful. In line with these findings, the let-7 8mer BS in the UHRF2 3'–UTR is experimentally confirmed in human A549 lung cancer cells (168). Furthermore, let-7 interacts with MLLT10 in a breast cancer cell line according to data from a HITS-CLIP study (104). However, the let-7 BS in the MLLT10 3'-UTR has not been previously studied.

4.4. Differences between mouse and human ECs in post-transcriptional regulation of let-7b targets

Due to the identical seed sequence, let-7 family members may share the same canonical targets. However, distinct roles of individual let-7 family members have been described. For example, let-7b mimic treatment increases mitochondrial respiration in bone marrow-derived

murine macrophages, in contrast to let-7a and let-7i (156). This effect may be due to non-canonical targeting, e.g., via seedless or 3'-complementary interactions.

miRNA mimic transfection allows to study strand-specific effects of miRNA and thus the role of individual let-7 family members (169). However, one limitation of this approach is that let-7b mimic treatment may not downregulate genes that are suppressed by endogenous let-7 to a very low expression level. This was probably why let-7b mimic treatment did not downregulate UHRF2 at the protein level in human ECs. To circumvent this limitation, let-7b inhibitor treatment was additionally performed in the functional assays. Accordingly, the UHRF2 protein levels were increased by let-7b inhibitor treatment in mouse and human ECs, demonstrating that let-7b suppresses UHRF2 in ECs. However, inhibiting let-7b increased the UHRF2 mRNA only in MECs but not in HECs, suggesting that let-7b degrades UHRF2 mRNA in MECs, whereas it inhibits UHRF2 translation in HECs. Accordingly, let-7 inhibits the initiation of translation in human cells (170).

In contrast to inhibition of translational initiation, degradation of the mRNA requires more time due to the recruitment of proteins of the deadenylation and decapping complexes. Therefore, the miRNA-mediated protein downregulation response may be time-dependent and occur at different times in mouse and human cells (171, 172). Another factor that plays a role in miRNA-mediated protein downregulation is the complementarity between the miRNA and its target RNA. Whereas high complementarity mainly results in mRNA decay, low complementarity, e.g., due to mismatches, favors translational inhibition (173). However, different degrees of complementarity cannot cause the differences in the UHRF2 mRNA targeting by let-7b in mouse and human ECs, since the UHRF2 BS region has identical flanking sequences in both species (Fig. 49A).

Let-7b inhibitors block the interaction between let-7b and all its targets. Therefore, besides UHRF2, let-7b inhibition most probably upregulated many other let-7b targets that could be different between mouse and human ECs (Fig. 49B). The differential regulation of other let-7b targets between the two types of ECs may explain why the mRNA level of UHRF2 did not change after let-7b inhibition in HECs. Interestingly, let-7b mimic treatment regulated RNA-related pathways differently in mouse and human ECs. For instance, let-7b mimic treatment upregulated CELF1 in HECs but not MECs. CELF1 promotes mRNA degradation by binding to UG-rich regions in the 3'–UTR (174, 175). Therefore, in contrast to MECs, inhibiting let-7b in HECs may reduce the expression of proteins that mediate mRNA decay, such as CELF1. Thus, the different outcomes of UHRF2 targeting in mouse and human ECs may be partially due to the differential regulation of other genes by let-7b in the two species.

To avoid the effect of other let-7b targets, TSBs were designed to block the interaction between let-7b and UHRF2. In contrast to let-7b inhibitor treatment, UHRF2-TSB treatment increased only the UHRF2 mRNA expression level in HECs and MECs (Fig. 49C). Thus, in comparison to the UHRF2-TSB treatment, the effect of the let-7b inhibitor on the UHRF2 mRNA level in HECs may be the net result of the up-regulation of multiple let-7b targets.

Like UHRF2, let-7b inhibitor treatment increased Mllt10 mRNA expression levels only in MECs and not HECs. Moreover, identical to UHRF2, MLLT10-TSB increased MLLT10

mRNA expression levels in mouse and human ECs. The similar let-7b-mediated regulation of MLLT10 and UHRF2 in HECs supports the hypothesis that individual interactions between the target and let-7b result in changes in the target mRNA level. The high similarity between the UHRF2 3'–UTR sequences allowed the design of the same TSBs for mouse and human ECs, whereas two different TSBs had to be designed for MLLT10 due to nucleotide differences that flank the BS. Indeed, in MECs, Mllt10-TSB treatment increased the expression of only Mllt10, whereas, in HECs, the MLLT10-TSB treatment also increased UHRF2 expression. Thus, TSBs with a design specific for the interaction between let-7b and MLLT10 had to be studied in HECs. In addition, MLLT10 protein expression values need to be determined after TSB and let-7b inhibitor treatment to compare its regulation by let-7b in mouse and human ECs.

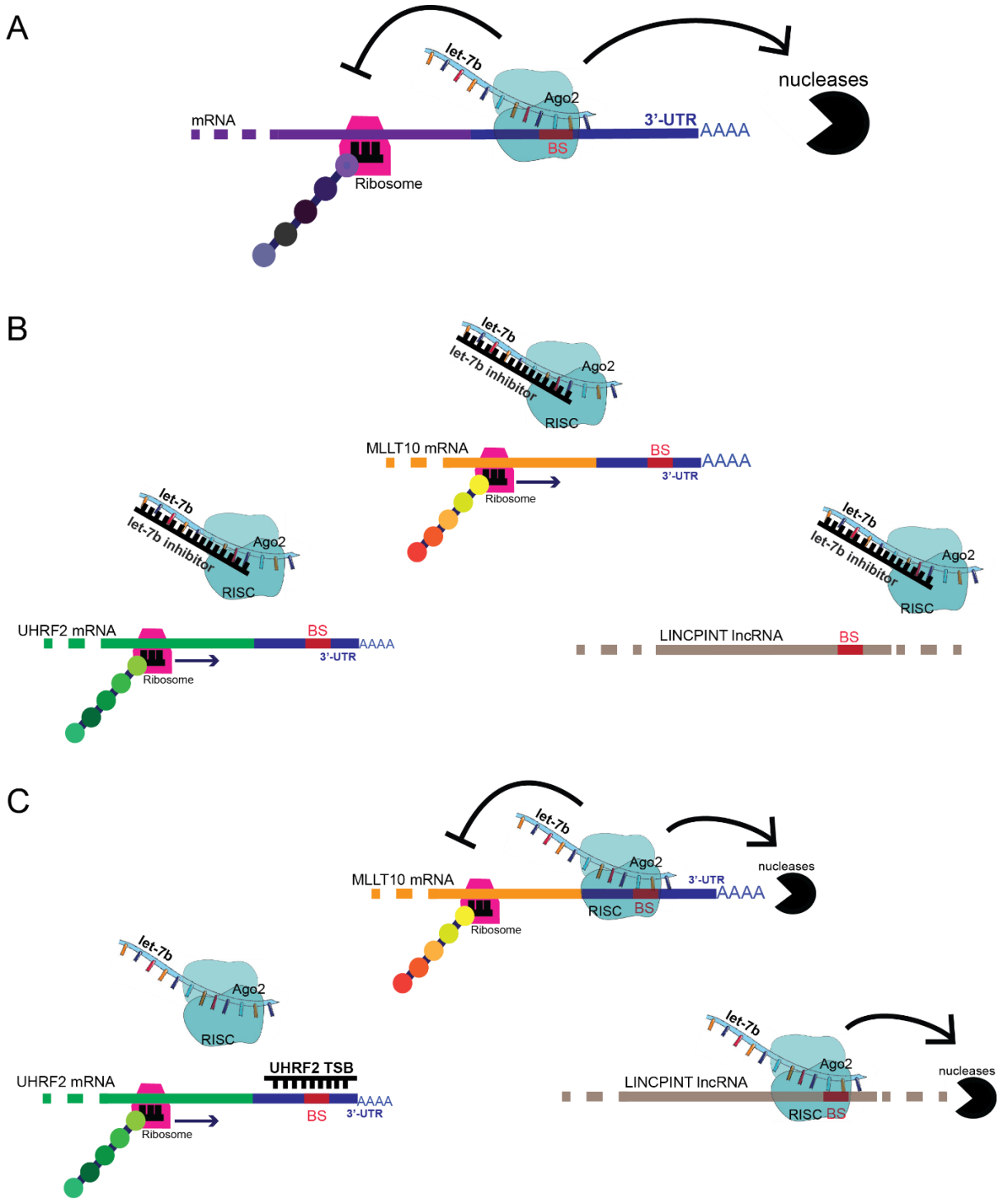

Fig. 49: Functional differences between let-7b inhibitors and TSBs

(A) Binding of let-7b in the RISC reduces the protein level of the mRNA target by translational inhibition or mRNA degradation. (B) Inhibitor treatment blocks the interaction of let-7b with all its targets, including MLLT10 and LINCPINT. (C) UHRF2-TSB treatment inhibits the interaction between let-7b and its BS in the 3'–UTR of UHRF2, but not between let-7b and its other targets, such as MLLT10 and LINCPINT.

The effect of let-7b inhibitor treatment on the expression of other let-7 family members was also different between mouse and human ECs, which could contribute to the differential impact of the let-7b inhibitor on both cell types. Whereas let-7b inhibitor treatment upregulated let-7g expression in MECs, it did not affect let-7g expression in HECs. Because miRNAs can also target other miRNAs (158), the let-7b inhibitor treatment may derepress let-7g in MECs. The difference in let-7g expression between mouse and human ECs after inhibiting let-7b could play a role in the regulation of UHRF2 in both cell types because the let-7b inhibitor may not block let-7g targeting due to four nucleotide differences in 3'complementary region. Conclusively, regulation of let-7 members by let-7b inhibition varies between mouse and human ECs and thus may influence UHRF2 mRNA regulation in both species.

4.5. Assessment of ncRNA and lncRNA gene expression in ECs

Mammalian nuclear genomes transcribe thousands of ncRNA genes, mostly lower expressed than protein-coding genes (176). Interestingly, some of the most highly expressed transcripts in human and mouse ECs were ncRNAs encoded in the mitochondrial genome. In the human heart, 70% of the lncRNAs are encoded in the mitochondrial genome (177). Some of these lncRNAs may not play a role in mitochondria. For instance, blood levels of the lncRNA LIPCAR, encoded in the mitochondrial and nuclear genome, indicate the risk for cardiovascular death after myocardial infarction (178). Moreover, two mitochondrial-encoded lncRNAs, MDL1 and MDL1AS, have been described in mice and humans (179, 180).

The mitochondrial-encoded mRNAs and lncRNAs were similar, but the highly expressed nuclear-encoded ncRNAs differed between mice and humans. For instance, MALAT1 was among the ten highly expressed ncRNAs in HECs but not MECs. MALAT1 contains BSs for more than 50 miRNAs, acts as a miRNA sponge (6), and promotes proliferation and vascularization of ECs (61, 181). Therefore, nuclear-encoded ncRNAs may contribute to the differences between mouse and human ECs.

In general, lncRNA gene and transcript numbers evolve more rapidly compared to protein-coding sequences (59) and can be up to 2-fold higher in humans than in mice (182). However, another study reported similar numbers of lncRNAs expressed in humans and mice (183). In ECs, ncRNA transcripts were 8.5-fold higher in HECs than in MECs, supporting that lncRNAs are more abundant in humans than in mice. Alternatively, ncRNA differences between mice and humans may be more prominent in ECs than in other cell types, which may explain species-specific effects of let-7b-mediated regulation of RNA transcript expression.

4.6. Assessment of lncRNA targets of let-7b in ECs

In addition to mRNAs, miRNAs can target ncRNAs (184-186), including pseudogenes and lncRNAs (60, 187). Interestingly, EC-specific *Dicer* deletion in mice downregulates miRNAs, such as miR-103 and let-7b, and upregulates a group of lncRNA transcripts,

including lncWDR59 and linc051468 in atherosclerotic arteries (60). Interestingly, linc051468 (5031425E22Rik or ENSMUSG00000073147), which contains a canonical let-7 BS, was also a target of let-7b in MECs. Most upregulated lncRNAs contain BS for miR-103 and let-7b, indicating that both miRNAs play a critical role in lncRNA targeting. Accordingly, in the current study, 50% of the non-coding transcripts in the RISC were let-7b targets, supporting the statement that, compared with other miRNAs, let-7b preferentially targets lncRNAs in MECs. Moreover, *Dicer* expression in mice ECs promotes atherosclerosis, partly due to the targeting of lncWDR59 by miR-103 (60). This finding suggests that targeting lncRNAs by let-7b in ECs may increase atherosclerotic plaque formation.

Only 11% and 21% of the let-7b targets were lncRNAs in mouse and human ECs, respectively. Thus, mRNAs are the main class of let-7b targets in ECs. This finding is in accordance with the miRNA interactome in HEK293 cells analyzed by the CLASH method (158). However, in ECs, the percentage of lncRNA targets of let-7b is much higher than that of all miRNAs in 293 cells (0.4%) (158). Similarly, CLIP-sequencing data indicate that 2% of all let-7b interactions are with lncRNAs in various mouse and human tissues (161, 188). Together, these findings suggest that miRNA-mediated targeting of lncRNAs is more critical in ECs than in other cell types. Furthermore, targeting of lncRNAs by let-7b is more frequent in human than in mouse ECs. Because the fraction of ncRNAs targeted by let-7b was similar between both species, the expansion of ncRNA expression may lead to an increased percentage of lncRNA targets of let-7b in HECs compared with MECs (47, 162, 163).

Notably, the miR-155 host gene (MIR155HG) was among the highly enriched let-7b lncRNA targets in HECs. This indicates that let-7b can interact with lncRNAs that are miRNA regulators and may indirectly regulate other miRNAs. Transfer of miR-155 to ECs via neutrophil-derived microvesicles promotes inflammation and atherogenesis (189). Therefore, regulating this miRNA by endothelial let-7b may play a role in atherosclerotic disease progression.

4.7. Canonical let-7b BSs in lncRNA genes

miRNAs target mRNA and lncRNA sequences through canonical and non-canonical interactions. Although miRNA BSs can be found on the entire mRNA sequence, the canonical miRNA targeting occurs in the 3’–UTR (46). Therefore, the predicted BSs in the 3’–UTRs were assessed in this study. lncRNAs lack a 3’-UTR, and miRNA BSs were predicted along the entire lncRNA sequence. Notably, more BSs were predicted in lncRNA sequences than in 3’–UTR sequences. One reason for this difference could be that the lncRNA transcript sequences are longer than the 3’–UTRs of the mRNAs, resulting in the prediction of more BSs in lncRNAs. However, like protein-coding genes, nearly one-third of the lncRNA targets contained a canonical BS in their transcript sequence.

According to the ENCORI database (161, 188), 8mer BSs are the most common type (42%) of interaction between let-7b and lncRNAs in mice and humans. In the current study, 8mer sites were also the most common predicted BSs in mouse let-7b lncRNA targets. However,

7mer-m8 and 7mer-A1 BSs in lncRNA targets were more frequent in HECs. Accordingly, mouse lncRNA targets were enriched more than human lncRNA targets by let-7b in the RISC, which aligns with the more substantial targeting effect of 8mer BSs. However, it is unclear why human lncRNA targets of let-7b mainly contain BSs other than 8mers.

A small group of conserved and highly expressed lncRNAs, like MALAT1, contain many BSs for miRNAs and interact with them in the RISC, known as the sponging effect (6). Sponging by lncRNAs reduces the regulatory impact of a miRNA on other RNA targets (190). For instance, sponging of let-7 by the H19 lncRNA reduces the suppression of HMGA2 and DICER proteins in SMCs (191). Accordingly, the current finding that lncRNA targets contain more let-7b BSs than mRNAs targets indicates that lncRNAs sponge up let-7b in ECs. One of the let-7b lncRNA targets with multiple BSs in MECs and HECs was LINCPINT. Because LINCPINT sponges multiple miRNAs, like miR-543, miR-208a-3p, and miR-155-5p (192-198), it may act as a let-7b sponge in ECs.

Like the mRNA targets, let-7b inhibitor treatment regulated LINCPINT expression only in MECs. Because lncRNAs are not translated, the posttranscriptional effect of let-7b on LINCPINT cannot be detected at the protein level. Thus, the finding that let-7b inhibition does not affect the transcript level of LINCPINT in HECs indicates that it primarily acts by sponging let-7b away from other mRNA targets. However, the finding that let-7b inhibition did not affect LINCPINT levels in HECs could also be due to the targeting by different miRNAs. Notably, LINCPINT also exists in a circular form (circRNA) in human cells, encoding a peptide that interacts with polymerase-associated factor complex (PAF1c) and inhibits elongation of oncogenes (199). However, the regulation of the circLINCPINT-derived peptide was not investigated further. Therefore, it cannot be excluded that let-7b inhibition regulates the translation of the LINCPINT peptide.

Various studies have reported 1000 to 2000 orthologous lncRNAs in mice and humans with the same function in the two species (182), indicating that lncRNA functions are conserved (200). Conservation of lncRNA structure and sequence is also probable but rare; however, the BS sequence conservation is critical to determine whether let-7b-mediated lncRNA targeting is conserved in mice and humans. Of the two let-7b BSs in MECs and three let-7b BSs in HECs predicted in LINCPINT, only the validated 7mer-A1 BS was identical and conserved in mouse and human ECs. Interestingly, blocking the conserved let-7b BS in LINCPINT by TSB treatment did not alter the Lincpint expression in MECs. This finding could be due to the binding of let-7b to the other predicted canonical BSs or non-canonical BSs in Lincpint. Thus, blocking the conserved let-7b BS is insufficient to inhibit Lincpint targeting by let-7b.

LINCPINT expression reduces tumorigenesis, cell growth, and cell proliferation in various cancers (201-207). Therefore, LINCPINT may inhibit EC proliferation. However, the role of let-7b-mediated LINCPINT targeting still needs to be elucidated.

4.8. Effects of let-7b on endothelial gene expression

miRNAs regulate gene expression through complementary binding to the mRNA target (173), which ultimately decreases its expression at the protein level. Moreover, miRNAs can indirectly regulate the expression of non-target proteins. In the current study, overexpression of let-7b regulated the expression of nearly 3% of the detected proteins in mouse and human ECs. This is in line with the finding that let-7b modulates protein expression of thousands of genes in HeLa cells (37). The regulated proteins by let-7b mimics included genes of identified let-7b targets (significantly enriched in the RISC) or contained an often conserved let-7b BS in their 3'–UTRs. In general, miRNA overexpression mildly (less than 2-fold) downregulates the transcript and protein expression of many targets with complimentary BSs in the 3'–UTRs (37, 208).

Whereas let-7b regulated proteins involved in RNA processing in MECs, it controlled proteins related to translation in HECs. Although this finding indicates that let-7b regulates different protein networks in mouse and human ECs, the functional role of the differentially regulated proteins appears to be pro-proliferative in both cell types. For example, the murine Fus and the human PUM1 proteins, downregulated by let-7b mimics, have a pro-proliferative effect on cancer cells (140, 209).

Among the regulated proteins by let-7b, no common proteins were detected between HECs and MECs. Moreover, the conserved let-7b targets' protein expression was mainly undetectable. In LC-MS/MS approach, quantities of only the detected proteins in control and treatment groups can be compared; therefore, if a protein is not expressed in the treatment or control group, it will not be included in the analysis. Thus, it is probable that these targets either are low expressed or are very efficiently downregulated by let-7b mimic treatment. The strict gene inclusion strategy may have excluded many of the proteins regulated by let-7b from the target enrichment analysis.

Besides the canonical pathway of miRNA-mediated downregulation of proteins, reports have shown that miRNAs can upregulate proteins (210, 211). Notably, many proteins were conversely upregulated by let-7b mimic transfection in murine and human ECs. The proteins upregulated by let-7b mimics also contained a conserved BS or were among the enriched targets by let-7b, indicating that let-7b interaction with 3'–UTRs may also lead to the upregulation of proteins. Upregulation of proteins by miRNAs like let-7 has been previously shown in serum-starved growth-arrested cells (211). miRNA-mediated translational repression of targets occurs in cycling cells, whereas in quiescent cells, miRNAs, including let-7, can mediate translational activation (212). miR-206 induces translational repression or activation of KLF4 in proliferating cells (213). MiR-145 has also been shown to mediate Myocardin overexpression by binding to its 3'–UTR and inducing vascular SMC differentiation (214). Cellular stress in HEK293 cells causes remodeling of the Ago2–mRNA interactions that release Ago2-bound mRNA sites (113), which might explain the

translational increase of the targets. Thus, depending on the cellular state, let-7b targeting could probably have a different outcome on protein regulation.

4.9. The let-7b targeting effect on ECs

Inflammatory activation, apoptosis, and ineffective regeneration due to decreased proliferation characterize EC maladaptation (6). Notably, let-7b targets TLR4 in human epithelial cells and affects inflammation by regulating NFκB activation and downstream genes involved in inflammation (150). Interestingly, let-7b overexpression did not alter CCL2, ICAM-1, and VCAM-1 gene expression in ECs, indicating that let-7 does not play a role in the inflammatory activation of ECs. This finding contrasts the inhibition of inflammation in HUVECs by let-7g. Let-7g overexpression in HUVECS inhibits inflammatory activation by targeting TGF-β pathway genes, i.e., THBS1 (thrombospondin 1), TGFBR1 (transforming growth factor beta receptor I), and SMAD2 (SMAD family member) (86). Moreover, let-7g and mir-98 target CCL2 and CCL5 to decrease leukocyte adhesion to microvascular ECs (215). Therefore, detection of inflammatory marker expression changes in this study may have been hindered due to let-7b mimic treatment in ECs. Conclusively, assessment of inflammatory markers after let-7b inhibition would clarify the role of let-7b in inflammatory activation of ECs.

Let-7 inhibits the proliferation of cancer cells and is a well-known tumour suppressor (216); however, in the current study, let-7b enhanced the proliferation of murine and human aortic ECs after injury. Although MECs and HECs appear to be very different, let-7b mediated increase of proliferation was similar in ECs from the two species. This data reveals that regulating proliferation by let-7b is a conserved function in both species. However, in a diabetic retinopathy model, let-7 inhibited the proliferation of HUVECs and reduced the formation of tubular structures (152), indicating that the effect of let-7 on proliferation depends on the disease context.

Inducing an injury to a confluent monolayer of ECs triggers cell proliferation (217-219). Because let-7 represses its targets during the proliferating phase of the cells and increases target gene expression levels in quiescent cells (212), the final effect of let-7b on proliferation may depend on the cell cycle phase.

Let-7b increased regeneration of HECs but not of MECs after injury. The regeneration of the EC layer depends on the combinatorial effect of proliferation, migration, and apoptosis. In HECs, decreased wound repair after let-7b inhibition may be due to reduced cell proliferation. In MECs, however, despite decreased cell proliferation after let-7b inhibition, wound repair efficiency was not altered. Interestingly, in HUVECs, up-regulation of let-7a attenuates migration (220); therefore, similar to HUVECS, MEC migration might have increased after let-7b inhibition. Thus, increased MEC migration during wound closure may compensate for the decreased proliferation.

Let-7 members also play a role in the apoptotic regulation of different cell types. In this study, let-7b inhibition increased apoptosis of HECs, but not MECs. This effect of let-7b on EC apoptosis is another factor that can explain the difference in wound regeneration between murine and human ECs. However, different phenotypes regarding let-7-mediated apoptosis regulation are reported. In a HUVEC-derived cell line, let-7g targets the 3'–UTR of caspase 3 and reduces apoptosis (151). Moreover, let-7a targets caspase 3 in cancer cells (221) and let-7e in PC12 cell line (222). Furthermore, let-7g overexpression attenuates apoptosis in oxLDL-treated SMCs (223), and let-7a/b reduces oxLDL-induced apoptosis of HUVECs (63) further supporting an anti-apoptotic role of let-7. In contrast, let-7c overexpression in HUVECs increases oxLDL-induced apoptosis and caspase 3 activity by targeting the anti-apoptotic protein Bcl-xl (149). Let-7b inhibition regulates mouse-specific and human-specific let-7b targets, which may affect apoptosis differently. Therefore, different effects on apoptosis may be detected depending on the let-7 target and the cell type.

In this study, apoptosis was not a result of DNA damage or ROS generation. DNA damage accumulation in ECs, due to inefficient DNA damage repair and excessive oxLDL-mediated reactive oxygen species (ROS) production negatively affects EC regeneration. Various studies show that let-7 contributes to DNA damage and repair pathways (224-227). However, no change in DNA damage levels or DNA damage-mediated MN formation was detected after let-7b inhibition in murine and human ECs. Furthermore, ROS generated at a physiological level in cells can induce oxidative stress if its production exceeds the antioxidant system's buffering capacity (228). Oxidative stress in ECs leads to a pro-inflammatory and pro-coagulatory phenotype (229). Additionally, oxidative stress can lower NO levels and impair vascular growth. (229). In MECs, let-7b protected against ROS generation; however, let-7b inhibition did not alter ROS levels in HECs. In contrast, let-7b and let-7a reduce ROS generation, the NO deficit, and the downregulation of eNOS in oxLDL-treated HUVECs (63). Moreover, in primary human VSMCs, overexpression of let-7g reduces, and inhibition of let-7g enhances ROS production (230). Conclusively, the protective effect of let-7 on ROS generation appears to be cell-type specific (Fig. 50).

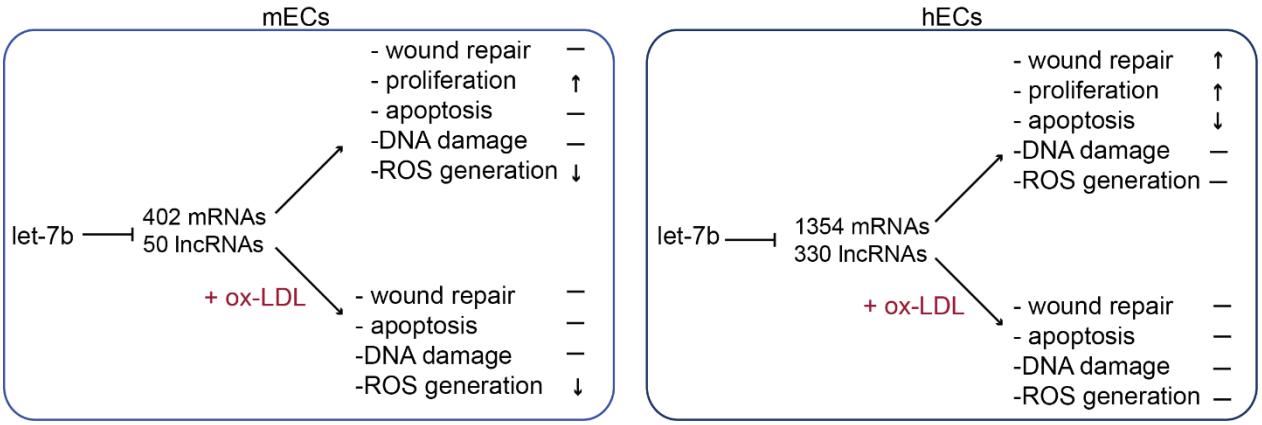

Fig. 50: Effects of let-7b inhibition on murine and human ECs.

Let-7b targets more uncommon mRNAs and lncRNAs than common RNAs in mouse and human ECs. Inhibiting let-7b (and, as a result, other let-7 members) by let-7b inhibitor alleviates the inhibitory effect of let-7b on all the common and uncommon targets, resulting in a different functional outcome between mouse and human ECs. Decreased EC proliferation after let-7b inhibition was similar in mouse and human ECs.

4.10. The effect of let-7b/UHRF2 interaction on ECs

Among the let-7b targets, one of the highly conserved targets in mice and humans with a canonical and identical BS was UHRF2 [also known as Np95/ICBP90-like RING finger protein (NIRF)]. This protein had the lowest combined P value of the mean enrichment compared to the other targets, making it an interesting target in ECs. UHRF2 is a nuclear protein interacting with the PEST-containing nuclear protein (PCNP) (231). UHRF2 is expressed in differentiated cells (232) and contains several functional domains interacting with diverse proteins (231, 233, 234), indicating its complex and broad activity. Interestingly, UHRF2 is one of the central nodes in the cell cycle network that interacts with cell cycle regulatory proteins, i.e., retinoblastoma (pRb), tumor protein P53 (p53), proliferating cell nuclear antigen (PCNA), and cyclins A2, B1, D1, and E1 (235) and Cdk2 (236). Moreover, UHRF2 binds the cyclin-dependent kinase inhibitor 1A (p21) cell cycle protein and negatively regulates it, most probably through ubiquitination (237); therefore, this protein is interesting in ECs since it plays a role in the cell cycle and cell proliferation control.

Increasing UHRF2 expression levels by blocking its interaction with let-7b promoted endothelial proliferation and regeneration. Endothelial proliferation promotes the repair of the endothelium at predilection sites by replacing apoptotic cells (6). Therefore, let-7b may impair endothelial regeneration at predilection sites by targeting UHRF2.

Interestingly, the UHRF2 expression level in lung fibroblast cell lines changes during the cell cycle, with high levels in the proliferative and low levels in the G0/G1 phase (231). Moreover, targeting UHRF2 by let-7a reduces cell proliferation and upregulates $p21^{WAF1}$ protein levels in cancer (168, 238), further supporting the current findings. Conclusively, let-7b mediated inhibition of EC proliferation by downregulating UHRF2 is conserved in mice and humans.

In contrast, targeting UHRF2 by let-7b had different effects on the apoptosis of MECs and HECs. oxLDL treatment attenuated the wound healing efficiency of HECs but not MECs, indicating that murine ECs are more resistant to oxLDL-induced injury. Blocking the interaction between let-7b and UHRF2 in MECs increased apoptosis after oxLDL treatment, which may hinder wound healing despite higher cell proliferation and thus compromise endothelial regeneration. In HECs, however, blocking let-7b-UHRF2 targeting in the presence of ox-LDL treatment decreased apoptosis and may therefore improve wound healing. The role of UHRF2 in apoptosis is contradictory (239, 240) and may depend on the cell type. Moreover, the effect of let-7b-mediated UHRF2 downregulation on apoptosis may be due to the different pathways in mouse and human ECs regulated downstream of this targeting pathway. Therefore, let-7b-mediated UHRF2 targeting effect on apoptosis is not conserved between mouse and human ECs.

DNA damage is evaluated by assessing the degree of phosphorylated (γ-) H2AX, a variant of the H2A histone, is incorporated evenly into the genome. After DNA double-strand breaks, the H2AX located near the damaged DNA regions is phosphorylated at serine 139 by a group of PI3-like protein kinases (241), stabilizing DNA damage repair factors and enabling DNA damage repair (242). High proliferation rates increase the probability of accumulating DNA damage due to the inactive cell repair mechanisms (243). Blocking the let-7b-UHRF2-interaction probably increases DNA damage that cannot be repaired in time in MECs. Accumulating DNA damage may lead to cell apoptosis without altering DNA damage extents. In HECs, however, blocking let-7b-UHRF2-interaction results in high DNA damage accumulation in proliferating cells, which is even higher with ox-LDL induced stress. Interestingly, UHRF2 is highly expressed in the mouse aortae and mouse VSMCs and is recruited to the DNA damage sites to facilitate H2AX phosphorylation (234). In HeLa cells, UHRF2 senses inter-strand crosslink (ICL) sites of damaged DNA and facilitates recruitment and maintenance of DNA damage repair factors (244). Accordingly, UHRF2 upregulation after blocking let-7b targeting in ECs may facilitate DNA damage repair in MECs. UHFR2 interacts with and is essential for activating ataxia telangiectasia and rad3-related (ATR) protein in a DNA damage-dependent manner (245). Moreover, UHRF2 interacts with PCNA, which is a sliding clamp protein involved in DNA replication and repair (246), therefore studying the interaction of UHRF2 with ATR and PCNA could also aid us in understanding its role in DNA damage formation and repair and that why it is different between mouse and human ECs.

Let-7b mediated inhibition of UHRF2 partially contributes to ROS decrease in MECs but not in HECs. This is the first report on the ROS-promoting effects of UHRF2.

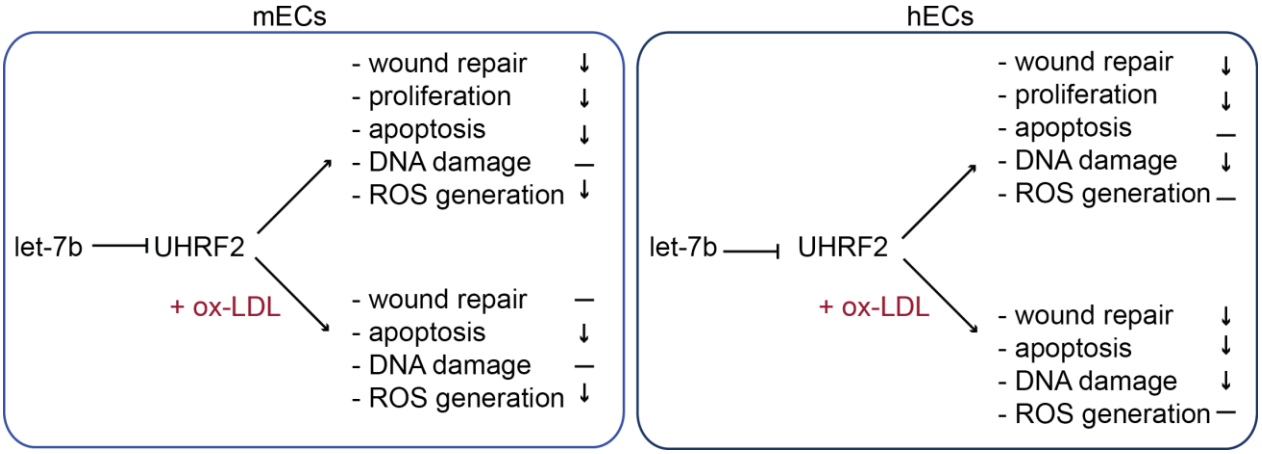

Fig. 51: The effect of let-7b-mediated UHRF2 downregulation on mouse and human ECs

Let-7b targets UHRF2 mRNA in mouse and human ECs. Inhibiting UHRF2-let-7b (and probably other let-7 members) interaction by UHRF2-TSBs increases the proliferation of cells and EC wound repair in mouse and human ECs. High proliferation rates in MECs likely increase DNA damage and activate the cell's damage repair pathways. Due to the unrepairable damage, cells undergo apoptosis. In HECs, high proliferation rates result in the accumulation of DNA damage in the cells. Since the DNA damage repair may not be activated, the cells do not undergo apoptosis.

4.11. Differences between MECs and HECs

Using model organisms in clinical research aids us in understanding the pathological and physiological mechanisms that cause disease. Despite the development and use of humanized mouse models, more than 80% of drug candidates fail in clinical trials (247), mainly due to the physiological and homeostatic differences between human and model organisms. In mice, atherosclerosis progresses primarily in the aortic root, aortic arch, and innominate artery. In contrast, in humans, apart from the aortic arch, it develops in the carotid and coronary arteries (248). Moreover, unlike humans, mouse atherosclerotic lesions are rarely unstable, do not cause thrombosis, and do not produce a thick fibrous cap (248). Given the differences between mouse and human atherogenesis, finding the common pathway in mouse and human cells that affects this disease would be more relevant and more translatable in the clinic.

References

1. Wilkins E, Wilson L, Wickramasinghe K, Bhatnagar P, Leal J, Luengo-Fernandez R, et al. European cardiovascular disease statistics 2017. 2017.
2. Hansson GK, Libby P. The immune response in atherosclerosis: a double-edged sword. Nature reviews immunology. 2006;6(7):508.
3. Libby P, Ridker PM, Hansson GK. Progress and challenges in translating the biology of atherosclerosis. Nature. 2011;473(7347):317.
4. Lusis AJ. Atherosclerosis. Nature. 2000;407(6801):233-41.
5. Gimbrone MA, Jr. Vascular endothelium: nature's blood-compatible container. Annals of the New York Academy of Sciences. 1987;516:5-11.
6. Schober A, Maleki SS, Nazari-Jahantigh M. Regulatory Non-coding RNAs in Atherosclerosis. Handbook of experimental pharmacology. 2021.
7. Hahn C, Schwartz MA. Mechanotransduction in vascular physiology and atherogenesis. Nature reviews Molecular cell biology. 2009;10(1):53-62.
8. Tabas I, García-Cardeña G, Owens GK. Recent insights into the cellular biology of atherosclerosis. J Cell Biol. 2015;209(1):13-22.
9. Libby P. The molecular mechanisms of the thrombotic complications of atherosclerosis. Journal of internal medicine. 2008;263(5):517-27.
10. Cahill PA, Redmond EM. Vascular endothelium - Gatekeeper of vessel health. Atherosclerosis. 2016;248:97-109.
11. Aird WC. Phenotypic heterogeneity of the endothelium: I. Structure, function, and mechanisms. Circ Res. 2007;100(2):158-73.
12. Pugsley MK, Tabrizchi R. The vascular system. An overview of structure and function. Journal of pharmacological and toxicological methods. 2000;44(2):333-40.
13. Hall JE, Hall ME. Guyton and Hall textbook of medical physiology e-Book: Elsevier Health Sciences; 2020.
14. Medical B. Medical gallery of blausen medical 2014. WikiJournal of Medicine. 2014;1(2):1-79.
15. Rajendran P, Rengarajan T, Thangavel J, Nishigaki Y, Sakthisekaran D, Sethi G, et al. The vascular endothelium and human diseases. International journal of biological sciences. 2013;9(10):1057-69.
16. Mehta D, Malik AB. Signaling mechanisms regulating endothelial permeability. Physiological reviews. 2006;86(1):279-367.
17. Pober JS, Sessa WC. Evolving functions of endothelial cells in inflammation. Nature reviews Immunology. 2007;7(10):803-15.
18. Chiu JJ, Chien S. Effects of disturbed flow on vascular endothelium: pathophysiological basis and clinical perspectives. Physiological reviews. 2011;91(1):327-87.
19. Kunes P, Holubcová Z, Krejsek J. Occurrence and significance of the nuclear transcription factor Krüppel-like factor 4 (KLF4) in the vessel wall. Acta medica (Hradec Kralove). 2009;52(4):135-9.
20. Schober A, Nazari-Jahantigh M, Weber C. MicroRNA-mediated mechanisms of the cellular stress response in atherosclerosis. Nature reviews Cardiology. 2015;12(6):361-74.
21. Lin Z, Kumar A, SenBanerjee S, Staniszewski K, Parmar K, Vaughan DE, et al. Kruppel-like factor 2 (KLF2) regulates endothelial thrombotic function. Circ Res. 2005;96(5):e48-57.

22. van Thienen JV, Fledderus JO, Dekker RJ, Rohlena J, van Ijzendoorn GA, Kootstra NA, et al. Shear stress sustains atheroprotective endothelial KLF2 expression more potently than statins through mRNA stabilization. Cardiovascular research. 2006;72(2):231-40.
23. Kim M, Kim S, Lim JH, Lee C, Choi HC, Woo CH. Laminar flow activation of ERK5 protein in vascular endothelium leads to atheroprotective effect via NF-E2-related factor 2 (Nrf2) activation. The Journal of biological chemistry. 2012;287(48):40722-31.
24. Kim S, Woo CH. Laminar Flow Inhibits ER Stress-Induced Endothelial Apoptosis through PI3K/Akt-Dependent Signaling Pathway. Molecules and cells. 2018;41(11):964-70.
25. Silva Rd, editor Anatomical study of the variation in the branching patterns and histology of the aorta in a South African population2013.
26. Chistiakov DA, Orekhov AN, Bobryshev YV. Effects of shear stress on endothelial cells: go with the flow. Acta physiologica (Oxford, England). 2017;219(2):382-408.
27. van Hinsbergh VW, Scheffer M, Havekes L, Kempen HJ. Role of endothelial cells and their products in the modification of low-density lipoproteins. Biochimica et biophysica acta. 1986;878(1):49-64.
28. Salvayre R, Auge N, Benoist H, Negre-Salvayre A. Oxidized low-density lipoprotein-induced apoptosis. Biochimica et biophysica acta. 2002;1585(2-3):213-21.
29. Mazière C, Alimardani G, Dantin F, Dubois F, Conte MA, Mazière JC. Oxidized LDL activates STAT1 and STAT3 transcription factors: possible involvement of reactive oxygen species. FEBS letters. 1999;448(1):49-52.
30. Cominacini L, Rigoni A, Pasini AF, Garbin U, Davoli A, Campagnola M, et al. The binding of oxidized low density lipoprotein (ox-LDL) to ox-LDL receptor-1 reduces the intracellular concentration of nitric oxide in endothelial cells through an increased production of superoxide. The Journal of biological chemistry. 2001;276(17):13750-5.
31. Singh S, Nguyen H, Michels D, Bazinet H, Matkar PN, Liu Z, et al. BReast CAncer susceptibility gene 2 deficiency exacerbates oxidized LDL-induced DNA damage and endothelial apoptosis. Physiological reports. 2020;8(13):e14481.
32. Blackford AN, Stucki M. How Cells Respond to DNA Breaks in Mitosis. Trends in biochemical sciences. 2020;45(4):321-31.
33. Kopp F, Mendell JT. Functional Classification and Experimental Dissection of Long Noncoding RNAs. Cell. 2018;172(3):393-407.
34. Lee RC, Feinbaum RL, Ambros V. The C. elegans heterochronic gene lin-4 encodes small RNAs with antisense complementarity to lin-14. Cell. 1993;75(5):843-54.
35. Ruvkun G. The perfect storm of tiny RNAs. Nat Med. 2008;14(10):1041-5.
36. Baek D, Villén J, Shin C, Camargo FD, Gygi SP, Bartel DP. The impact of microRNAs on protein output. 2008.
37. Selbach M, Schwanhäusser B, Thierfelder N, Fang Z, Khanin R, Rajewsky N. Widespread changes in protein synthesis induced by microRNAs. Nature. 2008;455(7209):58-63.
38. Feinberg MW, Moore KJ. MicroRNA regulation of atherosclerosis. Circulation research. 2016;118(4):703-20.
39. Kumar S, Kim CW, Simmons RD, Jo H. Role of flow-sensitive microRNAs in endothelial dysfunction and atherosclerosis: mechanosensitive athero-miRs. Arteriosclerosis, thrombosis, and vascular biology. 2014:ATVBAHA. 114.303425.
40. Zeng Y. Principles of micro-RNA production and maturation. Oncogene. 2006;25(46):6156-62.

41. Schober A, Weber C. Mechanisms of MicroRNAs in Atherosclerosis. Annu Rev Pathol. 2016;11:583-616.
42. Winter J, Jung S, Keller S, Gregory RI, Diederichs S. Many roads to maturity: microRNA biogenesis pathways and their regulation. Nature cell biology. 2009;11(3):228.
43. Krol J, Loedige I, Filipowicz W. The widespread regulation of microRNA biogenesis, function and decay. Nature Reviews Genetics. 2010;11(9):597.
44. Lim LP, Lau NC, Weinstein EG, Abdelhakim A, Yekta S, Rhoades MW, et al. The microRNAs of Caenorhabditis elegans. Genes & development. 2003;17(8):991-1008.
45. Roush S, Slack FJ. The let-7 family of microRNAs. Trends in cell biology. 2008;18(10):505-16.
46. Bartel DP. MicroRNAs: target recognition and regulatory functions. Cell. 2009;136(2):215-33.
47. Bartel DP. Metazoan MicroRNAs. Cell. 2018;173(1):20-51.
48. Chipman LB, Pasquinelli AE. miRNA Targeting: Growing beyond the Seed. Trends in genetics : TIG. 2019;35(3):215-22.
49. Schirle NT, Sheu-Gruttadauria J, MacRae IJ. Structural basis for microRNA targeting. Science (New York, NY). 2014;346(6209):608-13.
50. Kuosmanen SM, Kansanen E, Sihvola V, Levonen AL. MicroRNA Profiling Reveals Distinct Profiles for Tissue-Derived and Cultured Endothelial Cells. Scientific reports. 2017;7(1):10943.
51. Cheng XW, Wan YF, Zhou Q, Wang Y, Zhu HQ. MicroRNA-126 inhibits endothelial permeability and apoptosis in apolipoprotein E-knockout mice fed a high-fat diet. Molecular medicine reports. 2017;16(3):3061-8.
52. Schober A, Nazari-Jahantigh M, Wei Y, Bidzhekov K, Gremse F, Grommes J, et al. MicroRNA-126-5p promotes endothelial proliferation and limits atherosclerosis by suppressing Dlk1. Nat Med. 2014;20(4):368-76.
53. Fang Y, Davies PF. Site-specific microRNA-92a regulation of Kruppel-like factors 4 and 2 in atherosusceptible endothelium. Arterioscler Thromb Vasc Biol. 2012;32(4):979-87.
54. Loyer X, Potteaux S, Vion A-C, Guérin CL, Boulkroun S, Rautou P-E, et al. Inhibition of microRNA-92a prevents endothelial dysfunction and atherosclerosis in mice. Circulation research. 2014;114(3):434-43.
55. Akhtar S, Hartmann P, Karshovska E, Rinderknecht FA, Subramanian P, Gremse F, et al. Endothelial Hypoxia-Inducible Factor-1α Promotes Atherosclerosis and Monocyte Recruitment by Upregulating MicroRNA-19a. Hypertension (Dallas, Tex : 1979). 2015;66(6):1220-6.
56. Qin X, Wang X, Wang Y, Tang Z, Cui Q, Xi J, et al. MicroRNA-19a mediates the suppressive effect of laminar flow on cyclin D1 expression in human umbilical vein endothelial cells. Proceedings of the National Academy of Sciences. 2010;107(7):3240-4.
57. Finnerty JR, Wang WX, Hébert SS, Wilfred BR, Mao G, Nelson PT. The miR-15/107 group of microRNA genes: evolutionary biology, cellular functions, and roles in human diseases. Journal of molecular biology. 2010;402(3):491-509.
58. Hartmann P, Zhou Z, Natarelli L, Wei Y, Nazari-Jahantigh M, Zhu M, et al. Endothelial Dicer promotes atherosclerosis and vascular inflammation by miRNA-103-mediated suppression of KLF4. Nature communications. 2016;7:10521.
59. Ulitsky I, Bartel DP. lincRNAs: genomics, evolution, and mechanisms. Cell. 2013;154(1):26-46.

60. Natarelli L, Geißler C, Csaba G, Wei Y, Zhu M, di Francesco A, et al. miR-103 promotes endothelial maladaptation by targeting lncWDR59. Nature communications. 2018;9(1):2645.
61. Uchida S, Dimmeler S. Long noncoding RNAs in cardiovascular diseases. Circ Res. 2015;116(4):737-50.
62. Chen K-C, Hsieh I-C, Hsi E, Wang Y-S, Dai C-Y, Chou W-W, et al. Negative feedback regulation between microRNA let-7g and the oxLDL receptor LOX-1. J Cell Sci. 2011:jcs. 092767.
63. Bao M-h, Zhang Y-w, Lou X-y, Cheng Y, Zhou H-h. Protective effects of let-7a and let-7b on oxidized low-density lipoprotein induced endothelial cell injuries. PLoS One. 2014;9(9):e106540.
64. Reinhart BJ, Slack FJ, Basson M, Pasquinelli AE, Bettinger JC, Rougvie AE, et al. The 21-nucleotide let-7 RNA regulates developmental timing in Caenorhabditis elegans. nature. 2000;403(6772):901.
65. Pasquinelli AE, Reinhart BJ, Slack F, Martindale MQ, Kuroda MI, Maller B, et al. Conservation of the sequence and temporal expression of let-7 heterochronic regulatory RNA. Nature. 2000;408(6808):86-9.
66. Lee H, Han S, Kwon CS, Lee D. Biogenesis and regulation of the let-7 miRNAs and their functional implications. Protein & cell. 2016;7(2):100-13.
67. Bracht J, Hunter S, Eachus R, Weeks P, Pasquinelli AE. Trans-splicing and polyadenylation of let-7 microRNA primary transcripts. Rna. 2004;10(10):1586-94.
68. Heo I, Ha M, Lim J, Yoon MJ, Park JE, Kwon SC, et al. Mono-uridylation of pre-microRNA as a key step in the biogenesis of group II let-7 microRNAs. Cell. 2012;151(3):521-32.
69. Sampson VB, Rong NH, Han J, Yang Q, Aris V, Soteropoulos P, et al. MicroRNA let-7a down-regulates MYC and reverts MYC-induced growth in Burkitt lymphoma cells. Cancer research. 2007;67(20):9762-70.
70. Chang TC, Yu D, Lee YS, Wentzel EA, Arking DE, West KM, et al. Widespread microRNA repression by Myc contributes to tumorigenesis. Nature genetics. 2008;40(1):43-50.
71. Heo I, Joo C, Cho J, Ha M, Han J, Kim VN. Lin28 mediates the terminal uridylation of let-7 precursor MicroRNA. Mol Cell. 2008;32(2):276-84.
72. Heo I, Joo C, Kim YK, Ha M, Yoon MJ, Cho J, et al. TUT4 in concert with Lin28 suppresses microRNA biogenesis through pre-microRNA uridylation. Cell. 2009;138(4):696-708.
73. Faehnle CR, Walleshauser J, Joshua-Tor L. Mechanism of Dis3l2 substrate recognition in the Lin28-let-7 pathway. Nature. 2014;514(7521):252-6.
74. Michlewski G, Cáceres JF. Antagonistic role of hnRNP A1 and KSRP in the regulation of let-7a biogenesis. Nature structural & molecular biology. 2010;17(8):1011-8.
75. Trabucchi M, Briata P, Garcia-Mayoral M, Haase AD, Filipowicz W, Ramos A, et al. The RNA-binding protein KSRP promotes the biogenesis of a subset of microRNAs. Nature. 2009;459(7249):1010-4.
76. Johnson SM, Grosshans H, Shingara J, Byrom M, Jarvis R, Cheng A, et al. RAS is regulated by the let-7 microRNA family. Cell. 2005;120(5):635-47.
77. Jérôme T, Laurie P, Louis B, Pierre C. Enjoy the Silence: The Story of let-7 MicroRNA and Cancer. Current genomics. 2007;8(4):229-33.

78. Kumar MS, Erkeland SJ, Pester RE, Chen CY, Ebert MS, Sharp PA, et al. Suppression of non-small cell lung tumor development by the let-7 microRNA family. Proceedings of the National Academy of Sciences of the United States of America. 2008;105(10):3903-8.
79. Johnson CD, Esquela-Kerscher A, Stefani G, Byrom M, Kelnar K, Ovcharenko D, et al. The let-7 microRNA represses cell proliferation pathways in human cells. Cancer research. 2007;67(16):7713-22.
80. Yu F, Yao H, Zhu P, Zhang X, Pan Q, Gong C, et al. let-7 regulates self renewal and tumorigenicity of breast cancer cells. Cell. 2007;131(6):1109-23.
81. Park SM, Shell S, Radjabi AR, Schickel R, Feig C, Boyerinas B, et al. Let-7 prevents early cancer progression by suppressing expression of the embryonic gene HMGA2. Cell cycle (Georgetown, Tex). 2007;6(21):2585-90.
82. Emmrich S, Rasche M, Schöning J, Reimer C, Keihani S, Maroz A, et al. miR-99a/100~125b tricistrons regulate hematopoietic stem and progenitor cell homeostasis by shifting the balance between TGFβ and Wnt signaling. Genes & development. 2014;28(8):858-74.
83. Bao MH, Feng X, Zhang YW, Lou XY, Cheng Y, Zhou HH. Let-7 in cardiovascular diseases, heart development and cardiovascular differentiation from stem cells. Int J Mol Sci. 2013;14(11):23086-102.
84. McCall MN, Kent OA, Yu J, Fox-Talbot K, Zaiman AL, Halushka MK. MicroRNA profiling of diverse endothelial cell types. BMC medical genomics. 2011;4:78.
85. Otsuka M, Zheng M, Hayashi M, Lee J-D, Yoshino O, Lin S, et al. Impaired microRNA processing causes corpus luteum insufficiency and infertility in mice. The Journal of clinical investigation. 2008;118(5):1944-54.
86. Liao Y-C, Wang Y-S, Guo Y-C, Lin W-L, Chang M-H, Juo S-HH. Let-7g improves multiple endothelial functions through targeting transforming growth factor-beta and SIRT-1 signaling. Journal of the American College of Cardiology. 2014;63(16):1685-94.
87. Cambronne XA, Shen R, Auer PL, Goodman RH. Capturing microRNA targets using an RNA-induced silencing complex (RISC)-trap approach. Proceedings of the National Academy of Sciences. 2012;109(50):20473-8.
88. Dunnett CW. A Multiple Comparison Procedure for Comparing Several Treatments with a Control. Journal of the American Statistical Association. 1955;50(272):1096-121.
89. Hothorn LA. The two-step approach—a significant ANOVA F-test before Dunnett's comparisons against a control—is not recommended. Communications in Statistics - Theory and Methods. 2016;45(11):3332-43.
90. Raudvere U, Kolberg L, Kuzmin I, Arak T, Adler P, Peterson H, et al. g:Profiler: a web server for functional enrichment analysis and conversions of gene lists (2019 update). Nucleic Acids Research. 2019;47(W1):W191-W8.
91. Howe KL, Achuthan P, Allen J, Allen J, Alvarez-Jarreta J, Amode MR, et al. Ensembl 2021. Nucleic Acids Research. 2020;49(D1):D884-D91.
92. Fang S, Zhang L, Guo J, Niu Y, Wu Y, Li H, et al. NONCODEV5: a comprehensive annotation database for long non-coding RNAs. Nucleic Acids Res. 2018;46(D1):D308-d14.
93. Kozomara A, Griffiths-Jones S. miRBase: integrating microRNA annotation and deep-sequencing data. Nucleic Acids Research. 2010;39(suppl_1):D152-D7.
94. Rehmsmeier M, Steffen P, Hochsmann M, Giegerich R. Fast and effective prediction of microRNA/target duplexes. Rna. 2004;10(10):1507-17.

95. Agarwal V, Bell GW, Nam JW, Bartel DP. Predicting effective microRNA target sites in mammalian mRNAs. eLife. 2015;4.
96. Friedman RC, Farh KK-H, Burge CB, Bartel DP. Most mammalian mRNAs are conserved targets of microRNAs. Genome research. 2009;19(1):92-105.
97. Karagkouni D, Paraskevopoulou MD, Chatzopoulos S, Vlachos IS, Tastsoglou S, Kanellos I, et al. DIANA-TarBase v8: a decade-long collection of experimentally supported miRNA-gene interactions. Nucleic acids research. 2018;46(D1):D239-D45.
98. Kaseder M, Schmid N, Eubler K, Goetz K, Müller-Taubenberger A, Dissen GA, et al. Evidence of a role for cAMP in mitochondrial regulation in ovarian granulosa cells. Molecular human reproduction. 2022;28(10).
99. Jin Y, Chen Z, Liu X, Zhou X. Evaluating the microRNA targeting sites by luciferase reporter gene assay. Methods in molecular biology (Clifton, NJ). 2013;936:117-27.
100. Choi C, Han J, Thao Tran NT, Yoon S, Kim G, Song S, et al. Effective experimental validation of miRNA targets using an improved linker reporter assay. Genetics research. 2017;99:e2.
101. Iwasaki S, Kawamata T, Tomari Y. Drosophila Argonaute1 and Argonaute2 Employ Distinct Mechanisms for Translational Repression. Molecular Cell. 2009;34(1):58-67.
102. Yan Y, Song D, Song X, Song C. The role of lncRNA MALAT1 in cardiovascular disease. IUBMB life. 2020;72(3):334-42.
103. Johnsson P, Lipovich L, Grandér D, Morris KV. Evolutionary conservation of long non-coding RNAs; sequence, structure, function. Biochimica et biophysica acta. 2014;1840(3):1063-71.
104. Pillai MM, Gillen AE, Yamamoto TM, Kline E, Brown J, Flory K, et al. HITS-CLIP reveals key regulators of nuclear receptor signaling in breast cancer. Breast cancer research and treatment. 2014;146(1):85-97.
105. Skalsky RL, Corcoran DL, Gottwein E, Frank CL, Kang D, Hafner M, et al. The viral and cellular microRNA targetome in lymphoblastoid cell lines. PLoS pathogens. 2012;8(1):e1002484.
106. Boudreau RL, Jiang P, Gilmore BL, Spengler RM, Tirabassi R, Nelson JA, et al. Transcriptome-wide discovery of microRNA binding sites in human brain. Neuron. 2014;81(2):294-305.
107. Xue Y, Ouyang K, Huang J, Zhou Y, Ouyang H, Li H, et al. Direct conversion of fibroblasts to neurons by reprogramming PTB-regulated microRNA circuits. Cell. 2013;152(1-2):82-96.
108. Kameswaran V, Bramswig NC, McKenna LB, Penn M, Schug J, Hand NJ, et al. Epigenetic regulation of the DLK1-MEG3 microRNA cluster in human type 2 diabetic islets. Cell metabolism. 2014;19(1):135-45.
109. Gottwein E, Corcoran DL, Mukherjee N, Skalsky RL, Hafner M, Nusbaum JD, et al. Viral microRNA targetome of KSHV-infected primary effusion lymphoma cell lines. Cell host & microbe. 2011;10(5):515-26.
110. Balakrishnan I, Yang X, Brown J, Ramakrishnan A, Torok-Storb B, Kabos P, et al. Genome-wide analysis of miRNA-mRNA interactions in marrow stromal cells. Stem cells (Dayton, Ohio). 2014;32(3):662-73.

111. Kishore S, Jaskiewicz L, Burger L, Hausser J, Khorshid M, Zavolan M. A quantitative analysis of CLIP methods for identifying binding sites of RNA-binding proteins. Nature methods. 2011;8(7):559-64.
112. Whisnant AW, Bogerd HP, Flores O, Ho P, Powers JG, Sharova N, et al. In-depth analysis of the interaction of HIV-1 with cellular microRNA biogenesis and effector mechanisms. mBio. 2013;4(2):e000193.
113. Karginov FV, Hannon GJ. Remodeling of Ago2-mRNA interactions upon cellular stress reflects miRNA complementarity and correlates with altered translation rates. Genes & development. 2013;27(14):1624-32.
114. Dango S, Mosammaparast N, Sowa ME, Xiong LJ, Wu F, Park K, et al. DNA unwinding by ASCC3 helicase is coupled to ALKBH3-dependent DNA alkylation repair and cancer cell proliferation. Mol Cell. 2011;44(3):373-84.
115. Sugiura T, Nagano Y, Noguchi Y. DDX39, upregulated in lung squamous cell cancer, displays RNA helicase activities and promotes cancer cell growth. Cancer biology & therapy. 2007;6(6):957-64.
116. Awasthi S, Chakrapani B, Mahesh A, Chavali PL, Chavali S, Dhayalan A. DDX39B promotes translation through regulation of pre-ribosomal RNA levels. RNA biology. 2018;15(9):1157-66.
117. Jia R, Zhao XF. MicroRNA-497 functions as an inflammatory suppressor via targeting DDX3Y and modulating toll-like receptor 4/NF-κB in cigarette smoke extract-stimulated human bronchial epithelial cells. The journal of gene medicine. 2020;22(1):e3137.
118. Vakilian H, Mirzaei M, Sharifi Tabar M, Pooyan P, Habibi Rezaee L, Parker L, et al. DDX3Y, a Male-Specific Region of Y Chromosome Gene, May Modulate Neuronal Differentiation. Journal of proteome research. 2015;14(9):3474-83.
119. Ge L, Zhang Y, Zhao X, Wang J, Zhang Y, Wang Q, et al. EIF2AK2 selectively regulates the gene transcription in immune response and histones associated with systemic lupus erythematosus. Molecular Immunology. 2021;132:132-41.
120. Feng Y, Wu L. Knockdown of eukaryotic translation initiation factor 3 subunit B inhibits cell proliferation and migration and promotes apoptosis by downregulating WNT signaling pathway in acute myeloid leukemia. Int J Clin Exp Pathol. 2020;13(1):99-106.
121. Ishihara K, Kitamura H, Hiraizumi K, Kaneko M, Takahashi A, Zee O, et al. Mechanisms for the proliferation of eosinophilic leukemia cells by FIP1L1-PDGFRα. Biochemical and biophysical research communications. 2008;366(4):1007-11.
122. Wu Q, Ma J, Meng W, Hui P. DLX6-AS1 promotes cell proliferation, migration and EMT of gastric cancer through FUS-regulated MAP4K1. Cancer biology & therapy. 2020;21(1):17-25.
123. Suzuki H, Matsuoka M. Overexpression of nuclear FUS induces neuronal cell death. Neuroscience. 2015;287:113-24.
124. Gu Y, Chen L, Li Q. [PPP3CA silence regulates MET process, cell apoptosis, proliferation and migration in metanephric mesenchyme cells]. Sheng wu gong cheng xue bao = Chinese journal of biotechnology. 2020;36(10):2151-61.
125. Wang J, Xu L, Yun X, Yang K, Liao D, Tian L, et al. Proteomic analysis reveals that proteasome subunit beta 6 is involved in hypoxia-induced pulmonary vascular remodeling in rats. PLoS One. 2013;8(7):e67942.

126. Perucho L, Artero-Castro A, Guerrero S, Ramón y Cajal S, ME LL, Wang ZQ. RPLP1, a crucial ribosomal protein for embryonic development of the nervous system. PLoS One. 2014;9(6):e99956.
127. Taylor AM, Humphries JM, White RM, Murphey RD, Burns CE, Zon LI. Hematopoietic defects in rps29 mutant zebrafish depend upon p53 activation. Experimental hematology. 2012;40(3):228-37.e5.
128. Anchi T, Tamura K, Furihata M, Satake H, Sakoda H, Kawada C, et al. SNRPE is involved in cell proliferation and progression of high-grade prostate cancer through the regulation of androgen receptor expression. Oncology letters. 2012;3(2):264-8.
129. Yan J, Zhang D, Han Y, Wang Z, Ma C. Antitumor activity of SR splicing-factor 5 knockdown by downregulating pyruvate kinase M2 in non-small cell lung cancer cells. Journal of cellular biochemistry. 2019;120(10):17303-11.
130. Liu J, Bian T, Feng J, Qian L, Zhang J, Jiang D, et al. miR-335 inhibited cell proliferation of lung cancer cells by target Tra2β. Cancer science. 2018;109(2):289-96.
131. Storbeck M, Hupperich K, Gaspar JA, Meganathan K, Martínez Carrera L, Wirth R, et al. Neuronal-specific deficiency of the splicing factor Tra2b causes apoptosis in neurogenic areas of the developing mouse brain. PLoS One. 2014;9(2):e89020.
132. Lim S, Yoo BK, Kim HS, Gilmore HL, Lee Y, Lee HP, et al. Amyloid-β precursor protein promotes cell proliferation and motility of advanced breast cancer. BMC cancer. 2014;14:928.
133. Li J, Wang AS, Wang S, Wang CY, Xue S, Li WY, et al. Death-inducer obliterator 1 (DIDO1) silencing suppresses growth of bladder cancer cells through decreasing SAPK/JNK signaling cascades. Neoplasma. 2020;67(5):1074-84.
134. García-Domingo D, Ramírez D, González de Buitrago G, Martínez AC. Death inducer-obliterator 1 triggers apoptosis after nuclear translocation and caspase upregulation. Molecular and cellular biology. 2003;23(9):3216-25.
135. Zhang JY, Lin MT, Yi T, Tang YN, Fan LL, He XC, et al. Apoptosis sensitization by Euphorbia factor L1 in ABCB1-mediated multidrug resistant K562/ADR cells. Molecules (Basel, Switzerland). 2013;18(10):12793-808.
136. Armistead J, Hemming R, Patel N, Triggs-Raine B. Mutation of EMG1 causing Bowen-Conradi syndrome results in reduced cell proliferation rates concomitant with G2/M arrest and 18S rRNA processing delay. BBA clinical. 2014;1:33-43.
137. Armistead J, Patel N, Wu X, Hemming R, Chowdhury B, Basra GS, et al. Growth arrest in the ribosomopathy, Bowen-Conradi syndrome, is due to dramatically reduced cell proliferation and a defect in mitotic progression. Biochimica et biophysica acta. 2015;1852(5):1029-37.
138. Li H, Liu Q, Xiao K, He Z, Wu C, Sun J, et al. PDIA4 Correlates with Poor Prognosis and is a Potential Biomarker in Glioma. OncoTargets and therapy. 2021;14:125-38.
139. Qian S, Zhang S, Wu Y, Ding Y, Li X. Protein Disulfide Isomerase 4 Drives Docetaxel Resistance in Prostate Cancer. Chemotherapy. 2020;65(5-6):125-33.
140. Guan X, Chen S, Liu Y, Wang LL, Zhao Y, Zong ZH. PUM1 promotes ovarian cancer proliferation, migration and invasion. Biochemical and biophysical research communications. 2018;497(1):313-8.
141. Dai H, Shen K, Yang Y, Su X, Luo Y, Jiang Y, et al. PUM1 knockdown prevents tumor progression by activating the PERK/eIF2/ATF4 signaling pathway in pancreatic adenocarcinoma cells. Cell death & disease. 2019;10(8):595.

142. Liu Z, Li W, Pang Y, Zhou Z, Liu S, Cheng K, et al. SF3B4 is regulated by microRNA-133b and promotes cell proliferation and metastasis in hepatocellular carcinoma. EBioMedicine. 2018;38:57-68.
143. Hamada J, Shoda K, Masuda K, Fujita Y, Naruto T, Kohmoto T, et al. Tumor-promoting function and prognostic significance of the RNA-binding protein T-cell intracellular antigen-1 in esophageal squamous cell carcinoma. Oncotarget. 2016;7(13):17111-28.
144. Huang S, Liu N, Li H, Zhao J, Su L, Zhang Y, et al. TIA1 interacts with annexin A7 in regulating vascular endothelial cell autophagy. The international journal of biochemistry & cell biology. 2014;57:115-22.
145. Zhang S, Yan L, Cui C, Wang Z, Wu J, Zhao M, et al. Identification of TYMS as a promoting factor of retroperitoneal liposarcoma progression: Bioinformatics analysis and biological evidence. Oncology reports. 2020;44(2):565-76.
146. Panieri E, Santoro MM. ROS signaling and redox biology in endothelial cells. Cellular and molecular life sciences : CMLS. 2015;72(17):3281-303.
147. Braasch DA, Corey DR. Locked nucleic acid (LNA): fine-tuning the recognition of DNA and RNA. Chemistry & biology. 2001;8(1):1-7.
148. Kuehbacher A, Urbich C, Zeiher AM, Dimmeler S. Role of Dicer and Drosha for endothelial microRNA expression and angiogenesis. Circulation research. 2007;101(1):59-68.
149. Qin B, Xiao B, Liang D, Li Y, Jiang T, Yang H. MicroRNA let-7c inhibits Bcl-xl expression and regulates ox-LDL-induced endothelial apoptosis. BMB reports. 2012;45(8):464-9.
150. Teng GG, Wang WH, Dai Y, Wang SJ, Chu YX, Li J. Let-7b is involved in the inflammation and immune responses associated with Helicobacter pylori infection by targeting Toll-like receptor 4. PLoS One. 2013;8(2):e56709.
151. Zhang Y, Chen N, Zhang J, Tong Y. Hsa-let-7g miRNA targets caspase-3 and inhibits the apoptosis induced by ox-LDL in endothelial cells. International journal of molecular sciences. 2013;14(11):22708-20.
152. Zhou Q, Frost RJA, Anderson C, Zhao F, Ma J, Yu B, et al. let-7 Contributes to Diabetic Retinopathy but Represses Pathological Ocular Angiogenesis. Molecular and cellular biology. 2017;37(16).
153. Hou W, Tian Q, Steuerwald NM, Schrum LW, Bonkovsky HL. The let-7 microRNA enhances heme oxygenase-1 by suppressing Bach1 and attenuates oxidant injury in human hepatocytes. Biochimica et biophysica acta. 2012;1819(11-12):1113-22.
154. Shimizu S, Takehara T, Hikita H, Kodama T, Miyagi T, Hosui A, et al. The let-7 family of microRNAs inhibits Bcl-xL expression and potentiates sorafenib-induced apoptosis in human hepatocellular carcinoma. Journal of hepatology. 2010;52(5):698-704.
155. Jiang S, Yan W, Wang SE, Baltimore D. Let-7 Suppresses B Cell Activation through Restricting the Availability of Necessary Nutrients. Cell metabolism. 2018;27(2):393-403.e4.
156. Wei Y, Corbalán-Campos J, Gurung R, Natarelli L, Zhu M, Exner N, et al. Dicer in Macrophages Prevents Atherosclerosis by Promoting Mitochondrial Oxidative Metabolism. Circulation. 2018;138(18):2007-20.
157. Kiriakidou M, Nelson PT, Kouranov A, Fitziev P, Bouyioukos C, Mourelatos Z, et al. A combined computational-experimental approach predicts human microRNA targets. Genes & development. 2004;18(10):1165-78.

158. Helwak A, Kudla G, Dudnakova T, Tollervey D. Mapping the human miRNA interactome by CLASH reveals frequent noncanonical binding. Cell. 2013;153(3):654-65.
159. Chi SW, Zang JB, Mele A, Darnell RB. Argonaute HITS-CLIP decodes microRNA-mRNA interaction maps. Nature. 2009;460(7254):479-86.
160. Hafner M, Landthaler M, Burger L, Khorshid M, Hausser J, Berninger P, et al. Transcriptome-wide identification of RNA-binding protein and microRNA target sites by PAR-CLIP. Cell. 2010;141(1):129-41.
161. Li JH, Liu S, Zhou H, Qu LH, Yang JH. starBase v2.0: decoding miRNA-ceRNA, miRNA-ncRNA and protein-RNA interaction networks from large-scale CLIP-Seq data. Nucleic Acids Res. 2014;42(Database issue):D92-7.
162. Mao X, Li L, Cao Y. Evolutionary comparisons of miRNA regulation system in six model organisms. Genetica. 2014;142(1):109-18.
163. Fromm B, Billipp T, Peck LE, Johansen M, Tarver JE, King BL, et al. A Uniform System for the Annotation of Vertebrate microRNA Genes and the Evolution of the Human microRNAome. Annual review of genetics. 2015;49:213-42.
164. Reczko M, Maragkakis M, Alexiou P, Grosse I, Hatzigeorgiou AG. Functional microRNA targets in protein coding sequences. Bioinformatics (Oxford, England). 2012;28(6):771-6.
165. Grey F, Tirabassi R, Meyers H, Wu G, McWeeney S, Hook L, et al. A viral microRNA down-regulates multiple cell cycle genes through mRNA 5'UTRs. PLoS pathogens. 2010;6(6):e1000967.
166. McGeary SE, Lin KS, Shi CY, Pham TM, Bisaria N, Kelley GM, et al. The biochemical basis of microRNA targeting efficacy. Science (New York, NY). 2019;366(6472).
167. Martin HC, Wani S, Steptoe AL, Krishnan K, Nones K, Nourbakhsh E, et al. Imperfect centered miRNA binding sites are common and can mediate repression of target mRNAs. Genome biology. 2014;15(3):R51.
168. He X, Duan C, Chen J, Ou-Yang X, Zhang Z, Li C, et al. Let-7a elevates p21(WAF1) levels by targeting of NIRF and suppresses the growth of A549 lung cancer cells. FEBS letters. 2009;583(21):3501-7.
169. Bramsen JB, Laursen MB, Damgaard CK, Lena SW, Babu BR, Wengel J, et al. Improved silencing properties using small internally segmented interfering RNAs. Nucleic Acids Res. 2007;35(17):5886-97.
170. Pillai RS, Bhattacharyya SN, Artus CG, Zoller T, Cougot N, Basyuk E, et al. Inhibition of translational initiation by Let-7 MicroRNA in human cells. Science (New York, NY). 2005;309(5740):1573-6.
171. Djuranovic S, Nahvi A, Green R. miRNA-mediated gene silencing by translational repression followed by mRNA deadenylation and decay. Science (New York, NY). 2012;336(6078):237-40.
172. Béthune J, Artus-Revel CG, Filipowicz W. Kinetic analysis reveals successive steps leading to miRNA-mediated silencing in mammalian cells. EMBO reports. 2012;13(8):716-23.
173. Bartel DP. MicroRNAs: genomics, biogenesis, mechanism, and function. Cell. 2004;116(2):281-97.
174. Chang KT, Wang LH, Lin YM, Cheng CF, Wang GS. CELF1 promotes vascular endothelial growth factor degradation resulting in impaired microvasculature in heart

failure. FASEB journal : official publication of the Federation of American Societies for Experimental Biology. 2021;35(5):e21512.
175. Chang KT, Cheng CF, King PC, Liu SY, Wang GS. CELF1 Mediates Connexin 43 mRNA Degradation in Dilated Cardiomyopathy. Circ Res. 2017;121(10):1140-52.
176. Clark MB, Amaral PP, Schlesinger FJ, Dinger ME, Taft RJ, Rinn JL, et al. The reality of pervasive transcription. PLoS biology. 2011;9(7):e1000625; discussion e1102.
177. Yang K-C, Yamada KA, Patel AY, Topkara VK, George I, Cheema FH, et al. Deep RNA sequencing reveals dynamic regulation of myocardial noncoding RNAs in failing human heart and remodeling with mechanical circulatory support. Circulation. 2014;129(9):1009-21.
178. Kumarswamy R, Bauters C, Volkmann I, Maury F, Fetisch J, Holzmann A, et al. Circulating long noncoding RNA, LIPCAR, predicts survival in patients with heart failure. Circ Res. 2014;114(10):1569-75.
179. Jin X, Cheng Z, Wang B, Yau TO, Chen Z, Barker SC, et al. Precise annotation of human, chimpanzee, rhesus macaque and mouse mitochondrial genomes leads to insight into mitochondrial transcription in mammals. RNA biology. 2020;17(3):395-402.
180. Gao S, Tian X, Chang H, Sun Y, Wu Z, Cheng Z, et al. Two novel lncRNAs discovered in human mitochondrial DNA using PacBio full-length transcriptome data. Mitochondrion. 2018;38:41-7.
181. Michalik KM, You X, Manavski Y, Doddaballapur A, Zörnig M, Braun T, et al. Long Noncoding RNA MALAT1 Regulates Endothelial Cell Function and Vessel Growth. Circulation research. 2014;114(9):1389-97.
182. Breschi A, Gingeras TR, Guigó R. Comparative transcriptomics in human and mouse. Nature reviews Genetics. 2017;18(7):425-40.
183. Hezroni H, Koppstein D, Schwartz MG, Avrutin A, Bartel DP, Ulitsky I. Principles of long noncoding RNA evolution derived from direct comparison of transcriptomes in 17 species. Cell Rep. 2015;11(7):1110-22.
184. Chen ZH, Wang WT, Huang W, Fang K, Sun YM, Liu SR, et al. The lncRNA HOTAIRM1 regulates the degradation of PML-RARA oncoprotein and myeloid cell differentiation by enhancing the autophagy pathway. Cell death and differentiation. 2017;24(2):212-24.
185. Chiyomaru T, Fukuhara S, Saini S, Majid S, Deng G, Shahryari V, et al. Long non-coding RNA HOTAIR is targeted and regulated by miR-141 in human cancer cells. The Journal of biological chemistry. 2014;289(18):12550-65.
186. Wang D, Xu H, Wu B, Jiang S, Pan H, Wang R, et al. Long non-coding RNA MALAT1 sponges miR-124-3p.1/KLF5 to promote pulmonary vascular remodeling and cell cycle progression of pulmonary artery hypertension. International journal of molecular medicine. 2019;44(3):871-84.
187. Poliseno L, Salmena L, Zhang J, Carver B, Haveman WJ, Pandolfi PP. A coding-independent function of gene and pseudogene mRNAs regulates tumour biology. Nature. 2010;465(7301):1033-8.
188. ENCORI: The Encyclopedia of RNA Interactomes [Internet]. 2021. Available from: https://starbase.sysu.edu.cn/index.php.
189. Gomez I, Ward B, Souilhol C, Recarti C, Ariaans M, Johnston J, et al. Neutrophil microvesicles drive atherosclerosis by delivering miR-155 to atheroprone endothelium. Nat Commun. 2020;11(1):214.

190. Paraskevopoulou MD, Hatzigeorgiou AG. Analyzing MiRNA-LncRNA Interactions. Methods in molecular biology (Clifton, NJ). 2016;1402:271-86.
191. Kallen AN, Zhou XB, Xu J, Qiao C, Ma J, Yan L, et al. The imprinted H19 lncRNA antagonizes let-7 microRNAs. Mol Cell. 2013;52(1):101-12.
192. Zhou X, Wang Y, Li Q, Ma D, Nie A, Shen X. LncRNA Linc-PINT inhibits miR-523-3p to hamper retinoblastoma progression by upregulating Dickkopf-1 (DKK1). Biochemical and biophysical research communications. 2020;530(1):47-53.
193. Zhang L, Chen J, Wang L, Chen L, Du Z, Zhu L, et al. Linc-PINT acted as a tumor suppressor by sponging miR-543 and miR-576-5p in esophageal cancer. Journal of cellular biochemistry. 2019;120(12):19345-57.
194. Wang S, Jiang W, Zhang X, Lu Z, Geng Q, Wang W, et al. LINC-PINT alleviates lung cancer progression via sponging miR-543 and inducing PTEN. Cancer medicine. 2020;9(6):1999-2009.
195. Wang J, Zhao Q. LncRNA LINC-PINT increases SOCS1 expression by sponging miR-155-5p to inhibit the activation of ERK signaling pathway in rheumatoid arthritis synovial fibroblasts induced by TNF-α. International immunopharmacology. 2020;84:106497.
196. Jia M, Li Z, Pan M, Tao M, Wang J, Lu X. LINC-PINT Suppresses the Aggressiveness of Thyroid Cancer by Downregulating miR-767-5p to Induce TET2 Expression. Molecular therapy Nucleic acids. 2020;22:319-28.
197. Hao T, Huang S, Han F. LINC-PINT suppresses tumour cell proliferation, migration and invasion through targeting miR-374a-5p in ovarian cancer. Cell biochemistry and function. 2020;38(8):1089-99.
198. Zhu J, Gu H, Lv X, Yuan C, Ni P, Liu F. LINC-PINT Activates the Mitogen-Activated Protein Kinase Pathway to Promote Acute Myocardial Infarction by Regulating miR-208a-3p. Circulation journal : official journal of the Japanese Circulation Society. 2018;82(11):2783-92.
199. Zhang M, Zhao K, Xu X, Yang Y, Yan S, Wei P, et al. A peptide encoded by circular form of LINC-PINT suppresses oncogenic transcriptional elongation in glioblastoma. Nat Commun. 2018;9(1):4475.
200. Chen J, Shishkin AA, Zhu X, Kadri S, Maza I, Guttman M, et al. Evolutionary analysis across mammals reveals distinct classes of long non-coding RNAs. Genome biology. 2016;17:19.
201. Liu W. LncRNA LINC-PINT Inhibits Cancer Cell Proliferation, Invasion, and Migration in Osteosarcoma by Downregulating miRNA-21. Cancer biotherapy & radiopharmaceuticals. 2019;34(4):258-63.
202. Marín-Béjar O, Mas AM, González J, Martinez D, Athie A, Morales X, et al. The human lncRNA LINC-PINT inhibits tumor cell invasion through a highly conserved sequence element. Genome biology. 2017;18(1):202.
203. Zhu H, Chen Z, Shen L, Tang T, Yang M, Zheng X. Long Noncoding RNA LINC-PINT Suppresses Cell Proliferation, Invasion, and EMT by Blocking Wnt/β-Catenin Signaling in Glioblastoma. Frontiers in pharmacology. 2020;11:586653.
204. Xu Y, Wang H, Li F, Heindl LM, He X, Yu J, et al. Long Non-coding RNA LINC-PINT Suppresses Cell Proliferation and Migration of Melanoma via Recruiting EZH2. Frontiers in cell and developmental biology. 2019;7:350.

205. Lu H, Yang D, Zhang L, Lu S, Ye J, Li M, et al. Linc-pint inhibits early stage pancreatic ductal adenocarcinoma growth through TGF-β pathway activation. Oncology letters. 2019;17(5):4633-9.
206. Hong L, Wang J, Wang H, Wei S, Zhang F, Han J, et al. Linc-pint overexpression inhibits the growth of gastric tumors by downregulating HIF-1α. Molecular medicine reports. 2019;20(3):2875-81.
207. Garitano-Trojaola A, José-Enériz ES, Ezponda T, Unfried JP, Carrasco-León A, Razquin N, et al. Deregulation of linc-PINT in acute lymphoblastic leukemia is implicated in abnormal proliferation of leukemic cells. Oncotarget. 2018;9(16):12842-52.
208. Lim LP, Lau NC, Garrett-Engele P, Grimson A, Schelter JM, Castle J, et al. Microarray analysis shows that some microRNAs downregulate large numbers of target mRNAs. Nature. 2005;433(7027):769-73.
209. Feng Y, Yang Y, Zhao X, Fan Y, Zhou L, Rong J, et al. Circular RNA circ0005276 promotes the proliferation and migration of prostate cancer cells by interacting with FUS to transcriptionally activate XIAP. Cell death & disease. 2019;10(11):792.
210. Valinezhad Orang A, Safaralizadeh R, Kazemzadeh-Bavili M. Mechanisms of miRNA-Mediated Gene Regulation from Common Downregulation to mRNA-Specific Upregulation. International journal of genomics. 2014;2014:970607.
211. Vasudevan S, Tong Y, Steitz JA. Switching from repression to activation: microRNAs can up-regulate translation. Science (New York, NY). 2007;318(5858):1931-4.
212. Vasudevan S, Tong Y, Steitz JA. Cell-cycle control of microRNA-mediated translation regulation. Cell cycle (Georgetown, Tex). 2008;7(11):1545-9.
213. Lin CC, Liu LZ, Addison JB, Wonderlin WF, Ivanov AV, Ruppert JM. A KLF4-miRNA-206 autoregulatory feedback loop can promote or inhibit protein translation depending upon cell context. Molecular and cellular biology. 2011;31(12):2513-27.
214. Cordes KR, Sheehy NT, White MP, Berry EC, Morton SU, Muth AN, et al. miR-145 and miR-143 regulate smooth muscle cell fate and plasticity. Nature. 2009;460(7256):705-10.
215. Rom S, Dykstra H, Zuluaga-Ramirez V, Reichenbach NL, Persidsky Y. miR-98 and let-7g* protect the blood-brain barrier under neuroinflammatory conditions. Journal of cerebral blood flow and metabolism : official journal of the International Society of Cerebral Blood Flow and Metabolism. 2015;35(12):1957-65.
216. Büssing I, Slack FJ, Grosshans H. let-7 microRNAs in development, stem cells and cancer. Trends in molecular medicine. 2008;14(9):400-9.
217. Bazzoni G, Dejana E. Endothelial cell-to-cell junctions: molecular organization and role in vascular homeostasis. Physiological reviews. 2004;84(3):869-901.
218. Grazia Lampugnani M, Zanetti A, Corada M, Takahashi T, Balconi G, Breviario F, et al. Contact inhibition of VEGF-induced proliferation requires vascular endothelial cadherin, beta-catenin, and the phosphatase DEP-1/CD148. The Journal of cell biology. 2003;161(4):793-804.
219. Caveda L, Martin-Padura I, Navarro P, Breviario F, Corada M, Gulino D, et al. Inhibition of cultured cell growth by vascular endothelial cadherin (cadherin-5/VE-cadherin). J Clin Invest. 1996;98(4):886-93.
220. O'Toole TE, Abplanalp W, Li X, Cooper N, Conklin DJ, Haberzettl P, et al. Acrolein decreases endothelial cell migration and insulin sensitivity through induction of let-7a. Toxicological sciences : an official journal of the Society of Toxicology. 2014;140(2):271-82.

221. Tsang WP, Kwok TT. Let-7a microRNA suppresses therapeutics-induced cancer cell death by targeting caspase-3. Apoptosis. 2008;13(10):1215-22.
222. Peng G, Yuan Y, He Q, Wu W, Luo B-y. MicroRNA let-7e regulates the expression of caspase-3 during apoptosis of PC12 cells following anoxia/reoxygenation injury. Brain research bulletin. 2011;86(3-4):272-6.
223. Ding Z, Wang X, Khaidakov M, Liu S, Mehta JL. MicroRNA hsa-let-7g targets lectin-like oxidized low-density lipoprotein receptor-1 expression and inhibits apoptosis in human smooth muscle cells. Experimental Biology and Medicine. 2012;237(9):1093-100.
224. Xie C, Chen W, Zhang M, Cai Q, Xu W, Li X, et al. MDM4 regulation by the let-7 miRNA family in the DNA damage response of glioma cells. FEBS letters. 2015;589(15):1958-65.
225. Saleh AD, Savage JE, Cao L, Soule BP, Ly D, DeGraff W, et al. Cellular stress induced alterations in microRNA let-7a and let-7b expression are dependent on p53. PLoS One. 2011;6(10):e24429.
226. Hu H, Zhao X, Jin Z, Hou M. Hsa-let-7g miRNA regulates the anti-tumor effects of gastric cancer cells under oxidative stress through the expression of DDR genes. The Journal of toxicological sciences. 2015;40(3):329-38.
227. Liu B, Liu M, Wang J, Zhang X, Wang X, Wang P, et al. DICER-dependent biogenesis of let-7 miRNAs affects human cell response to DNA damage via targeting p21/p27. Nucleic Acids Res. 2015;43(3):1626-36.
228. Incalza MA, D'Oria R, Natalicchio A, Perrini S, Laviola L, Giorgino F. Oxidative stress and reactive oxygen species in endothelial dysfunction associated with cardiovascular and metabolic diseases. Vascul Pharmacol. 2018;100:1-19.
229. Cai H, Harrison DG. Endothelial dysfunction in cardiovascular diseases: the role of oxidant stress. Circ Res. 2000;87(10):840-4.
230. Ding Z, Wang X, Schnackenberg L, Khaidakov M, Liu S, Singla S, et al. Regulation of autophagy and apoptosis in response to ox-LDL in vascular smooth muscle cells, and the modulatory effects of the microRNA hsa-let-7 g. International journal of cardiology. 2013;168(2):1378-85.
231. Mori T, Li Y, Hata H, Ono K, Kochi H. NIRF, a novel RING finger protein, is involved in cell-cycle regulation. Biochemical and biophysical research communications. 2002;296(3):530-6.
232. Pichler G, Wolf P, Schmidt CS, Meilinger D, Schneider K, Frauer C, et al. Cooperative DNA and histone binding by Uhrf2 links the two major repressive epigenetic pathways. Journal of cellular biochemistry. 2011;112(9):2585-93.
233. Aasland R, Gibson TJ, Stewart AF. The PHD finger: implications for chromatin-mediated transcriptional regulation. Trends in biochemical sciences. 1995;20(2):56-9.
234. Luo T, Cui S, Bian C, Yu X. Uhrf2 is important for DNA damage response in vascular smooth muscle cells. Biochemical and biophysical research communications. 2013;441(1):65-70.
235. Mori T, Ikeda DD, Fukushima T, Takenoshita S, Kochi H. NIRF constitutes a nodal point in the cell cycle network and is a candidate tumor suppressor. Cell cycle (Georgetown, Tex). 2011;10(19):3284-99.
236. Li Y, Mori T, Hata H, Homma Y, Kochi H. NIRF induces G1 arrest and associates with Cdk2. Biochemical and biophysical research communications. 2004;319(2):464-8.

237. Wang Y, Yan X, Zeng S, Zhang T, Cheng F, Chen R, et al. UHRF2 promotes DNA damage response by decreasing p21 via RING finger domain. Biotechnology letters. 2018;40(8):1181-8.
238. Wang F, Zhang P, Ma Y, Yang J, Moyer MP, Shi C, et al. NIRF is frequently upregulated in colorectal cancer and its oncogenicity can be suppressed by let-7a microRNA. Cancer letters. 2012;314(2):223-31.
239. Lu H, Hallstrom TC. The nuclear protein UHRF2 is a direct target of the transcription factor E2F1 in the induction of apoptosis. The Journal of biological chemistry. 2013;288(33):23833-43.
240. Fang XY, Sun JJ, Chen SY, Wu KJ, Yu Y, Zhang C, et al. IGF2BP1/UHRF2 Axis Mediated by miR-98-5p to Promote the Proliferation of and Inhibit the Apoptosis of Esophageal Squamous Cell Carcinoma. Annals of clinical and laboratory science. 2021;51(3):329-38.
241. Rogakou EP, Pilch DR, Orr AH, Ivanova VS, Bonner WM. DNA Double-stranded Breaks Induce Histone H2AX Phosphorylation on Serine 139*. Journal of Biological Chemistry. 1998;273(10):5858-68.
242. Paull TT, Rogakou EP, Yamazaki V, Kirchgessner CU, Gellert M, Bonner WM. A critical role for histone H2AX in recruitment of repair factors to nuclear foci after DNA damage. Current Biology. 2000;10(15):886-95.
243. Wang JY, Cho SK. Coordination of repair, checkpoint, and cell death responses to DNA damage. Advances in protein chemistry. 2004;69:101-35.
244. Motnenko A, Liang CC, Yang D, Lopez-Martinez D, Yoshikawa Y, Zhan B, et al. Identification of UHRF2 as a novel DNA interstrand crosslink sensor protein. PLoS genetics. 2018;14(10):e1007643.
245. Hanaki S, Habara M, Shimada M. UV-induced activation of ATR is mediated by UHRF2. Genes to cells : devoted to molecular & cellular mechanisms. 2021;26(6):447-54.
246. Georgescu RE, Kim S-S, Yurieva O, Kuriyan J, Kong X-P, O'Donnell M. Structure of a Sliding Clamp on DNA. Cell. 2008;132(1):43-54.
247. Ito R, Takahashi T, Ito M. Humanized mouse models: Application to human diseases. Journal of cellular physiology. 2018;233(5):3723-8.
248. Getz GS, Reardon CA. Animal models of atherosclerosis. Arteriosclerosis, thrombosis, and vascular biology. 2012;32(5):1104-15.

Acknowledgements

Words cannot express my gratitude to my Supervisor and the chair of my thesis advisory committee, Prof. Dr. Andreas Schober for his invaluable patience and feedback. This work wouldn't have been possible without his extra ordinary scientific mindset.

I also could not have undertaken this journey without my thesis Advisory comitee members, Prof. Dr. Alexander Bartelt and Prof. Dr. Sabine Steffens who generously provided knowledge and expertise. Additionally, this endeavor would not have been possible without the generous support from the Deutsche Forschungsgemeinschaft (German Research Foundation) Collaborative Research Centre 1123 and the director of Institute for Cardiovascular Prevention (IPEK), Prof. Dr. med. Christian Weber.

I am also grateful to Claudia Geissler for her priceless technical expertise and Anja Fusco for her great assisstance. I am thankful to my collegues, Nan, Lucia, Isabelle, Anna and Mengyu for their feedback and moral support. Thanks should also go to Ms. Iliriana Vatovci and Ms. Catherine Gunczi for the bureaucratic support they gave me during my work.

Lastly, I would be remiss in not mentioning my family, especially my parents and my spouse. Their belief in me has kept my spirits and motivation high during this process.

Affidavit

LMU LUDWIG-MAXIMILIANS-UNIVERSITÄT MÜNCHEN | Promotionsbüro Medizinische Fakultät | MMRS

Affidavit

Saboor Maleki, Saffiyeh

_____

Surname, first name

Pettenkoferstraße 8a und 9

_____

Street

80336, Munich, Germany

_____

Zip code, town, country

I hereby declare, that the submitted thesis entitled:

Targets of let-7b in endothelial cells

is my own work. I have only used the sources indicated and have not made unauthorised use of services of a third party. Where the work of others has been quoted or reproduced, the source is always given.

I further declare that the submitted thesis or parts thereof have not been presented as part of an examination degree to any other university.

Bischofsheim, 08.10.2022 Saffiyeh Saboor Maleki

_____

place, date Signature doctoral candidate

Confirmation of congruency

Confirmation of congruency between printed and electronic version of the doctoral thesis

Saboor Maleki, Saffiyeh

Surname, first name

Pettenkoferstraße 8a und 9

Street

80336, Munich, Germany

Zip code, town, country

I hereby declare, that the submitted thesis entitled:

Targets of let-7b in endothelial cells

is congruent with the printed version both in content and format.

Bischofsheim, 08.10.2022 Saffiyeh Saboor Maleki

place, date Signature doctoral candidate